Wood as a scour protection

MSc Graduation Work

Appendices

Author:
Laurens Beulink 4076532

Supervisors:
Prof. Dr. Ir. Uijttewaal, W.
Ir. Verhagen, H.J.
Dr. Dionisio Pires, L.M.
Dr. Ir. Bricker, J.D.
Dr. Ir. Sieben, J.

Table of Contents

Appendix A I

A1.1 Hydraulic resistance

Change in friction can be measured through a change in the depth and thus average flow velocity in a laboratory setting. The Darcy – Weisbach formula could be used to deduct the friction generated by the logs.

$$\frac{\Delta p}{L} = f_d * \frac{\rho_w}{2} * \frac{\bar{u}^2}{D}$$

$where$:
$\Delta p = Hydraulic\ head$
$L = Lenght\ of\ section$
$f_d = average\ friction\ over\ section$
$\rho_w = density\ water$
$\bar{u} = average\ flow\ velocity$
$D = hydraulic\ diameter = \left(\frac{4(d*w)}{2d+w}\right)$ (for open channel sections)

To obtain an indication of the friction changes, depth **(h)** and average flow velocity **($\bar{u}$)** must therefore be measured. As the average flow velocity outside of the constricted section is solely dependent on depth **(h)** due to a constant with, this parameter is essential to the secondary research objective with respect to the changes in hydraulic conditions.

A1.2 Shields & contraction scour predictions

The first secondary research question demands an assessment to be made of the potential scouring in the contraction. For this to be known a connection has to be made to the relevant knowledge which has to do with the so-called shields parameter, scour mode, relevant transport modes, and the knowledge with respect to contraction scour.

From practical considerations it is best to produce a situation in which clear water scour is simulated. Otherwise a source of sediment would have to be included, which is impractical. Starting from this, it is important to look at the research conducted by Shields, to produce a situation in which no scour occurs in the areas outside the constriction.

First one must look at the by shields defined modes of transport:

0. No movement at all
1. Occasional moment at some locations
2. Frequent movement at some locations
3. Frequent movement at several locations
4. Frequent movement at many locations
5. Frequent movement at all locations
6. Continuous movement at all locations
7. General transport of the grains

From a practical point of view mode 1 is assumed to generate no significant movement of bed particles outside of the constriction, so this mode is assumed which leads to a shields parameter that must not be exceeded of roughly 0,03 (Schiereck & Verhagen, 2012).

With this knowledge a connection can be made to the stability equation (Schiereck & Verhagen, 2012):

$$d_{50} = \frac{\overline{u_c}^2}{(\Psi_c * \Delta C^2)}$$

$where$:
$\overline{u_c} = Average\ critical\ velocity\ [m/s]$
$\Psi_c = Shields\ value\ for\ mode\ 1 = 0.03$
$\Delta = 1.65$
$C = Chezy\ coefficient = 18\log(12R/k_r)$
$k_r = 6d_{50}$

As the choice of sediment has been made to retain the scale relations as best as is possible, maximum average flow velocities can be estimated through iteration to be 0,2 [m/s] in the un-constricted section.

The relation that follows in the gradual constriction relation (Schiereck & Verhagen, 2012), and can be written as follows:

$$\frac{h_2}{h_1} = \left(\frac{B_1}{B_2}\right)^{\frac{m-1}{m}}$$

$where$:
$h_1 = water\ depth\ in\ front\ of\ constriction\ [m]$
$h_2 = water\ depth\ at\ constriction\ [m]$
$B_1 = width\ in\ front\ of\ constriction\ [m]$
$B_2 = width\ at\ constriction\ [m]$
$m = transport\ parameter\ 4{\sim}5\ [-]$

This then leads to an estimated scouring depth (s_d) of roughly 0,33-0,35 times the original flow depth. The depth of the erodible layer should be adjusted to accommodate this. In the light of this secondary research question it is therefore important to measure the water level heights **($\boldsymbol{h}$)** and Discharge **($\boldsymbol{Q}$)**

A1.3 Addition Secondary Research Question 3

Secondary question 3 requires the scouring depths **($\boldsymbol{d_s}$)** to be measured and compared between the experiments where the bottom surface has been replaced with logs. To get a conclusive understanding the depths must be measured after draining the flume but with the logs still on the bottom.

A1.4 Scour formulae

Although there hasn't been a lot of work done on this specific problem, there is extensive knowledge of scour generation around other objects like armor units, bridge piers & pipelines. The knowledge of these studies can therefore be helpful in obtaining an insight in the relevant measurable parameters, and will be discussed in this section.

A baseline design formula for pier scour can be found in (Schiereck & Verhagen, 2012) and can be seen below. Although it can give some indication to the to be expected scour depth alongside a single log, it is doubtful whether it holds up to a fully submerged object as bridge piers extend along the entire depth of a water column.

$$\frac{d_s}{B_s} = 2 * K_s * K_\alpha * K_u * \tanh\left(\frac{h_0}{B}\right)$$

$where$:
$d_s = scour\ depth$
$B_s = Shape\ corrrection\ factor\ (1.0)$
$K_\alpha = angle\ correction\ factor\ (1.0)$
$K_u = velocity\ factor\ (1.0)$
$h_0 = depth\ prior\ to\ scour$
$B = width\ object$

It is however interesting to note that the scour depth is dependent to a great extent on the diameter ($\boldsymbol{D}$) and length ($\boldsymbol{L_l}$) of the logs. The velocity factor is also important when the average flow speed does not reach the critical flow speed required for the movement of the sediment particles.

Another relevant source for scour around objects is (Mutlu Sumer & Fredsøe, 2005). The source is very explicit about erosion around pipelines, which bears to a certain extent significant similarities to tree logs. Unfortunately most of the information about this subject is to pipelines which are placed perpendicular to the flow while this research study will focus mainly on logs placed parallel to the flow. The source also contains significant knowledge with respect to erosion around slender piles and a group of slender piles, but as these piles extend throughout the entire water column the turbulences generated behind them might have a (slightly) different character. It could therefore be important to measure relative fluctuation intensity around the model trees ($\boldsymbol{r_u}$), ($\boldsymbol{r_v}$) & ($\boldsymbol{r_w}$). These can be derived from measuring the average velocity **($\boldsymbol{\overline{u}}$),** ($\boldsymbol{\overline{v}}$) & ($\boldsymbol{\overline{w}}$) and velocity fluctuations ($\boldsymbol{u`}$), ($\boldsymbol{v`}$) & ($\boldsymbol{w`}$).

A third source worth noting (Ettema, Melville, & Barkdoll, 1998), specifies the Froehlich equation, which is a more comprehensive pier scour formulation that can be written as follows:

$$\left(\frac{d_s}{D}\right)_{max} = 1.3\left(\frac{h}{D}\right)^{0.62}\left(\frac{u}{(gh)^{0.5}}\right)^{0.2}\left(\frac{D}{D_{50}}\right)^{0.08}$$

The formula is corrected for a square nose. As most of the quantities are predetermined, only the flow velocity ($\boldsymbol{u}$) and depth **($\boldsymbol{h}$)** are measurable.

A1.5 Scaling laws

The necessary scale of a model is chosen in such a manner that for the task at hand all important wave conditions and structural parameters are reproduced to an adequate degree and that a sufficient measuring accuracy is guaranteed. The scale of the model is determined by geometric, dynamic and kinematic similarity. Geometric similitude of a scale model is given when all geometric lengths in prototype have a constant relation to the corresponding lengths in the model. Kinematic similarity says that time-dependent processes in the model have a constant time relation to the processes in nature. Dynamic similarity entails that the forces in nature and model have a constant relation. Dynamic similarity is the premise that in geometrically similar models time dependent processes have kinematic similarity. Thus for a geometrically similar model the key to a correct representation is dynamic similarity.

There are in principia seven fundamental physical ratios to which a fluid experiment can be scaled to obtain this similitude with the prototype, namely Froude (Fr), Reynolds (Re), Weber (We), Mach (Ma), Cauchy (Ca), Richardson (Ri), and Euler (Eu). It is generally impossible to keep all ratios equal without changing the properties of for example the fluid that is used in the experiments. It is however possible to neglect some ratios or account for them in the results and apply correction factors. Of the given ratio above, the first three are most important in scale experiments and will be discussed in further detail in this section.

A1.5.1 Froude number scaling

Physical background

Of the scaling relationships Froude is generally considered to be the most applicable ratio. It describes the flow controlling force. The Froude number is expressed as follows:

$$Fr = \frac{u}{\sqrt{g * h}}$$

The Froude number describes three possible flow stages:

$Fr < 1$	$Fr = 1$	$Fr > 1$
Sub-critical flow	critical flow	super critical flow

When flow is critical or super critical information downstream of the flow is unable to propagate upstream. This can be visualized by a wave that cannot travel upstream because flow velocities are too large for the wave to overcome.

Scaling aspects

By keeping the Froude number similar in model as in prototype Froude scaling can for example be used to correctly scale the following hydro dynamical quantities:

- Time scales as $N_t = N_l^{0.5}$
- Current speeds scale as $N_U = N_l^{0.5}$
- Current drag coefficients in rough turbulent flows are identical in model and prototype
- Bed shear stresses in rough turbulent flow scale as $N_\tau = N_U^2 = N_l$

This does however require that the bed material is geometrically scaled to fit the model scale.

The downside of using the Froude number as the basis for scale experiments is most predominant when both the model and prototype make use of the same model fluid. This means that the other forces cannot be reproduced at a similar scale. When Froude scaling is applied flow velocities are always lower in scale models, which causes Reynolds number to be reduced and causes the viscous forces to become more pronounced in the scale model compared to the prototype. When the flow becomes so called “smooth turbulent” or “transitional” the last two bullet points above do not hold.

Beside these hydrodynamic quantities there are also a couple of sediment dynamic quantities that can be correctly scaled by using Froude scaling, with the requirement that the bed material has the same density and is geometrically scaled. If these requirements are fulfilled a correct representation of the following quantities can be obtained:

- Shield parameter in rough turbulent flow are identical in model and prototype
- Threshold shields parameter of rock-protection is almost identical in model and prototype provided that viscous effects can be ignored.

A1.5.2 Reynolds number scaling

Physical background

The Reynolds number is also a very common ratio applied in scaled experiments. It describes the ratio between inertial forces and viscous forces.

$$Re = \frac{u * h}{v}$$

The Reynolds number is used to classify three possible flow stages:

$Re < 2000$	$2000 < Re < 4000$	$Re > 4000$
Laminar flow	Transitional flow	Turbulent flow

When flow is laminar, viscous forces dominate and fluid tends to flow smoothly without disruption. When flow can be characterized as turbulent inertial forces dominate and rotation and the formation of eddies can be observed in the fluid motion.

Scaling aspects

When the viscous forces are dominant at prototype scale, the Reynolds number rather than the Froude number should be used to form the basis of the scaling. The dominance of viscous forces occurs in:

- Laminar wave boundary layers
- Permeability effects on percolation through sediment beds in beach dynamics and offshore foundations
- Settling velocities of fine sediments in suspension
- Wave friction factors in smooth and transitional turbulent flow

In some cases the usage of hot water can reduce the kinematic viscosity of the water at model scale and can therefor better represent the prototype this does however this has a limited applicability. Alternatively air can be used at very small scales.

If Froude scaling can be applied it is best to assure that the Reynolds number is at least in the same regime as in the prototype and perfect similitude is not required. With the lowest given flow parameters from **Error! Reference source not found.**, the Reynolds number is roughly 22,500 which classifies well in the turbulent flow regime, thus significant scaling errors are not expected.

A1.5.3 Weber number scaling

Physical background

The Weber number is the third common ratio applied in scaled experiments. It describes the ratio between inertial forces and surface tension force.

$$We = \frac{\rho_w * u^2}{\sigma}$$

If a model is created in which waves are modeled at a very small scale, capillary waves could be of a similar wavelength to gravity waves. In this case the capillary waves can disturb the wave dynamics. The influence of the surface tension force is assumed to be negligible when the weber number is larger than 120. With the given flow conditions from (Rijkswaterstaat, 2016), this requirement is met.

Scaling aspects

As discussed above, Weber number similitude only becomes important when waves are modeled at very small scales and capillary forces can disturb wave Dynamics. As this is not the case in this research study, and the requirements are well met, scaling errors are not expected.

A1.5.4 Other scale relationships

Beside the three most important scale relations the following are shortly discussed:

- Cauchy ratio (Ca) – ratio between inertial force and elastic force
- Richardson ratio (Ri) – ratio between kinetic energy and potential energy
- Mach ratio (Ma) – ratio between local flow speed and the speed of sound in the medium.
- Euler ratio (Eu) – ratio between pressure force and inertial force

Appendix A II

A2.1 Bed material properties

Six sieving tests were conducted to determine the grain distribution of the bed material. From the sieving tests, Table 1 was constructed. From these sieving tests the d50 was determined to be 127 [µm], slightly lower than factory specifications (Sibelco, 2017). Additionally three tests were conducted to determine porosity and density of the bed material.

Table 1; Sieving

Specimen number	Total weight prior [g]	0,25 [mm]	0,212 [mm]	0,18 [mm]	0,15 [mm]	0,125 [mm]	0,112 [mm]	0,106 [mm]	0,09 [mm]	Remainder [mm]	Total weight after [g]
1	175,8	1,5	2,1	12,8	26,6	91,8	20,6	3,3	5,2	3,8	167,7
2	170,6	1,9	1,6	7,9	26,2	84,0	22,8	0,3	10,0	8,1	162,8
3	175	1,5	1,4	11,6	23,8	79,4	26,6	4,4	13,8	5,8	168,3
4	178,8	1,1	0,8	7,4	26,8	79,4	32,4	2,8	15,9	5,1	171,7
5	200	1,2	1,4	1,9	24,8	94,6	32,6	6,6	14,2	8,3	185,6
6	107	0,6	0,5	3,0	11,2	51,2	20,4	1,2	7,49	5,2	100,7
	1007,2	7,7	7,8	44,6	139,4	480,4	155,4	18,6	66,6	36,3	956,8
% of total		0,8	0,8	4,7	14,6	50,2	16,2	1,94	6,96	3,79	

Table 2; Porosity and density

Specimen number	Weight sand [gr]	Volume sand [ml]	Weight water [gr]	Volume water [ml]	Combined weight [gr]	Combined volume [ml]	Density [kg/m^3]	Porosity [-]
1	142,8	100	293,8	293,8	436,6	350	2540,9	0,438
2	198,6	150	290,0	290,0	488,6	370	2482,5	0,467
3	198,2	150	296,0	296,0	494,2	376	2477,5	0,467
Average							2500,3	0,457

Appendix A III

Determination of flow conditions

Determination of the required flow conditions were derived from applying the shields methodology. The following discusses the parameters and formulae used in combination with the approach strategy. To determine the flow conditions the shields curve with respect to the dimensionless particle diameter d_* is used (Figure 1). From the obtained values of the shields parameter, an estimation of depth averaged flow velocity can be made.

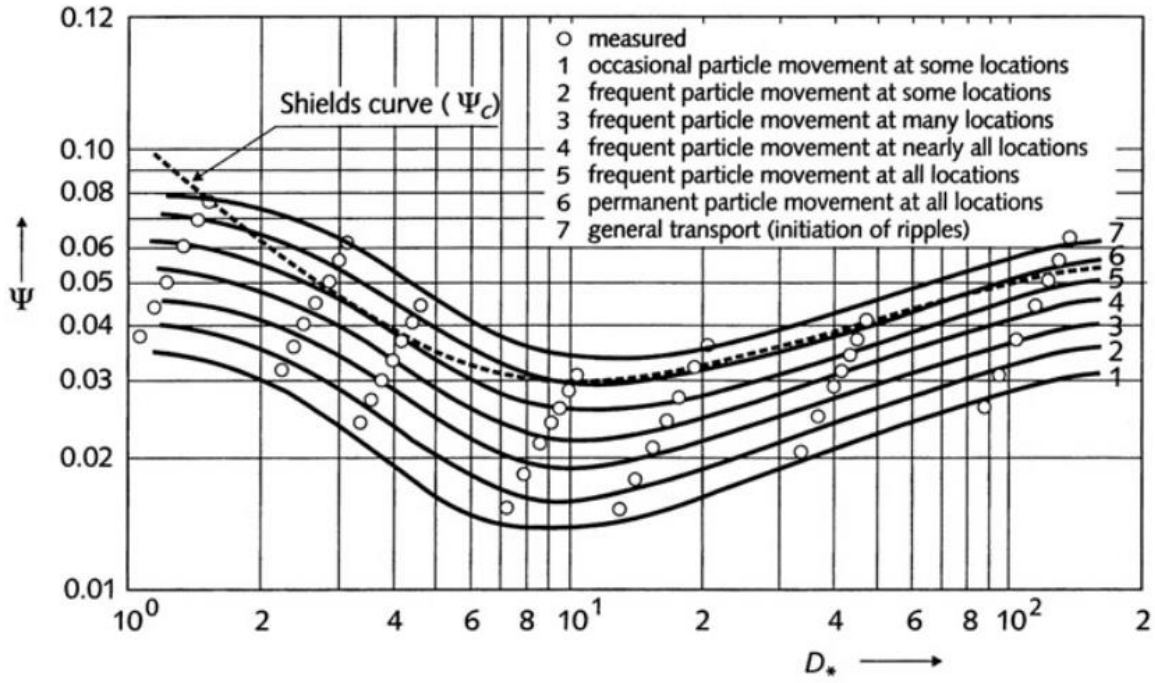

Figure 1; Shields diagram

The first step incorporates the determination of dimensionless particle diameter d_* must be made. From the sieving's of the sand the d_{50} was determined to be about 127 [mm]. With Equation 1, the dimensionless particle diameter is determined to be 2,6 [-].

Equation 1; dimensionless particle diameter

$$d_* = d\left(\frac{\Delta g}{v^2}\right)$$

With the dimensionless particle number know, the shields parameter for all transport stages can be estimated (Figure 2 & Table 3). Following iterative calculations with Equation 2. It can be determined that for a depth of 0.4 [m], flow velocities should not exceed values in Table 3

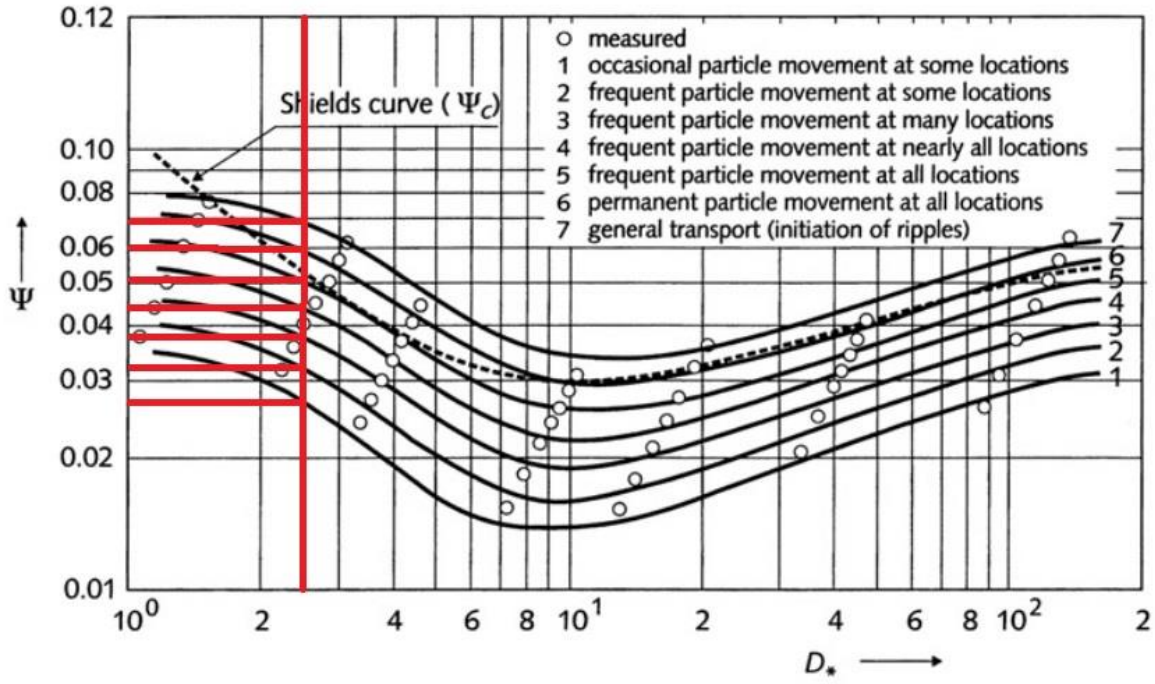

Figure 2; Shields diagram

Table 3;

Stage of shields transport	1	2	3	4	5	6	7
Shields parameter [-]	0.028	0.032	0.038	0.044	0.05	0.06	0.07
Estimation of depth average velocity [m/s]	0.177	0.190	0.205	0.220	0.235	0.26	0.28

Equation 2;

$$d_{50} = \overline{u_c}^2/(\psi_c \Delta C^2)$$

Appendix B I

I Introduction

Basic scour I is the first experiment conducted. Bed, velocity and fluctuation intensity development is measured during a 96 [h] run as the reference to follow up experiments. In this experiment only the influence of the contraction on the set – up is monitored. This report includes all measured findings during this particular experiment. Conclusions are drawn in the main report on the basis of multiple similarly conducted experiments. A short preliminary conclusion is however included at the end of this report.

Summary

Table 4 represents relevant scour quantities after 96 [h]. Note that the absolute is measured relative to the measurement of the bed at 0 [h], excluding the maximum scour depth which is measured to a reference bed with a 0 [mm] elevation. Measurements of scour volume in the column with respect to reference include missing volume with respect to a reference be of 0 [mm].

Table 4; Summary of quantities

	Quantity	With respect to reference
Maximum Scour Depth [mm]	151	151
Total Scoured volume [cm^3]	-46448	-48517
Scoured volume Upstream-sector [cm^3]	+60	-426
Scoured volume Contracting-sector [cm^3]	-17011	-18322
Scoured volume Constricted-sector [cm^3]	-25424	-25838
Scoured volume Expanding-sector [cm^3]	-5303	-5193
Scoured volume Downstream-sector [cm^3]	+1231	+1263

Measurements at 0h

Bed level

A projection of the bed at the moment of initiation of flow during the first scour experiment can be seen in Figure 3. It can be observed that the bed was relatively flat, except for two minor bumps visible about 2000 [mm] into the set-up. These bumps where remains of a test run conducted prior to the first official scour experiment. The bumps were roughly 1.5 [cm] high and located in the expanding section of the set-up.

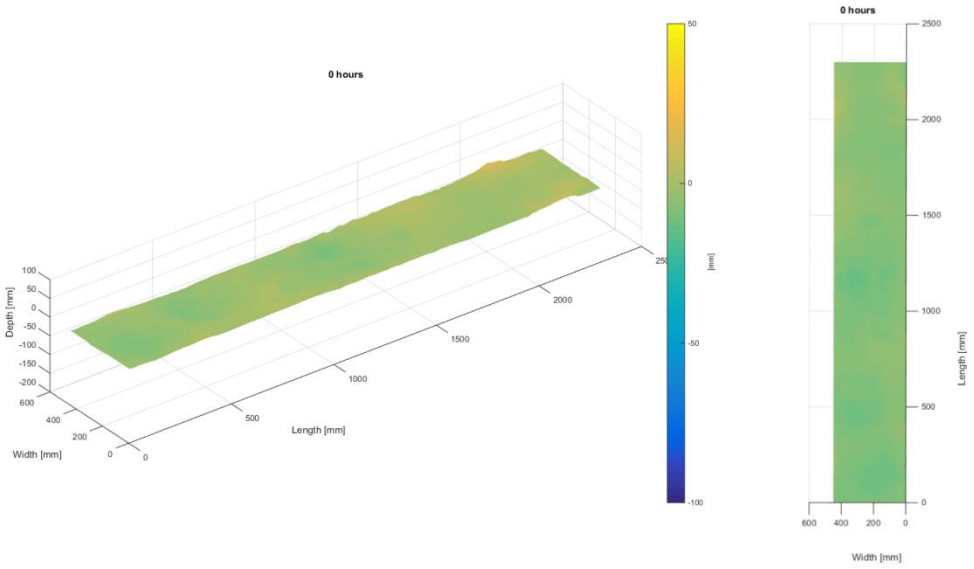

Figure 3; Bed map 0[h]

The average transect, observable in Figure 4, was calculated from the 16 transects taken over the entire length of the laboratory set-up. As can be seen, the bed shows minor indentures along the set-up ranging between 0.5 – 1.0 [cm]. Due to the difficulty of obtaining a near smooth bed it was accepted that the bed showed these minor deformations prior to initiating the flow.

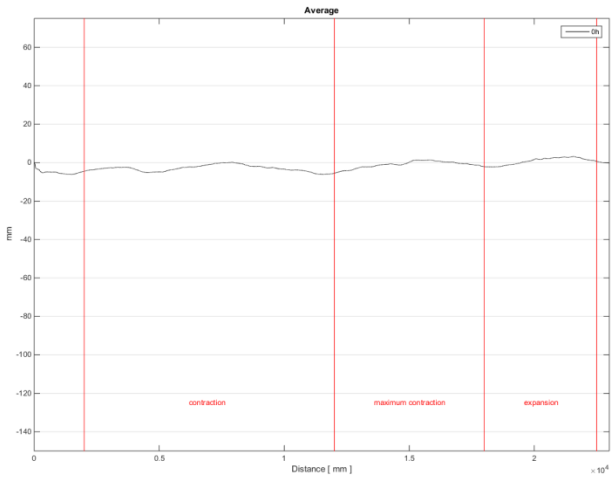

Figure 4; 0 [h] average transect

Velocity Profiles & Fluctuation intensity

Even though measurements were taken just after start of the experiment, these were not included in this report. The measurements showed severe inconsistencies that are attributed to misuse of the equipment and a lack of experience by the user. User experience and the usage of some Chinese clay improved measurements conducted at different moments during the experiment. Therefor these later measurements are included in this report, as they showed a more consistent data.

Measurements after 24h

Bed level

A projection of the bed after running for 24 [h] can be observed in Figure 5. The bed showed the development of bed forms starting close to the end of the contracting zone. Furthermore it could clearly be observed that erosion and transport of sediment towards the downstream part of the model had occurred, originating primarily from the maximum contracted area. The absence of erosion in the upstream part of the model followed calculations with respects to the shields parameter.

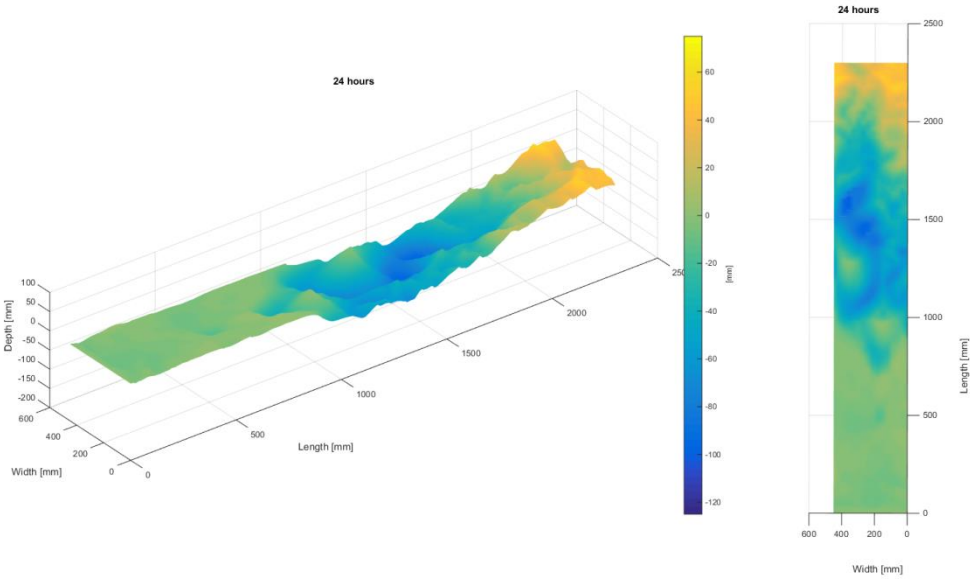

Figure 5; 24[h] bed projection

This can be confirmed with the average transect, observable in Figure 6. It shows the largest on average scour at the center of the maximum contracted section.

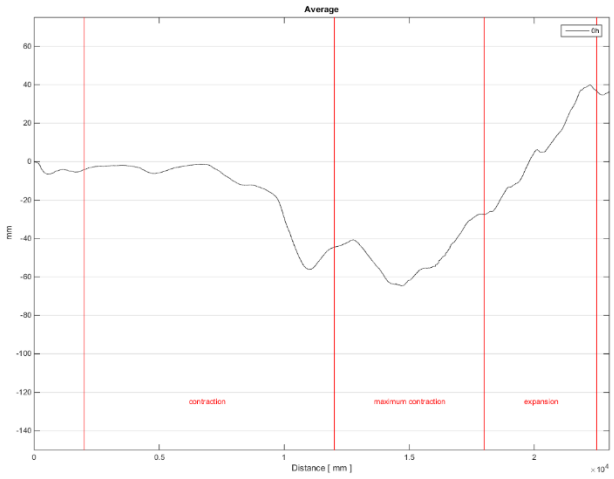

Figure 6; 24[h] average transect

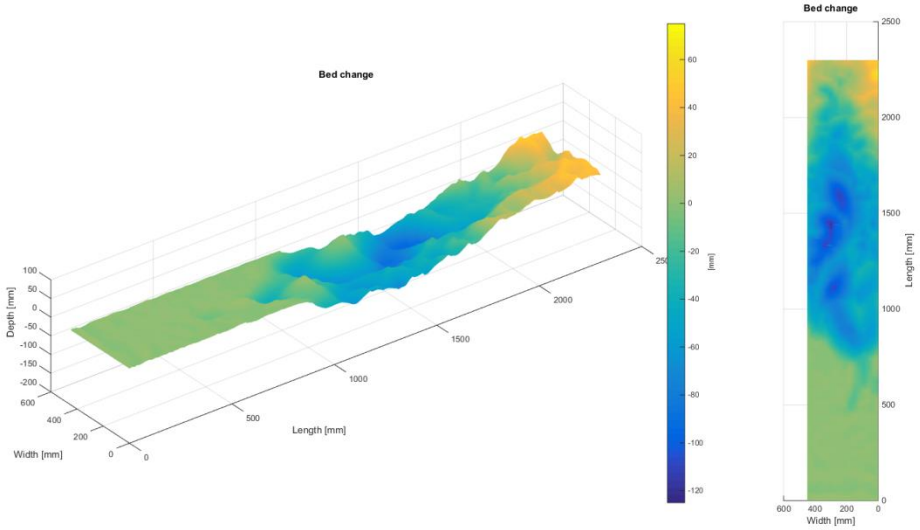

Figure 7; 0[h]-24[h] bed change projection

If the bed change in Figure 7 is observed, it can be clearly seen that the first 1000 [mm] is barely affected, but some scour has started to penetrate the contracting-section (first 200-1200 [mm]). Some of the deepest spots already reach up to 100 [mm] of scour. From the sediment transport table (Table 5), it can be observed that the bulk of the scour occurs in the area of maximum contraction. But the contracting section also experiences a significant amount of scour. The import from upstream is attributed to a small amount of sediment that was just upstream of the scanning threshold.

Table 5; Volume change per sector in [cm^3]

	Upstream	Contraction	Constriction	Expansion	Downstream
Volume	+51,6	-4614,8	-14016,0	-435,0	+1774,6

Velocity Profiles

In this section, individual flow profiles of locations marked above are shown. It can be observed that the flow cannot be considered to be uniform upon arrival in model (location 1) (Schiereck & Verhagen, 2012). This was as expected; as the length of the false bottom was not long enough facilitate the full development of the boundary layer. It can therefore be seen that flow is not logarithmically distributed, but instead has a turbulent flow structure. The data of location 5 was incomplete and therefor an accurate curve could not be fitted.

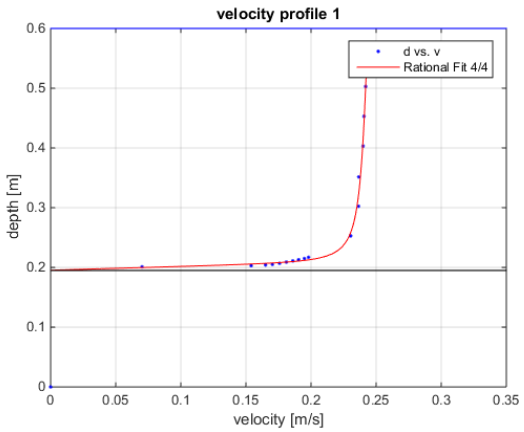

Figure 8; Velocity profile location 1 24h]

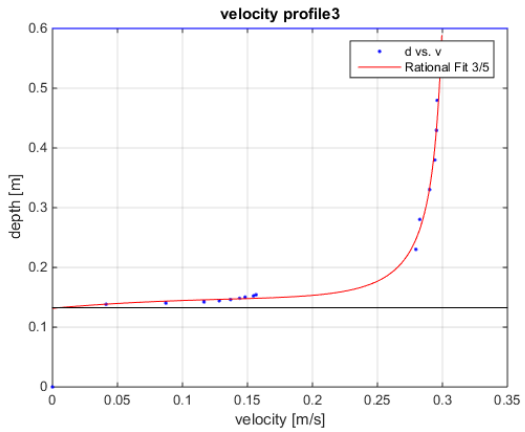

Figure 9; Velocity profile location 3 24h]

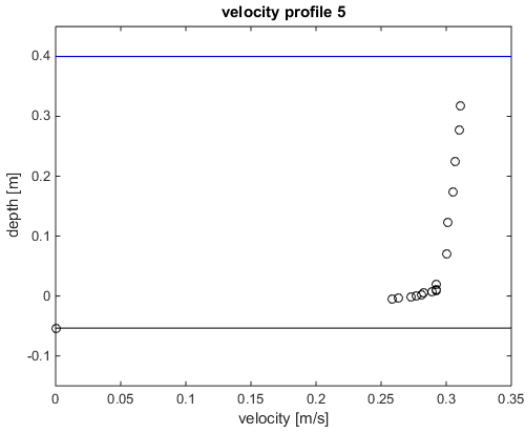

Figure 10; Velocity profile location 5 24h]

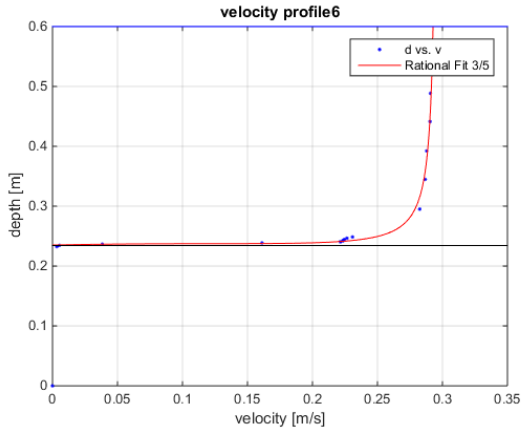

Figure 11; Velocity profile location 6 24h]

Relative fluctuation intensity

Fluctuation intensity measurements were not taken well enough to include in this section.

Measurements after 48h

Bed level

As can be seen, the bed shows the largest amount of scour around 1.5 [m] into the experiment, which is at a point of maximum contraction. Furthermore the bed in front of the contracting section of the experiment is still fairly stable as can be seen from Figure 12 & Figure 13.

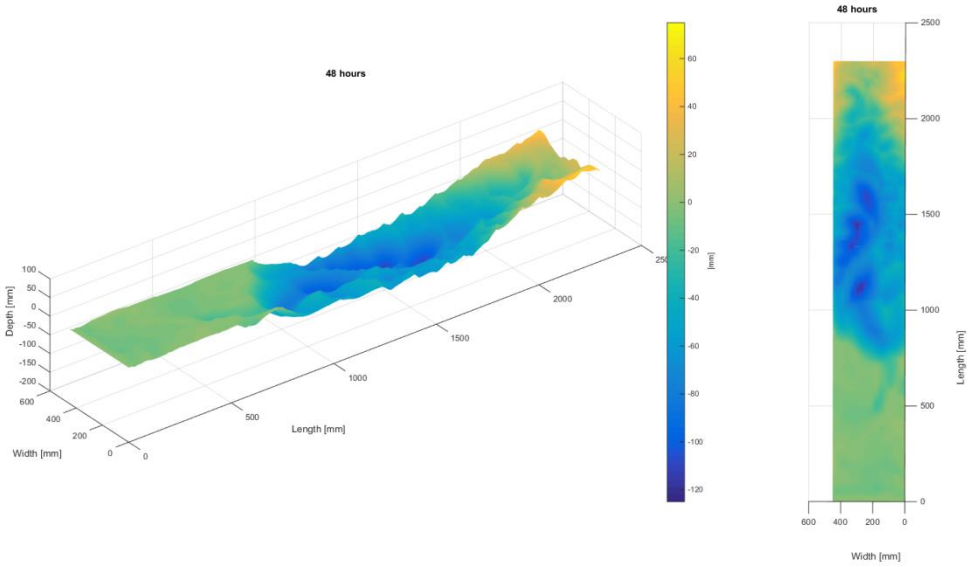

Figure 12; 48[h] bed projection

The average transect observable in Figure 13, shows scouring has stabilized at around 80 [mm]. The bed in front of the contraction and up till half way of the contracting section still is fairly unaffected.

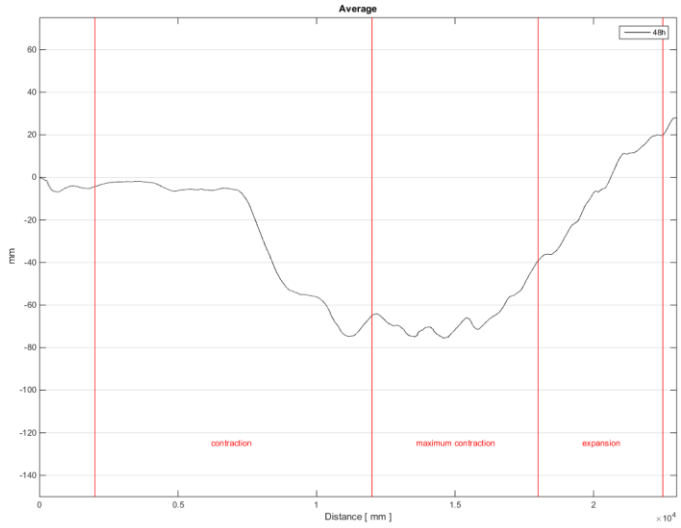

Figure 13; 48[h] average transect

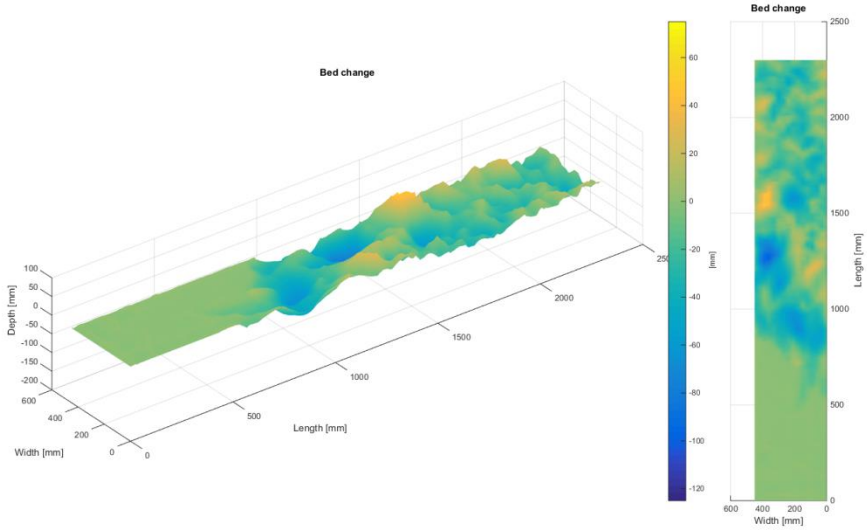

Figure 14; 24[h]-48[h] bed change projection

Furthermore Figure 14 shows that erosion is clearly moving upstream, observable by the accretion areas downstream of the eroding segments. These eroding areas are there for located within the contraction section. From Table 6, it can indeed be observed that this area is now eroding at this area has in total volume now eroded most.

Table 6; Volume change per sector in [cm^3]

	Upstream	Contraction	Constriction	Expansion	Downstream
Volume	+4,3	-5202,5	-5173,8	-2681,5	-716,5

Velocity Profiles

It can be concluded from the velocity profile, that flow velocities decreased on average. Location 1 shows a slight decrease of velocity while locations 3 & 5 show a strong decrease of velocity, this is in accordance with these locations having been afflicted by a larger amount of scour, thus increasing the wet surface area.

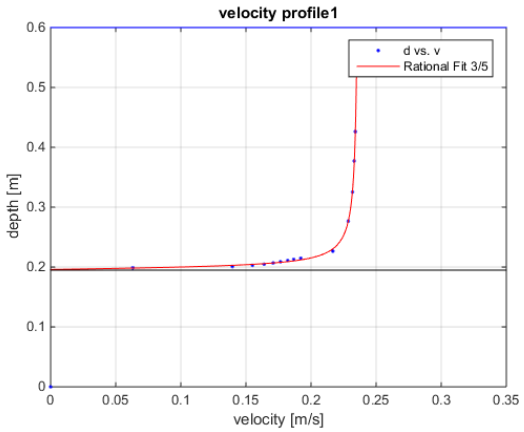

Figure 15; Velocity profile location 1 48 [h]

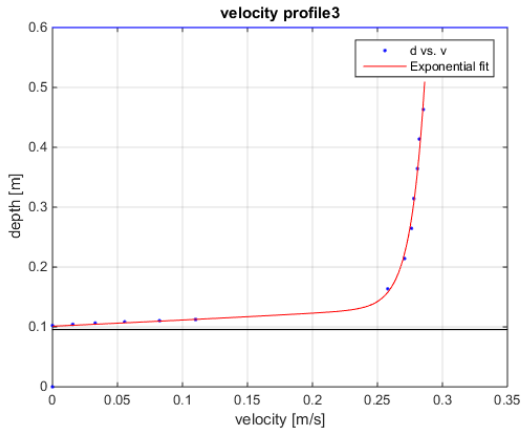

Figure 16; Velocity profile location 3 48 [h]

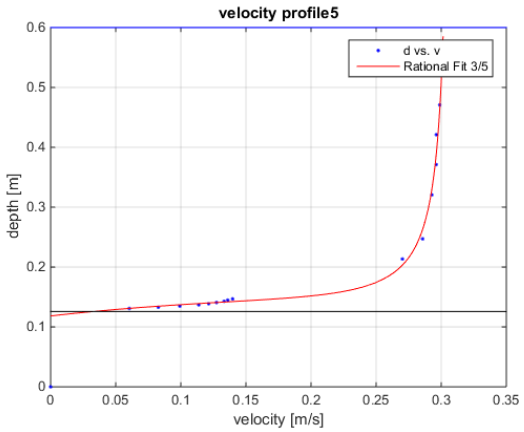

Figure 17; Velocity profile location 5 48 {h]

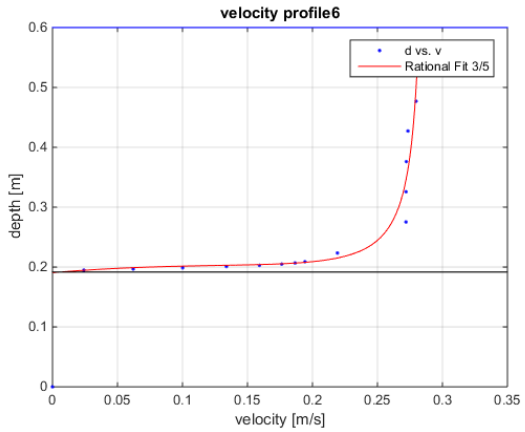

Figure 18; Velocity profile location 6 48 [h]

Relative fluctuation intensity

Calculated fluctuation intensity shows that during the contraction of the flow this fluctuation drops significantly (Location 2) with respect the fluctuation intensity upstream (Location 1) and flow therefor tends to become smoother, this is as was expected from theory. Furthermore the fluctuation intensity tends to increase exponentially at the point of maximum contraction location 3. At the end of the maximum contracted zone, this again reduces and flow tends to smooth out. This is attributed to the fact that flow again contracts due to the sloping bed.

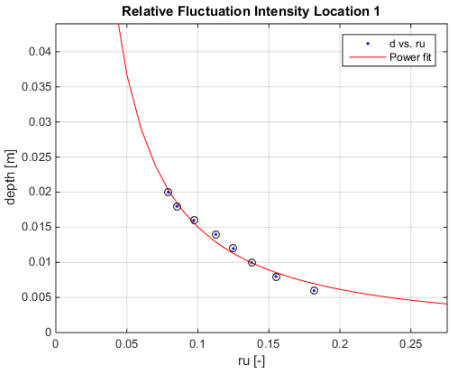

Figure 19; Fluctuation intensity location 1 48[h]

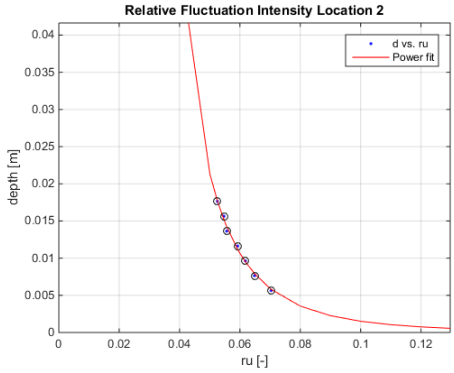

Figure 20; Fluctuation intensity location 2 48[h]

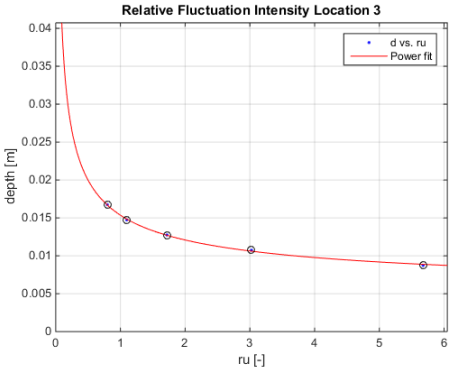

Figure 21; Fluctuation intensity location 3 48[h]

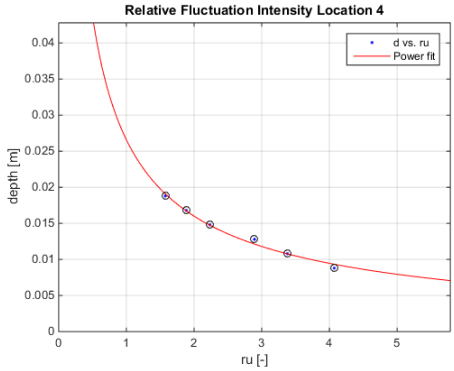

Figure 22; Fluctuation intensity location 4 48[h]

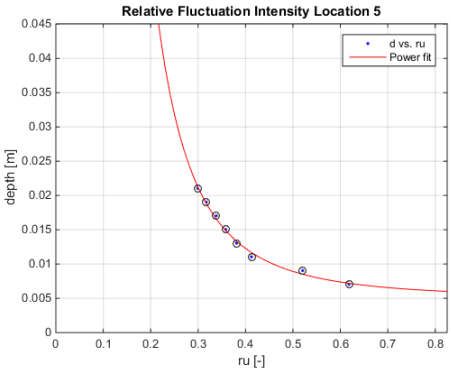

Figure 23; Fluctuation intensity location 5 48[h]

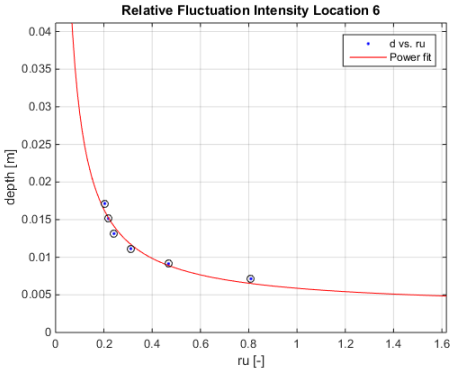

Figure 24; Fluctuation intensity location 6 48[h]

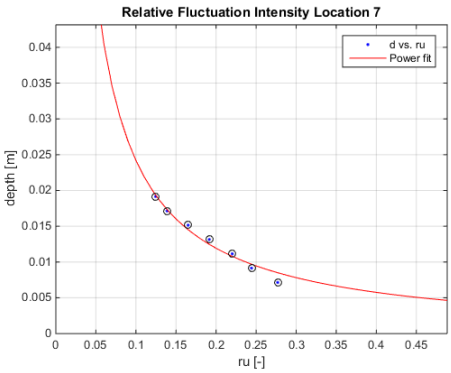

Figure 25; Fluctuation intensity location 7 48[h]

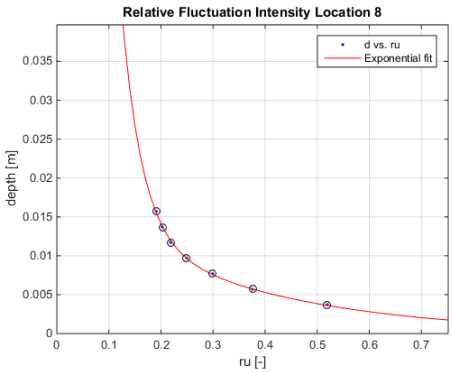

Figure 26; Fluctuation intensity location 8 48[h]

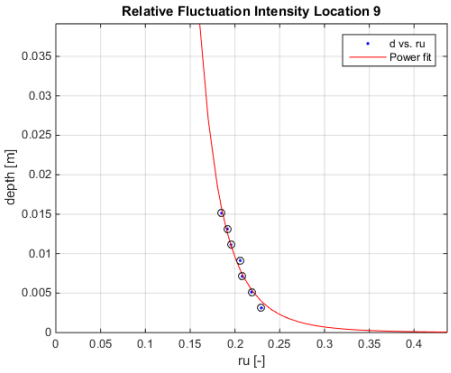

Figure 27; Fluctuation intensity location 9 48[h]

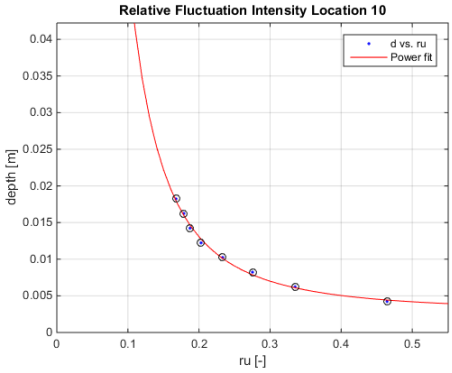

Figure 28; Fluctuation intensity location 10 48[h]

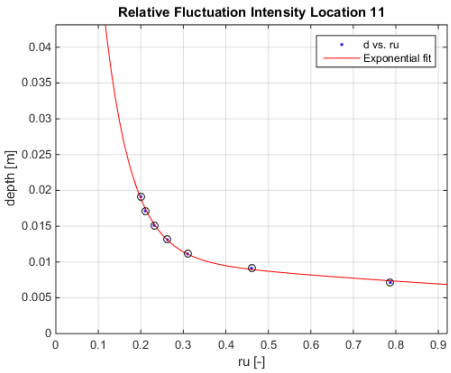

Figure 29; Fluctuation intensity location 11 48[h]

For locations near the wall (Locations 7-11) this effect was also observed but in a far smaller magnitude. Downstream of the contraction (Location 11) we see the flow again become more turbulent, especially near the bottom. This is attributed to the flow deceleration due to the expansion and large bedforms that have developed near that location.

Measurements after 72h

Bed level

As can be seen, the bed shows the largest amount of scour around 1.4 [m] into the experiment, which is at a point of maximum contraction. Furthermore the bed in front of the contracting section of the experiment is still fairly stable as can be seen from Figure 30 & Figure 31.

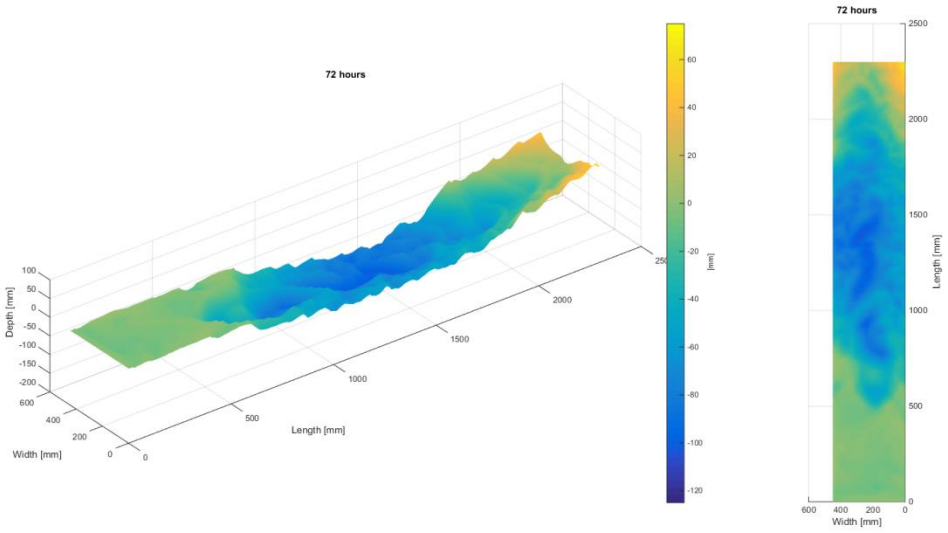

Figure 30; 72[h] bed projection

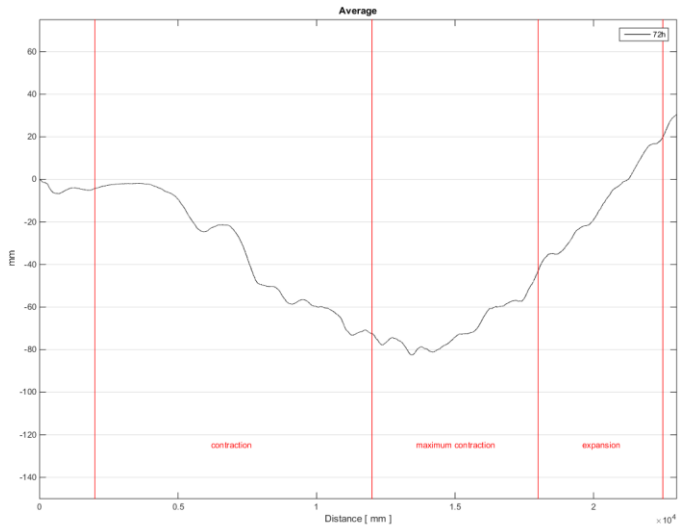

Figure 31; 72[h] average transect

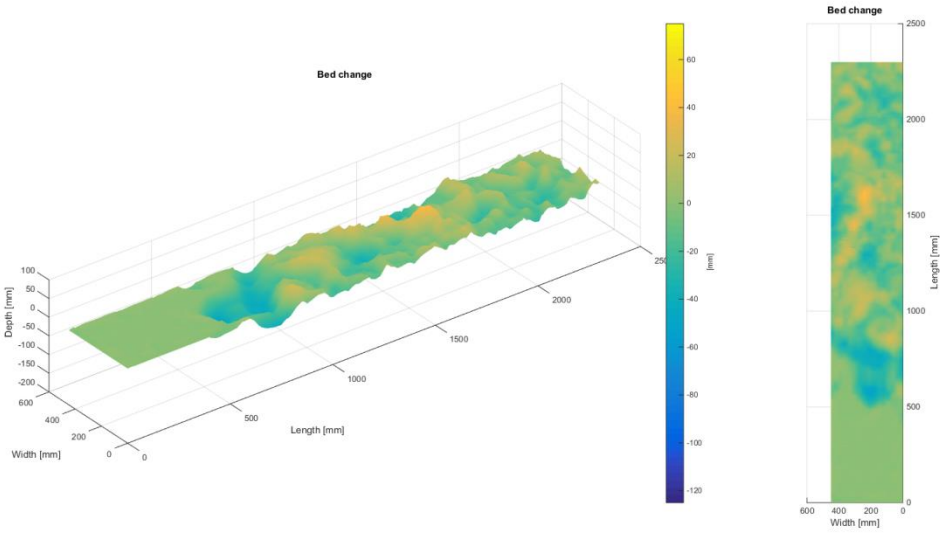

Figure 32; 48[h]-72[h] bed change projection

It can be observed from Figure 32 that the area of the bed halfway of the contracting area (500-700 [mm]) has experienced the largest amount of scour. This seems to be deposited at the entry point of the area of maximum contraction (1000-1200 [mm]). This is also supported by the fact that the sediment transport Table 7 shows little scour has occurred in this section.

Table 7; Volume change per sector in [cm^3]

	Upstream	Contraction	Constriction	Expansion	Downstream
Volume	+5,3	-3095,8	-1017,3	-1226,0	-18,7

Velocity Profiles

It can be concluded from the velocity profiles, that flow velocities at locations 1 & 3 remained nearly the same, but the profile at location 3 assumed a more turbulent pattern. Flow profiles at locations 5 & 6 showed a far more disturbed flow regime, and on average lower flow velocities as observed earlier.

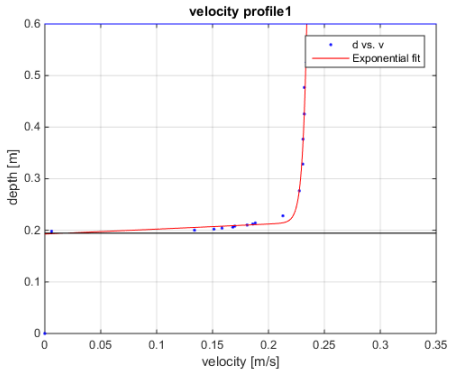

Figure 33; Velocity profile location 1 72h]

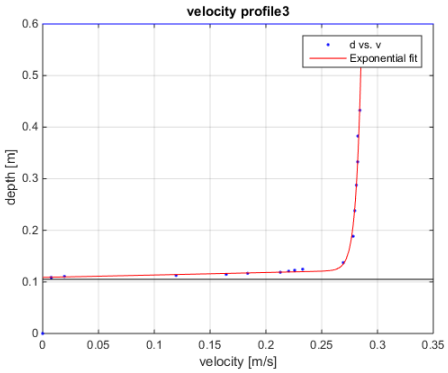

Figure 34; Velocity profile location 3 72h]

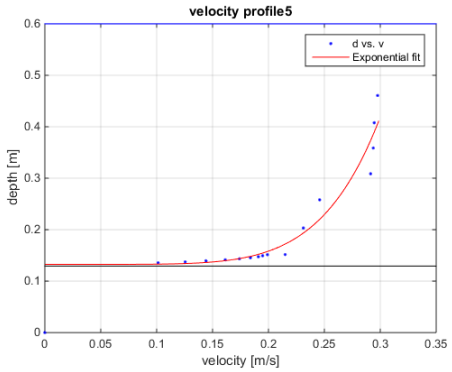

Figure 35; Velocity profile location 5 72h]

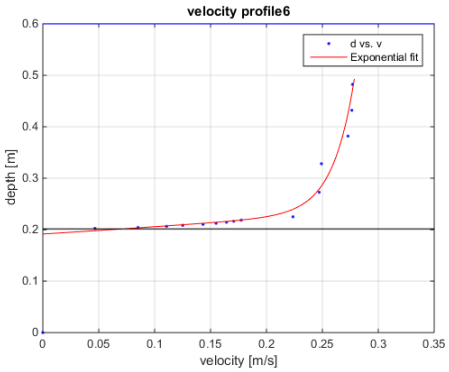

Figure 36; Velocity profile location 6 72h]

Relative fluctuation intensity

Looking at the fluctuation intensity, we can observe that halfway the contracting section (Location 2), it seems to reduce which is in agreement with the fact that erosion here is still relatively modest thus the acceleration of flow has still caused the turbulence to be reduced in comparison with Location 1. When we observe other locations in the model, we can see that the relative fluctuation intensity is fairly stable for all these areas at three times the magnitude with respect to Location 1 & 2.

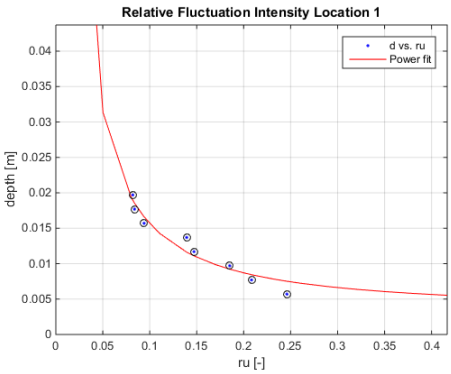

Figure 37; Fluctuation intensity location 1 72[h]

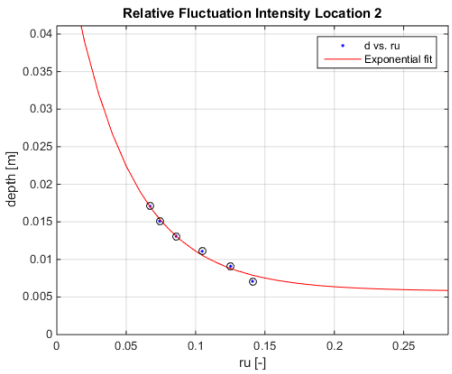

Figure 38; Fluctuation intensity location 2 72[h]

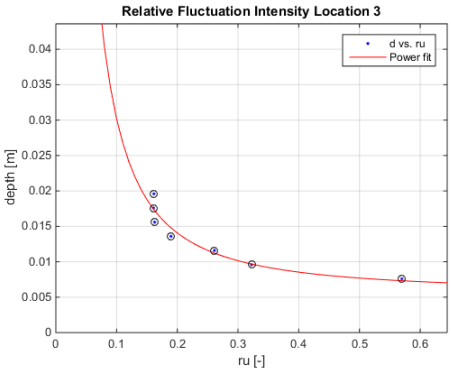

Figure 39; Fluctuation intensity location 3 72[h]

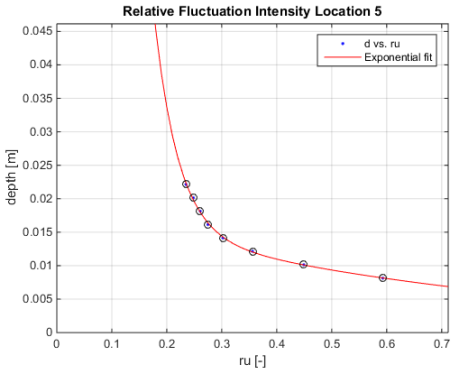

Figure 40; Fluctuation intensity location 5 72[h]

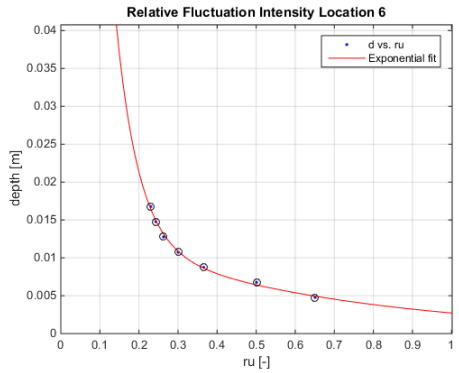

\

Figure 41; Fluctuation intensity location 6 72[h]

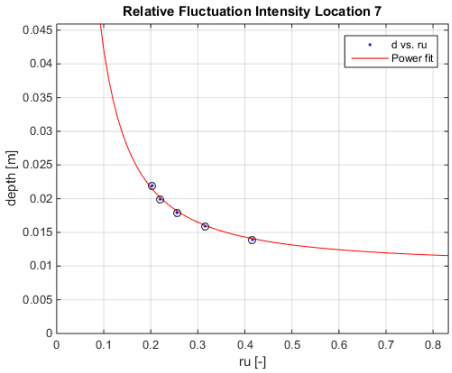

Figure 42; Fluctuation intensity location 7 72[h]

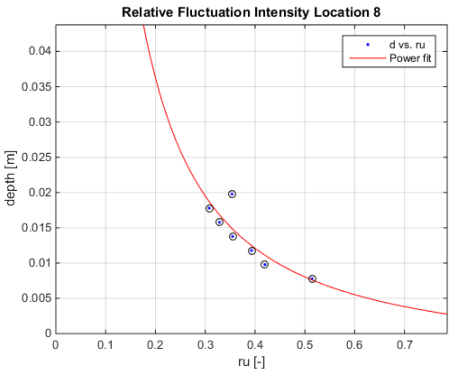

Figure 43; Fluctuation intensity location 8 72[h]

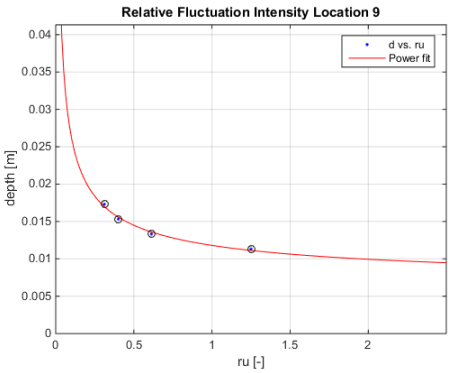

Figure 44; Fluctuation intensity location 9 72[h]

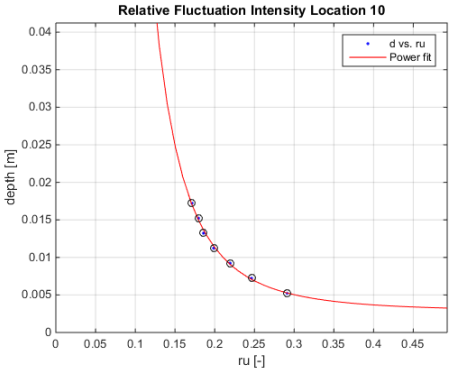

Figure 45; Fluctuation intensity location 10 72[h]

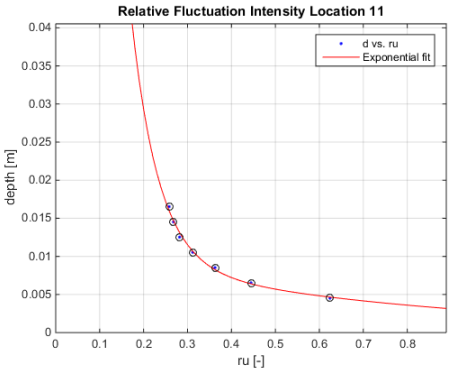

Figure 46; Fluctuation intensity location 11 72[h]

We can observe that Locations 1,2,7 & 9 have seen an increase of fluctuation intensity. The other locations remained either similar or showed a significant decrease (Location 3). Location 4 could not be compared as this location was missing valid data.

Measurements after 96h

Bed level

The bed after 96 [h] shows an even further intensification of scour, scour rates do seem to reduce after this time. Maximum scour can be observed to be around 1250 [mm] into the setup, which is at the entry point of maximum contraction (see Figure 47 & Figure 48).

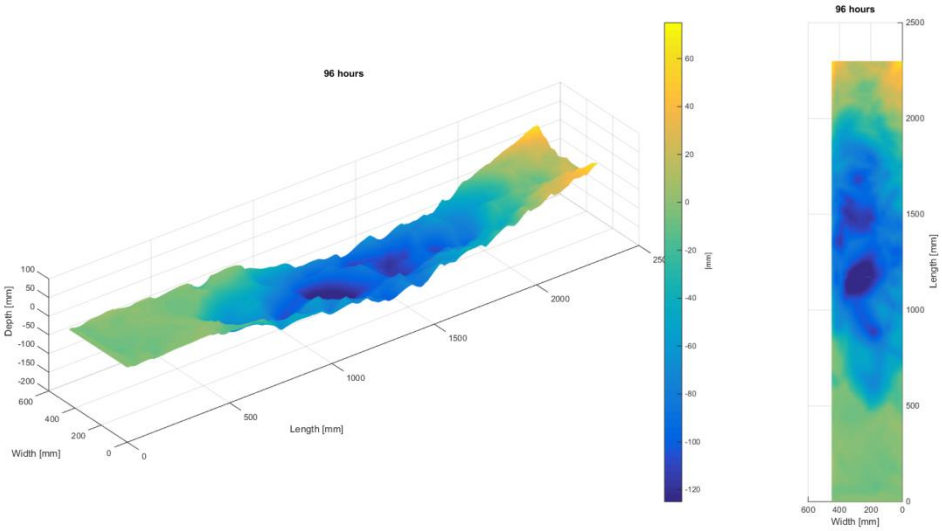

Figure 47; Bed map after 96 [h]

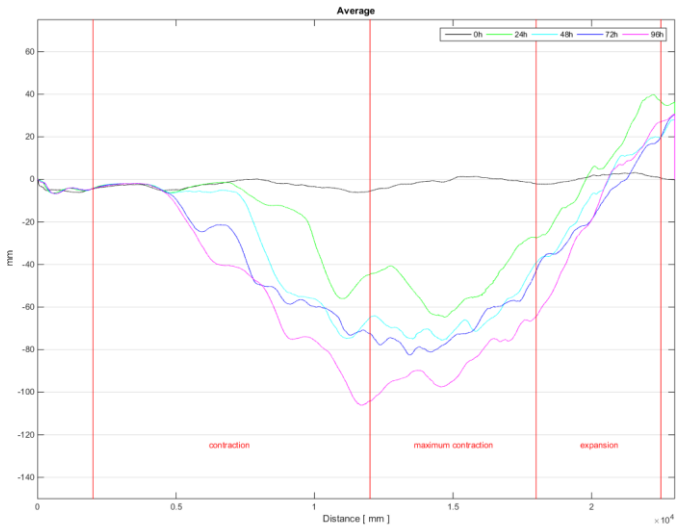

Figure 48; Average transects through time

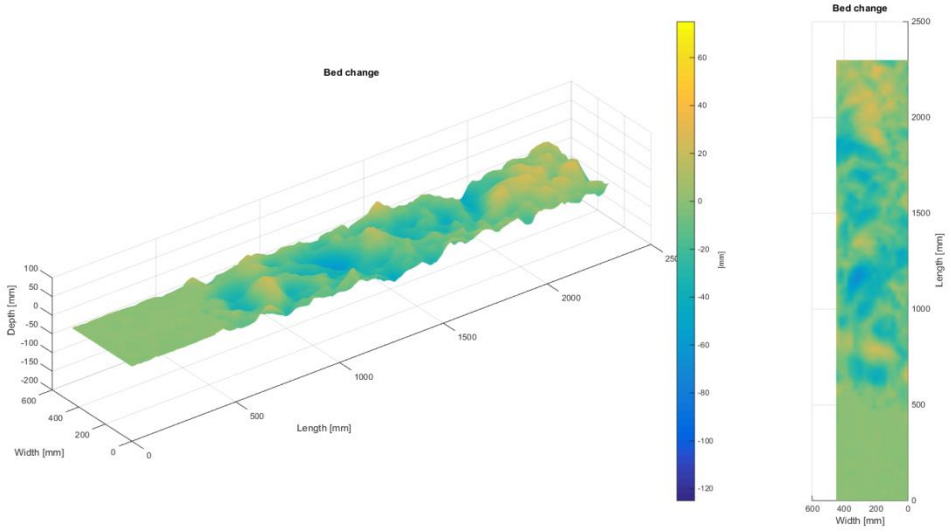

Figure 49; Bed change with respect to 72[h]

Figure 49 shows further accretion in the expansion and downstream sectors of the set-up, the contracting and the constricted section show similar scour patterns. This is again supported by the sediment transport Table 8. The total scour rate has doubled in this interval compared with the previous 24 hours.

Table 8; Volume change per sector in [cm^3]

	Upstream	Contraction	Constriction	Expansion	Downstream
Volume	-1,6	-4097,9	5217,5	960,0	221,0

Concluding Remarks

This first basic scour experiment showed areas of improvement for the usage of the vectrino Doppler, the bed maps however showed a clear development of scour starting at the end of the maximum contracted section of the set-up, and a slow progression upstream. After 96 hours the maximum scour was around 15 [cm] while the cross section average maximum scour was around 11 [cm].

Appendix B II

I Introduction

Basic scour II is the second experiment conducted. Bed, velocity and fluctuation intensity development is measured during a 96 [h] run as the reference to past and follow up experiments. In this experiment only the influence of the contraction on the set – up is monitored. This report includes all measured findings during this particular experiment. Conclusions are drawn in the main report on the basis of multiple similarly conducted experiments. A short preliminary conclusion is however included at the end of this report.

Summary

Table 9 represents relevant scour quantities after 96 [h]. Note that the absolute is measured relative to the measurement of the bed at 0 [h], excluding the maximum scour depth which is measured to a reference bed with a 0 [mm] elevation. Measurements of scour volume in the column with respect to reference include missing volume with respect to a reference be of 0 [mm].

Table 9; Summary of quantities

	Absolute	With respect to reference
Maximum Scour Depth [mm]	94,4	94,4
Total Scoured volume [cm^3]	-18617	-35308
Scoured volume Upstream-sector [cm^3]	+15	-351
Scoured volume Contracting-sector [cm^3]	-11844	-16786
Scoured volume Constricted-sector [cm^3]	-12259	-18681
Scoured volume Expanding-sector [cm^3]	+2399	-1903
Scoured volume Downstream-sector [cm^3]	+3071	+2412

Measurements at 0h

Bed level

A projection of the bed at the moment of initiation of flow during the first scour experiment can be seen in Figure 50. It can be observed that the bed was relatively flat, but sloped downwards towards the area of maximum contraction. This section was on average 20 [mm] lower.

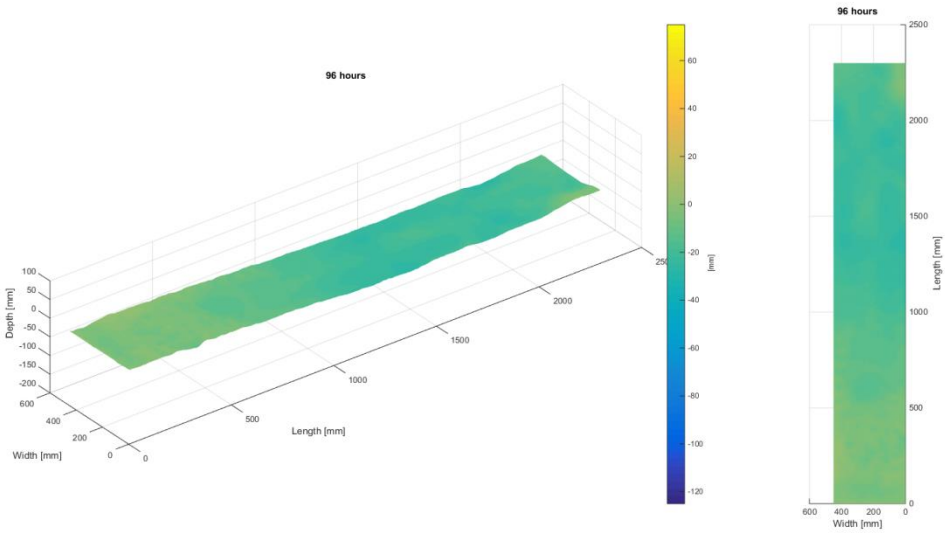

Figure 50; Bed map 0[h]

The average transect, observable in Figure 51, shows this slope rather well. Due to the difficulty of obtaining a near smooth bed it was accepted that the bed showed this deformation.

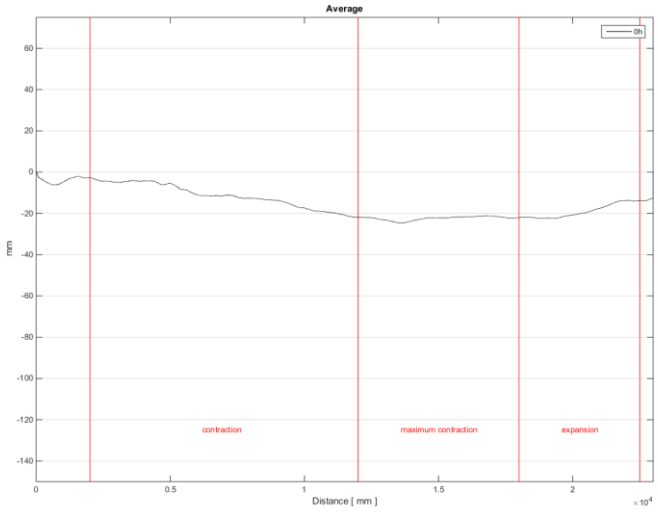

Figure 51; 0 [h] average transect

Velocity Profiles

In this section, individual flow profiles of locations marked above are shown. It can be observed that flow is not logarithmic upon arrival in the model. Location 1 and 3 show a profile which is similar to flow profiles in turbulent conditions. Location 5 shows a slight upwards shift with comparison to profile 3, while profile 6 again shows a shift towards a more turbulent profile, but at higher velocities in comparison with location 1, while the wet perimeter is equal. This is attributed to the fact that flow is, due to the expansion of the wet perimeter, probably more unequally distributed between the center of the flume and the areas close to the walls.

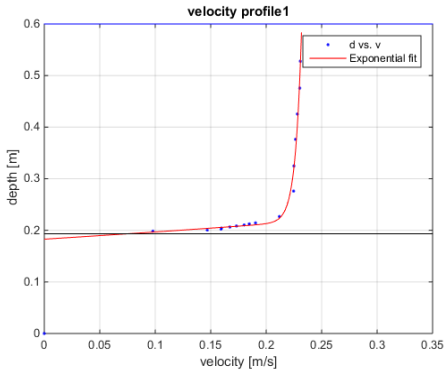

Figure 52; Velocity profile location 1 0[h]

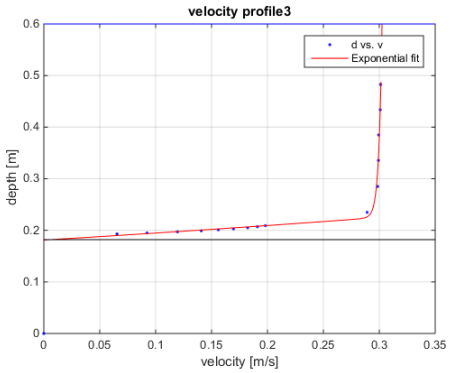

Figure 53; Velocity profile location 3 0[h]

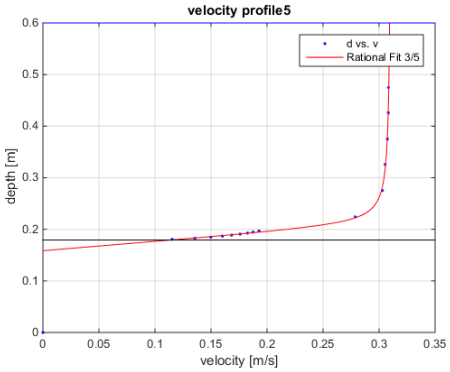

Figure 54; Velocity profile location 5 0[h]

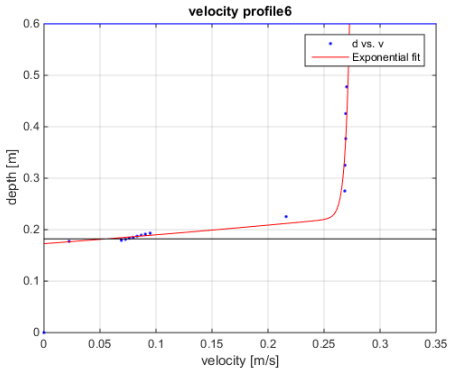

Figure 55; Velocity profile location 6 0[h]

Table 10; Average Velocity

Location	Average Velocity [m/s]
1	0,2211
3	0,2861
5	0,2912
6	0,2449

Relative fluctuation intensity

Relative fluctuation Intensity seemingly increases from location 1-3, this is in contrast with acceleration theory and the previously conducted experiment. As all conditions are the same, only the difference in initial bed is suspected to be the cause for this. The magnitude of relative fluctuation intensity is of a similar magnitude at all locations in the zone of maximum contraction (3-4-5-8-9-10). Locations downstream of the area of maximum contraction show much higher relative fluctuation intensity, which is in accordance with expectations of deceleration.

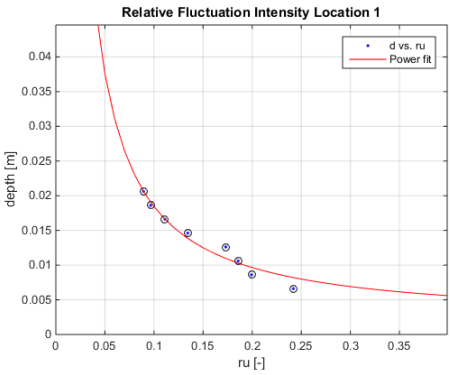

Figure 56; Fluctuation intensity location 1 0[h]

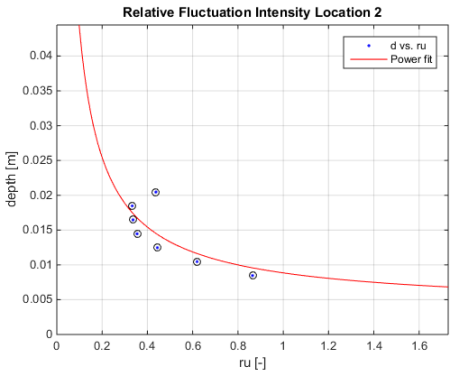

Figure 57; Fluctuation intensity location 2 0[h]

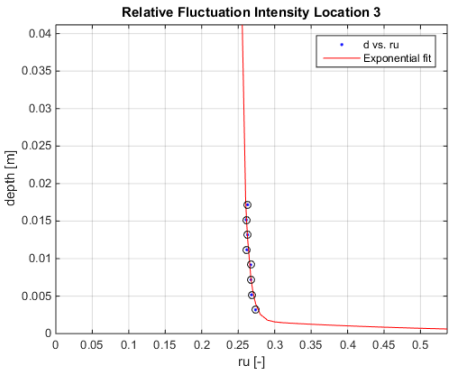

Figure 58; Fluctuation intensity location 3 0[h]

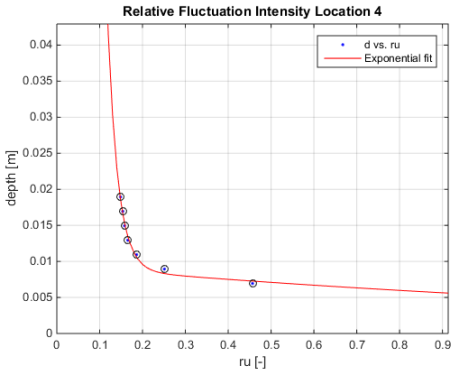

Figure 59; Fluctuation intensity location 4 0[h]

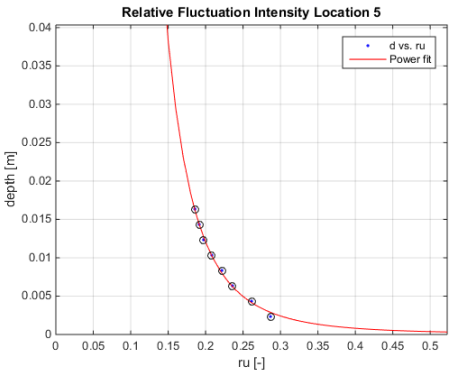

Figure 60; Fluctuation intensity location5 0[h]

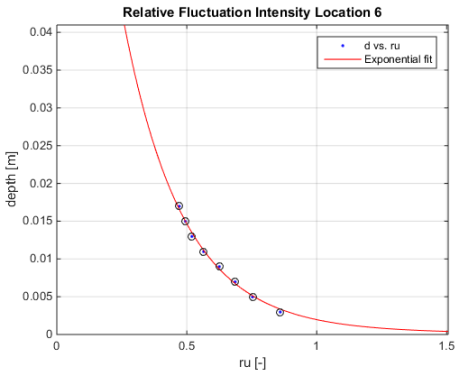

Figure 61; Fluctuation intensity location 6 0[h]

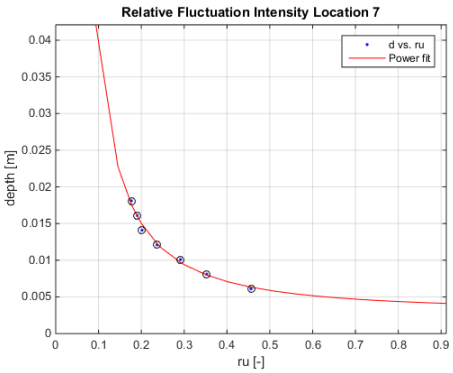

Figure 62; Fluctuation intensity location 7 0[h]

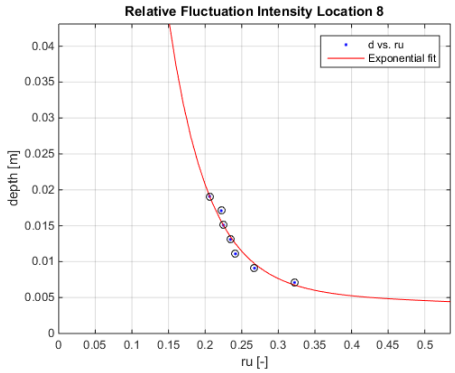

Figure 63; Fluctuation intensity location 8 0[h]

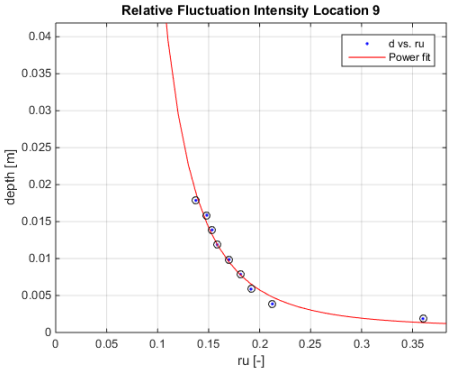

Figure 64; Fluctuation intensity location 9 0[h]

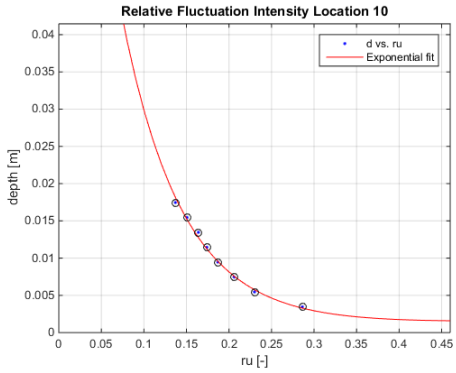

Figure 65; Fluctuation intensity location 10 0[h]

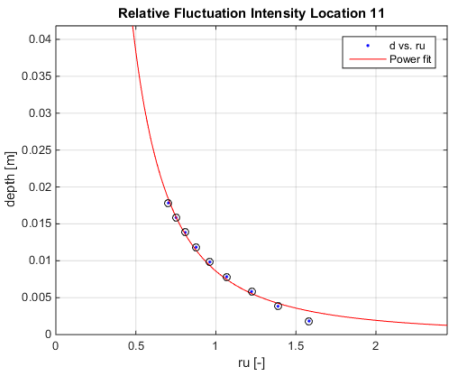

Figure 66; Fluctuation intensity location 11 0[h]

Bed Shear stress

The bed shear stress was determined with Reynolds formula stated in (Schiereck & Verhagen, 2012). Bed shear stresses are determined by averaging the estimation for bed shear stress, over the centimeter measured above the bottom for a time frame of 3 minutes measuring at 50 [hz] per second, excluding all measured values that do not confirm with a signal to noise ratio above 15 and a correlation of 90%.

Observable is that bed shear stresses are highest in the center of constriction-sector (Locations 3,4,5). Other locations with high values are in the constriction-sector near the interface with the expansion sector (location 10) and the area in the center of the downstream-section (location 6).

Table 11; Bed shear stresses [n/m^2]

Location	1	2	3	4	5	6	7	8	9	10	11
	-0,050	-0,013	-0,467	-0,118	-0,274	-0,139	-0,084	-0,057	-0,076	-0,330	-0,090

Estimation of transport

Following the formulations of the bed load transport by van Rijn (van Rijn, 2018). The results are represented as such, that locations at the same longitudinal location are coupled and transport is averaged over these locations (Table 12). The results are also depicted per sector by calculating the area underneath each cross-sectional measurement. In this way it is observed that scour is to be expected at the interface of the contraction and constriction sector (location 3 & 8), as well as the interface of the constriction and expansion sector (location 5 &10). Other locations do not meet the required bed shear stresses for transport to occur.

Table 12; Bed load transport [kg/m/s]

Location	1	2 & 7	3 & 8	4 & 9	5 & 10	6 & 11
	NaN	NaN	0,001112	NaN	0,002232	NaN

Table 13; Bed load transport per sector [kg/day]

Location	Upstream	Contraction	Constriction	Expansion	Downstream
	NaN	12,49	22,54	22,56	NaN

Measurements after 24h

Bed level

A projection of the bed after running for 24 [h] can be observed in Figure 67. The bed showed development of bedforms and scour throughout a very large part of the model. Scour started to occur about 500 mm into the projection, which is 300 [mm] into the contracting part of the model. It can be observed that the bedforms and scour that are present tend to increase in magnitude towards the point of maximum contraction. This is somewhat in agreement with the shields theorem, as the capacity for flow to transport particles increases in this area

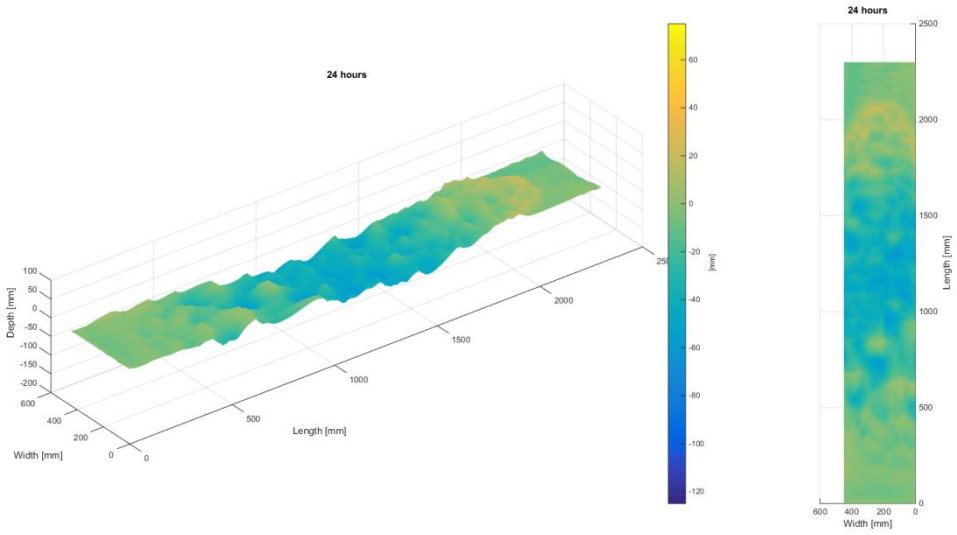

Figure 67; 24[h] bed projection

This analysis can be confirmed with the average transect, observable in Figure 68. It shows the largest at the point of maximum contraction and an increase in magnitude of bedforms and scour originating 500 [mm] into the model.

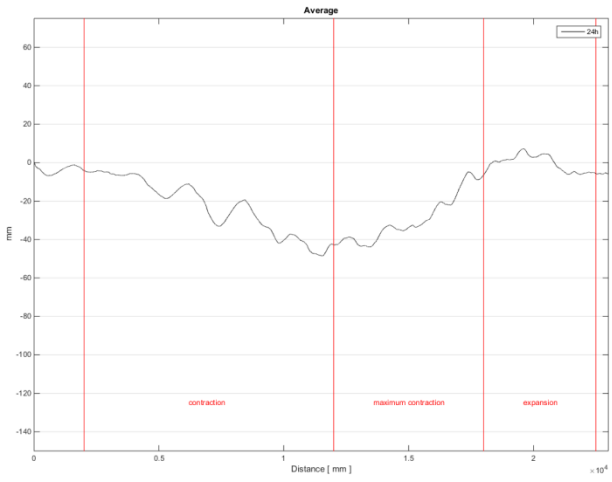

Figure 68; 24[h] average transect

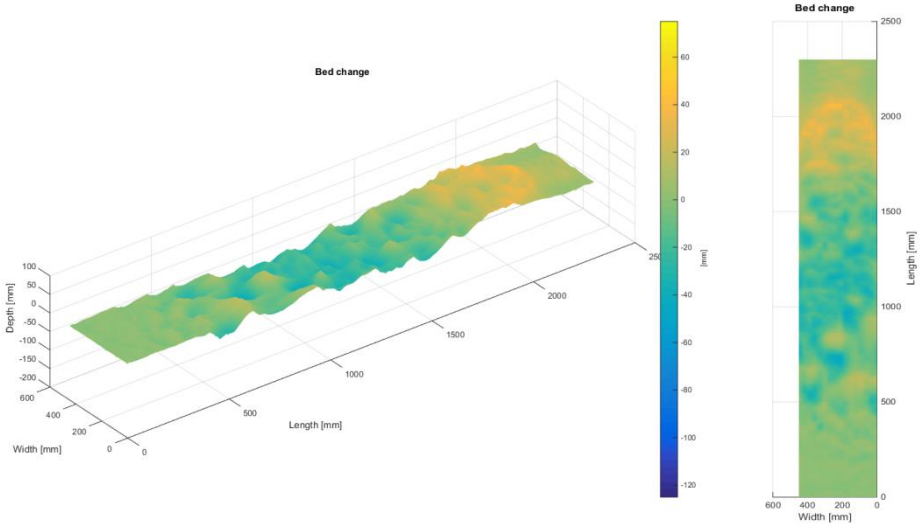

Figure 69; 0[h]-24[h] bed change projection

If the bed change in Figure 69 is observed, it can be seen that scour appears to occur in both the constriction-sector (1200-1600 [mm]) and the contraction sector (200-1200 [mm]) a strong deposition of sediment is seen downstream, which is located in the expansion sector. Table 14 Furthermore, the bulk of scour appears to occur in the contracting section, near the interface with the constriction-sector.

Table 14; Volume change per sector in [cm^3]

	Upstream	Contraction	Constriction	Expansion	Downstream
Volume	+8,1	-4944,3	-2942,7	+4174,2	+395,8

Velocity Profiles

Analyzing the flow profiles, it can be observed that however velocity increases between location 1 & 3, the flow profile changes significantly. Looking at the changes in bed topography it can be explained that the bedforms disturb the flow profile. Locations 3-5-6 show a very similar flow profile; clearly indicting flow close to the bed is strongly disturbed by the bed forms. Location 9 has a profile in between these shapes and also a maximum velocity that is in between these extremes, showing that this profile is less affected by the acceleration of flow and the disturbances by bedforms, probably due to the fact this location is very close to the wall.

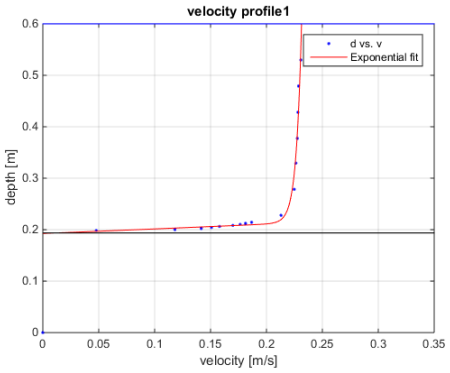

Figure 70; Velocity profile location 1 24[h]

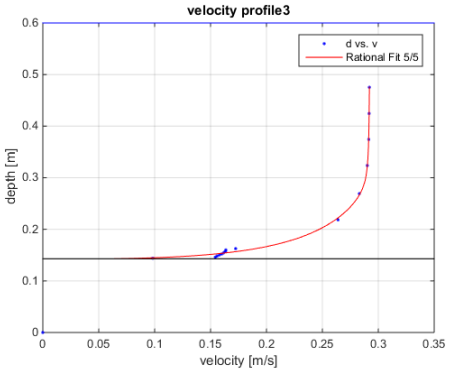

Figure 71; Velocity profile location 3 24[h]

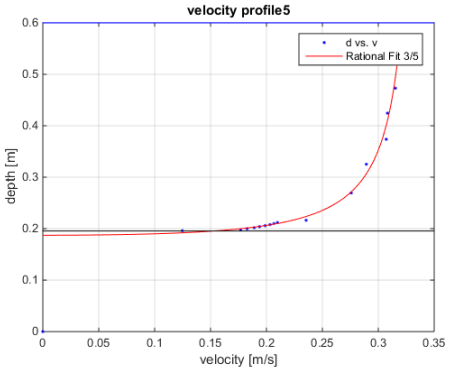

Figure 72; Velocity profile location 5 24[h]

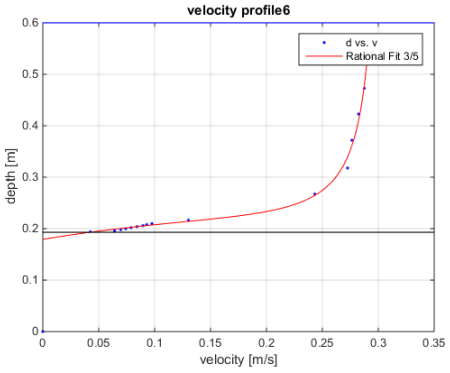

Figure 73; Velocity profile location 6 24[h]

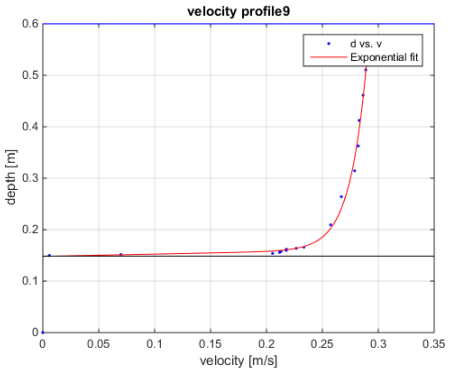

Figure 74; Velocity profile location 9 24[h]

Table 15; Average Velocity

Location	Average Velocity [m/s]
1	0,2204
3	0,2668
5	0,2872
6	0,2487
9	0,2686

Relative fluctuation intensity

From the relative fluctuation plots, we can see an increase halfway the contracting section of the flume. At locations 3-4-5-8-9-10 this decreases intensity decreases. At locations 10-11 this intensity strongly increases as a result of expanding and thus decelerating flow. Relative fluctuation intensity could not be produced for location 7 due to faulty data.

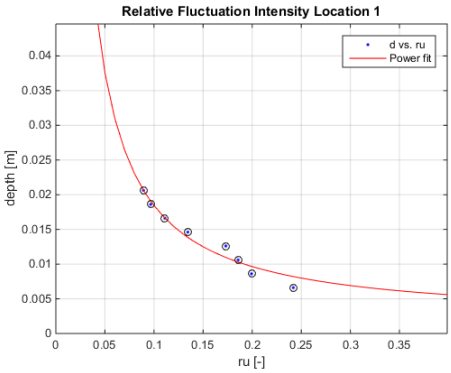

Figure 75; Fluctuation intensity location 1 24[h]

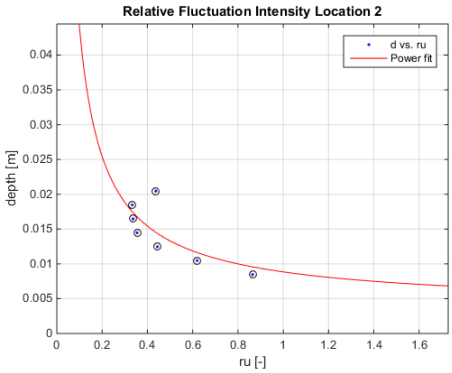

Figure 76; Fluctuation intensity location 2 24[h]

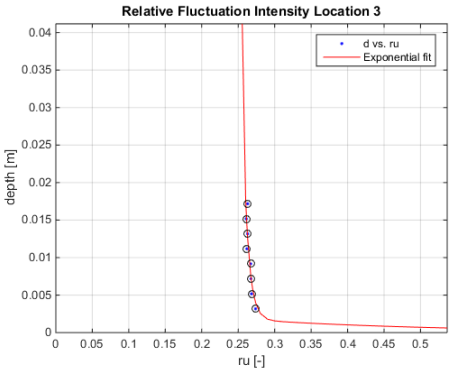

Figure 77; Fluctuation intensity location 3 24[h]

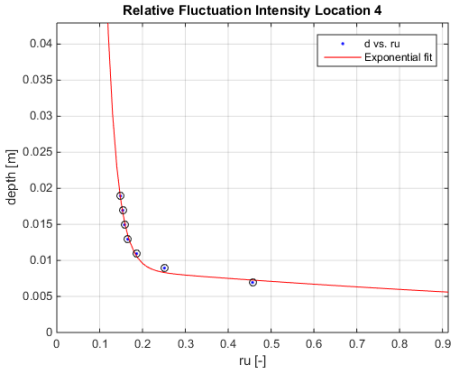

Figure 78; Fluctuation intensity location 4 24[h]

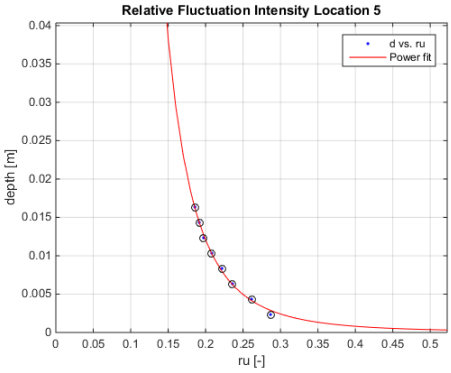

Figure 79; Fluctuation intensity location 5 24[h]

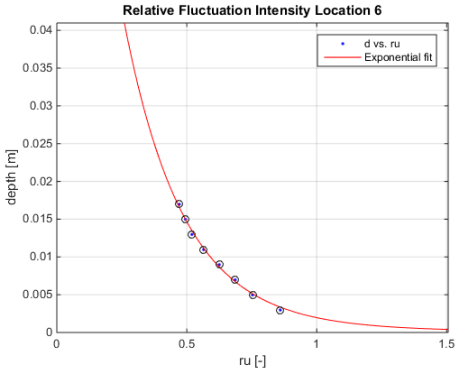

Figure 80; Fluctuation intensity location 6 24[h]

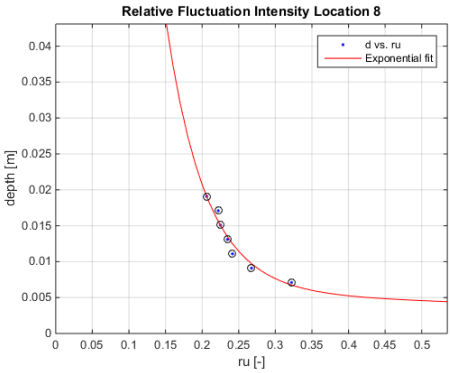

Figure 81; Fluctuation intensity location 8 24[h]

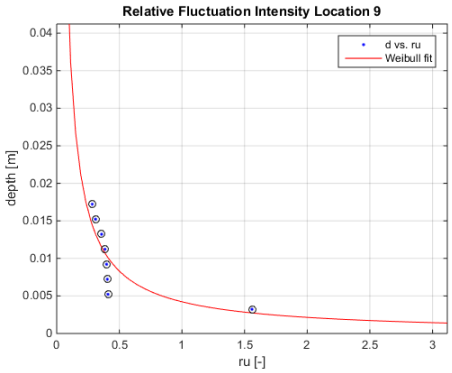

Figure 82; Fluctuation intensity location 9 24[h]

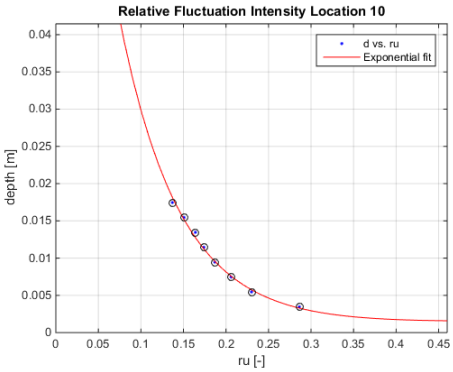

Figure 83; Fluctuation intensity location 10 24[h]

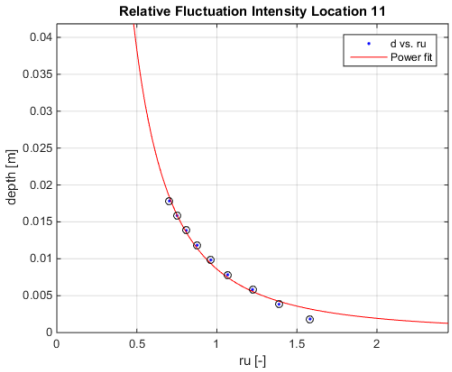

Figure 84; Fluctuation intensity location 11 24[h]

Bed Shear stress

The bed shear stress was determined with Reynolds formula stated in (Schiereck & Verhagen, 2012). Bed shear stresses are determined by averaging the estimation for bed shear stress, over the centimeter measured above the bottom for a time frame of 3 minutes measuring at 50 [hz] per second, excluding all measured values that do not confirm with a signal to noise ratio above 15 and a correlation of 90%.

Observable is that bed shear stresses are high in the center of constriction-sector (Location 4). Other locations with high values are in the constriction-sector near the wall (locations 8,9,10) and locations in the downstream sector (9 & 11)

Table 16; Bed shear stresses [g/ms2]

Location	1	2	3	4	5	6	7	8	9	10	11
	-0,090	-0,084	0,064	-0,348	-0,031	-0,213	-0,016	-0,367	0,755	-0,294	-0,138

Estimation of transport

Following the formulations of the bed load transport by van Rijn (van Rijn, 2018). The results are represented as such, that locations at the same longitudinal location are coupled and transport is averaged over these locations (Table 17). For the calculations the absolute value was taken of the measured bed shear stresses. The results are also depicted per sector by calculating the area underneath each cross-sectional measurement. In this way it is observed that scour is to be expected at locations 3|8, 4|9, 5|10, & 6|11. The results predict an enormous acceleration of scour in the constriction, this is however questionable given the actual observations. Interesting to note is that this area contains both positive and negative values which may indicate the scour rate is different from the estimated values.

Table 17; Bed load transport [kg/m/s]

Location	1	2 & 7	3 & 8	4 & 9	5 & 10	6 & 11
	NaN	NaN	0,000292	0,016322	$2{,}05*10^{-7}$	$1{,}56*10^{-5}$

Table 18; Bed load transport per sector [kg/day]

Location	Upstream	Contraction	Constriction	Expansion	Downstream
	NaN	3,28	221,96	0,32	NaN

Measurements after 48h

Bed level

As can be observed in Figure 85, strongest scour occurs about 1400 [mm] into the model, this is at the section of maximum contraction, and is roughly 85 [mm]. Furthermore scour occurs in almost all upstream areas now, and bedforms clearly show starting from 250 [mm] into the model.

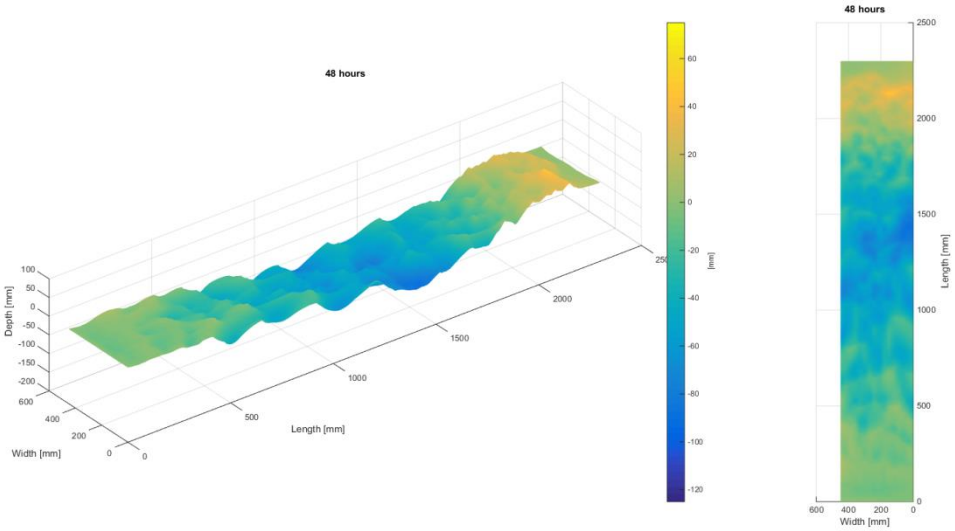

Figure 85; 48[h] bed projection

The average transect observable in Figure 86 shows average maximum scour has reached about 70 [mm], and is located well within the section of maximum contraction. A strong deposition of sediment is located in the expanding section.

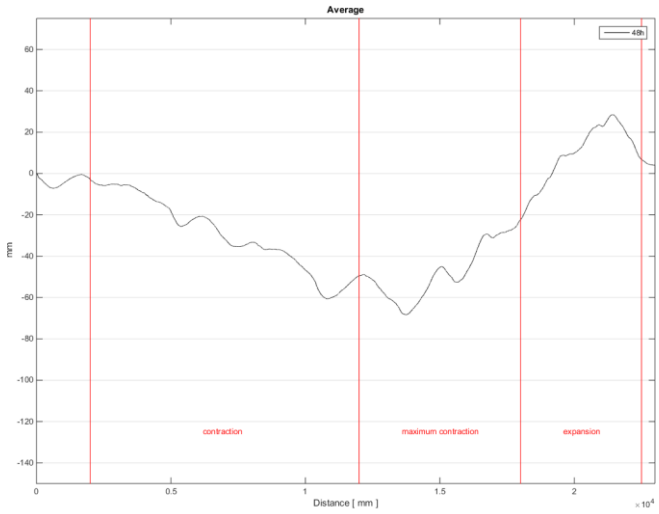

Figure 86; 48[h] average transect

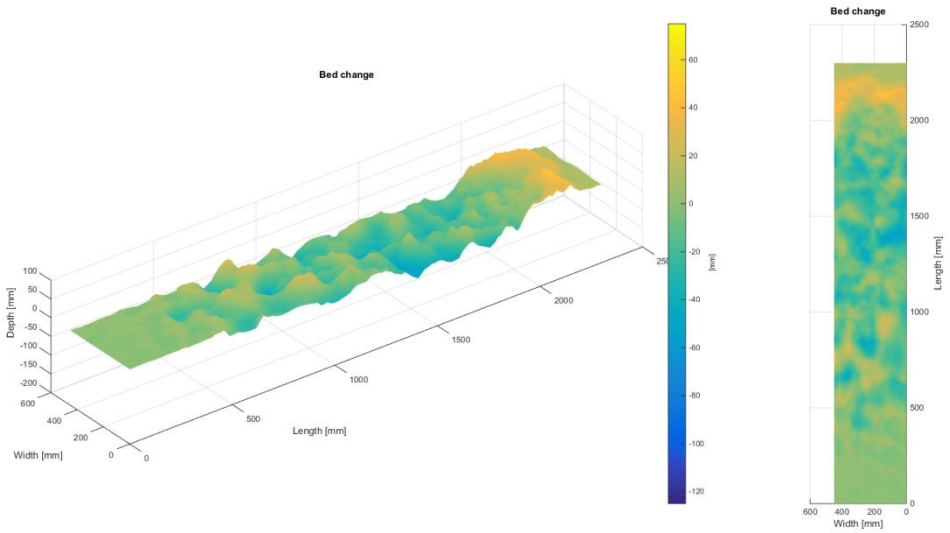

Figure 87; 24[h]-48[h] bed change projection

Furthermore Figure 87 shows that erosion is clearly occurring both in the area of maximum contraction as well as the contracting section. Strong accretion occurred in areas downstream of the contraction in the expanding section (1800 [mm] and beyond). Furthermore, the bulk of the total erosion appears to originate from the area of maximum contraction (Table 19). The total scour rate has doubled with respect to the first 24 hours.

Table 19; Volume change per sector in [cm^3]

	Upstream	Contraction	Constriction	Expansion	Downstream
Volume	+21,5	-2979,3	-4966,2	+1,2	+683,9

Velocity Profiles

It can be observed that upstream velocity profile 1 shows little to no change with respect to the profile measured at 24 [h]. As location 1 has seen almost no change in bed topography, this is as expected. Location 3-5-6 al show a slight downward shift but keep their shape while location 9 has now attained a more disturbed profile and shifted upwards.

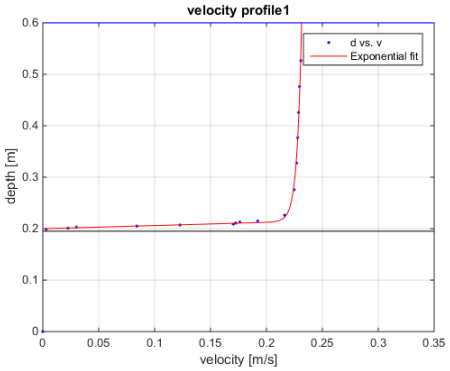

Figure 88; Velocity profile location 1 48[h]

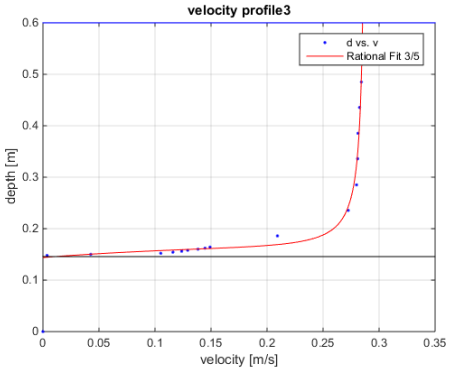

Figure 89; Velocity profile location 3 48[h]

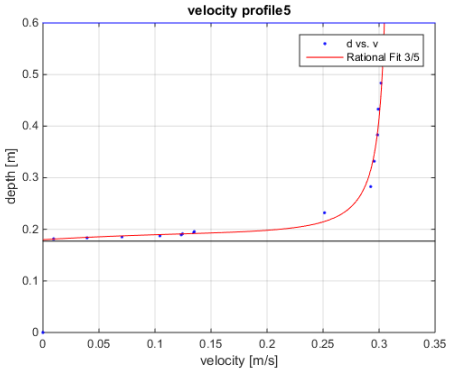

Figure 90; Velocity profile location 5 48[h]

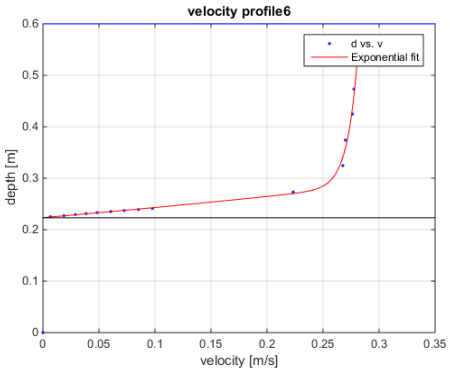

Figure 91; Velocity profile location 6 48[h]

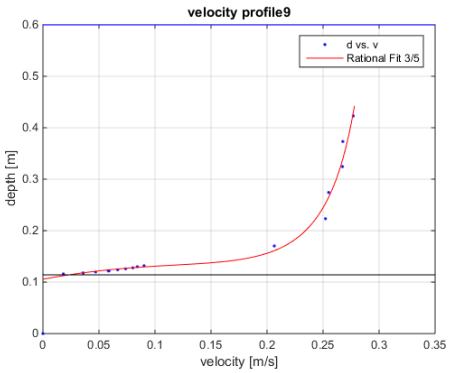

Figure 92; Velocity profile location 9 48[h]

Table 20; Average Velocity

Location	Average Velocity [m/s]
1	0,2191
3	0,2585
5	0,2727
6	0,2437
9	0,2313

Relative fluctuation intensity

From the relative fluctuation plots, we can see this intensity now stays roughly the same between locations 1-2. But increases especially near the bed between locations 2-3. A similar phenomenon can be witnessed between locations 7-8. Locations 5-9 now show very strong relative fluctuation intensity. This strongly decreases between locations 9-10 and tends to again increase in the decelerating section of the model resulting in significantly large values for locations 6 & 11.

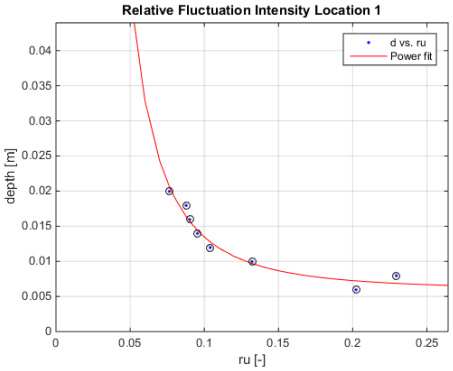

Figure 93; Fluctuation intensity location 1 48[h]

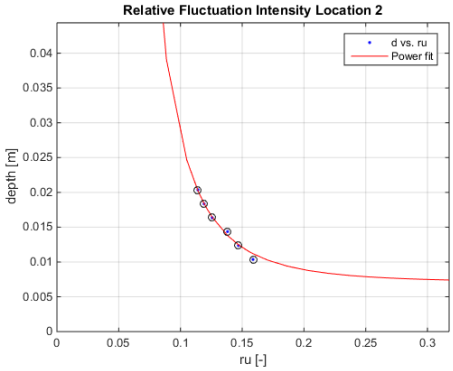

Figure 94; Fluctuation intensity location 2 48[h]

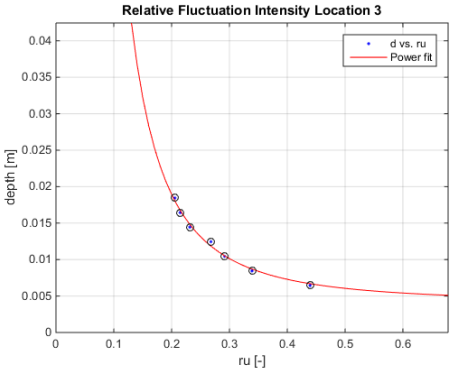

Figure 95; Fluctuation intensity location 3 48[h]

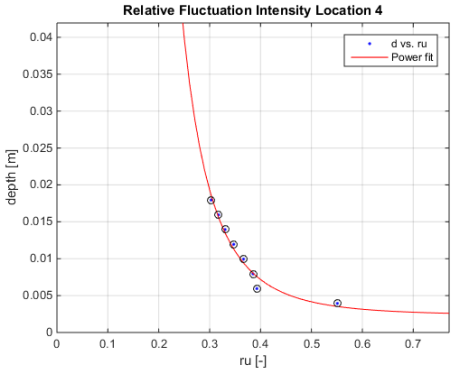

Figure 96; Fluctuation intensity location 4 48[h]

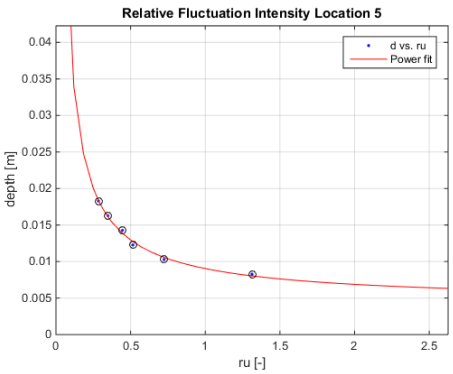

Figure 97; Fluctuation intensity location 5 48[h]

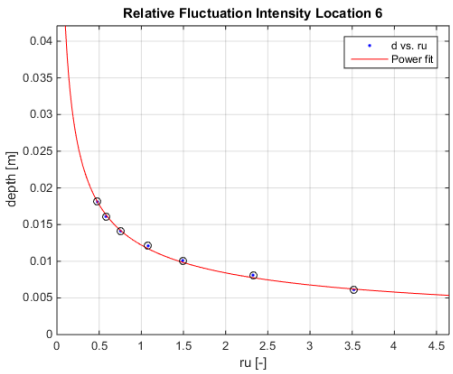

Figure 98; Fluctuation intensity location 6 48[h]

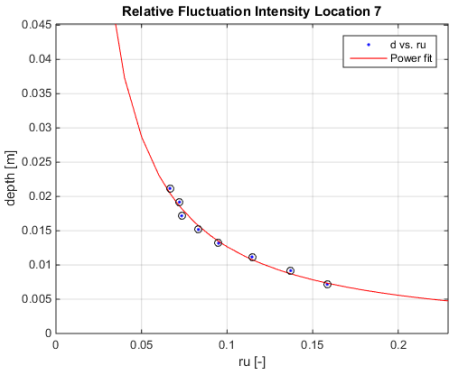

Figure 99; Fluctuation intensity location 7 48[h]

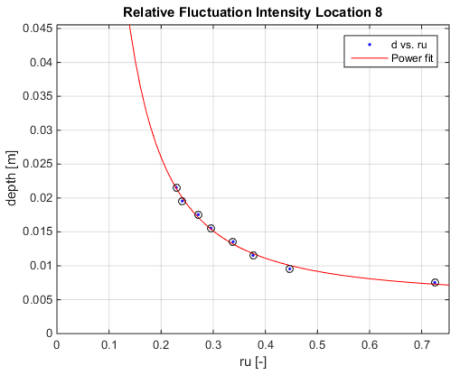

Figure 100; Fluctuation intensity location 8 48[h]

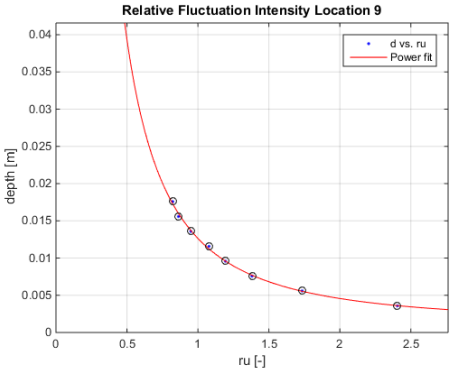

Figure 101; Fluctuation intensity location 9 48[h]

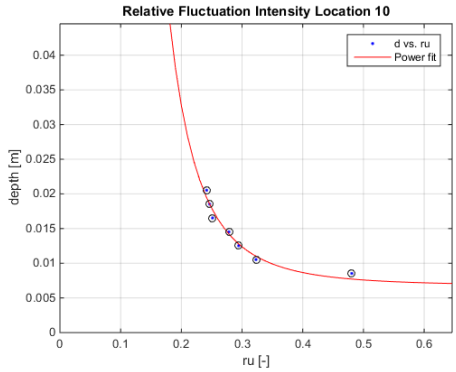

Figure 102; Fluctuation intensity location 10 48[h]

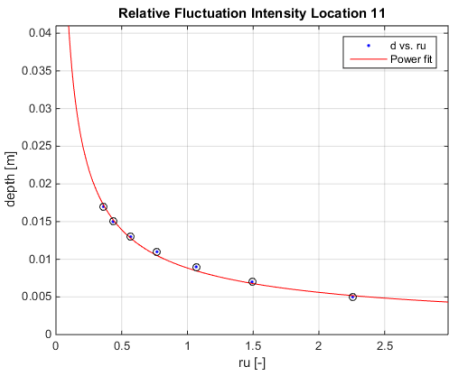

Figure 103; Fluctuation intensity location 11 48[h]

Bed Shear stress

The bed shear stress was determined with Reynolds formula stated in (Schiereck & Verhagen, 2012). Bed shear stresses are determined by averaging the estimation for bed shear stress, over the centimeter measured above the bottom for a time frame of 3 minutes measuring at 50 [hz] per second, excluding all measured values that do not confirm with a signal to noise ratio above 15 and a correlation of 90%.

The bed shear stress was determined with the conventions stated in (Schiereck & Verhagen, 2012). All locations show negative bed shear stresses with the exception of location 10. Locations 5-6-8-9-10-11 show values indicative of scour.

Table 21; Bed shear stresses [n/m^2]

Location	1	2	3	4	5	6	7	8	9	10	11
	-0,004	-0,035	-0,024	-0,073	-0,360	-0,221	-0,005	-0,202	-0,339	0,815	-0,316

Estimation of transport

Following the formulations of the bed load transport by van Rijn (van Rijn, 2018). The results are represented as such, that locations at the same longitudinal location are coupled and transport is averaged over these locations (Table 22). For the calculations the absolute value was taken of the measured bed shear stresses. The results are also depicted per sector (Table 23) by calculating the area underneath each cross-sectional measurement. In this way it is observed that scour is to be expected at locations 4|9, 5|10, & 6|11. The results predict strong scour in the constriction, this is however questionable given the actual observations. Interesting to note is that this area contains both positive and negative values which may indicate the scour rate is different from the estimated values. If for the constriction locations 5&10 are dropped the scour rate reduces to 5,2 [kg/day] which seems to be more reasonable.

Table 22; Bed load transport [kg/m/s]

Location	1	2 & 7	3 & 8	4 & 9	5 & 10	6 & 11
	NaN	NaN	NaN	0,000193	0,019183	0,001268

Table 23; Bed load transport per sector [kg/day]

Location	Upstream	Contraction	Constriction	Expansion	Downstream
	NaN	NaN	131,88	0,32	NaN

Measurements after 72h

Bed level

As can be seen in Figure 104, the largest amount of scour occurs at roughly 1300 [mm] into the model, which is again inside the maximum contracted zone. Maximum scour is about 85 [mm].

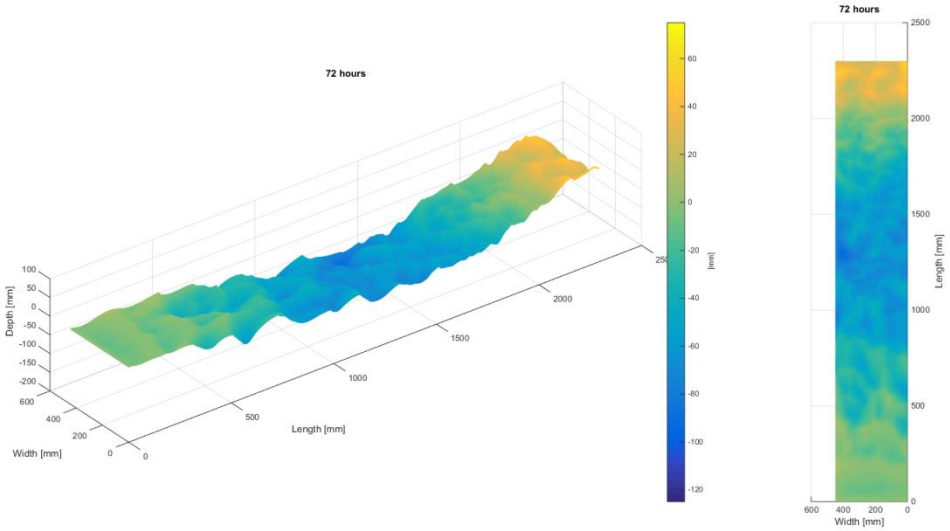

Figure 104; 72[h] bed projection

The average transect observable in Figure 105 shows average maximum scour is still at 70 [mm], but has moved upstream. The average scour over the entire maximum contracted section has however increased. And the bedforms that were clearly observable before have smoothed out significantly.

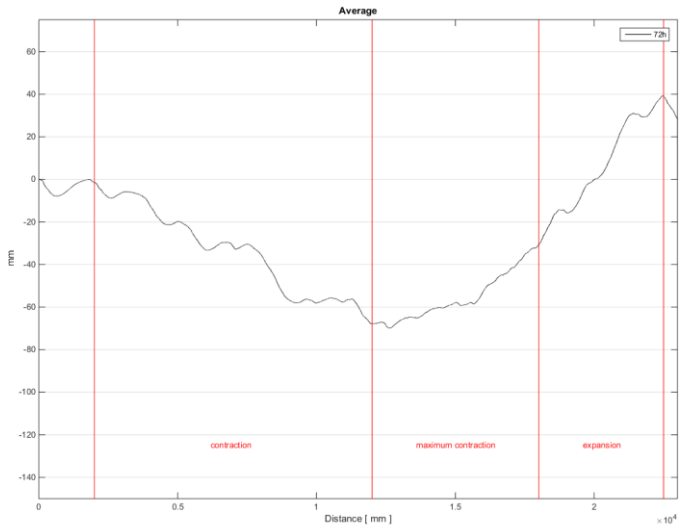

Figure 105; 72[h] average transect

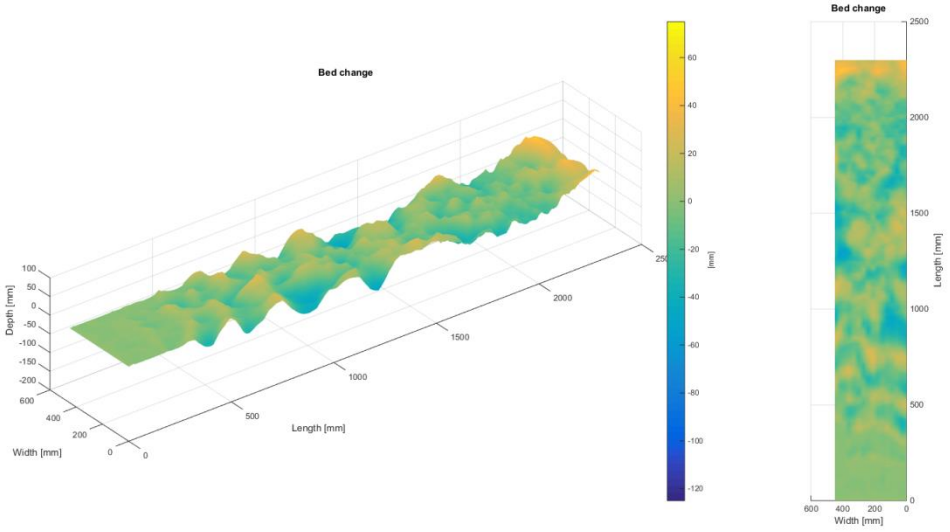

Figure 106; 48[h]-72[h] bed change projection

It can be observed from Figure 106, that the bed shows progressing erosion in the contracting section, furthermore some accretion has occurred in the constriction-sector, but in total this area still shows scour Table 24, however at a significantly reduced rate. The total scour rate has decreased 25% compared to the 24 hour interval measured before.

Table 24; Volume change per sector in [cm^3]

	Upstream	Contraction	Constriction	Expansion	Downstream
Volume	-4,9	-2014,0	-2434,4	-1401,1	+1252,2

Velocity Profiles

Again, little to no change of the flow profile at location 1 was observed. Location 3 also has maintained a similar shape. Location 5 shows the flow profile shifted upwards slightly, while profile 6 now shows much higher velocities very near to the bed with respect to the measurements taken at 48 [h]. Location 9 also shows this increase of velocity near the bed, this might be attributed to the fact that strong bedforms have ever so slightly smoothed out, as was observed in the previous section.

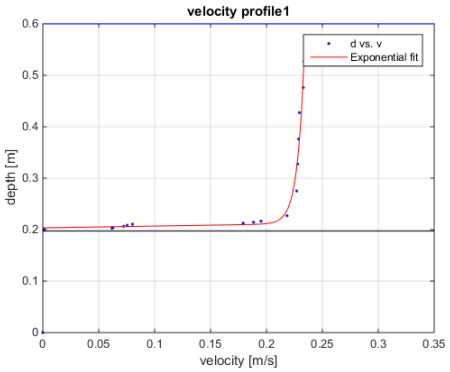

Figure 107; Velocity profile location 1 72[h]

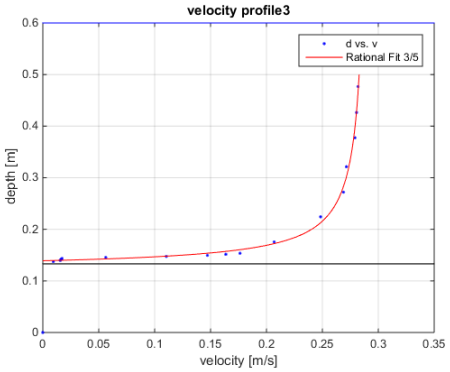

Figure 108; Velocity profile location 3 72[h]

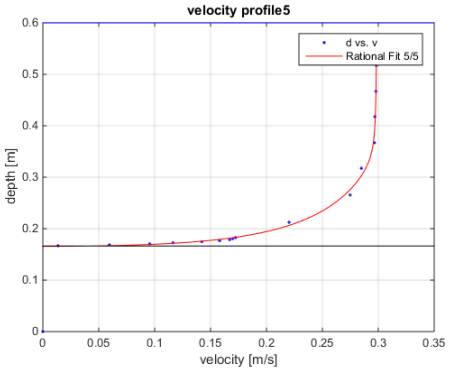

Figure 109; Velocity profile location 5 72[h]

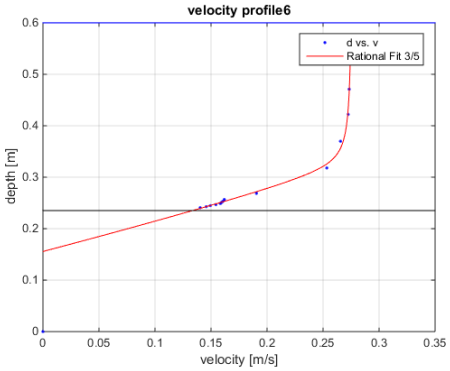

Figure 110; Velocity profile location 6 72[h]

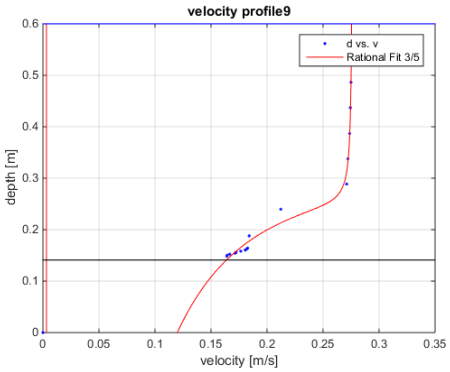

Figure 111; Velocity profile location 9 72[h]

Table 25; Average Velocity

Location	Average Velocity [m/s]
1	0,2205
3	0,2507
5	0,2684
6	0,2553
9	0,2456

Relative fluctuation intensity

Location 1 now shows a very disturbed relative fluctuation intensity. Around 15-20 [mm] above the bed this is similar with respect to earlier measurements, but close to the bed fluctuation intensity tends to spike. A clear increase can be observed between locations 2-3 & 7-8. A reduction occurs between locations 3-4 and then increases again from 4-5 and from 5-6. Between locations 8-9 intensity increases but becomes more uniform and decreases again between locations 9-10-11.

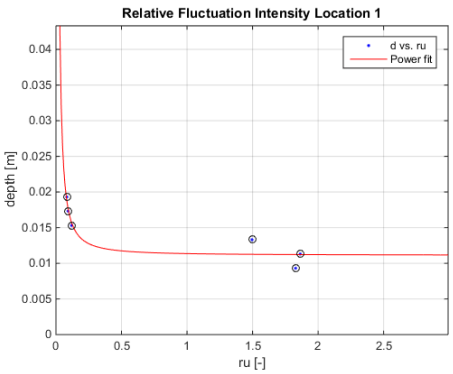

Figure 112; Fluctuation intensity location 1 72[h]

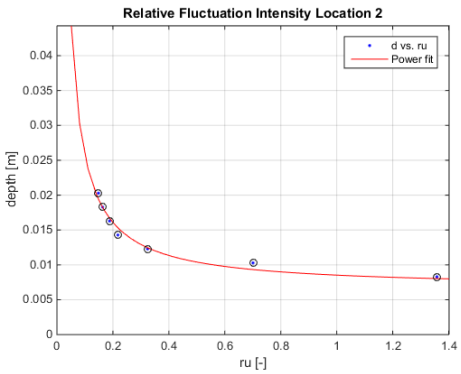

Figure 113; Fluctuation intensity location 2 72[h]

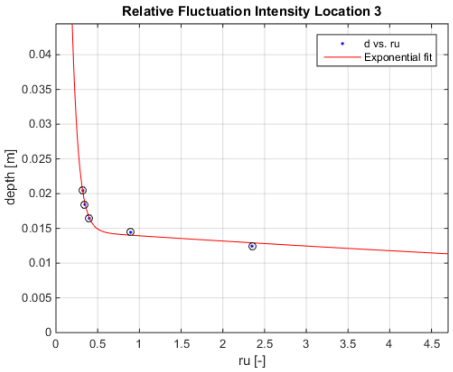

Figure 114; Fluctuation intensity location 3 72[h]

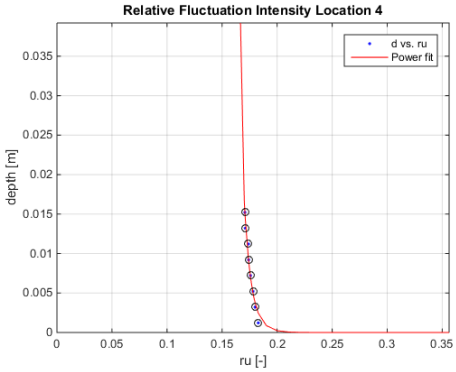

Figure 115; Fluctuation intensity location 4 72[h]

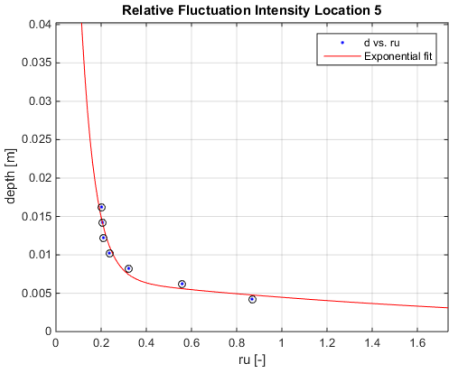

Figure 116; Fluctuation intensity location 5 72[h]

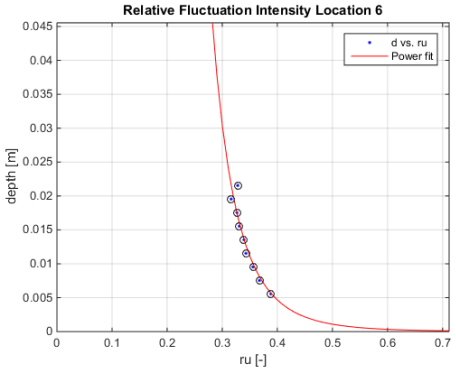

Figure 117; Fluctuation intensity location 6 72[h]

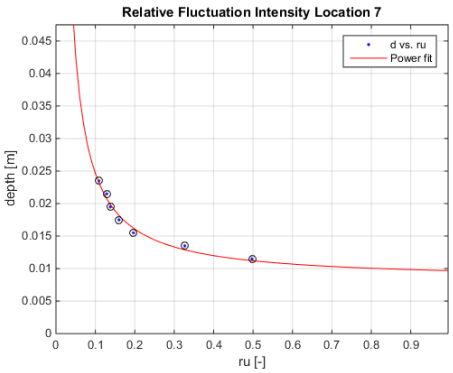

Figure 118; Fluctuation intensity location 7 72[h]

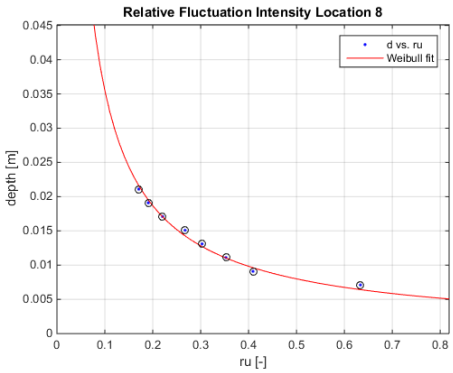

Figure 119; Fluctuation intensity location 8 72[h]

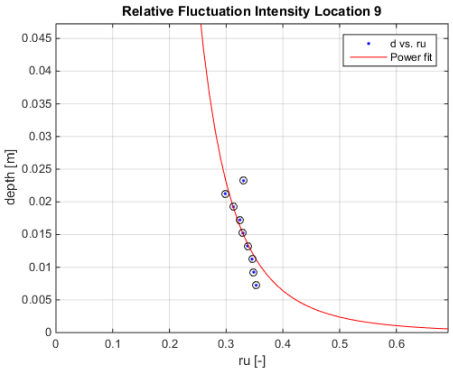

Figure 120; Fluctuation intensity location 9 72[h]

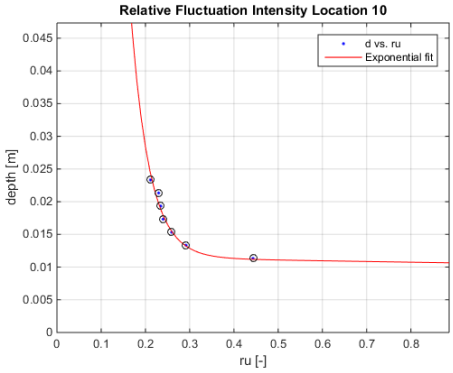

Figure 121; Fluctuation intensity location 10 72[h]

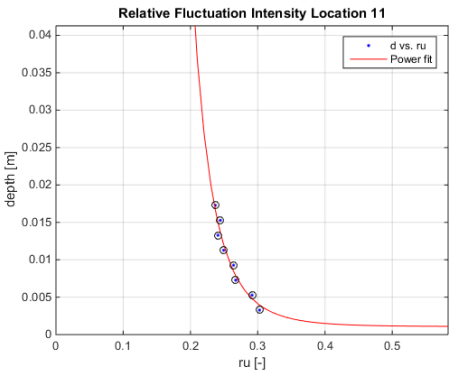

Figure 122; Fluctuation intensity location 11 72[h]

Bed Shear stress

The bed stress was determined with Reynolds formula stated in (Schiereck & Verhagen, 2012). Bed shear stresses are determined by averaging the estimation for bed shear stress, over the centimeter measured above the bottom for a time frame of 3 minutes, excluding all measured values that do not confirm with a signal to noise ratio above 15 and a correlation of 90%.

The bed shear stress was determined with the conventions stated in (Schiereck & Verhagen, 2012). Areas under high load were located on the interface between the contracting and constriction-sector (location 3 & 8), areas near the wall (location 9), and areas downstream of the expansion (10 & 11), see Table 26.

Table 26; Bed shear stresses [n/m^2]

Location	1	2	3	4	5	6	7	8	9	10	11
	-0,002	-0,123	-0,279	-0,053	0,053	0,240	-0,030	-0,239	-0,301	0,569	0,293

Estimation of transport

Following the formulations of the bed load transport by van Rijn (van Rijn, 2018). The results are represented as such, that locations at the same longitudinal location are coupled and transport is averaged over these locations (Table 27). For the calculations the absolute value was taken of the measured bed shear stresses. The results are also depicted per sector (Table 28) by calculating the area underneath each cross-sectional measurement. In this way it is observed that scour is to be expected at locations 3|8, 4|9, 5|10, & 6|11. The results predict strong scour in the constriction and the expansion, the results are large but not exceptional. The upward slope might prevent parts of this transport.

Table 27; Bed load transport [kg/m/s]

Location	1	2 & 7	3 & 8	4 & 9	5 & 10	6 & 11
	NaN	NaN	0,00104	$1{,}94*10^{-5}$	0,00253	0,001219

Table 28; Bed load transport per sector [kg/day]

Location	Upstream	Contraction	Constriction	Expansion	Downstream
	NaN	11,7	24,3	39,9	5,5

Measurements after 96h

Bed level

The bed after 96 [h] shows an even further intensification of scour, scour rates do seem to reduce after this time. Maximum scour can be observed to be around 1250 [mm] into the setup, which is at the entry point of maximum contraction (see Figure 123 & Figure 124).

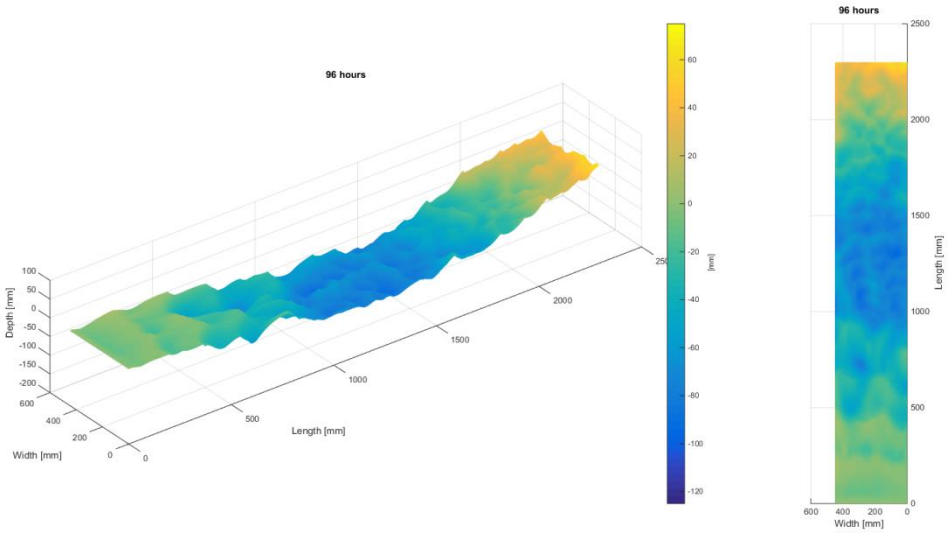

Figure 123; Bed map after 96 [h]

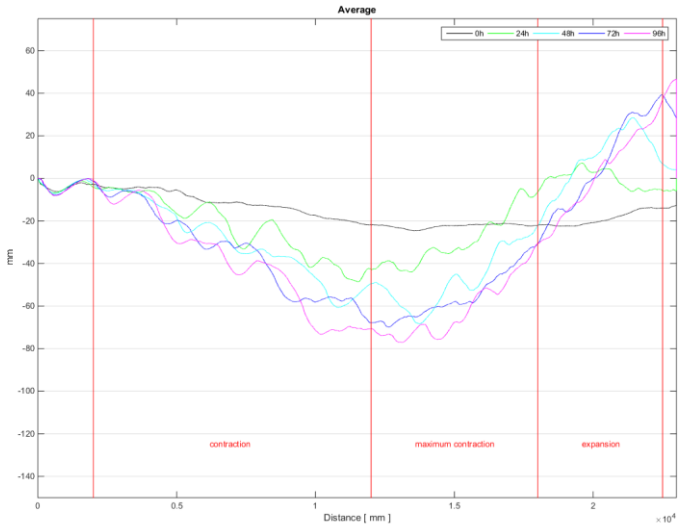

Figure 124; Average transects through time

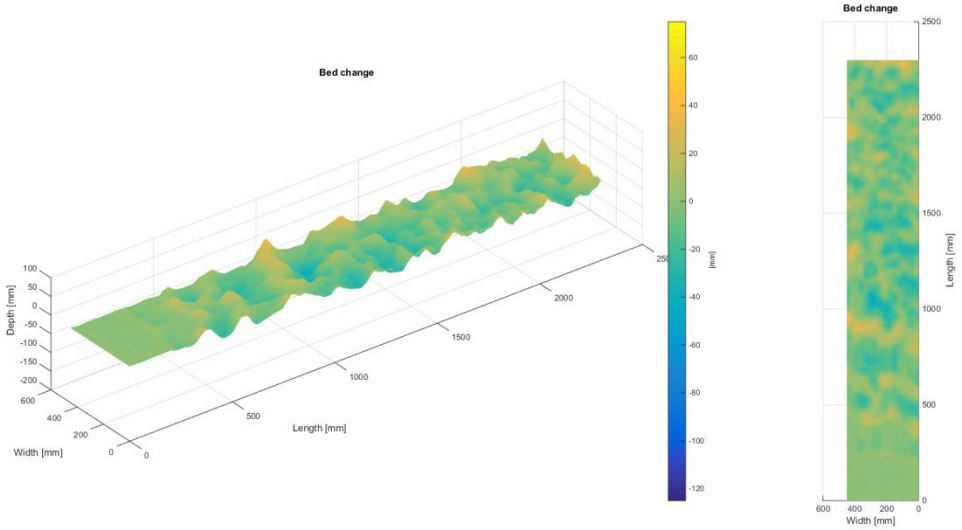

Figure 125; Bed change with respect to 72[h]

Figure 125 shows further progression of bedforms with areas of scour followed by areas of accretion, these areas are however relatively short. The total scour rate has stayed approximately the same, but this is only because the area downstream of the expansion has not accreted. Both the areas of maximum contraction as well as the contracting and expanding areas have eroded at a rate lower than before (Table 29).

Table 29; Volume change per sector in [cm^3]

	Upstream	Contraction	Constriction	Expansion	Downstream
Volume	-9,7	-1906,1	-1915,3	-919,1	-67,6

Concluding Remarks

This second basic scour experiment showed a similar development of scour and scour magnitude with respect to the first experiment, but scour occurred further upstream from the start. As the bed had a different initial profile, differences between these experiments are partially attributed due to this difference. The largest scour depth measured was approximately 94 [mm] and the maximum cross section average scour reached about 77 [mm].

Appendix B III

I Introduction

Basic scour III is the third experiment conducted. Bed, velocity and fluctuation intensity development is measured during a 96 [h] run as the reference to past and follow up experiments. In this experiment only the influence of the contraction on the set – up is monitored. This report includes all measured findings during this particular experiment. Conclusions are drawn in the main report on the basis of multiple similarly conducted experiments. A short preliminary conclusion is however included at the end of this report.

Summary

Table 30 represents relevant scour quantities after 96 [h]. Note that the absolute is measured relative to the measurement of the bed at 0 [h], excluding the maximum scour depth which is measured to a reference bed with a 0 [mm] elevation. Measurements of scour volume in the column with respect to reference include missing volume with respect to a reference be of 0 [mm].

Table 30; Summary of quantities

	Absolute	With respect to reference
Maximum Scour Depth [mm]	121,6	121,6
Total Scoured volume [cm^3]	-24634,6	-34693,3
Scoured volume Upstream-sector [cm^3]	+16,5	-688,8
Scoured volume Contracting-sector [cm^3]	-610,1	-6249,6
Scoured volume Constricted-sector [cm^3]	-16580	-18343,4
Scoured volume Expanding-sector [cm^3]	-7440,2	-9280,3
Scoured volume Downstream-sector [cm^3]	-20,8	-151,2

Measurements at 0h

Bed level

A projection of the bed at the moment of initiation of flow during the first scour experiment can be seen in Figure 126. It can be observed that the bed was relatively flat, except for a minor hill at the maximum contracted section.

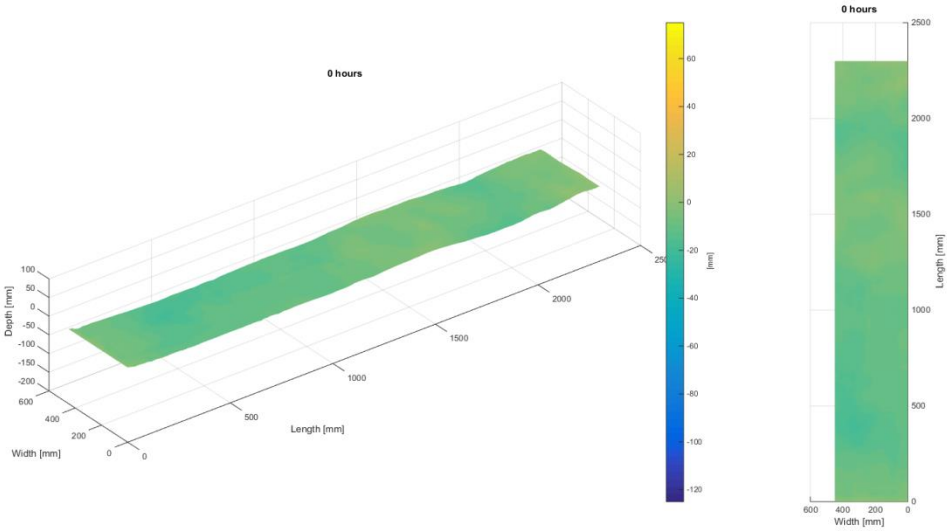

Figure 126; Bed map 0[h]

The average transect, observable in Figure 127, was calculated from the 16 transects taken over the entire length of the laboratory set-up. As can be seen, the bed shows minor indentures along the set-up ranging between 0.5 – 1.5 [cm]. Due to the difficulty of obtaining a near smooth bed it was accepted that the bed showed these minor deformations prior to initiating the flow.

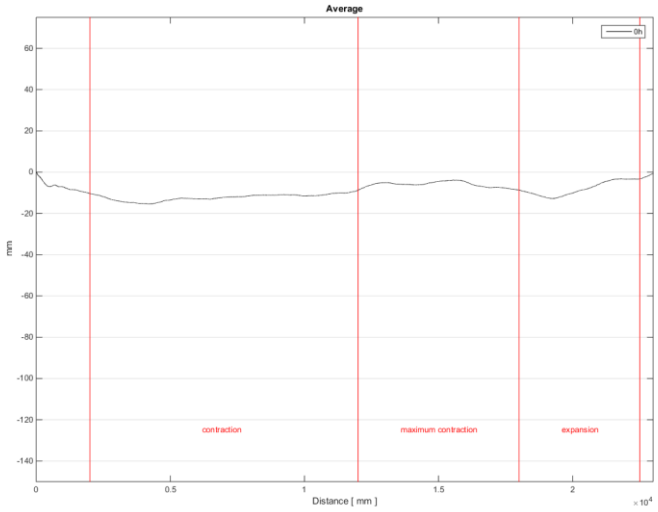

Figure 127; 0 [h] average transect

Velocity Profiles

In this section, individual flow profiles of locations marked above are shown. It can be observed that the flow cannot be considered to be uniform upon arrival in model (Figure 128). This was as expected; as the length of the false bottom was not long enough facilitate full development of the boundary layer. It can therefore be seen that flow is not logarithmically distributed, but instead has a turbulent flow structure. It can further be observed that at location 3 (Figure 129), the velocity profile further skews. Locations 5 (Figure 130) & 6 (Figure 131) have completely different profiles, and hint to changes in the flow structure. Location 9 (Figure 132), which is in the center and near the wall in the maximum contracted section, shows a structure similar to the entry point of the maximum contracted section.

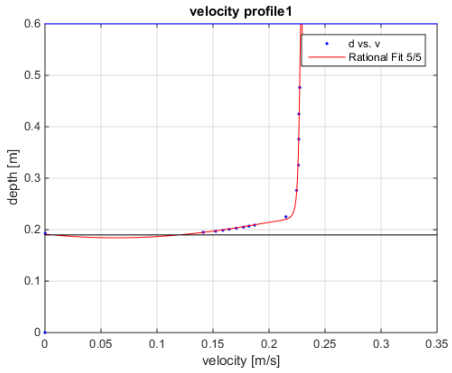

Figure 128; Velocity profile Location 1 [0h]

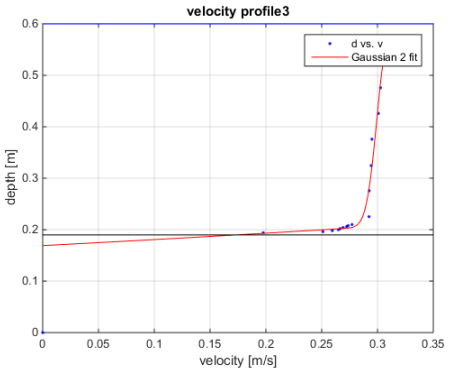

Figure 129; Velocity profile Location 3 [0h]

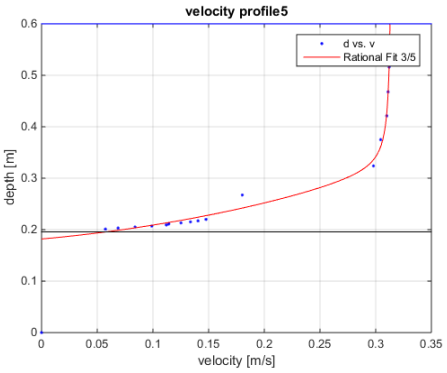

Figure 130; Velocity profile Location 5 [0h]

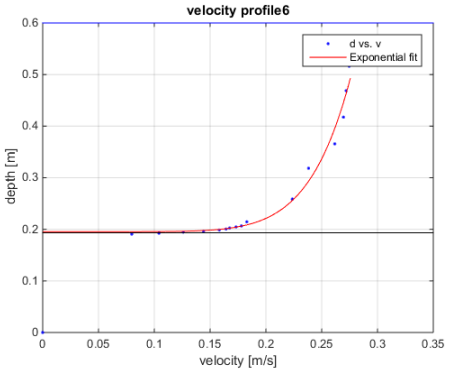

Figure 131; Velocity profile Location 6 [0h]

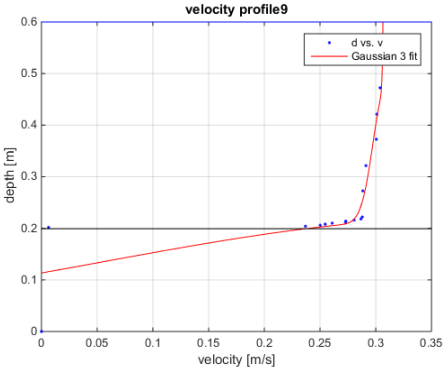

Figure 132; Velocity profile Location 9 [0h]

Table 31; Average Velocity

Location	Average Velocity [m/s]
1	0,2197
3	0,2938
5	0,2605
6	0,2414
9	0,2925

Relative fluctuation intensity

Looking at the relative fluctuation intensity, we can observe this decrease from location 1 to 3 and 7 to 8, due to the fact of contracting flow and this smooth out turbulences. This slightly increases at between locations 3-4 and 8-9 and increases strongly between locations 4-5 and 9-10. Upon leaving the section of maximum contraction a reduction can be observed between locations 5-6 and further increases between locations 10-11. The development of the relative fluctuation intensity is in accordance with the changes in flow profile observed and discussed in the previous section.

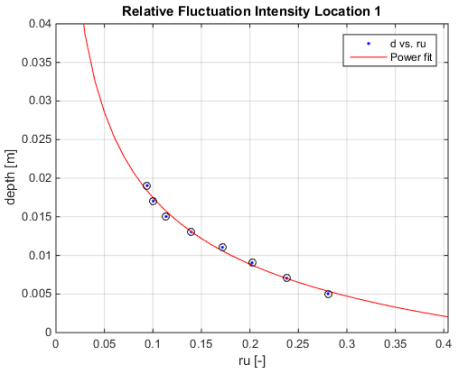

Figure 133; RU location 1 [0h]

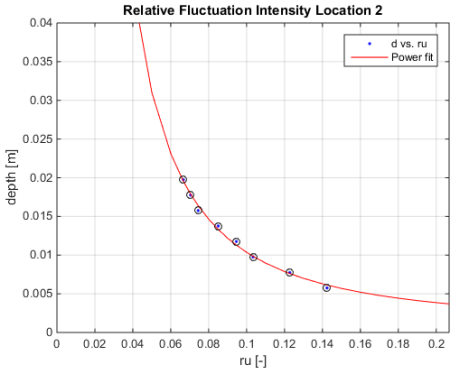

Figure 134; RU location 2 [0h]

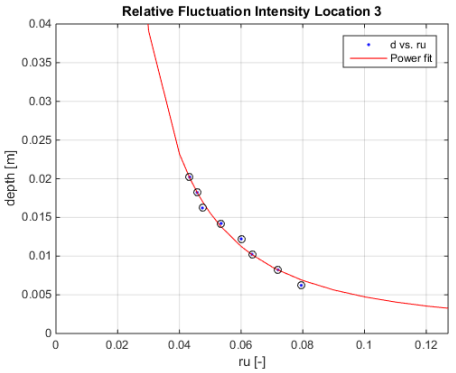

Figure 135; RU location 3 [0h]

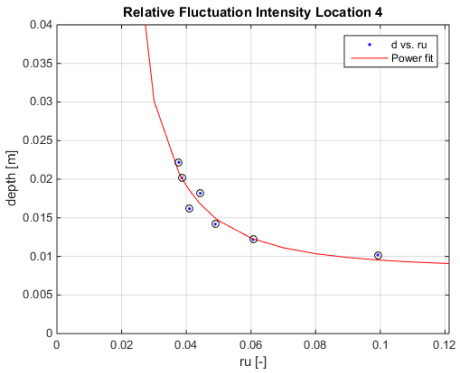

Figure 136; RU location 4 [0h]

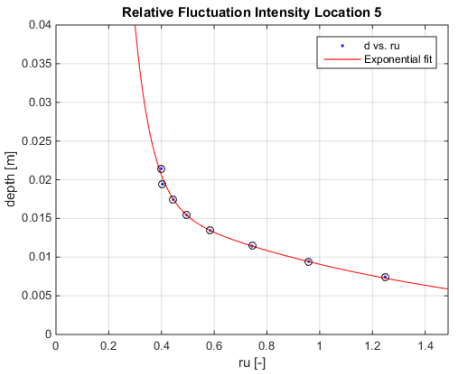

Figure 137; RU location 5 [0h]

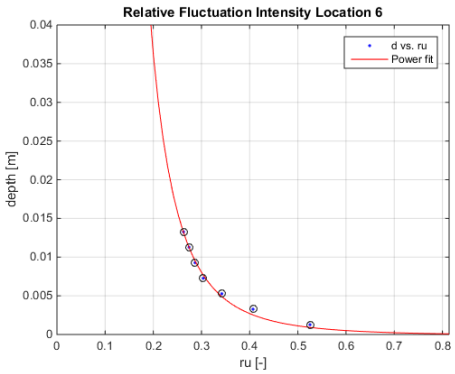

Figure 138; RU location 6 [0h]

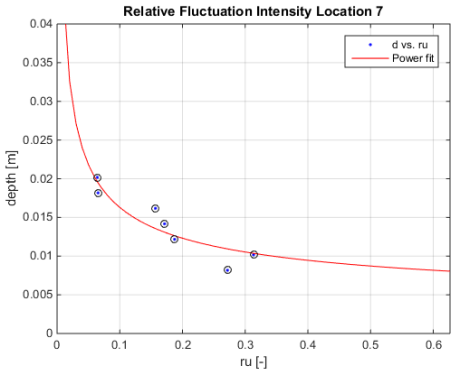

Figure 139; RU location 7 [0h]

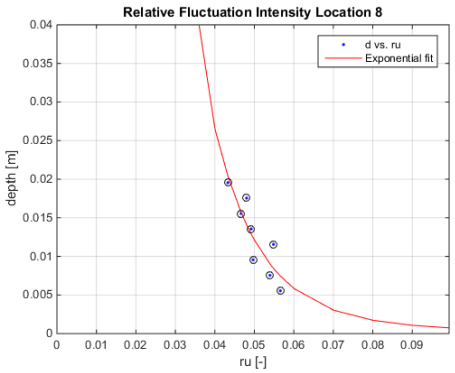

Figure 140; RU location 8 [0h]

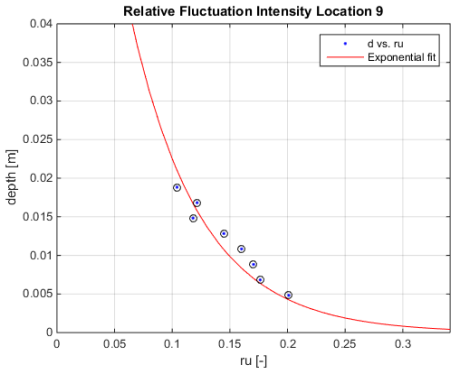

Figure 141; RU location 9 [0h]

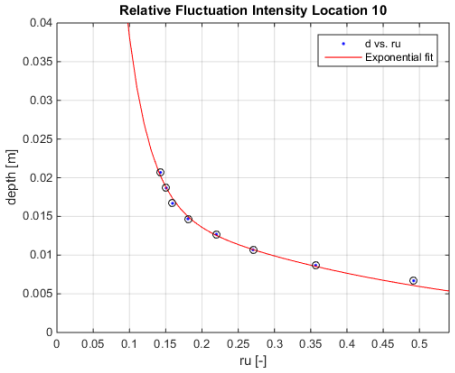

Figure 142; RU location 10 [0h]

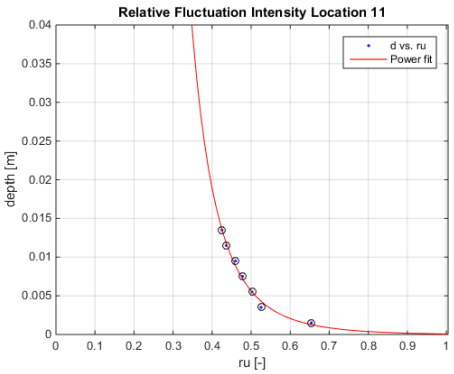

Figure 143; RU location 11 [0h]

Bed Shear stress

The bed shear stress was determined with Reynolds formula stated in (Schiereck & Verhagen, 2012). Bed shear stresses are determined by averaging the estimation for bed shear stress, over the centimeter measured above the bottom for a time frame of 3 minutes measuring at 50 [hz] per second, excluding all measured values that do not confirm with a signal to noise ratio above 15 and a correlation of 90%.

Observable is that bed shear stresses are alternating between positive and negative values. Values are highest (absolute) at locations near wall locations 9 & 10, and locations located in the downstream sector (locations 10 &11).

Table 32; Bed shear stresses [n/m^2]

Location	1	2	3	4	5	6	7	8	9	10	11
	-0,047	-0,045	-0,0174	0,076	0,002	-0,425	0,034	0,020	0,155	-0,453	-0,173

Estimation of transport

Following the formulations of the bed load transport by van Rijn (van Rijn, 2018). The results are represented as such, that locations at the same longitudinal location are coupled and transport is averaged over these locations (Table 33). For the calculations the absolute value was taken of the measured bed shear stresses. The results are also depicted per sector (Table 34) by calculating the area underneath each cross-sectional measurement. In this way it is observed that scour is to be expected at locations 5|10, & 6|11. The results predict scour located at the interface between the constriction and expansion sector, focused mainly near the side as well as scour at the interface between the expansion and the downstream sector.

Table 33; Bed load transport [kg/m/s]

Location	1	2 & 7	3 & 8	4 & 9	5 & 10	6 & 11
	NaN	NaN	NaN	NaN	0,00044	0,00213

Table 34; Bed load transport per sector [kg/day]

Sector	Upstream	Contraction	Constriction	Expansion	Downstream
	NaN	NaN	3,0	21,5	9,6

Water level

The water levels were measured at locations 1,3,5,6 they are depicted in Table 35Table 59. The levels were computed by measuring at 1000 [hz] for 15 seconds, and averaging those results. It is observed that the water level shows a drop of 0,6 [cm]. The water level seems to drop during constriction, while shortly downstream of the constriction the water level seems to stay approximately the same.

Table 35; Water level [cm]

Location	1	3	5	6
	39,9737	39,4417	39,2933	39,3350

Measurements after 24h

Bed level

A projection of the bed after running for 24 [h] can be observed in Figure 144. The bed showed a very particular development of scour, heavily favoring one side of the maximum contracted section of the flume. Furthermore it could clearly be observed that sand as deposited on the opposite side downstream of the maximum contracted section.

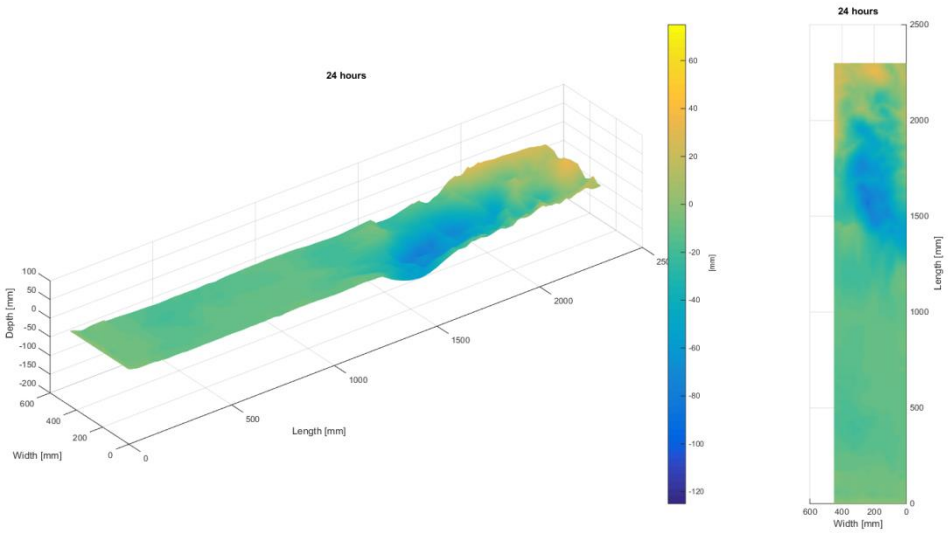

Figure 144; 24[h] bed projection

Erosion localized at the maximum contracted section can be confirmed with the average transect, observable in Figure 145. It shows the largest on average scour at the center of the maximum contracted section. This is in agreement with the bed shear stresses determined at initiation of flow.

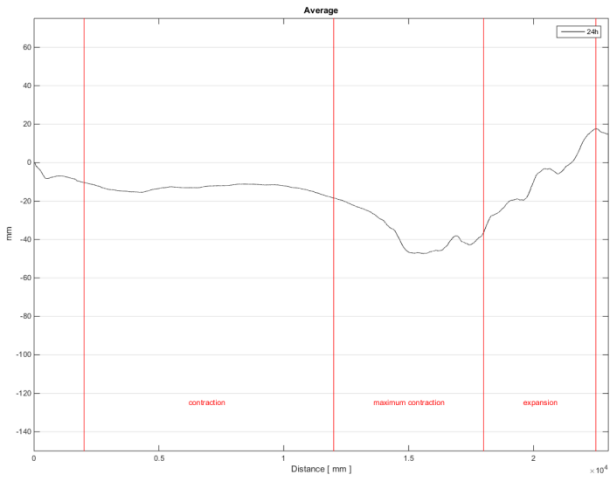

Figure 145; 24[h] average transect

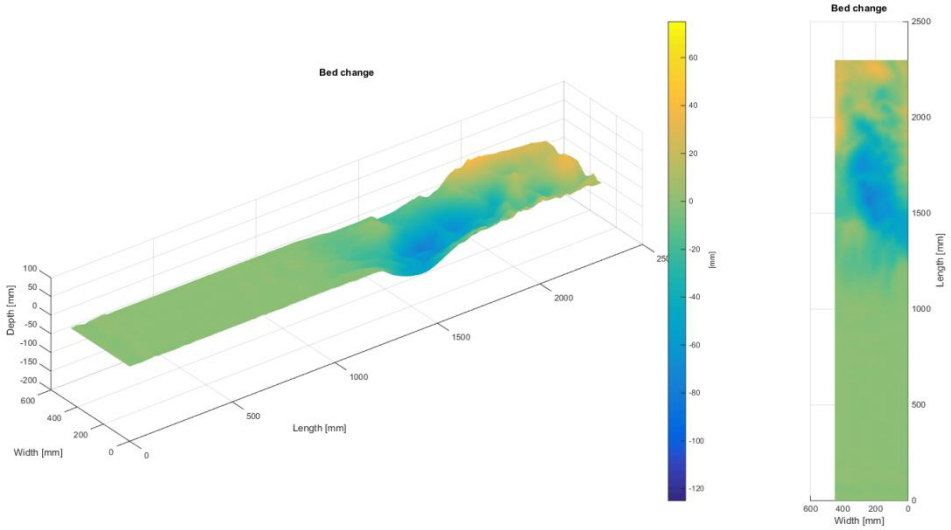

Figure 146; 0[h]-24[h] bed change projection

If the bed change in Figure 146 is observed, it can be clearly seen that the bed is barely affected in the first 1000 [mm]. Furthermore erosion can again be clearly observed to slightly favor the right half of the maximum contracted section between 1200 [mm] and 1600 [mm]. From the sediment transport table (Table 36) it can be observed that the bulk of the scour occurs in the area of maximum contraction.

Table 36; Volume change per sector in [cm^3]

	Upstream	Contraction	Constriction	Expansion	Downstream
Volume	-0,7	-255,2	-8024,3	-1458,8	+877,0

Velocity Profiles

It can observed that a similar velocity profile exists at location 1 & 3 as at the beginning of the experiment. This can easily be explained as the bed has not been affected at these locations. Location 5 shows a significant shift, and seemingly shows a more disturbed shape. Location 6 seems unaffected and remains the same while location 9 has moved from a profile like location 3 to a profile more like location 6.

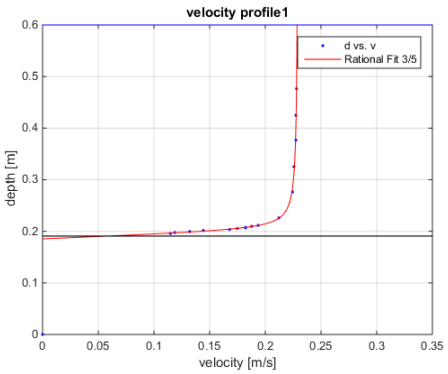

Figure 147; Velocity profile Location 1 [24h]

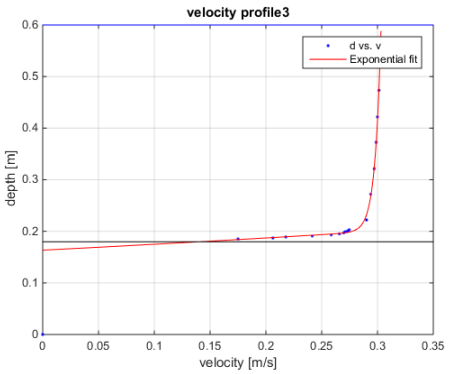

Figure 148; Velocity profile Location 3 [24h]

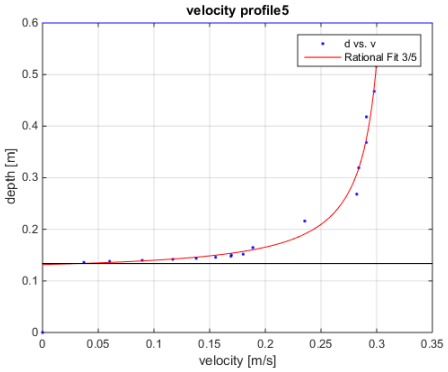

Figure 149; Velocity profile Location 5 [24h]

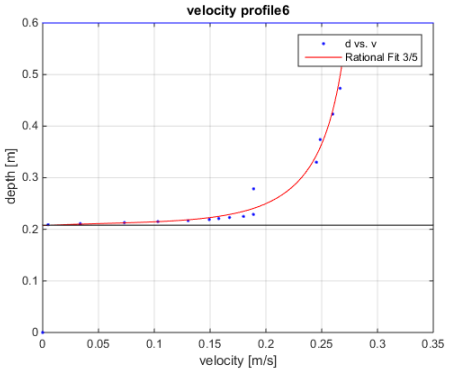

Figure 150; Velocity profile Location 6 [24h]

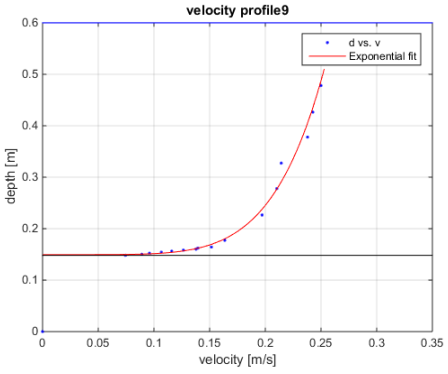

Figure 151; Velocity profile Location 9 [24h]

Table 37; Average Velocity

Location	Average Velocity [m/s]
1	0,2189
3	0,2936
5	0,2601
6	0,2309
9	0,2101

Relative fluctuation intensity

Looking at the relative fluctuation intensity, we can observe a slight increase at location 1, 2 & 7. The slight indenture that has formed at the entry point is most likely the cause for this. Furthermore little to no change has occurred at locations 3 & 4. All other locations show a strong increase in the relative fluctuation intensity. These locations also show the largest bed changes.

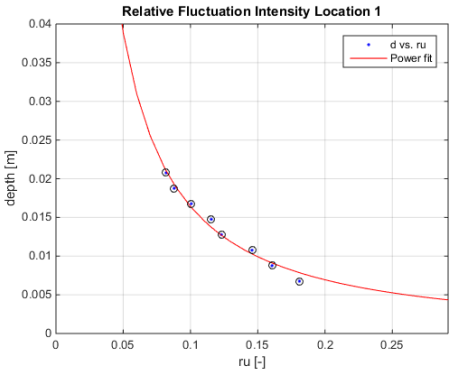

Figure 152; RU location 1 [24h]

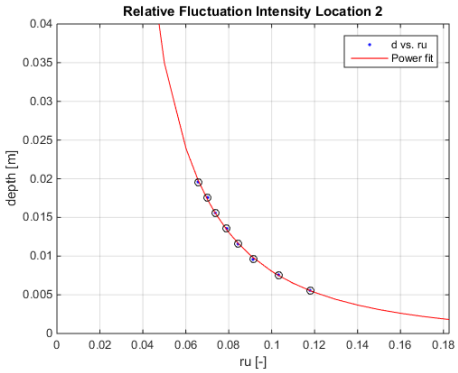

Figure 153; RU location 2 [24h]

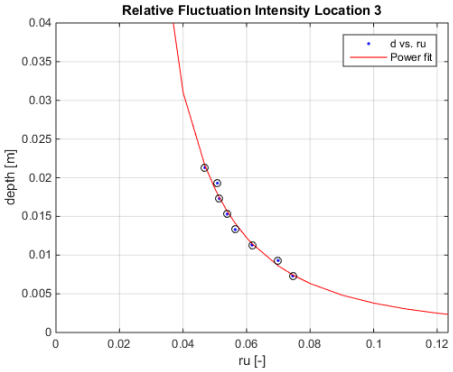

Figure 154; RU location 3 [24h]

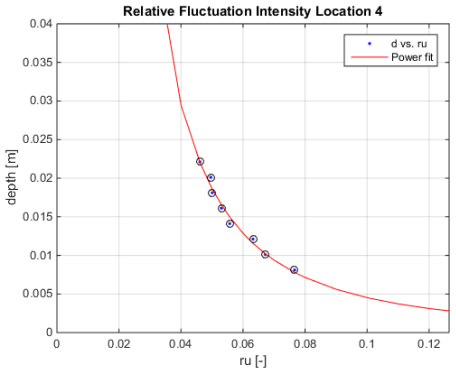

Figure 155; RU location 4 [24h]

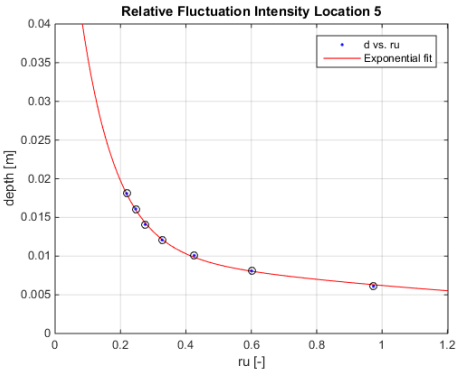

Figure 156; RU location 5 [24h]

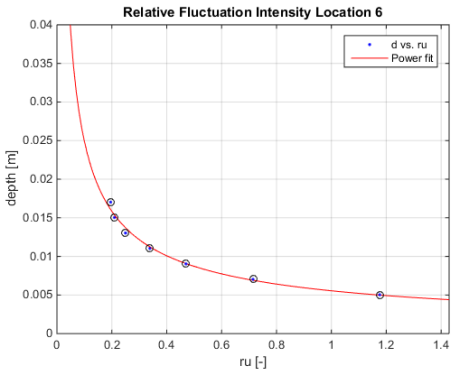

Figure 157; RU location 6 [24h]

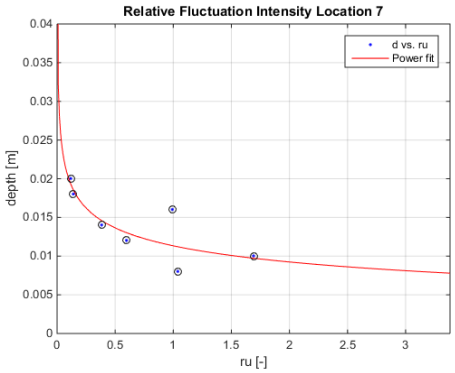

Figure 158; RU location 7 [24h]

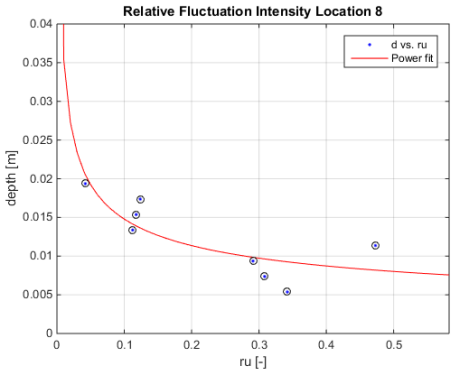

Figure 159; RU location 8 [24h]

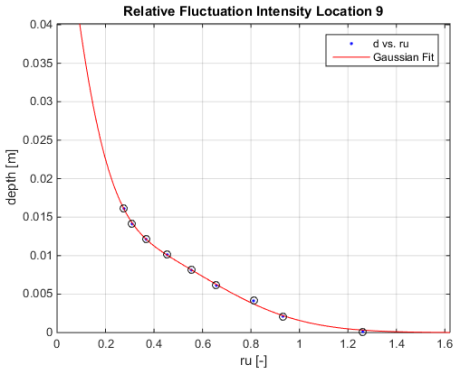

Figure 160; RU location 9 [24h]

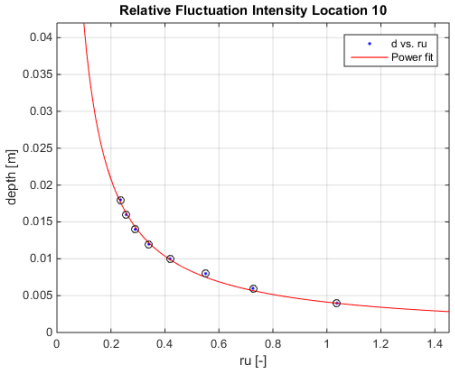

Figure 161; RU location 10 [24h]

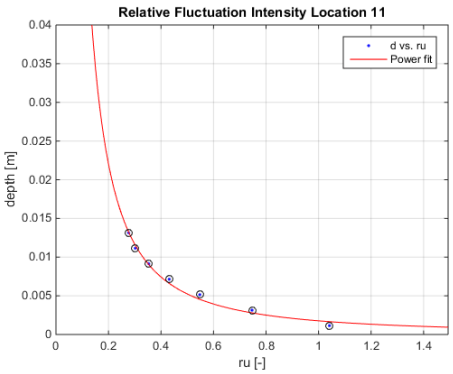

Figure 162; RU location 11 [24h]

Bed shear stress

The bed shear stress was determined with Reynolds formula stated in (Schiereck & Verhagen, 2012). Bed shear stresses are determined by averaging the estimation for bed shear stress, over the centimeter measured above the bottom for a time frame of 3 minutes measuring at 50 [hz] per second, excluding all measured values that do not confirm with a signal to noise ratio above 15 and a correlation of 90%. Observable is that bed shear stresses are highest in the constriction-sector (4-5-6 & 9,10) with the exception of location 8. Locations 6 and 11 in the downstream sector also experience high bed shear stresses.

Table 38; Bed shear stresses [n/m^2]

Location	1	2	3	4	5	6	7	8	9	10	11
	0,003	-0,083	-0,064	-0,125	-0,442	-0,367	-0,005	0,004	-0,391	-0,166	-0,337

Estimation of transport

Following the formulations of the bed load transport by van Rijn (van Rijn, 2018). The results are represented as such, that locations at the same longitudinal location are coupled and transport is averaged over these locations (Table 39). For the calculations the absolute value was taken of the measured bed shear stresses. The results are also depicted per sector (Table 40) by calculating the area underneath each cross-sectional measurement. In this way it is observed that scour is to be expected at locations 4|9, 5|10, & 6|11. The results predict strong scour at the interface between the constriction and the expansion sector as well as the interface between the expansion and the downstream sectors.

Table 39; Bed load transport [kg/m/s]

Location	1	2 & 7	3 & 8	4 & 9	5 & 10	6 & 11
	NaN	NaN	NaN	0,00102	0,00230	0,00413

Table 40; Bed load transport per sector [kg/day]

Sector	Upstream	Contraction	Constriction	Expansion	Downstream
	NaN	NaN	29,2	130,0	18,6

Water level

The water levels were measured at locations 1,3,5,6 they are depicted in Table 41. The levels were computed by measuring at 1000 [hz] for 15 seconds, and averaging those results. It is observed that the water level shows a drop of 0,4 [cm]. The water level seems to drop during constriction, while shortly downstream of the constriction the water level seems to increase slightly with 0,1 [cm]

Table 41; Water level [cm]

Location	1	3	5	6
	39,6820	39,2486	39,1301	39,2492

Measurements after 48h

Bed level

A projection of the bed after running for 24 [h] can be observed in Figure 163. The bed continued to show a very particular development of scour, heavily favoring one side of the maximum contracted section of the flume. Again, the absence of scour in the upstream part of the model followed predictions with respect to the in advance calculated values of shields transport for this section.

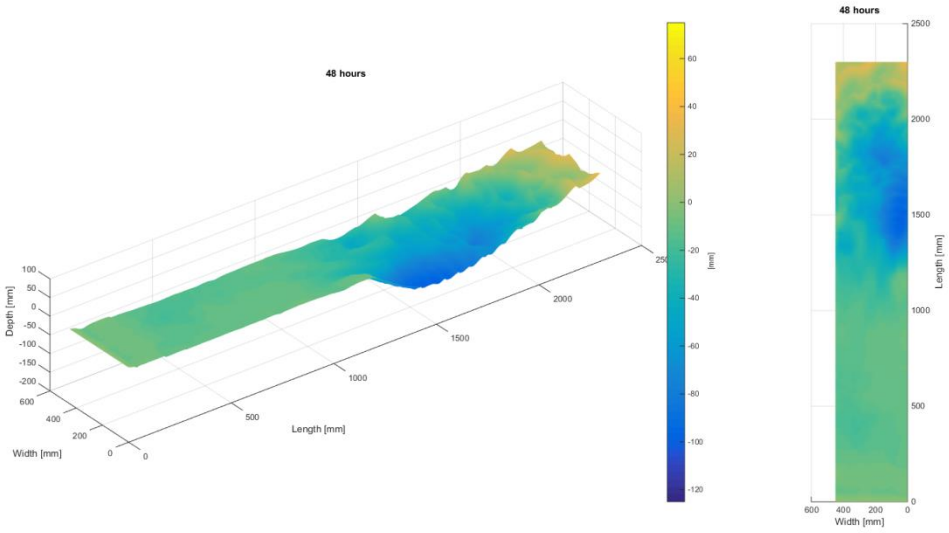

Figure 163; 48[h] bed projection

The average transect observable in Figure 164Figure 13, shows scouring has reached an average of 60 [mm]. This is however strongly skewed as one half of the maximum contracted section shows scour up till 100 [m] and the other side shows scour between 0-40 [mm]. The scour pattern is in agreement with the bed shear stresses determined at 24 hours after initiation of flow.

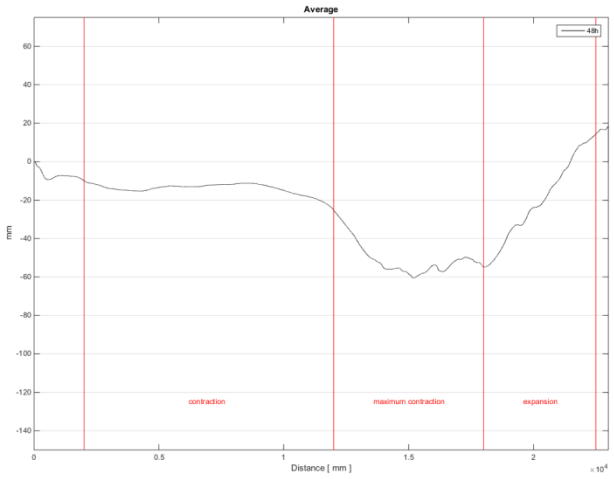

Figure 164; 48[h] average transect

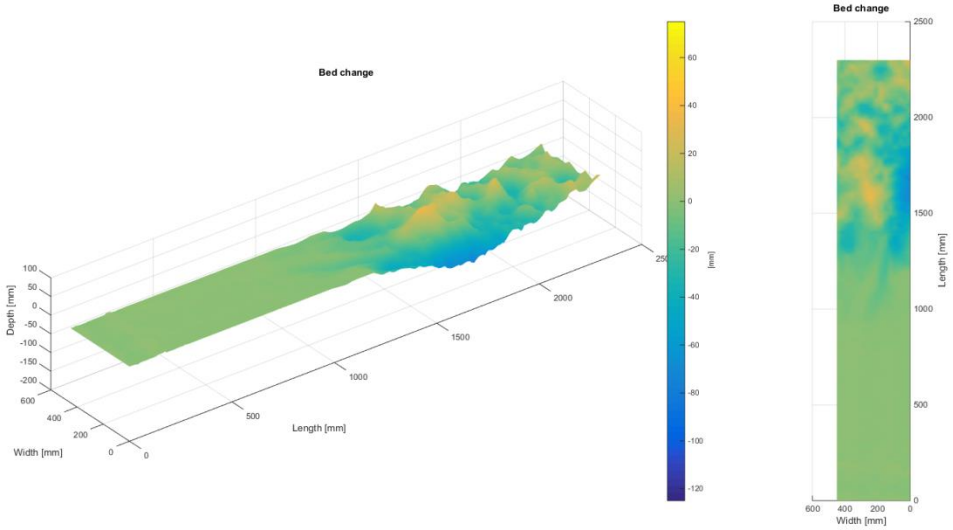

Figure 165; 24[h]-48[h] bed change projection

Furthermore Figure 165 shows that the particular erosion that had developed only further increased in magnitude towards the already eroded area. The sediment transport table (Table 42) also clearly shows that virtually no scour occurs in the contraction-sector while being concentrated in constriction-sector. On average total scour has slightly reduced with respect to the first 24 hours.

Table 42; Volume change per sector in [cm^3]

	Upstream	Contraction	Constriction	Expansion	Downstream
Volume	-0,8	-345,5	-4035,3	-2622,4	-74,2

Velocity Profiles

It can observed that a similar velocity profile exists at location 1 & 3 as at the beginning of the experiment. Locations 5 & 6 have also assumed a profile more alike to locations 1 & 3. Compared with the measurement at 24 hours, flow profile 9 seems to have been strongly disturbed. This is consequently also the location of maximum scour in the experiment and the disturbance is most like due to a sort of wake having been formed.

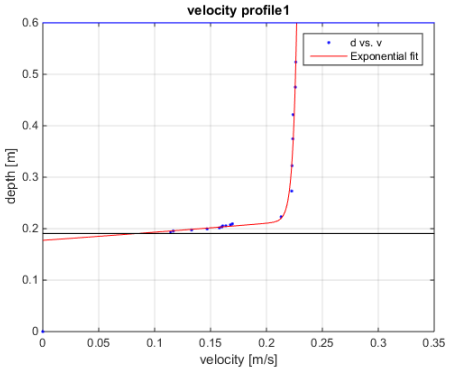

Figure 166; Velocity profile Location 1 [48h]

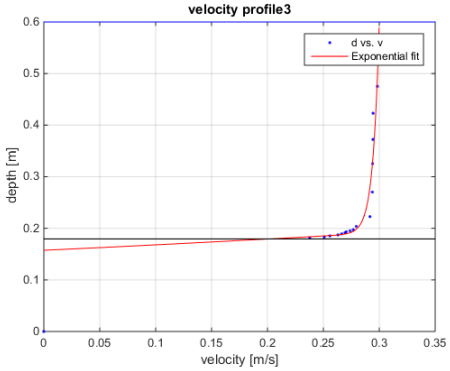

Figure 167; Velocity profile Location 3 [48h]

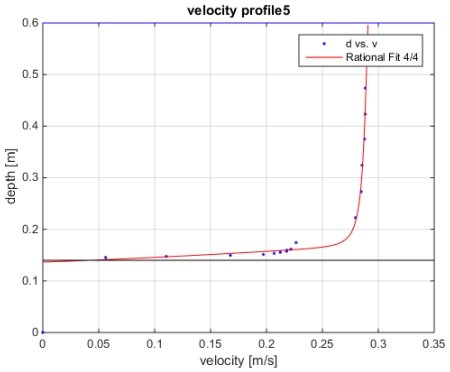

Figure 168; Velocity profile Location 5 [48h]

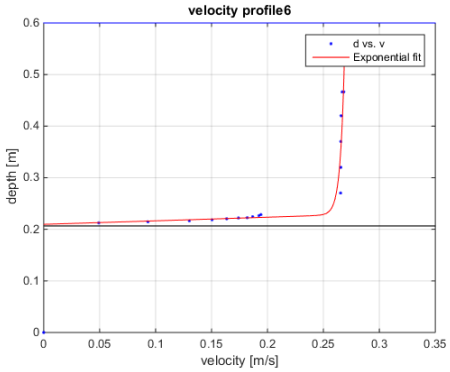

Figure 169; Velocity profile Location 6 [48h]

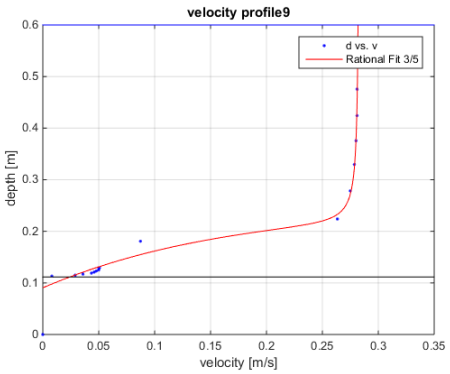

Figure 170; Velocity profile Location 9 [48h]

Table 43; Average Velocity

Location	Average Velocity [m/s]
1	0,2163
3	0,2914
5	0,2725
6	0,2510
9	0,2247

Relative fluctuation intensity

Locations 1,2,3 & 10 show little change with respect to relative fluctuation intensity measured at 24 [h], locations 5,6 & 7 saw a decrease while locations 4,8,9 & 11 showed a moderate to strong increase of relative fluctuation intensity. These locations were also locations of significant bed change.

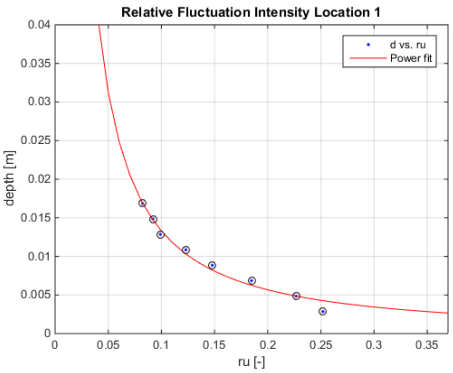

Figure 171; RU location 1 [48h]

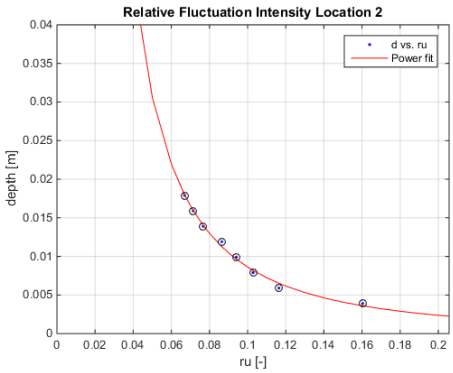

Figure 172; RU location 2 [48h]

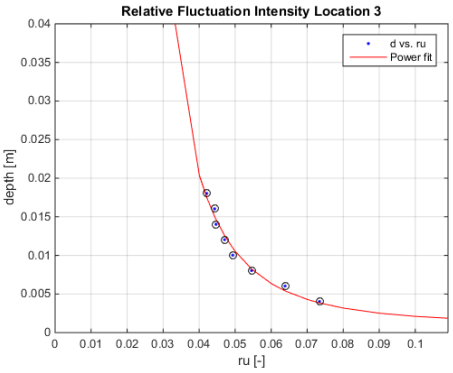

Figure 173; RU location 3 [48h]

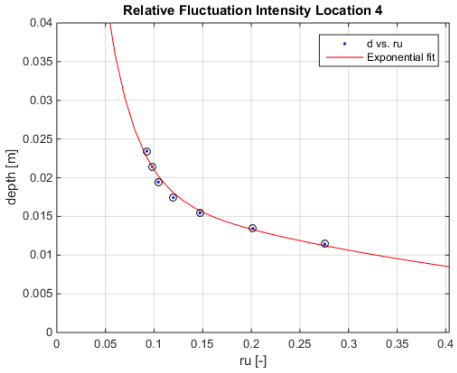

Figure 174; RU location 4 [48h]

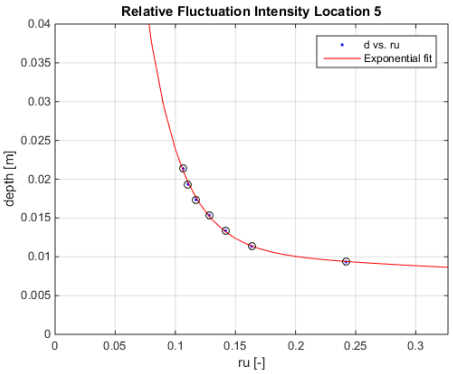

Figure 175; RU location 5 [48h]

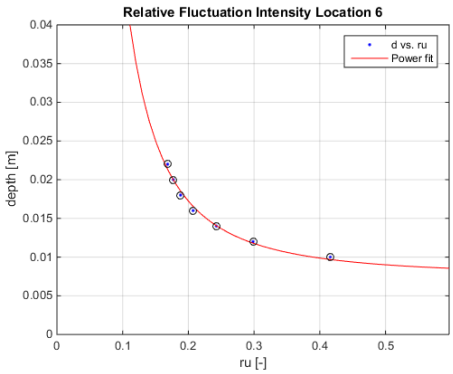

Figure 176; RU location 6 [48h]

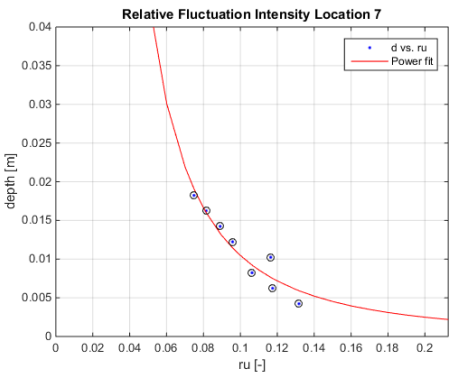

Figure 177; RU location 7 [48h]

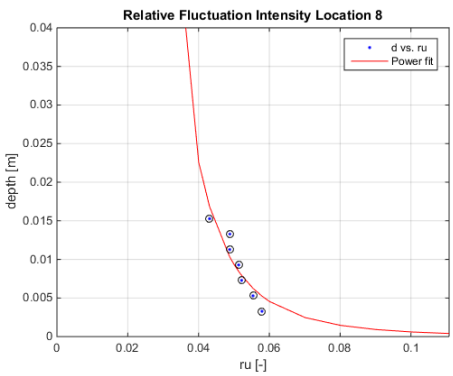

Figure 178; RU location 8 [48h]

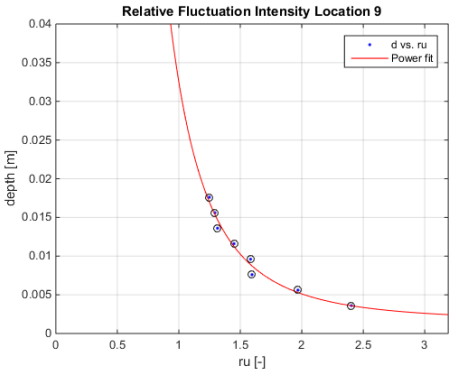

Figure 179; RU location 9 [48h]

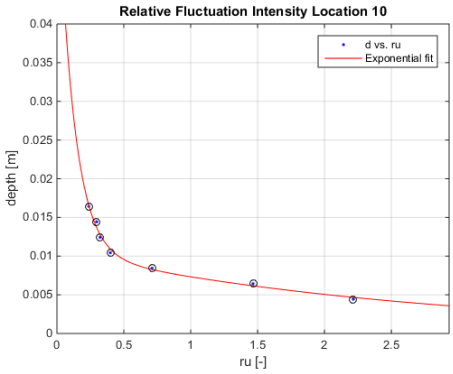

Figure 180; RU location 10 [48h]

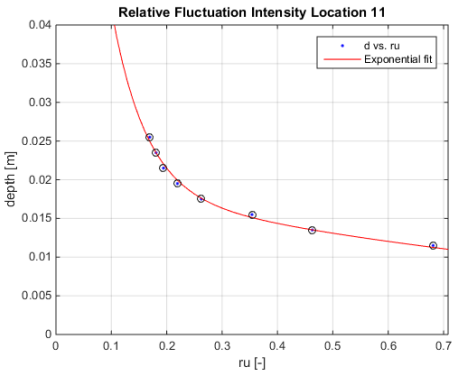

Figure 181; RU location 11 [48h]

Bed shear stress

The bed shear stress was determined with Reynolds formula stated in (Schiereck & Verhagen, 2012). Bed shear stresses are determined by averaging the estimation for bed shear stress, over the centimeter measured above the bottom for a time frame of 3 minutes measuring at 50 [hz] per second, excluding all measured values that do not confirm with a signal to noise ratio above 15 and a correlation of 90%. Observable is that bed shear stresses are highest in the center and near the end of the constriction-sector (locations 5-6). Locations 6 and 11 also experience high bed shear stresses although the magnitude has reduced with respect to earlier measurements.

Table 44; Bed shear stresses [n/m^2]

Location	1	2	3	4	5	6	7	8	9	10	11
	-0,043	-0,023	-0,040	-0,051	-0,109	-0,172	-0,059	0,071	0,068	0,026	0,114

Estimation of transport

Following the formulations of the bed load transport by van Rijn (van Rijn, 2018). The results are represented as such, that locations at the same longitudinal location are coupled and transport is averaged over these locations (Table 45). For the calculations the absolute value was taken of the measured bed shear stresses. The results are also depicted per sector (Table 46) by calculating the area underneath each cross-sectional measurement. In this way it is observed that scour is to be expected at location 6 only, but rates are very low and no sector should experience scour with the given bed shear stresses.

Table 45; Bed load transport [kg/m/s]

Location	1	2 & 7	3 & 8	4 & 9	5 & 10	6 & 11
	NaN	NaN	NaN	NaN	NaN	NaN

Table 46; Bed load transport per sector [kg/day]

Sector	Upstream	Contraction	Constriction	Expansion	Downstream
	NaN	NaN	NaN	NaN	NaN

Water level

The water levels were measured at locations 1,3,5,6 they are depicted in Table 47. The levels were computed by measuring at 1000 [hz] for 15 seconds, and averaging those results. It is observed that the water level shows a drop of 0,5 [cm]. The water level seems to drop during constriction, while shortly downstream of the constriction the water level seems to increase slightly with 0,1 [cm]

Table 47; Water level [cm]

Location	1	3	5	6
	40,1694	39,6525	39,5658	39,6514

Measurements after 72h

Bed level

After 72 hours, scour continued to occur only at the constriction-sector while still heavily favoring the right hand side. Scour depths up to 120 [mm] were observed (Figure 182). The average transect in Figure 183 showed the maximum scour to be around 80 [mm] and occurred at the end of the maximum contracted section of the model.

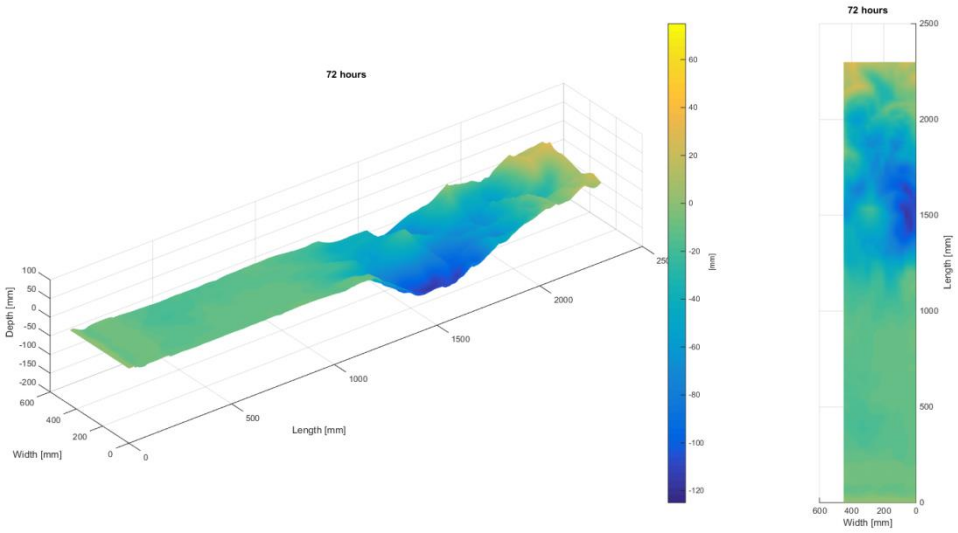

Figure 182; 72[h] bed projection

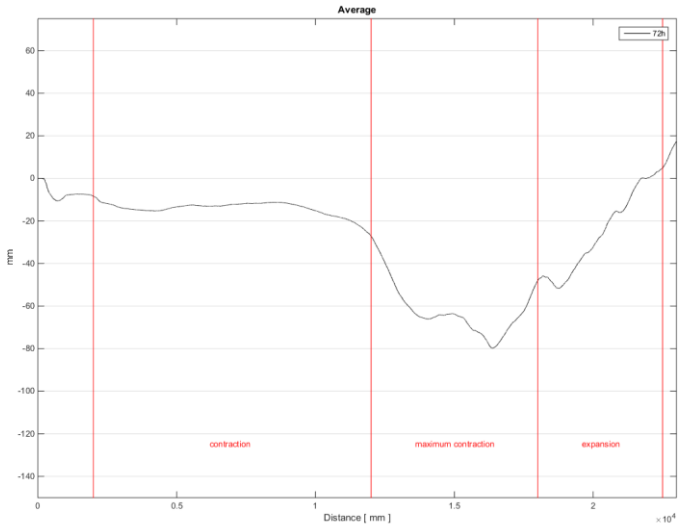

Figure 183; 72[h] average transect

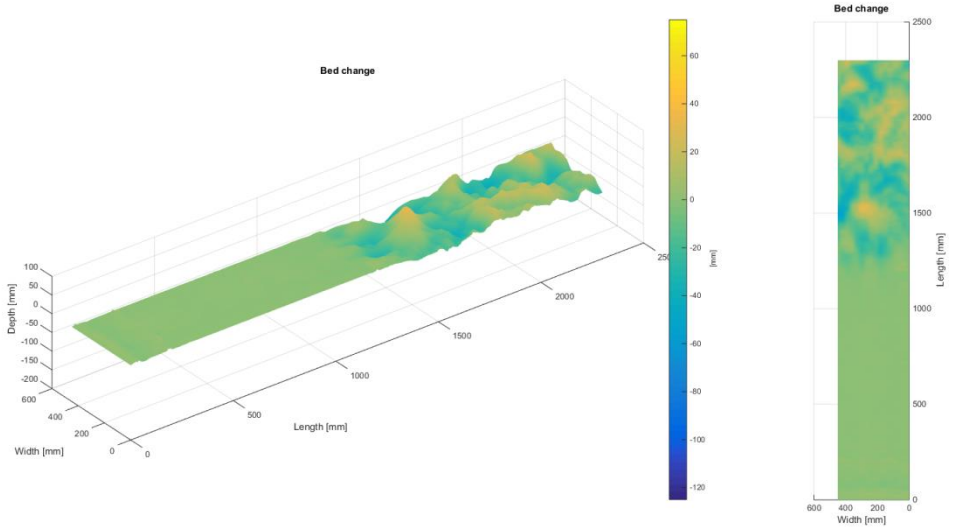

Figure 184; 0[h]-72[h] bed change projection

It can be observed from Figure 184 that scour now occurred more equally divided over the maximum contracted section of the experiment. And the strongest scour with respect to the measurement taken at 48 [h], occurred on the left side of the model. This is also in agreement with the bed shear stresses determined at 48 [h], which predicted a more even distributed scour pattern.

The sediment transport table (Table 48) now shows a strongly reduced scour rate with respect to earlier measurements, as total scour has now nearly halved in magnitude. As earlier noted, it can again be observed most of the scour occurs in constriction and expansion sectors while little to no scour occurs upstream of these regions.

Table 48; Volume change per sector in [cm^3]

	Upstream	Contraction	Constriction	Expansion	Downstream
Volume	+25,5	-9,9	-3232,1	-1006,2	-347,6

Velocity Profiles

Velocity profiles at location 1 & 3 are still unaffected, locations 5 showed a slight shift from a turbulent velocity profile to a logarithmic velocity profile. Profile 6 remained almost un-afflicted while the profile at location 9 shows a very distinct profile which points to a strong reduction in flow velocity at this location.

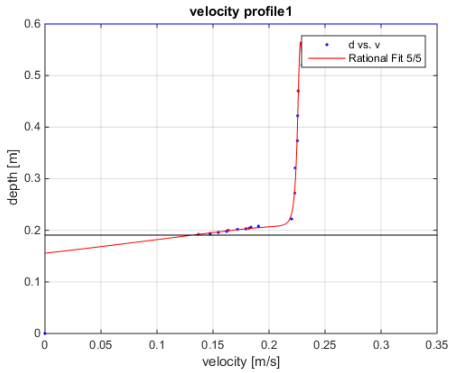

Figure 185; Velocity profile Location 1 [72h]

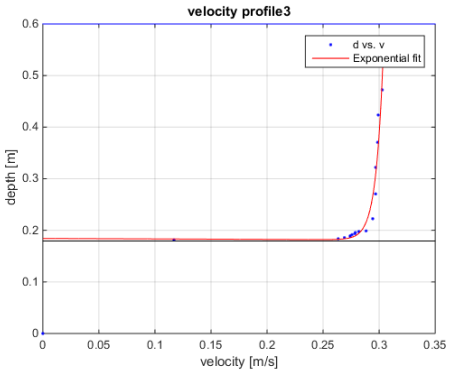

Figure 186; Velocity profile Location 3 [72h]

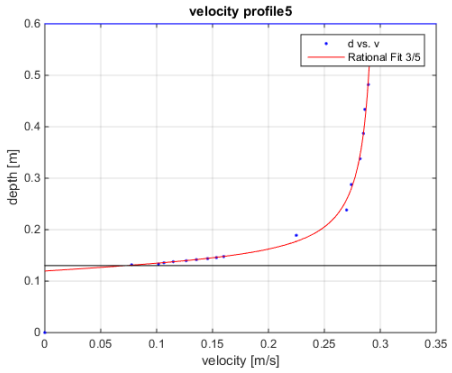

Figure 187; Velocity profile Location 5 [72h]

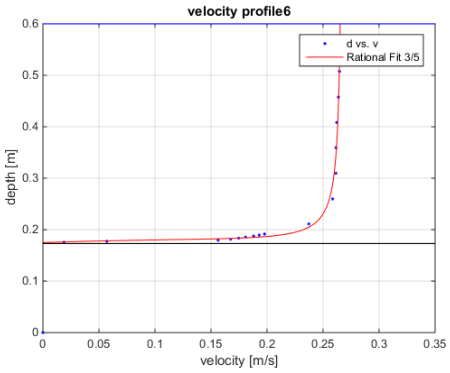

Figure 188; Velocity profile Location6 [72h]

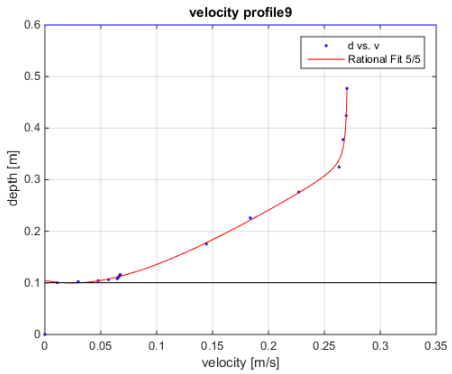

Figure 189; Velocity profile Location 9 [72h]

Table 49; Average Velocity

Location	Average Velocity [m/s]
1	0,2192
3	0,2940
5	0,2577
6	0,2507
9	0,2071

Relative fluctuation intensity

With respect to the measurements conducted at 48 hours no significant change of fluctuation intensity was observed at locations 1, 2, 3, 6, 7, 8 & 10. A reduction was observed at location 5 while locations 4 & 11 saw an increase and location 9 saw a strong increase. This can be attributed to the fact that the average flow velocity near the bed at location 10 has decreased such that similar fluctuations then start to have a much larger effect.

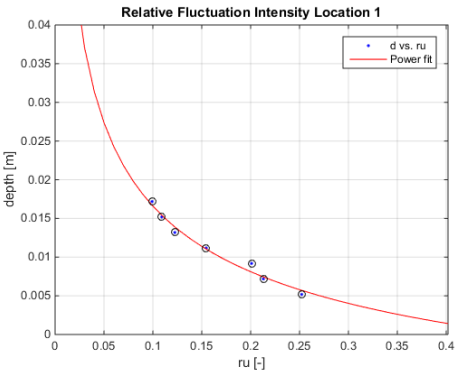

Figure 190; RU location 1 [72h]

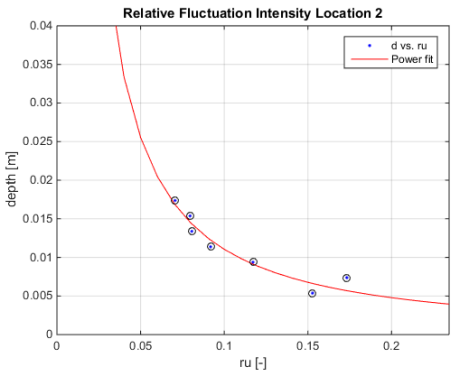

Figure 191; RU location 2 [72h]

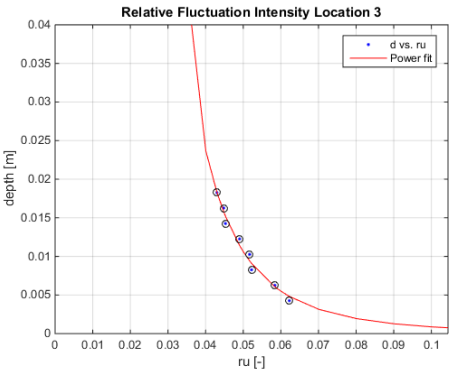

Figure 192; RU location 3 [72h]

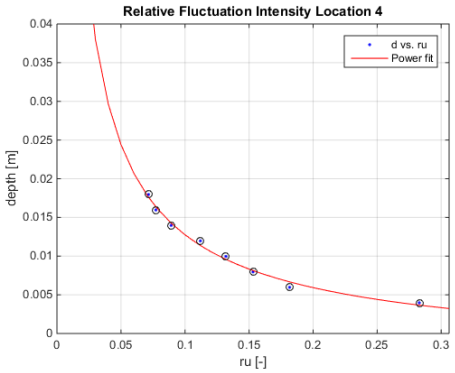

Figure 193; RU location 4 [72h]

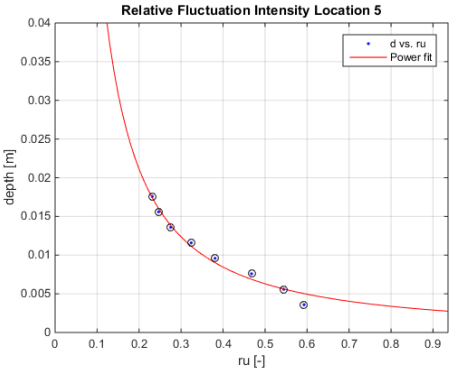

Figure 194; RU location 5 [72h]

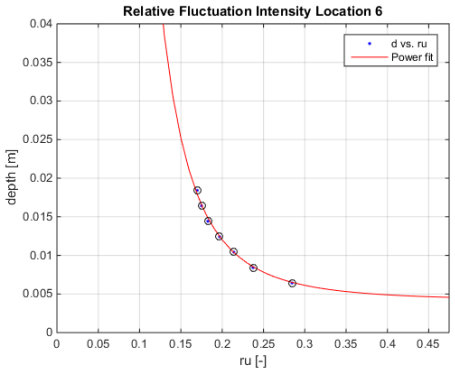

Figure 195; RU location 6 [72h]

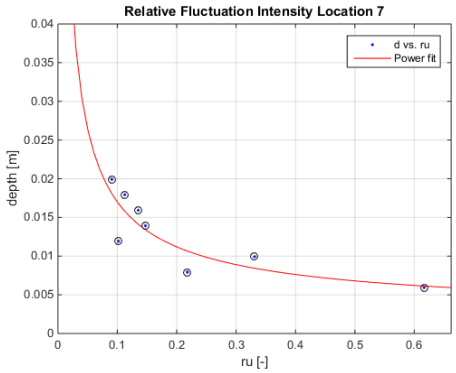

Figure 196; RU location 7 [72h]

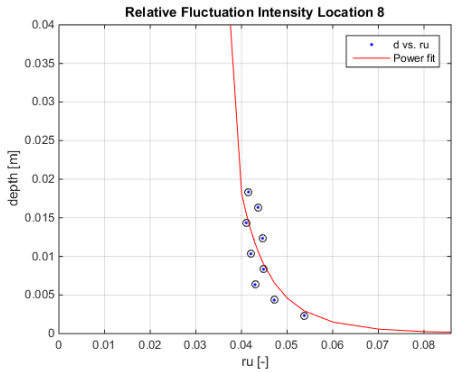

Figure 197; RU location 8 [72h]

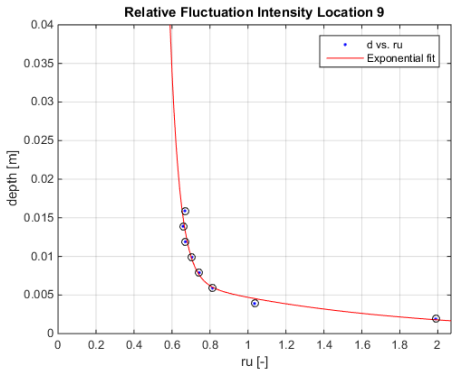

Figure 198; RU location 9 [72h]

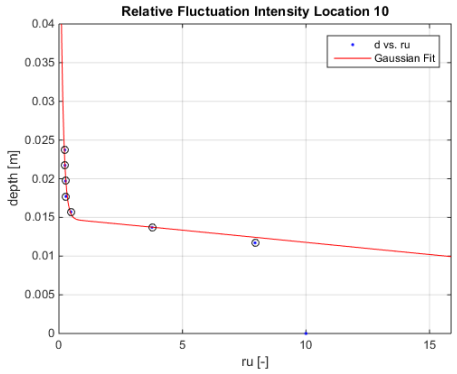

Figure 199; RU location 10 [72h]

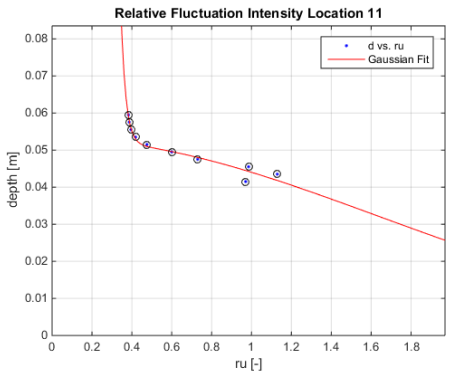

Figure 200; RU location 11 [72h]

Bed shear stress

The bed shear stress was determined with Reynolds formula stated in (Schiereck & Verhagen, 2012). Bed shear stresses are determined by averaging the estimation for bed shear stress, over the centimeter measured above the bottom for a time frame of 3 minutes measuring at 50 [hz] per second, excluding all measured values that do not confirm with a signal to noise ratio above 15 and a correlation of 90%. Observable is that bed shear stresses (Table 50) are still high at locations 5-6 and 10, locations that have already experienced a great deal of scour. Location 11 was measured to far above the bed to be included in the results.

Table 50; Bed shear stresses [n/m^2]

Location	1	2	3	4	5	6	7	8	9	10	11
	-0,114	-0,051	0,046	-0,095	-193,0	-0,178	-0,013	-0,018	-0,056	0,220	NaN

Estimation of transport

Following the formulations of the bed load transport by van Rijn (van Rijn, 2018). The results are represented as such, that locations at the same longitudinal location are coupled and transport is averaged over these locations (Table 51). For the calculations the absolute value was taken of the measured bed shear stresses. The results are also depicted per sector (Table 52) by calculating the area underneath each cross-sectional measurement. In this way it is observed that scour is to be expected at locations 5|10 & 6|11.

Table 51; Bed load transport [kg/m/s]

Location	1	2 & 7	3 & 8	4 & 9	5 & 10	6 & 11
	NaN	NaN	NaN	NaN	0,000197	$2{,}219*10^{-5}$

Table 52; Bed load transport per sector [kg/day]

Sector	Upstream	Contraction	Constriction	Expansion	Downstream
	NaN	NaN	1,3	4,4	0,1

Water level

The water levels were measured at locations 1,3,5,6 they are depicted in Table 53. The levels were computed by measuring at 1000 [hz] for 15 seconds, and averaging those results. It is observed that the water level shows a drop of 0,6 [cm]. The water level seems to drop during constriction, while shortly downstream of the constriction the water level seems to stay approximately the same.

Table 53; Water level [cm]

Location	1	3	5	6
	39,9297	39,5127	39,4150	39,3698

Measurements after 96h

Bed level

After 96 [h] it can be seen from Figure 201 & Figure 202 that scour still heavily favored the right side of the maximum contracted area of the flume. Scour was also almost completely within the area of maximum contraction and scour barely showed up outside of this region. This was in strong contradiction with Basic scour experiments I & II and also not in full agreement with the shields criterion. Some erosion should have occurred a bit further upstream. Possible culprits could be some intrusion of clay into the sand as well as washing out of some of the finer particles from previous experiments. Average maximum was around 80 [mm] after 96 hours.

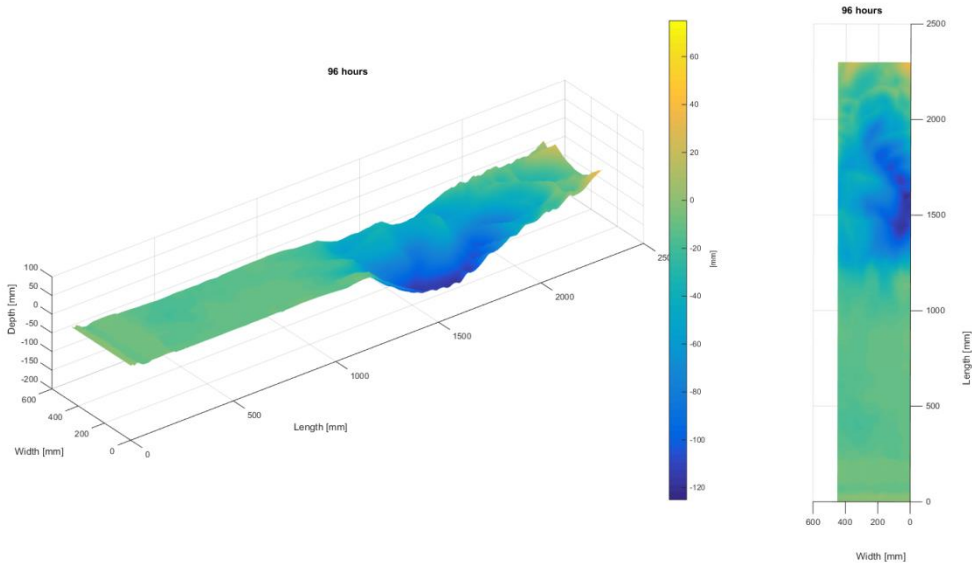

Figure 201; Bed map after 96 [h]

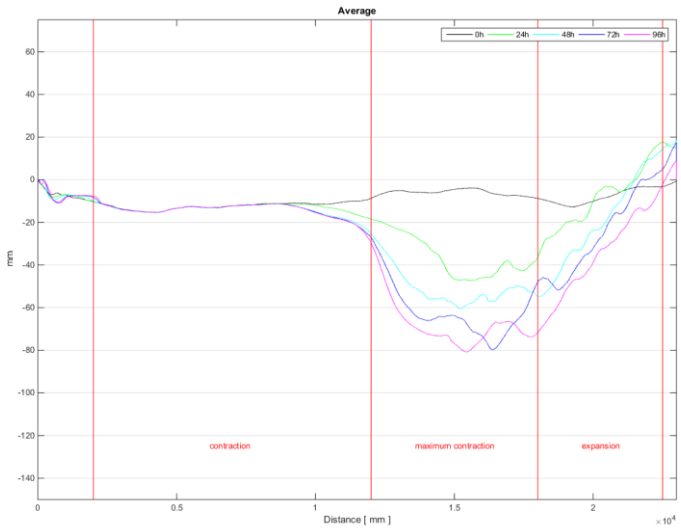

Figure 202; Average transects through time

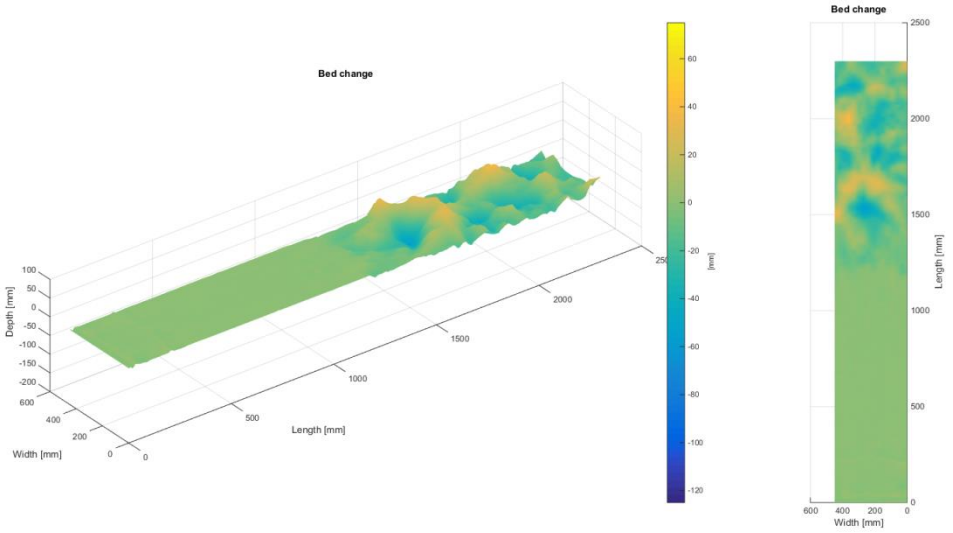

Figure 203; Bed change with respect to 72[h]

If Figure 49 is observed, it can be concluded that scour still favored the right side if the maximum contracted section of the experiment, even though this area had already undergone a significant amount of scour more than the left side.

The sediment transport Table 54, again shows a slight reduction of total scour and a strong reduction of scour in the area of maximum contraction. The largest amount of scour now occurred in the expanding section of the model. The total quantity of scour did amount to roughly 25000 [cm^3] after this time.

Table 54; Volume change per sector in [cm^3]

	Upstream	Contraction	Constriction	Expansion	Downstream
Volume	-7,5	+0,4	-1288,7	-2352,7	-434,9

Concluding Remarks

This third basic scour showed optimal usage of the vectrino Doppler, and bed maps showed a clear development of scour in the section of maximum contraction, virtually no upstream progression was shown to develop. Furthermore, after 96 hours scour maximum scour was about 122 [mm] and cross section average maximum scour was about 81 [mm].

Appendix C I

I Introduction

Burial scour experiments are the second type of experiments conducted. It includes the placement of a single log on the bed, and measuring/monitoring erosion/scour that occurs around the log. The log was placed in the area of maximum contraction and it was chosen to vary velocities in between experiments of this type to simulate a naturally non-eroding as well as an eroding bed. For this reason 5 similar experiments were conducted.

This report focuses on the first of this kind of experiment, with a water depth of 40[cm], a width of 0.52 [cm] and a discharge of 40 [l/s]. This would therefore lead to an average velocity of 0.19 [cm/s] which should not violate shields parameter 1 (only occasional movement at some locations).

Observations at 0h

In Figure 204, it can be observed that at imitation of flow, the bed was relatively flat around the log.

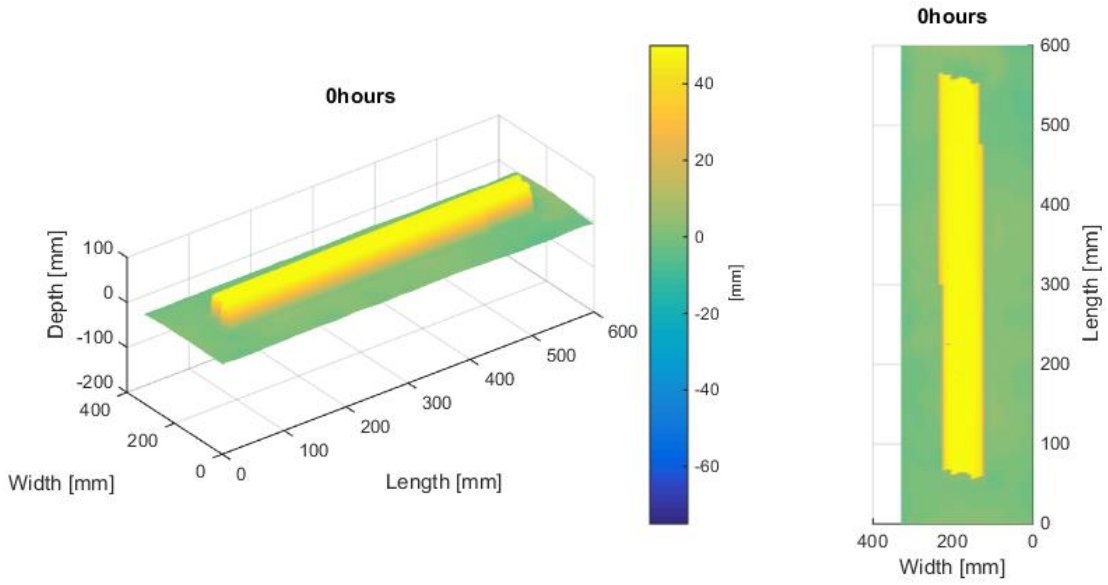

Figure 204; Bed topography at 0 hours

Observations at 18h

After 18 hours bed topography was measured and video footage that was taken during the previous 18 hours was analyzed. From Figure 205 it can be clearly observed that the bed has shown to develop relatively small bedforms around the log. A small indenture had started to develop at the face of the log and a wavy pattern of sand particles has started to appear around and near the sides of the log. The size of these bedforms were limited to less than a centimeter

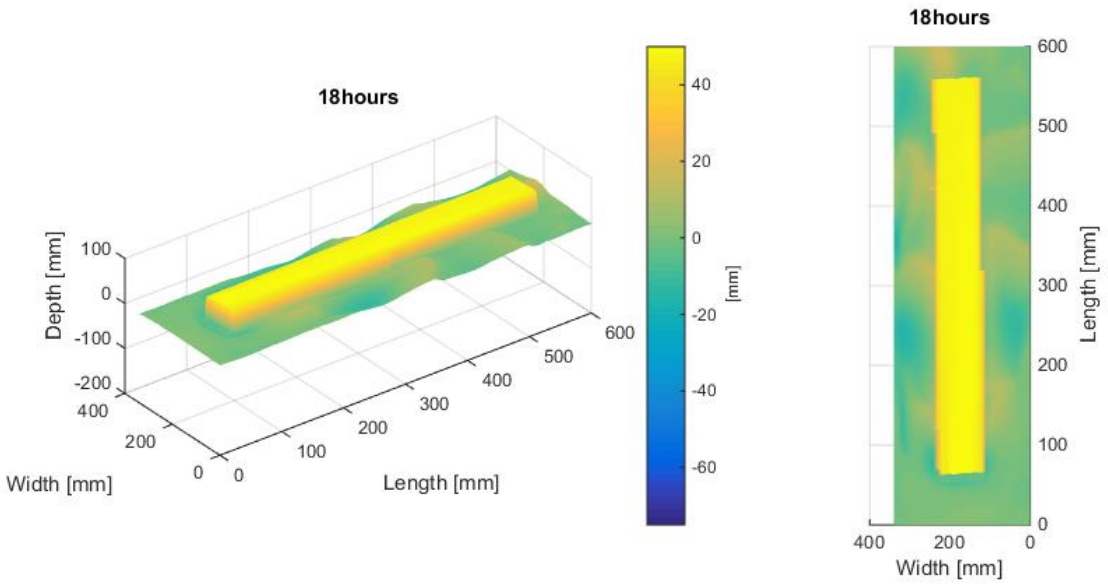

Figure 205; Bed topography after 18 hours

0h00m

At initiation of flow (Figure 206), it could be observed that the bed showed no visible bedforms. The log was placed parallel to the flow conditions with the help of the laser equipment installed on the overhead kart.

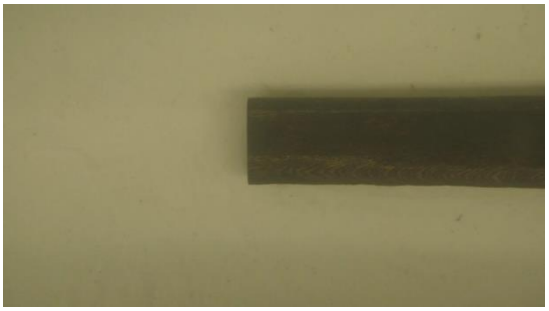

Figure 206; 0h00m

2h30m

After two and a half hour of flow (Figure 207) a minor indenture could be observed at the face of the log. Furthermore, some small bedforms have started to develop near the sides.

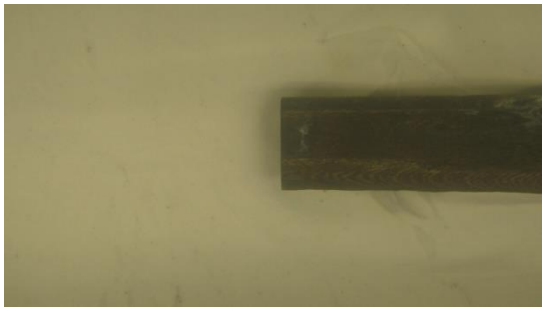

Figure 207; 2h30m

5h00m

After 5 hours (Figure 208) it could be observed that all the bedforms near the side grew in width. But from observations the magnitude of change was limited.

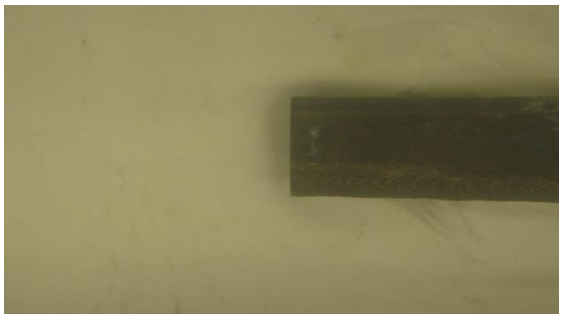

Figure 208; 5h00m

7h30m

At 7 and a half hour (Figure 208) the only observable change was the downstream movement of the bedforms close to the sides.

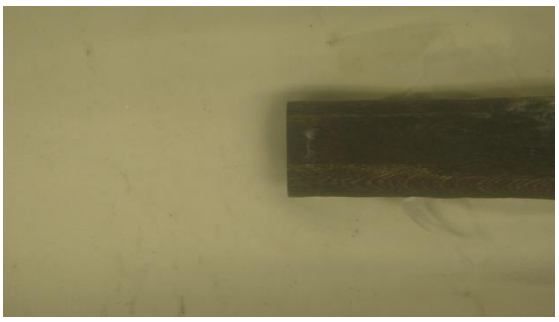

Figure 209; 7h30m

10h00m

After 10 hours (Figure 210), observable changes were again limited and it was decided to end the experiment after 24 hours due to the visibly slow progression of scour.

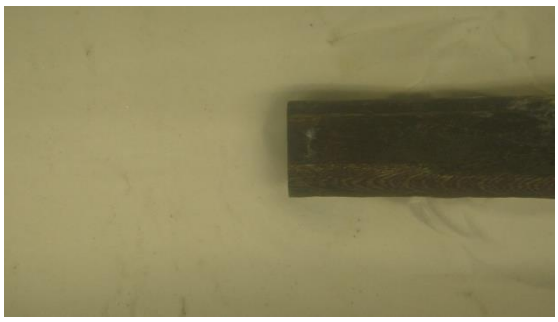

Figure 210; 10h00m

Observations at 24h

After 24 hours bed topography was measured. From Figure 211 it can be clearly observed that the bed has not shown to be that significant and only small indentures in and around the log were present. Because progression of the bedforms appeared to be slow, it was decided to end the experiment.

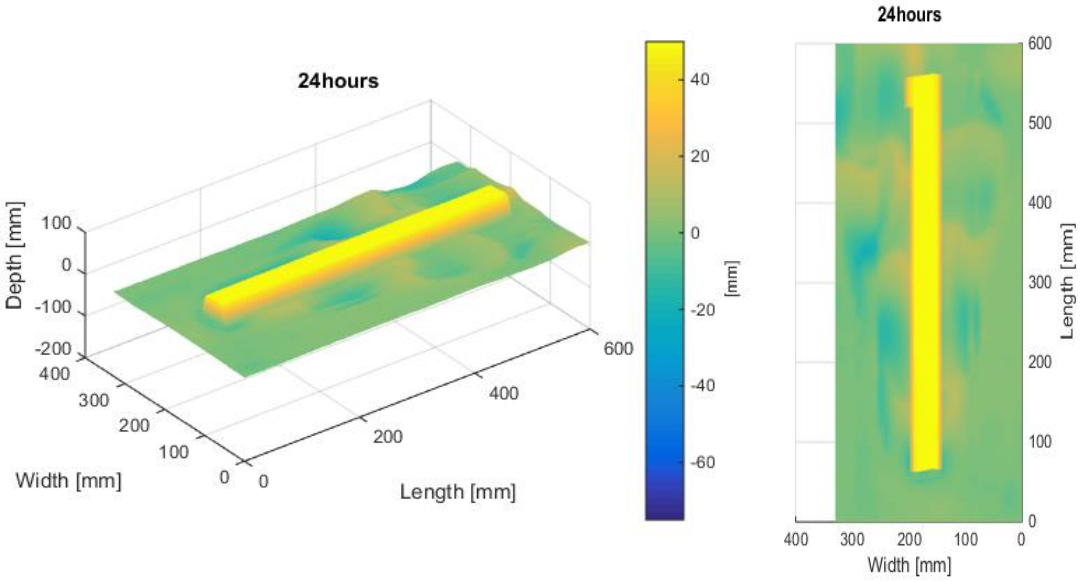

Figure 211; Bed topography after 24 hours

Concluding remarks

The placement of a log on a previously non-eroding bed has shown to develop some minor bedforms. This was as expected with respect to the theory with respect to pier scour. A slight horseshoe shaped scour hole has developed at the face and small bedforms appeared to have been shed from the small scour hole that developed underneath the face of the log. Because progression of these bedforms and scour formation was slow, it was decided to end the experiment and restart the experiment with a higher discharge and thus higher flow velocity; this will be discussed in burial scour II.

Appendix C II

I Introduction

Burial scour experiments are the second type of experiments conducted. It includes the placement of a single log on the bed, and measuring/monitoring erosion/scour that occurs around the log. The log was placed in the area of maximum contraction and it was chosen to vary velocities in between experiments of this type to simulate a naturally non-eroding as well as an eroding bed. For this reason 5 similar experiments were conducted.

This report focuses on the second of this kind of experiment, with a water depth of 40[cm], a width of 0.52 [cm] and a discharge of 45 [l/s]. This would therefore lead to an average velocity of 0.216 [cm/s].

Observations at 0h

In Figure 212, it can be observed that at initiation of flow, the bed was relatively flat around the log.

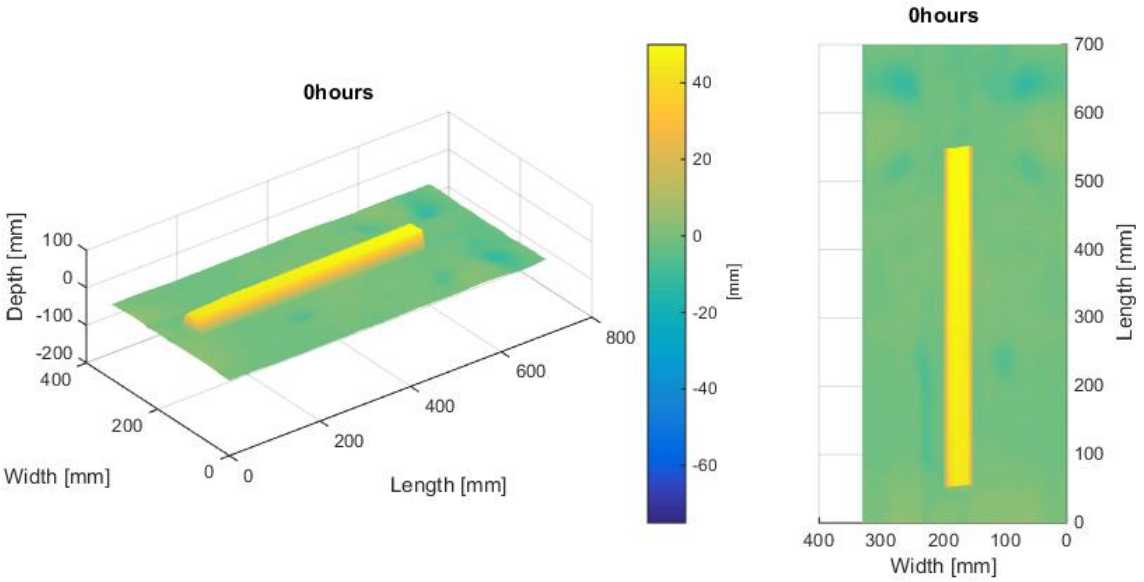

Figure 212; Bed topography at 0 hours

Observations at 24h

After 24 hours bed topography was measured and video footage that was taken during the previous 24 hours was analyzed. From Figure 213 it can be clearly observed that the bed has shown to develop a clear horseshoe shaped scour hole at the upstream face of the log. Furthermore it can be observed that the log has started to tilt into the hole, as the upstream face has dropped over 1 [cm] with respect to the downstream face.

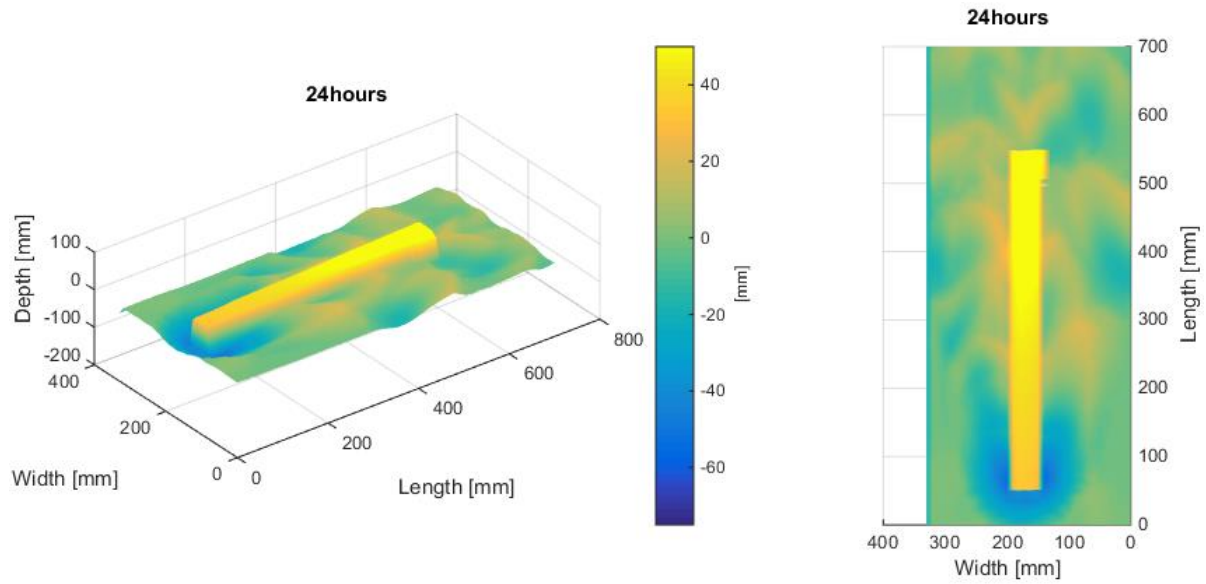

Figure 213; Bed topography after 18 hours

0h00m

At initiation of flow (Figure 214), it could be observed that the bed showed no visible bedforms. The log was placed exactly parallel to the governing flow direction.

Figure 214; 0h00m

0h15m

Shortly after initiation of flow (Figure 215), it could be observed that the bed quickly developed a seemingly symmetrical set of bedforms around the face of the log.

Figure 215; 0h15m

2h30m

After two and a half hour of flow (Figure 216) the bedforms still maintained their symmetry, but grew significantly in magnitude. It was clearly noticeable that the face of the log had completely detached from the surface

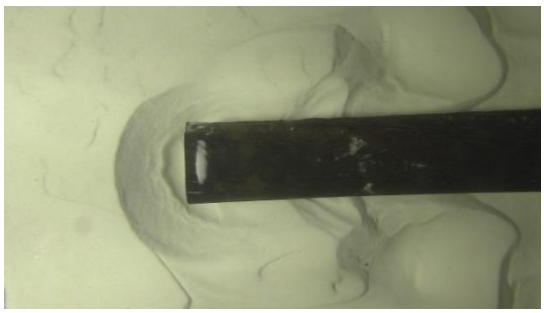

Figure 216; 2h30m

5h00m

After 5 hours (Figure 217) it could be observed that the horseshoe like erosion around the face of the log grew even further and deeper. The overhang of the log grew significantly.

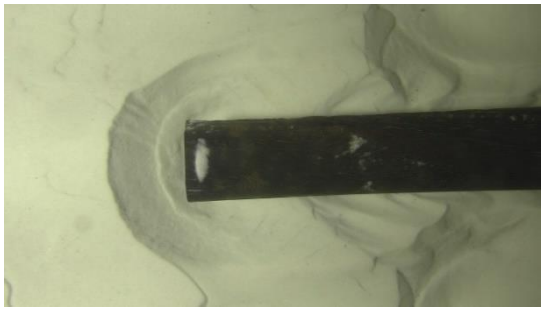

Figure 217; 5h00m

7h30m

At 7 and a half hour (Figure 218) the rate of scour on the slopes upstream reduced. Sediment was still being transported from underneath the log in downstream direction.

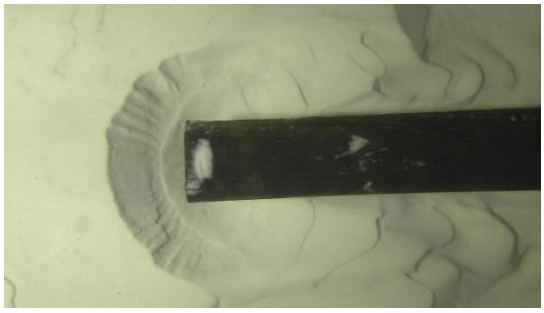

Figure 218; 7h30m

10h00m

After 10 hours (Figure 219), scour appeared to slow down even further, and only occasionally parts of the upstream slope would collapse.

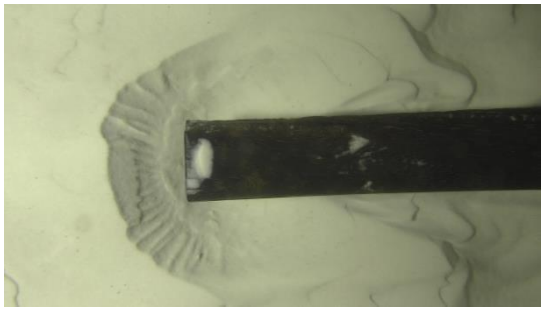

Figure 219; 10h00m

Observations at 48h

After 48 hours bed topography was measured. From Figure 220 it can be clearly observed that the bed forms that developed within the first 24 hours have increased in intensity and the tilting of the log has also increased. It can be observed that scouring at the upstream face of the log now reaches up to 7 [cm] compared with the bed level at the start of the experiment. The downstream face of the log clearly shows accretion limited to 1-3 [cm].

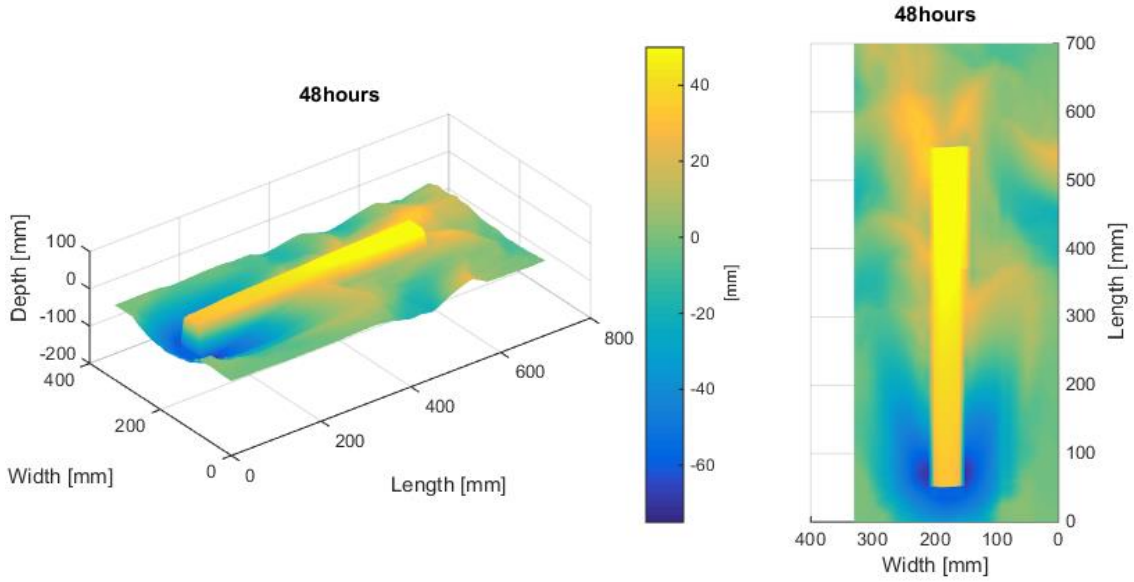

Figure 220; Bed topography after 48 hours

Concluding remarks

The placement of a log on a bed showing little to no movement of bed particles has shown to develop significant scour around the log. This was as expected with respect to the theory with respect to pier scour. A horseshoe shaped scour hole has developed at the face and bedforms appeared to have been shed from the scour hole that developed underneath the upstream face of the log. After 48 hours progression of these bedforms and scour formation appeared to be slow, it was decided to end the experiment and restart the experiment with a higher discharge and thus higher flow velocity; this will be discussed in burial scour III.

Appendix C III

I Introduction

Burial scour experiments are the second type of experiments conducted. It includes the placement of a single log on the bed, and measuring/monitoring erosion/scour that occurs around the log. The log was placed in the area of maximum contraction and it was chosen to vary velocities in between experiments of this type to simulate a naturally non-eroding as well as an eroding bed. For this reason 5 similar experiments were conducted.

This report focuses on the third of this kind of experiment, with a water depth of 40[cm], a width of 0.52 [cm] and a discharge of 50 [l/s]. This would therefore lead to an average velocity of 0.24 [cm/s].

Observations at 0h

In Figure 221, it can be observed that at initiation of flow, the log was placed on a flat surface.

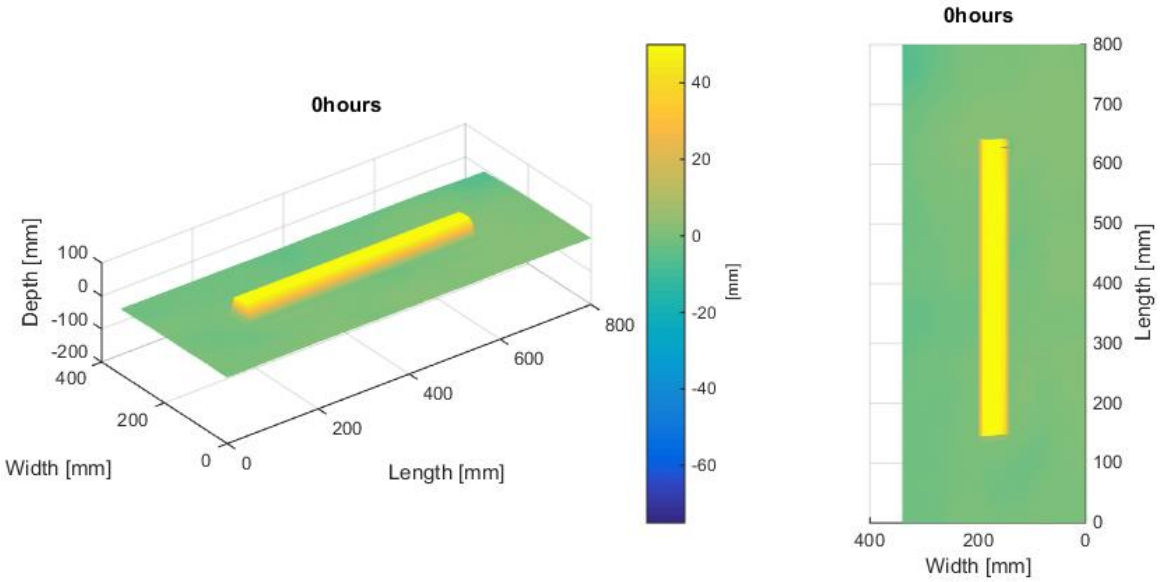

Figure 221; Bed topography at 0 hours

Observations at 24h

After 24 hours bed topography was measured and video footage that was taken during the previous 24 hours was analyzed. From Figure 222 it can be clearly observed that a significant amount of scour has occurred at the front face of the log, the scour showed a typical horseshoe shape and reached up to 70 [mm] at the front face of the log, which was also detached from the surface. It is also clearly visible that the log has slanted downwards, and the front face was almost at the same level as the remainder of the bed.

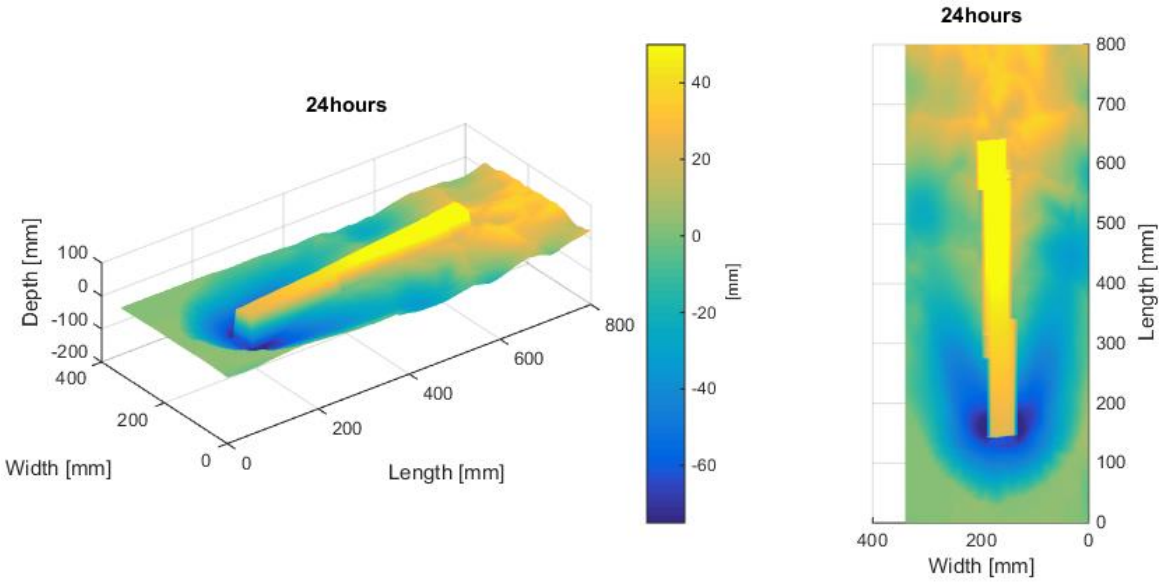

Figure 222; Bed topography after 18 hours

0h00m

Shortly after initiation of flow (Figure 223), it could be observed that the bed showed only small bedforms near the sides. The log was placed parallel to the governing flow direction.

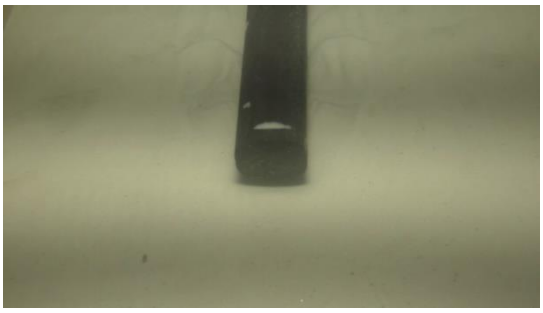

Figure 223; 0h00m

1h15m

After this time of flow (Figure 224), the bed developed a clear and symmetrical scour hole at the face of the log and bedforms progressing past the sides of the log.

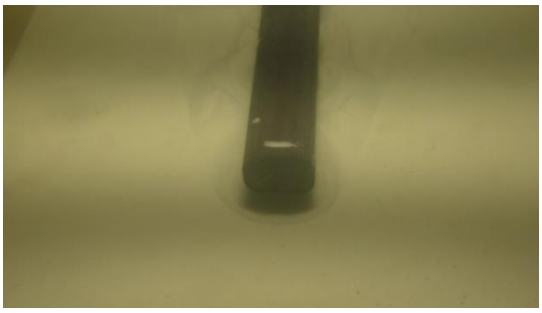

Figure 224; 1h15m

2h30m

After two and a half hour of flow (Figure 225) the bedforms still maintained their symmetry, and grew significantly in magnitude. It was clearly noticeable that the first 5 [cm] of the log was completely detached from the bed.

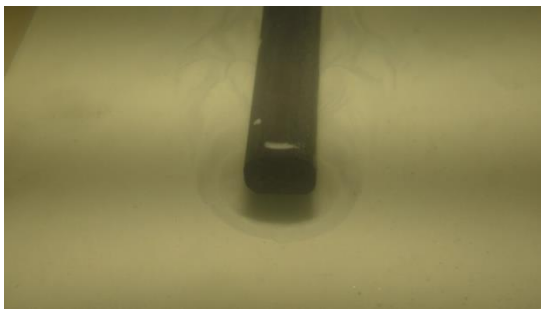

Figure 225; 2h30m

5h00m

After 5 hours (Figure 226) the camera angle was changed. Approximately 10 [cm] of the log starting from the upstream face was now detached and a cone shaped field of bedforms developed around the logs.

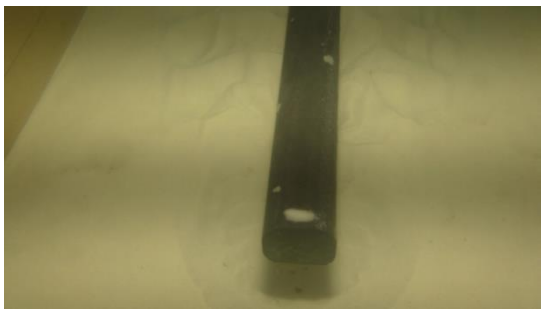

Figure 226; 5h00m

7h30m

After 7 and a half hour (Figure 227) the rate of scour reduced. Downstream bedforms slowly progressed further along the log. The scour hole at the front face also grew slowly.

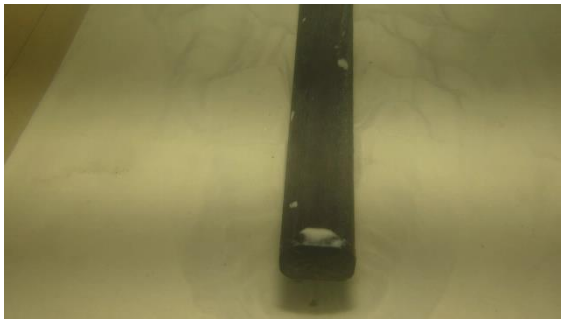

Figure 227; 7h30m

10h00m

After 10 hours (Figure 228), scour appeared to slow down even further. A strong reduction of bedforms shed from the front face can be observed.

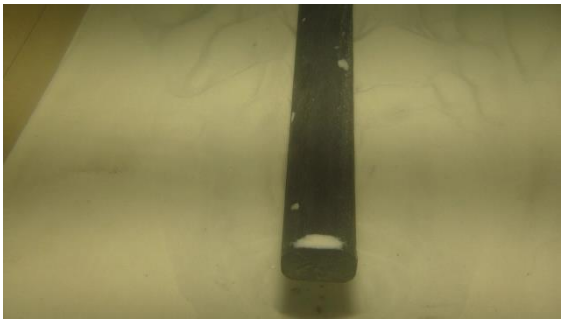

Figure 228; 10h00m

Observations at 48h

After 48 hours bed topography was measured. From Figure 229 it can be clearly observed that the front face of the log had now dropped far below the original bed level, furthermore the log had turned several degrees and the downstream end of the log now also developed a scour hole. Maximum scour was observed to be about 80 [mm] and similar at both the upstream and the downstream scour.

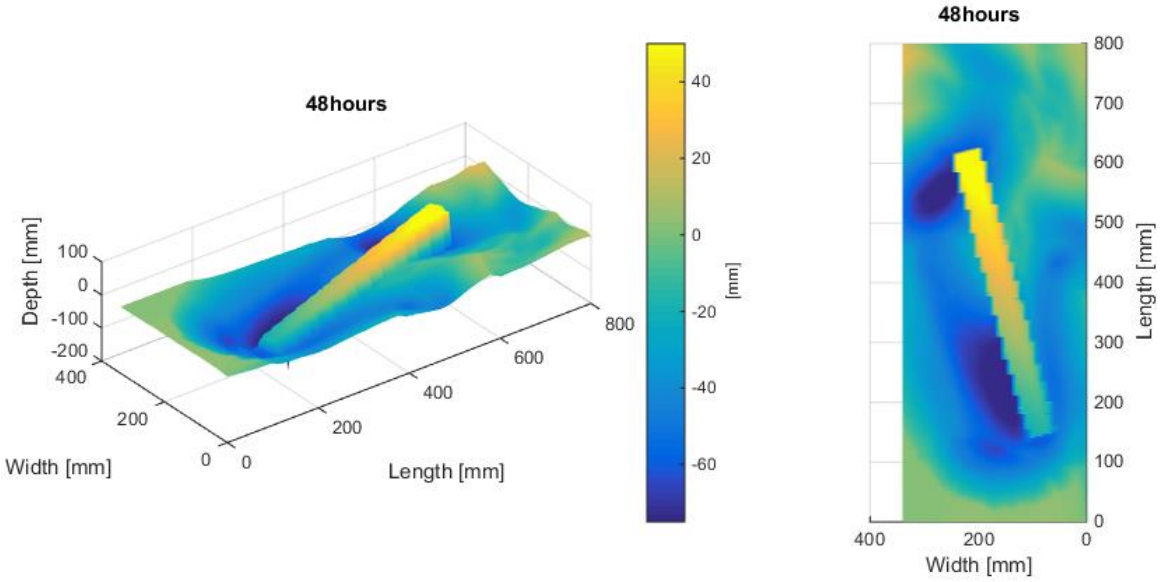

Figure 229; Bed topography after 48 hours

Observations at 72h

After 72 hours the log was now almost entirely below the original bed level. Maximum scour amounted to 90 [mm] and occurred slightly downstream of the front face in the wider part of the cross section. The scour hole at the downstream face disappeared due to the downstream sediment transport. Furthermore bedforms developed on the section which is narrow upstream.

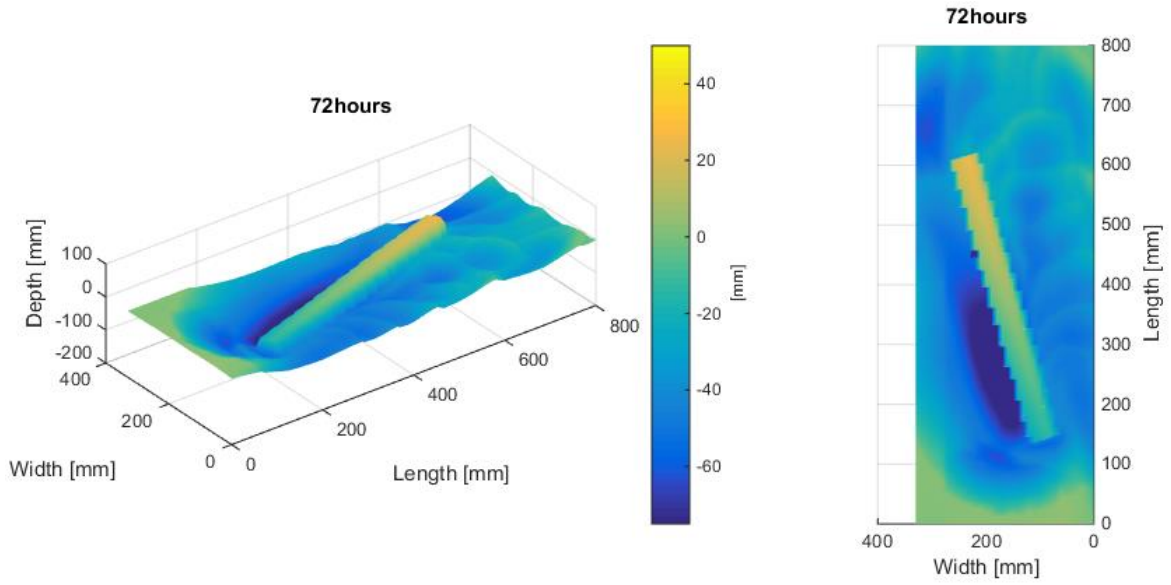

Figure 230; Bed topography after 72 hours

Concluding remarks

The placement of a log on a bed that should show some transport of bed particles has shown to result in a similar scour pattern with a strong increase in scour magnitude. Furthermore, the log was significantly displaced with respect to earlier experiments. It can therefore be expected that when flow velocity is increased even further, larger displacements can be observed. The traditional horseshoe shaped scour hole occurred in the beginning of the experiment but upon tilting and shifting of the log this scour pattern changed significantly, no longer following a clear and well defined model. After 72 hours progression of scour seemed to be slow, thus it was decided to end the experiment and restart the experiment with a higher discharge and thus higher flow velocity; this will be discussed in burial scour IV.

Appendix C IV

I Introduction

Burial scour experiments are the second type of experiments conducted. It includes the placement of a single log on the bed, and measuring/monitoring erosion/scour that occurs around the log. The log was placed in the area of maximum contraction and it was chosen to vary velocities in between experiments of this type to simulate a naturally non-eroding as well as an eroding bed. For this reason 5 similar experiments were conducted.

This report focuses on the third of this kind of experiment, with a water depth of 40[cm], a width of 0.52 [cm] and a discharge of 55 [l/s]. This would therefore lead to an average velocity of 0.265 [cm/s].

Observations at 0h

In Figure 231, it can be observed that at initiation of flow, the log was placed on a flat surface.

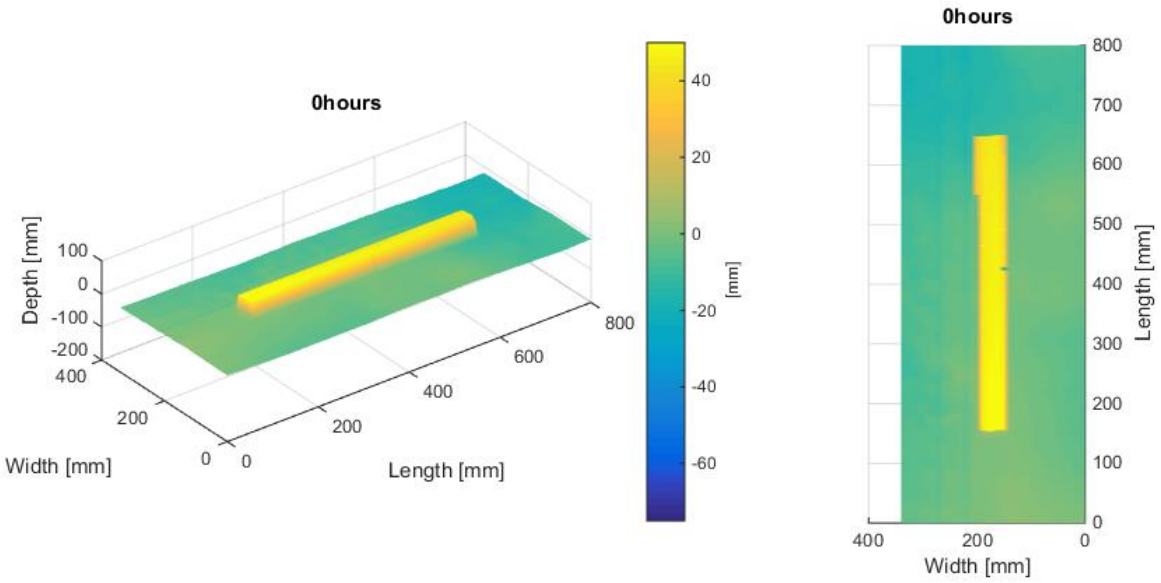

Figure 231; Bed topography at 0 hours

Observations at 3h

From visual observations it was decided to take a measurement of the bed after 3 hours (Figure 232). The log had already shown to tilt and shift significantly to one direction. It could also be observed that the bed had now started to erode ad nearly all locations. But the maximum amount of scour present was still located underneath the upstream face of the log, and reached up to 40 [mm].

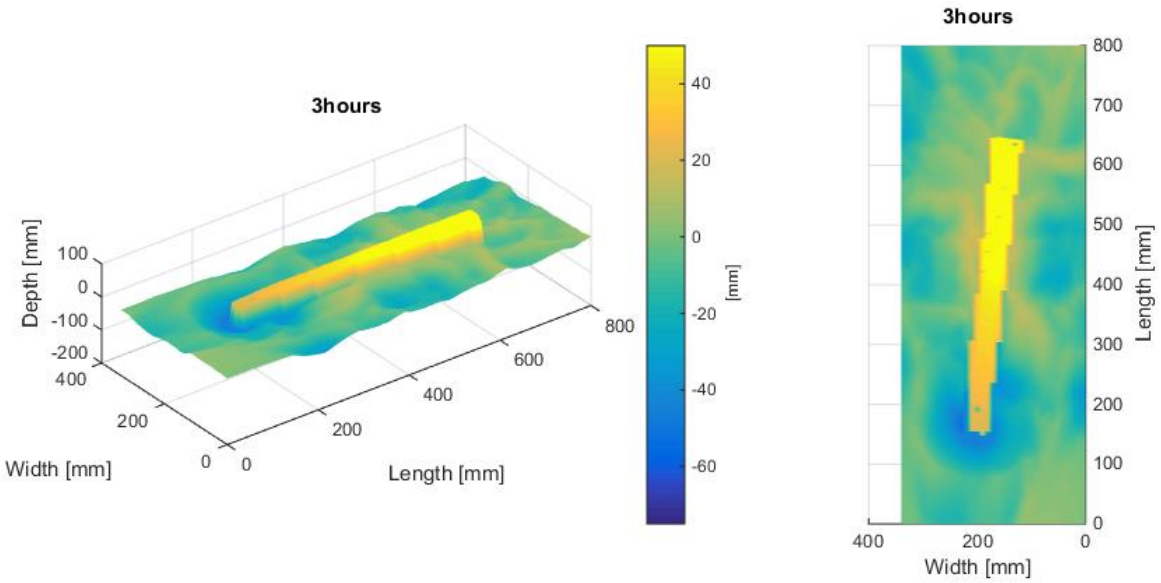

Figure 232; Bed topography after 3 hours

Observations at 24h

After 24 hours bed topography was measured and video footage that was taken during the previous 24 hours was analyzed. Upon inspection of the experiment it was observed that the log had turned over 90 degrees and was now placed almost perpendicular to the flow direction (Figure 233). It can be observed that the log developed two areas of scour, each at one end of the log, indicating that sediment was being transported around the log. The bed downstream of the log had shown to become rather smooth with no significant bedforms visible in the projection. The area upstream from the log did show the presence of bedforms.

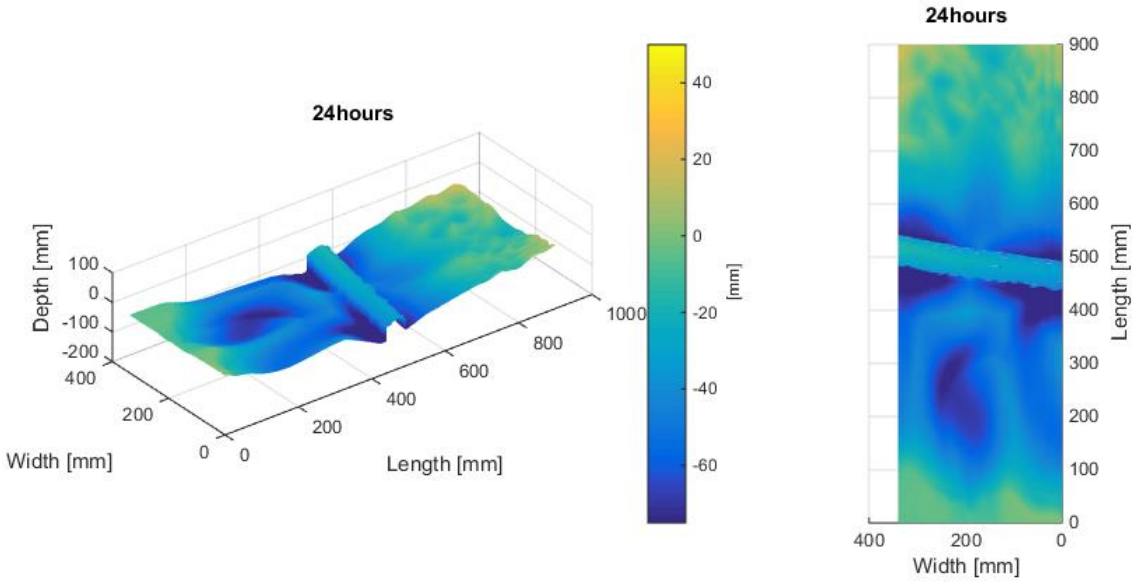

Figure 233; Bed topography after 24 hours

As it was expected, from previous experiments that the log would turn during the first 24 hour; a camera was mounted above the log to observe its movements during the night. Figure 234-Figure 245

0h00m

At initiation of flow (Figure 234), it could be observed that the bed showed no bedforms and. The log was placed exactly parallel to the flow.

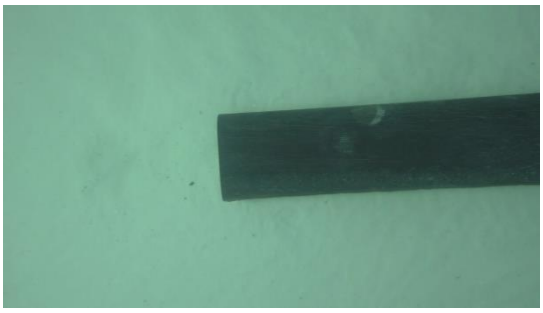

Figure 234; 0h00m

0h5m

After five minutes of flow (Figure 235), the bed developed minor bedforms upstream, while stronger and more defined bedforms developed around the log.

Figure 235; 0h5m

2h30m

After two and a half hour of flow (Figure 237) scour developed around the log, but did not resemble a horseshoe shape. It can be observed that sediment transport is limited with respect to scour caused by the log.

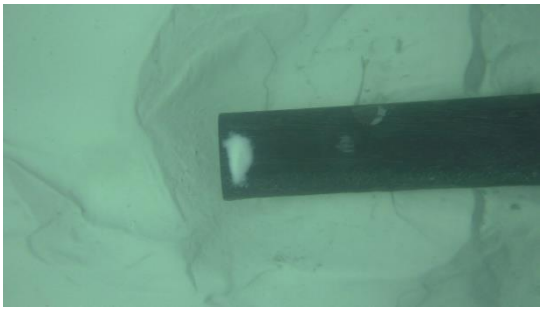

Figure 236; 2h30m

5h00m

After 5 hours (Figure 237) the camera settings were changed. At this point in time the log had started to shift significantly towards one side.

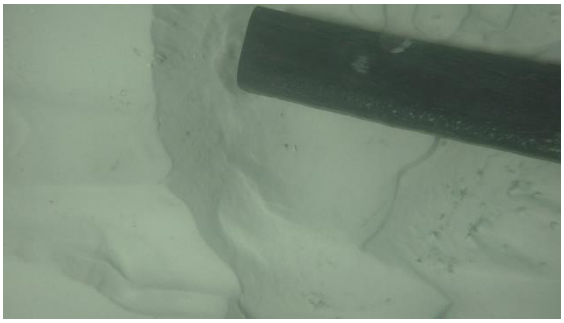

Figure 237; 5h00m

6h30m

After 6 and a half hour (Figure 238) the log had only rotated slightly more than before, and scour did not seem to have developed much further than after 5 hours.

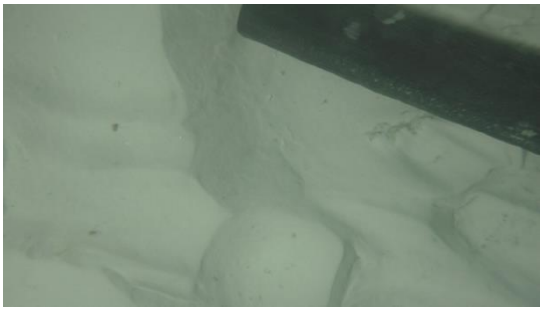

Figure 238; 6h30m

6h45m

After 6 hours and 45 minutes (Figure 239), the log had suddenly turned almost 90 degrees with respect to the initial placing.

Figure 239; 6h45m

8h00m

After 8 hours the log developed a trench upstream of its position (Figure 240). The log was now almost perfectly perpendicular with respect to the flow direction.

Figure 240; 8h00m

10h00m

After 10 hours (Figure 241) it could be observed that the trench upstream of the log showed the tendency to smoothen, and upstream transport was relatively slow.

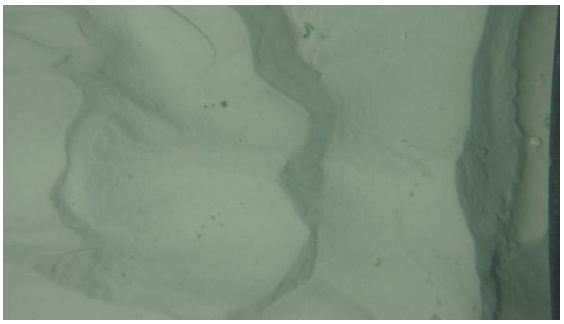

Figure 241; 10h00m

12h00m

After twelve hours (Figure 242) the trench was almost indistinguishable, indicating a further smoothing of the bed. Sediment was still slowly being transported from the upstream.

Figure 242; 12h00m

14h00m

After 14 hours (Figure 243), bedforms origination from upstream showed a long crested uniform pattern and were slowly nearing the log.

Figure 243; 14h00m

16h00m

After 16 and a half hour (Figure 244), the pattern observed after 14 hours continued. Irregularities just in front of the log again reduced.

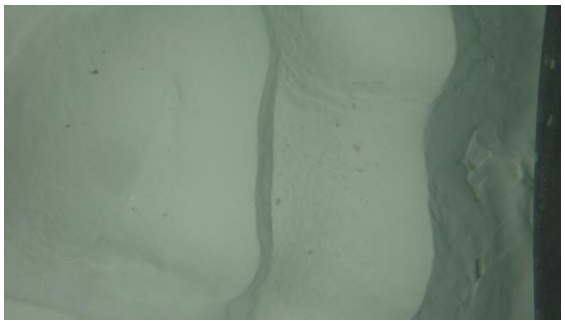

Figure 244; 16h00m

18h00m

After 18 hours (Figure 245), the bed upstream was now no longer showing sediment transport, the bed clearly showed to become smoother and more uniform.

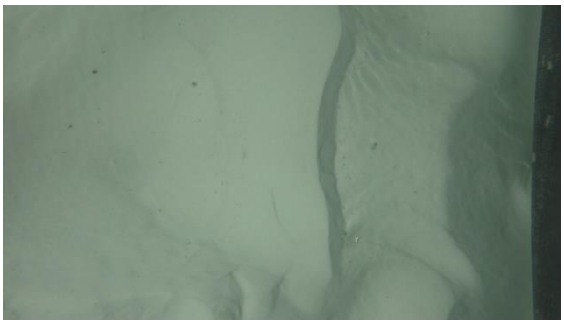

Figure 245; 18h00m

Observations at 48h

After 48 hours (Figure 246) it was observed that the bed downstream of the log had become even smoother and had started to attach itself to the logs originating from the sides.. The upstream bed still showed minor bedforms as well as a large scour hole right in front of the log. At this time, almost the entire bed that was measured had shown some degree of scour, up to a maximum of about 105 [mm].

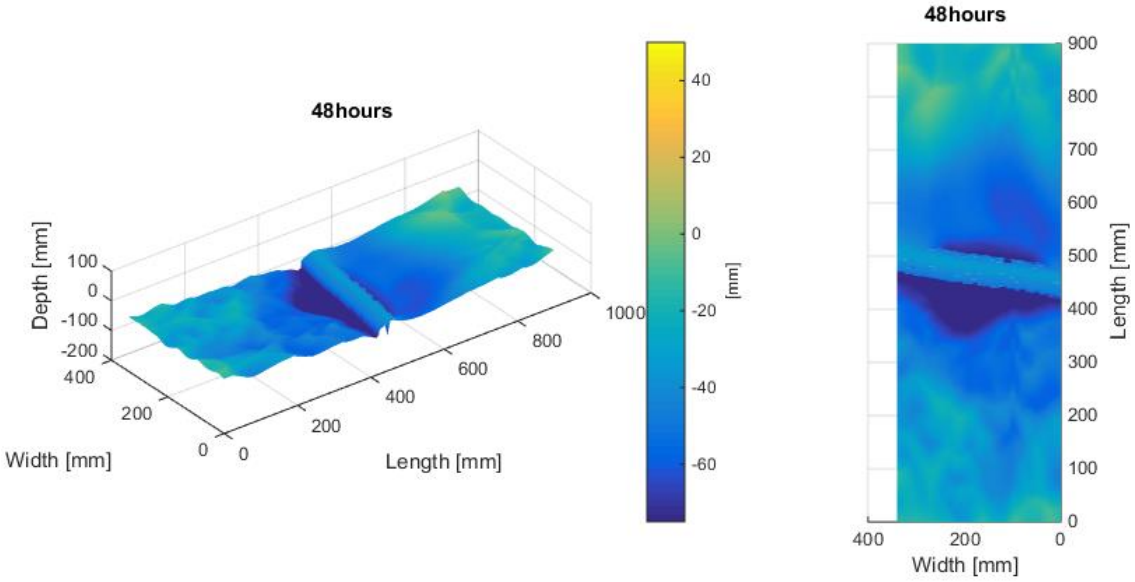

Figure 246; Bed topography after 48 hours

Observations at 72h

After 72 hours the log was now on the downstream side almost indistinguishable from the bed, as the bed had accreted to envelop the log completely, the scour hole that developed after 48 hours had shrunken in width and the magnitude was also reduced to about 100 [mm], with respect to 105 [mm] after 48 hours. Furthermore the bed downstream had retained it smoothness but did show to decrease slightly further downstream from the log.

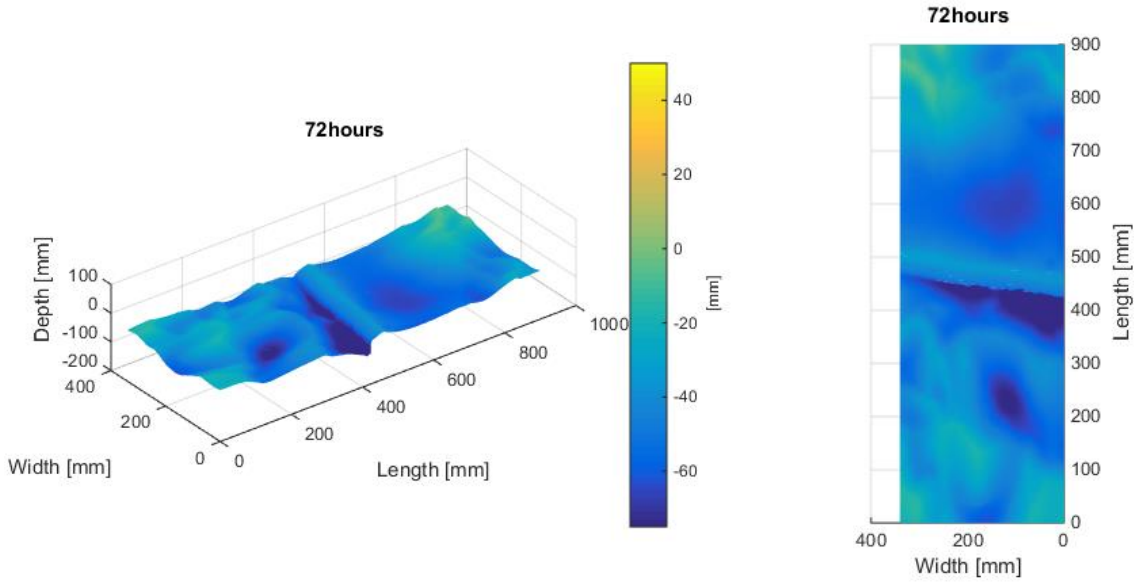

Figure 247; Bed topography after 72 hours

Concluding remarks

The placement of a log on an eroding bed showed that the log underwent a strong displacement and turned over 90 degrees to now assume a perpendicular position with respect to flow. The log started to act like a sort of silt. Downstream of the log the bed seems to become smoother and more stable than upstream of the log. The log tends to develop a trench immediately upstream of its location, which did seem to become less pronounced over time. As changes between 48 hours and 72 were small the experiment was stopped and it was decided to restart the experiment one more time with the maximum discharge and thus higher flow velocity; this will be discussed in burial scour V.

Appendix C V

Burial scour experiments are the second type of experiments conducted. It includes the placement of a single log on the bed, and measuring/monitoring erosion/scour that occurs around the log. The log was placed in the area of maximum contraction and it was chosen to vary velocities in between experiments of this type to simulate a naturally non-eroding as well as an eroding bed. For this reason 5 similar experiments were conducted.

This report focuses on the third of this kind of experiment, with a water depth of 40[cm], a width of 0.52 [cm] and a discharge of 60 [l/s]. This would therefore lead to an average velocity of 0.29 [cm/s]. This is also the same discharge as was used in the Basic scour experiments.

Observations at 0h

In Figure 248, it can be observed that at initiation of flow, the log was placed on a flat surface.

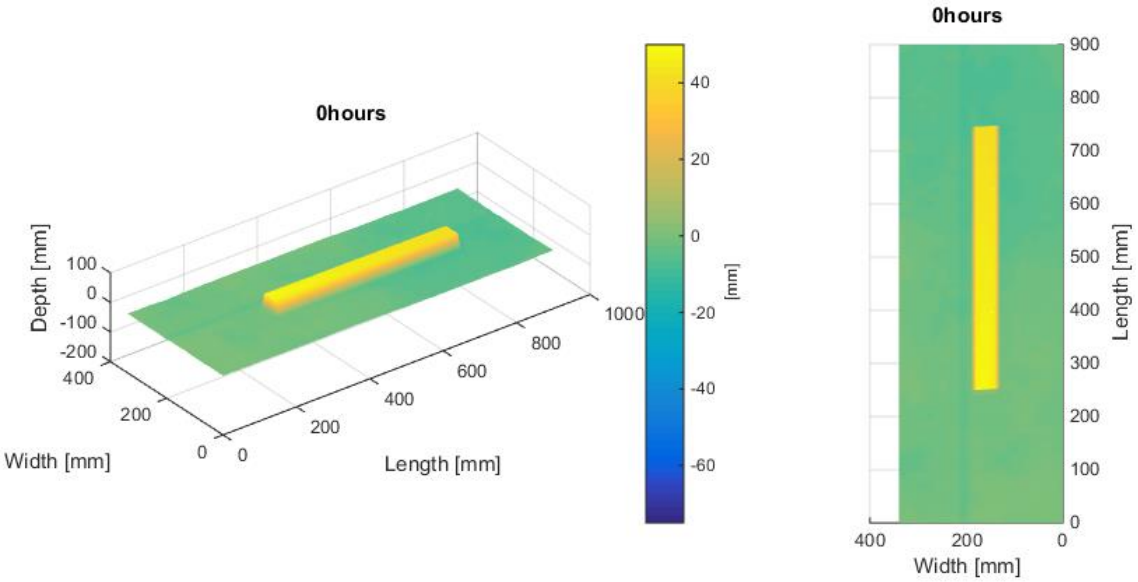

Figure 248; Local bed topography at 0 hours

Observations at 24h

After 24 hours bed topography was measured and video footage that was taken during the previous 24 hours was analyzed. Upon inspection of the experiment it was observed that the log had turned just short of 90 degrees and was now placed almost perpendicular to the flow direction (Figure 249). Scour concentrated close to the log on the upstream side and just downstream on the lower lying end of the log. The bed downstream of the log had yet again shown to become rather smooth with no significant bedforms visible in the projection. The area upstream from the log did show the presence of bedforms. Maximum scour was observed to be equal in both in the upstream scour hole as the downstream scour hole and amounted a local maximum of 70 [mm]

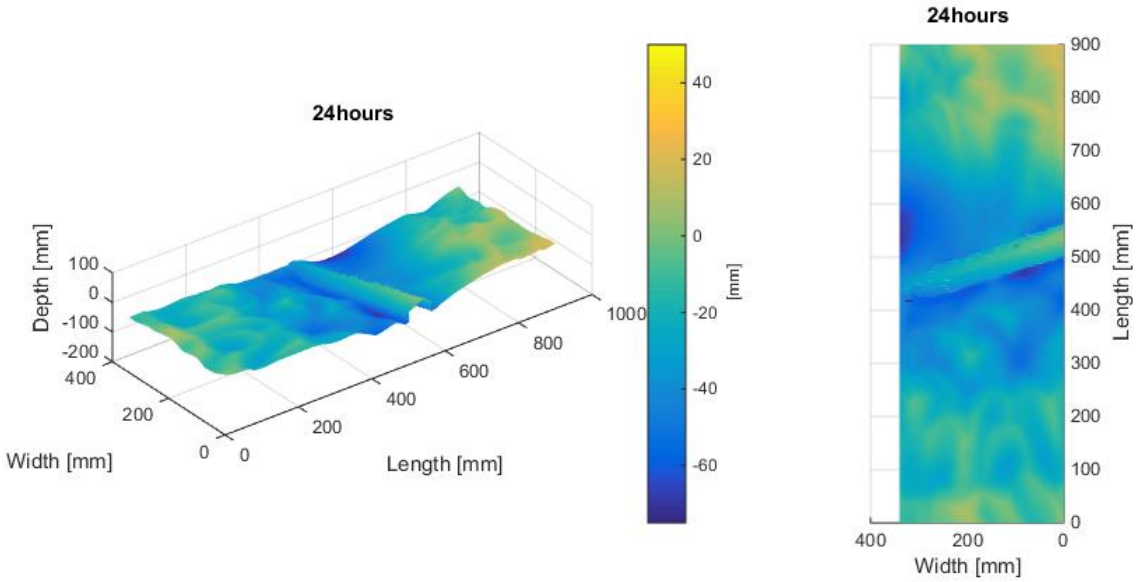

Figure 249; Local bed topography after 24 hours

As it was expected, from previous experiments that the log would turn during the first 24 hour; a camera was mounted downstream the log to observe its movements during the night. Figure 250-Figure 255 shows this phenomenon.

0h01m

Shortly after initiation of flow (Figure 250), it could be observed that the bed immediately showed movement at all locations. The largest bedforms again developed close to the sides of the log.

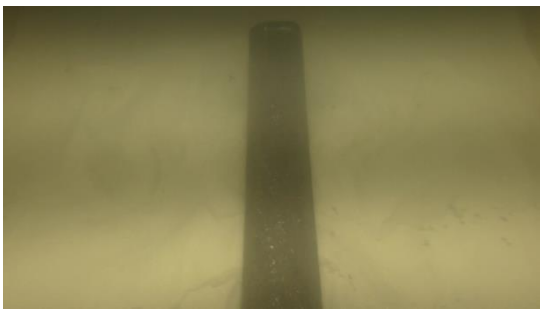

Figure 250; 0h01m

2h30m

After this time of flow (Figure 251), the bed developed a scour hole at the upstream face of the log continuously being fed with sediment from upstream. The log had shown to start to tilt and shift towards the right.

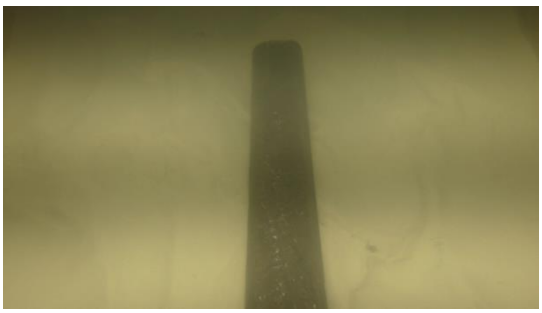

Figure 251; 2h30m

5h00m

After 5 hours of flow (Figure 252) the log had already turned almost 80 degrees with respect to its original position.

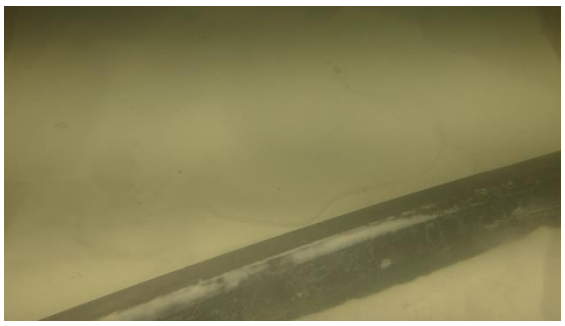

Figure 252; 5h00m

7h30m

After this time of flow (Figure 253) settled several cm further downstream. It could also be seen that the bed underneath the log eroded causing the log to lie lower.

Figure 253; 7h30m

10h00m

After ten hours of flow (Figure 254) the log showed to still be detached from the surface with a small trench downstream of the log.

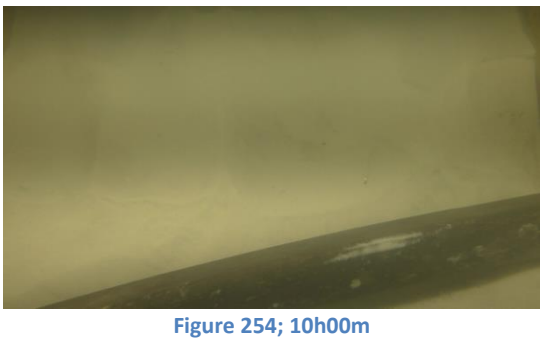

Figure 254; 10h00m

12h30m

After this time of flow (Figure 255), the log showed no significant further displacement except for sinking even slightly further.

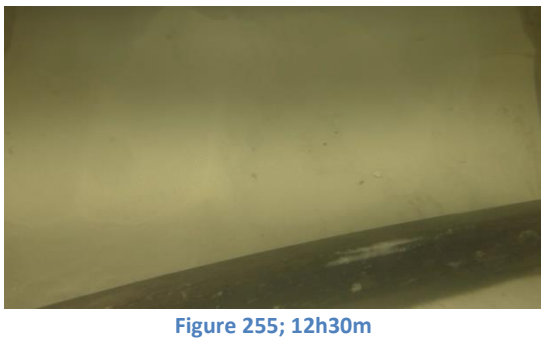

Figure 255; 12h30m

Observations at 48h

After 48 hours (Figure 256) it was observed that the bed downstream of the log had become somewhat smoother and trenches were still present on both sides of the log. A point of accretion was however observed on the downstream end of the log near the right wall. Maximum scour was around 95 [mm] located in the upstream trench. Maximum scour on the downstream trench was 80 [mm]

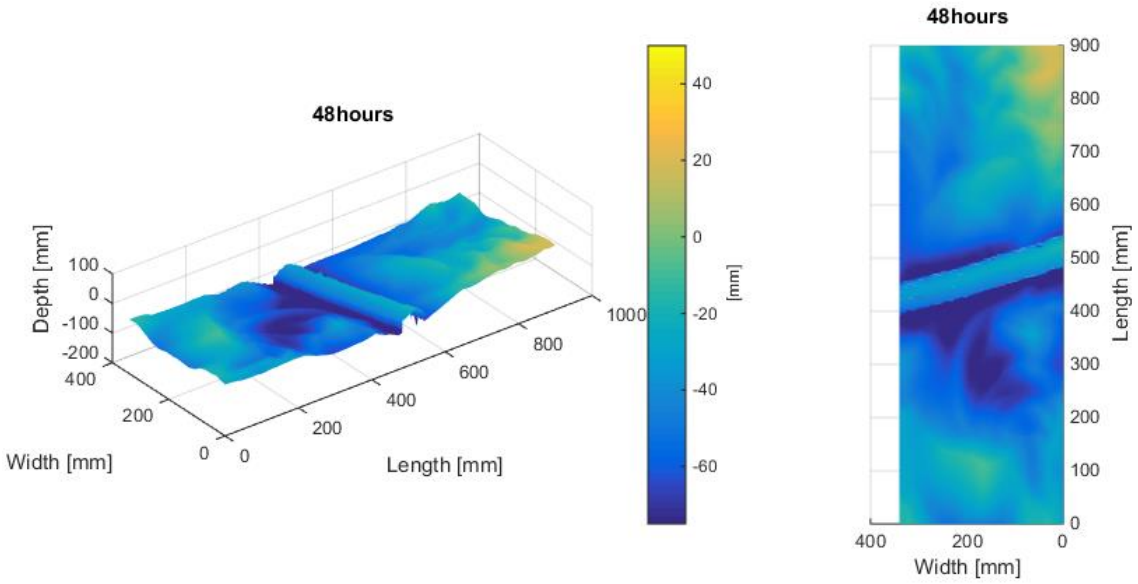

Figure 256; Local bed topography after 48 hours

Observations at 72h

After 72 hours (Figure 257 & Figure 258), the log was now on the downstream side almost indistinguishable from the bed, as the bed had accreted to envelop the log completely. If the bed levels are compared, it can be observed that the bed actually accreted around the log with respect to the measurement taken at 48 hours, potentially signaling that the log is acting as a significant barrier for sediment transport. Maximum scour was observed directly upstream of the log and amounted to 87 [mm], this is almost a centimeter less than the measurement at 48 hours. The total bed topography projection (Figure 258) shows a general scour pattern similar to basic scour experiments 1 & 2.

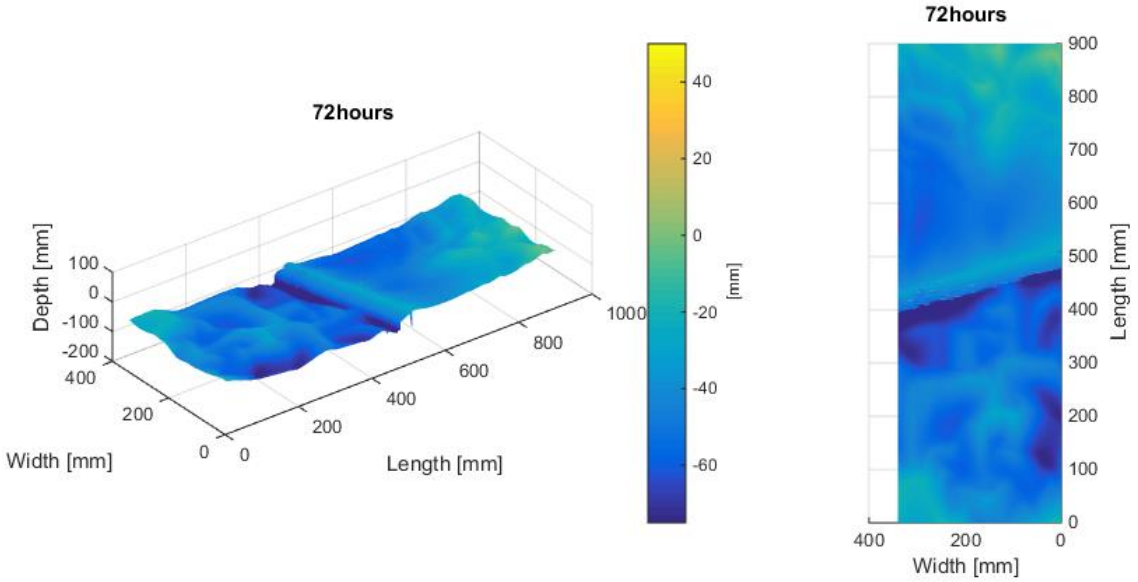

Figure 257; Local bed topography after 72 hours

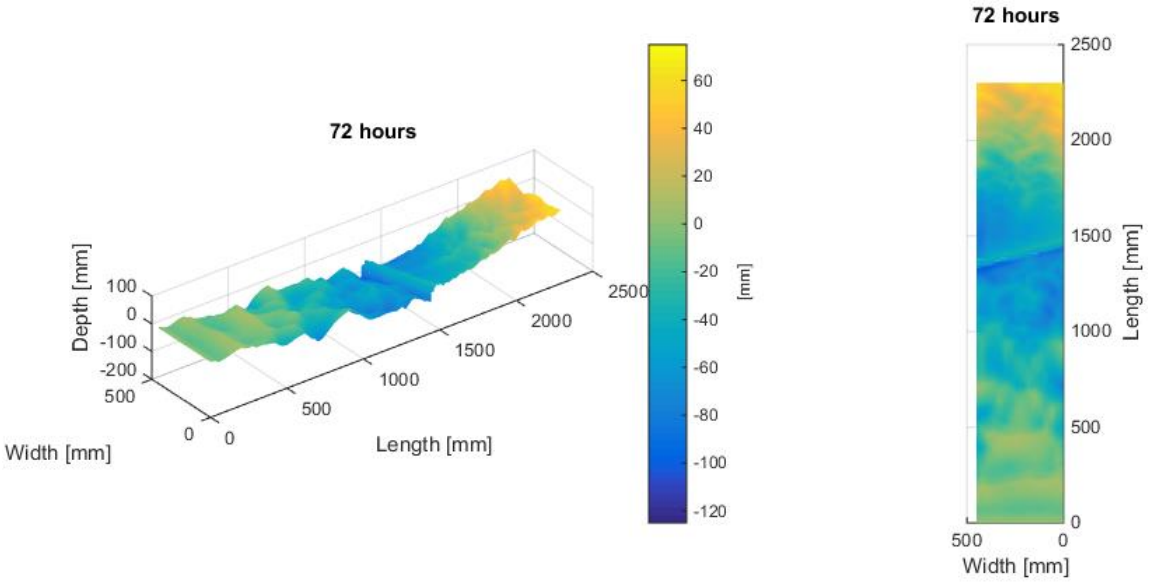

Figure 258; Total bed topography after 72h

Measurements at 96h

After 96 hours the log was now on the downstream uncovered again, and scour holes developed on both sides of the log moving from the faces towards the center. The scour pattern now resembled a pattern more similar to pipeline scour (Mutlu Sumer & Fredsøe, 2005). Maximum scour occurred towards the right log face and measured over 100 [mm]. This was the largest recorded scour magnitude up to this point in the experiment. Easily exceeding earlier maximum scour magnitudes found after 48 and 72 hours. Scour on the downstream side of the log was generally smaller with magnitudes between 75 & 90 [mm].

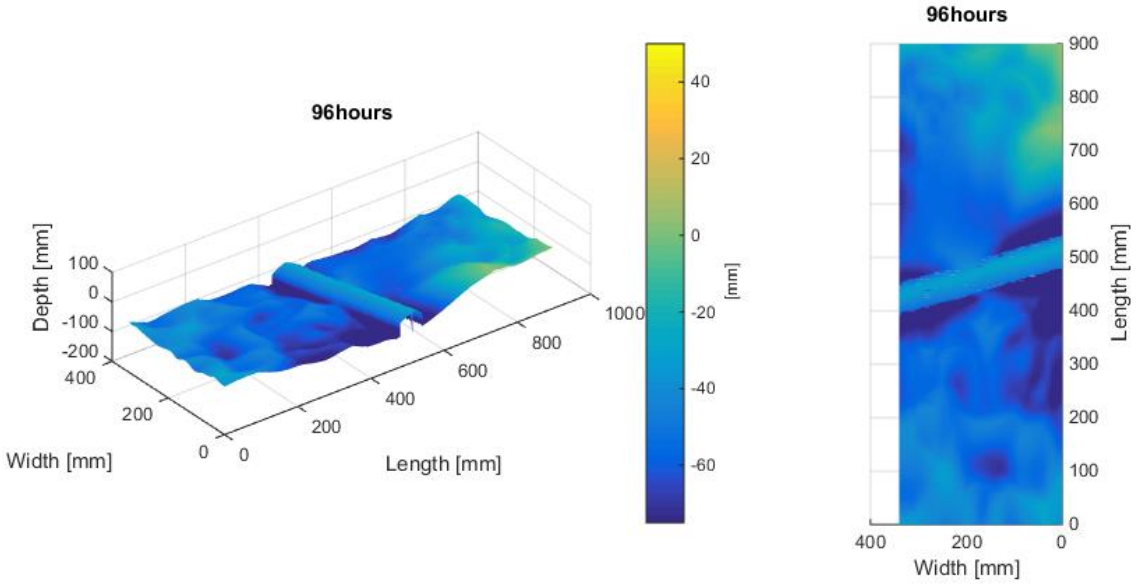

Figure 259; Local bed topography after 96 hours

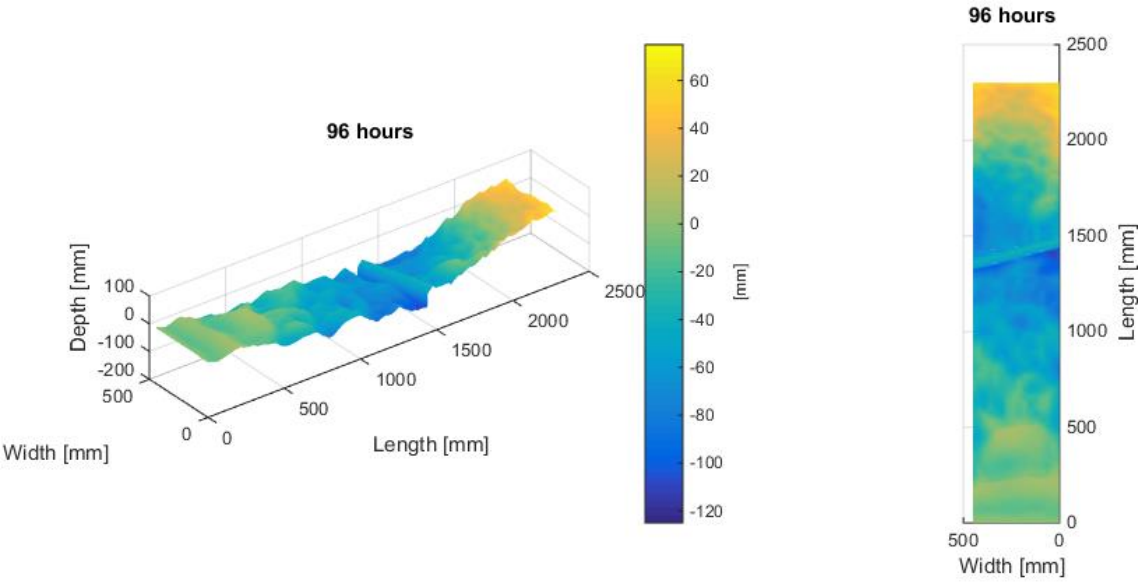

Figure 260; Total bed topography after 96 hours

Concluding remarks

The placement of a log on an eroding bed showed that the log again underwent a strong displacement and turned about 80 degrees to now assume a semi-perpendicular position with respect to flow. The log again started to act like a sort of silt. The log now clearly acted as a silt reducing erosion and scour on both sides. This effect is however temporary and over time the bed downstream of the log starts to erode. If the average transect is compared with that of the Basic Scour experiments (see Figure 261), it can be observed that the scour development followed a pattern close to basic scour experiments I & II. With respect to those experiments, Burial scour 5 showed the least amount of erosion of the three after 96 hours.

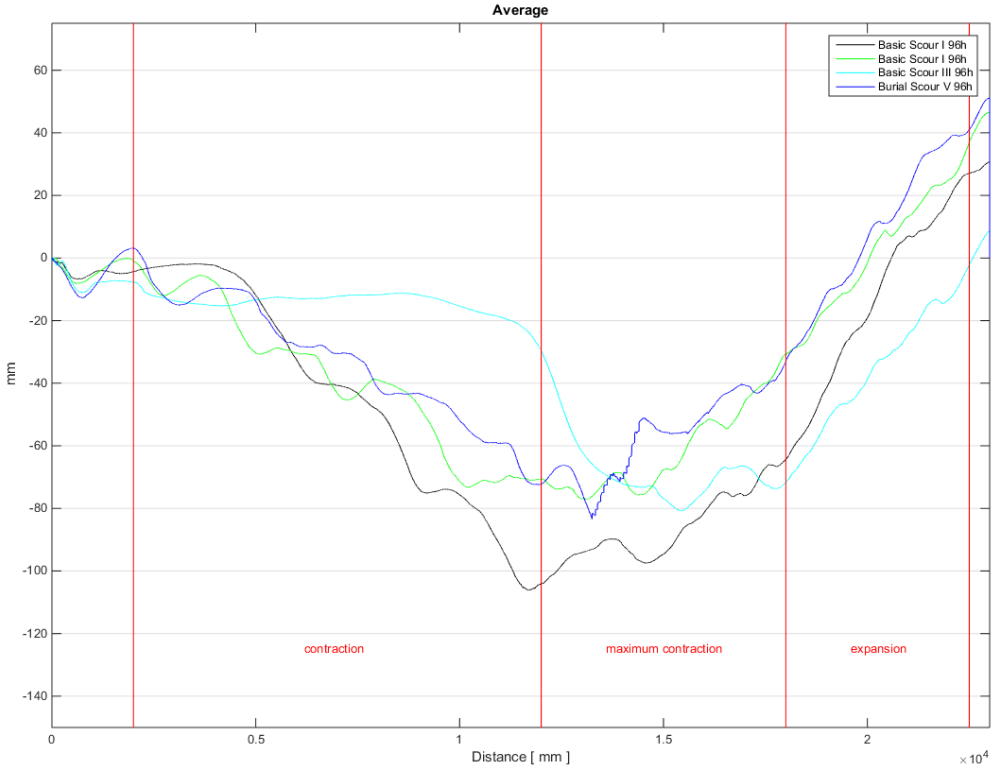

Figure 261; Average transects

Appendix D I

I Introduction

The protected Scour experiments are considered to be the baseline experiments for the application of wooden logs as a scour protection. The “Protected Scour A” experiments feature a flow parallel placed single layer of logs directly on top of the bed, in the area of maximum contraction. Similar to the basic scour experiments bed, velocity and fluctuation intensity development is measured during a 96 [h] run. This report includes all measured findings during this particular experiment. Conclusions are drawn in the main report on the basis of multiple similarly conducted experiments. A short preliminary conclusion is however included at the end of this report.

Summary

Table 55 represents relevant scour quantities after 96 [h]. Note that the absolute is measured relative to the measurement of the bed at 0 [h], excluding the maximum scour depth which is measured to a reference bed with a 0 [mm] elevation. Measurements of scour volume in the column with respect to reference include missing volume with respect to a reference be of 0 [mm] and corrected for the presence of logs .

Table 55; Summary of quantities (Negative values indicate scour, positive indicate accretion)

	Quantity	With respect to reference
Maximum Scour Depth [mm]	143	143
Total Scoured volume [cm^3]	-23111	-32674
Scoured volume Upstream-sector [cm^3]	+5	-496
Scoured volume Contracting-sector [cm^3]	-7051	-11093
Scoured volume Constricted-sector [cm^3]	-18839	-21769
Scoured volume Expanding-sector [cm^3]	+978	-819
Scoured volume Downstream-sector [cm^3]	+1796	+1504

Measurements at 0h

Bed level

A projection of the bed at the moment of initiation of flow during the first scour experiment can be seen in Figure 262. Clearly observable are the placed logs on the bed. They are roughly located in between 1200-1700 [mm] from the entry point of flow. The bed further seems to be relatively flat with only minor deformations with respect to the size of the logs.

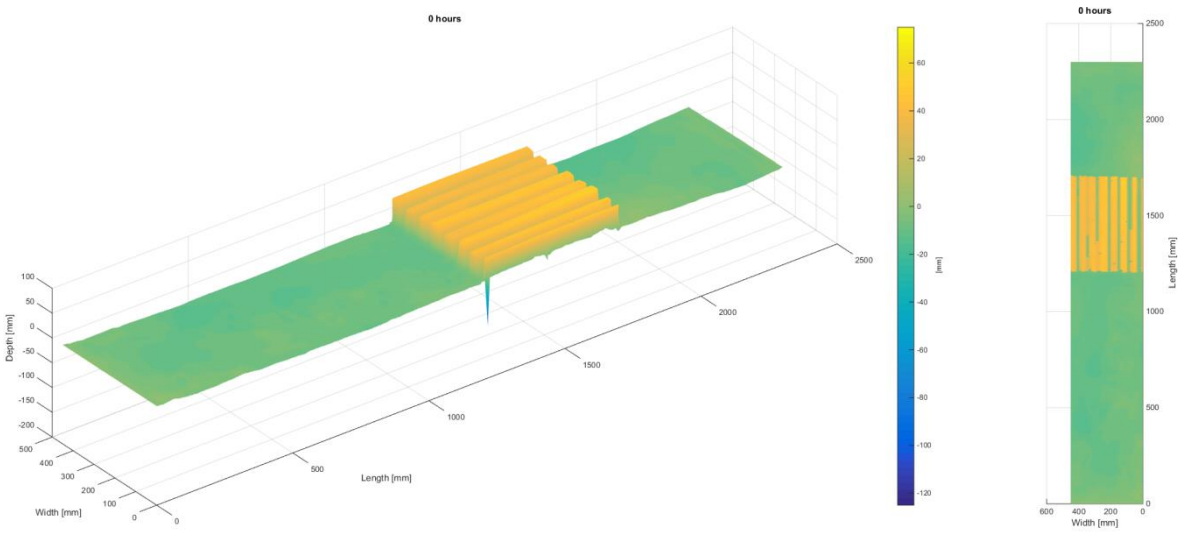

Figure 262; Bed map 0[h]

The average transect, observable in Figure 263, was calculated from the 31 transects taken over the entire length of the laboratory set-up. As can be seen, the bed is slightly below the target value of 0 [mm] with about 10 [mm]. Other than that the bed seems to be relatively flat. The position of the logs is also clearly observable within the area of maximum contraction.

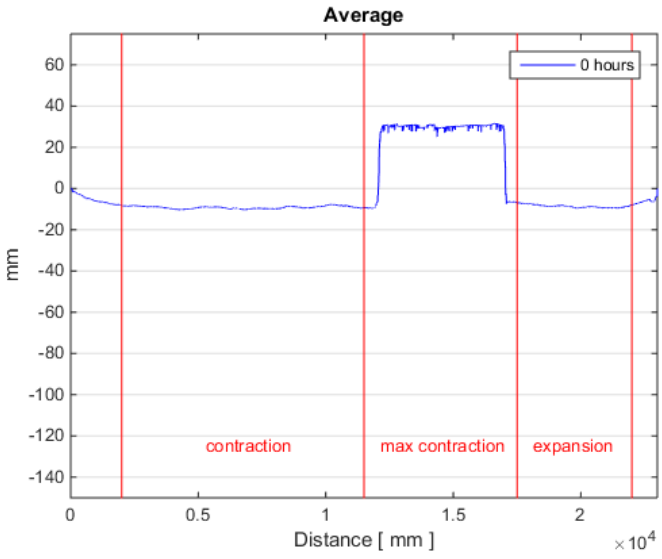

Figure 263; 0 [h] average transect

Velocity Profiles

In this section, individual flow profiles of locations marked above are shown. At location 3 the flow has accelerated significantly, except for the area close to the bottom, this is most likely caused by the logs and the disruption they create within the near bed flow near location 3. Location 5 shows a similar phenomenon, where flow near the bed almost reduces to zero in the wake of the logs. Flow in between the logs most likely causes a small residual current near the bed. Near location 6 flow velocity higher up the water column is much higher with respect to similar measurements during the Basic Scour Experiments. Although flow seemingly does try to redistribute, but clearly no equilibrium has yet been reached as near bed velocities are still significantly lower with respect to the Basic Scour Experiments.

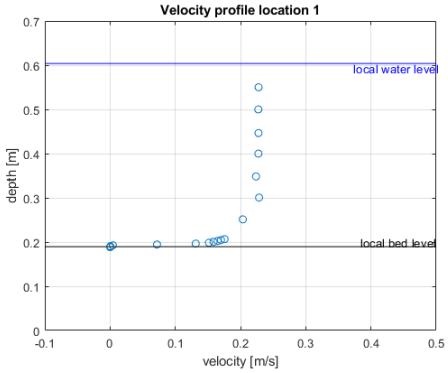

Figure 264; Velocity Profile location 1

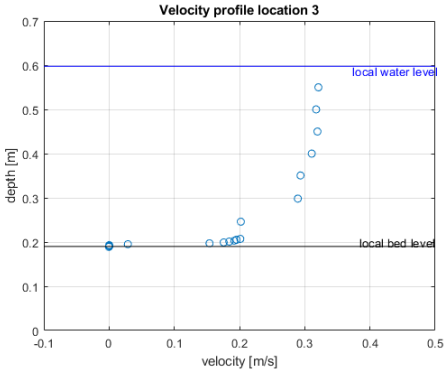

Figure 265; Velocity Profile location 3

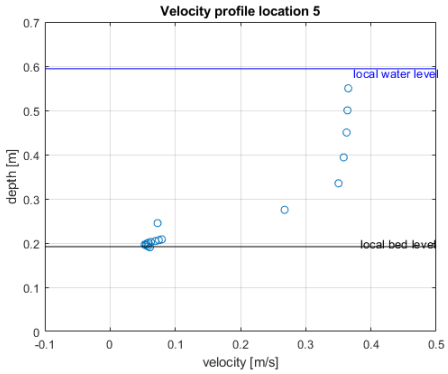

Figure 266; Velocity Profile location 5

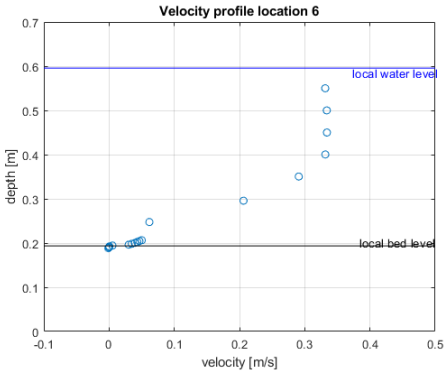

Figure 267; Velocity Profile location 6

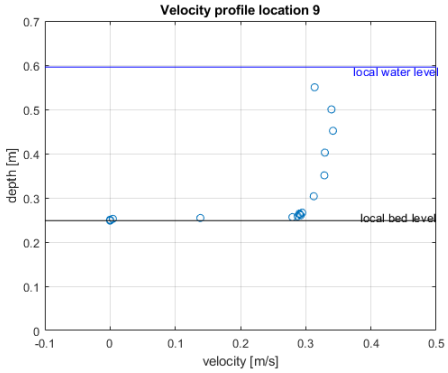

Figure 268; Velocity Profile location 9

Relative fluctuation intensity

Calculated fluctuation intensity shows that during flow contraction, in between location 1 & 2, this fluctuation drop now slightly increases again towards location 3. This same phenomenon is observed in between locations 7 and 8. At locations 4 and 9 (measured above the logs) the relative fluctuation intensity remains small. Wherever possible, curve fitting has been applied to make interpretation easier.

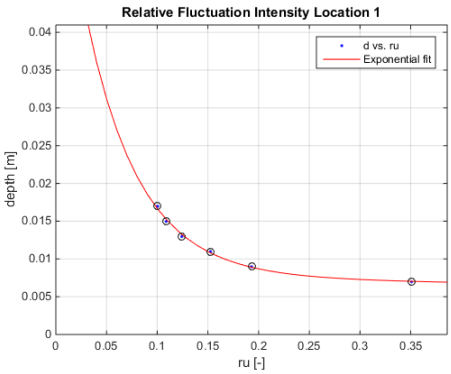

Figure 269; Relative fluctuation intensity location 1

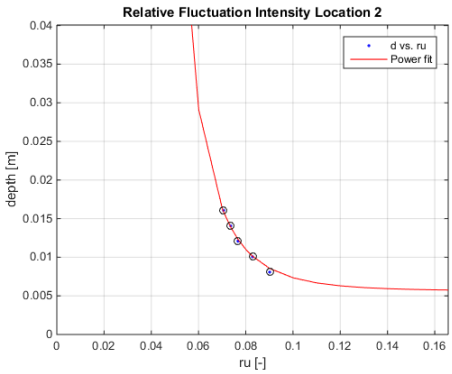

Figure 270; Relative fluctuation intensity location 2

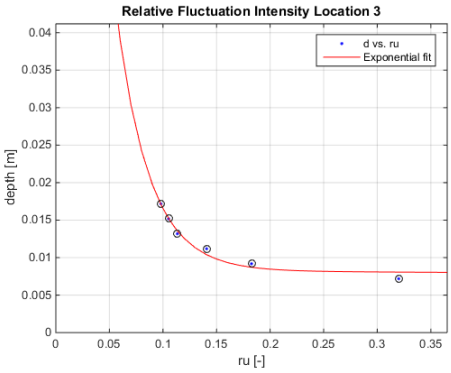

Figure 271; Relative fluctuation intensity location 3

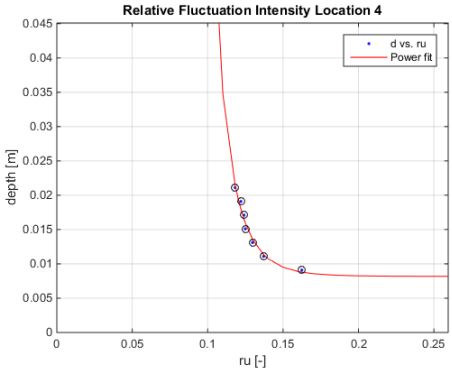

Figure 272; Relative fluctuation intensity location 4

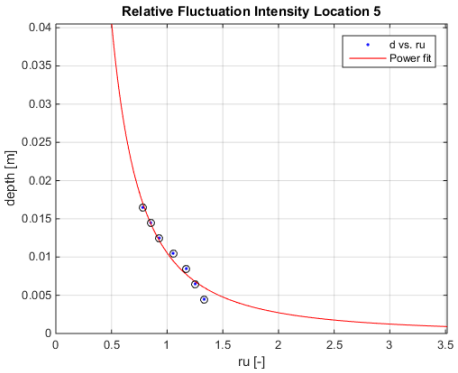

Figure 273; Relative fluctuation intensity location 5

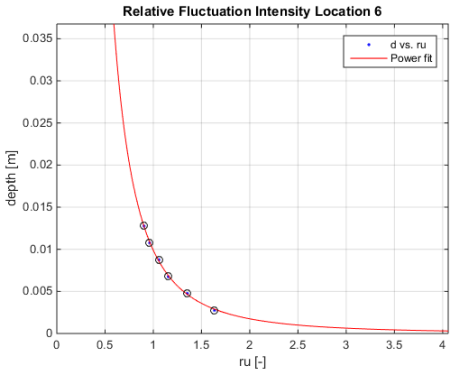

Figure 274 Relative fluctuation intensity location 6

It is at locations 5 & 10 where things start to become interesting. While fluctuation intensity is high at location 5, it is negative and still relatively small at location 10. The relatively high fluctuation intensity at location 5 can be explained by pointing out that this location is located within the wake of the logs, and thus average velocity is small, and the vortex formation causes relatively intense fluctuations with respect to the average flow velocity. At location 10 the negative relative fluctuation intensity is caused by a near bed flow that is opposite to the flow direction, and thus towards the logs. Locations 6 & 11 which are located close to the exit point show strong fluctuations with respect to average flow, caused by the flow not having reattached yet to the bottom.

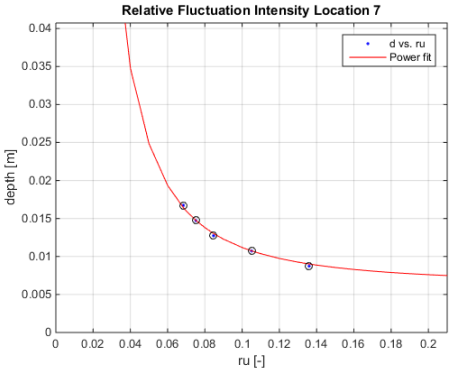

Figure 275; Relative fluctuation intensity location 7

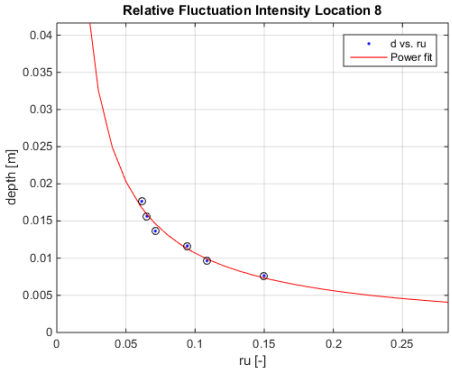

Figure 276; Relative fluctuation intensity location 8

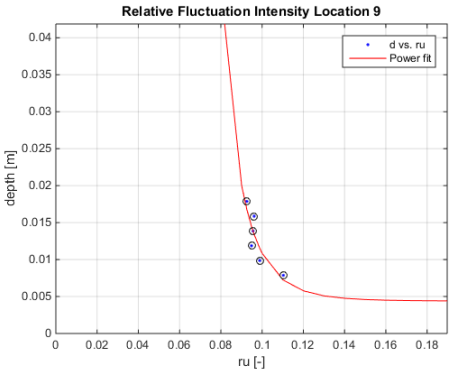

Figure 277; Relative fluctuation intensity location 9

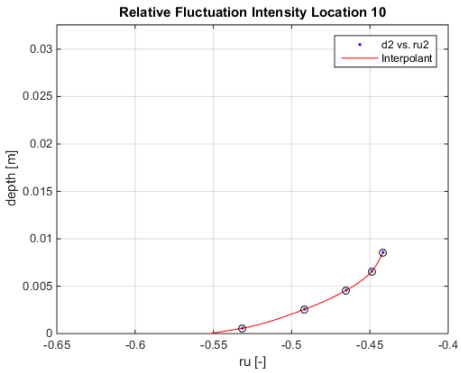

Figure 278; Relative fluctuation intensity location 10

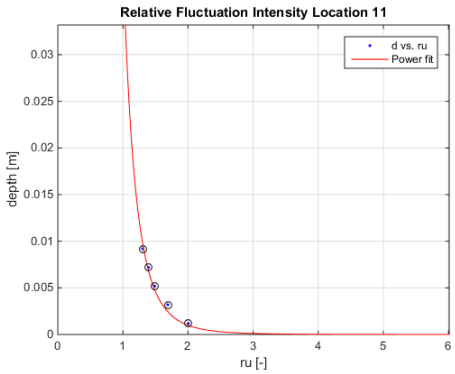

Figure 279 ; Relative fluctuation intensity location 11

Bed Shear stress

The bed shear stress was determined with Reynolds formula stated in (Schiereck & Verhagen, 2012). Bed shear stresses are determined by averaging the estimation for bed shear stress, over the centimeter measured above the bottom for a time frame of 3 minutes measuring at 50 [hz] per second, excluding all measured values that do not confirm with a signal to noise ratio above 15 and a correlation of 90%.

Observable is that bed shear stresses are highest in the center of constriction-sector (Locations 3,4,5). Other locations with high values are in the constriction-sector near the interface with the expansion sector (location 10) and the area in the center of the downstream-section (location 6).

Table 56; Bed shear stresses [n/m^2]

Location	1	2	3	4	5	6	7	8	9	10	11
	-0,052	-0,004	-0,047	-0,118	-0,307	-0,054	-0,009	-0,027	-0,062	-0,023	-0,288

Estimation of transport

Following the formulations of the bed load transport by van Rijn (van Rijn, 2018). The results are represented as such, that locations at the same longitudinal location are coupled and transport is averaged over these locations (Table 57). For the calculations the absolute value was taken of the measured bed shear stresses. The results are also depicted per sector (Table 58) by calculating the area underneath each cross-sectional measurement. In this way it is observed that almost no scour is expected in all sectors.

Table 57; Bed load transport [kg/m/s]

Location	1	2 & 7	3 & 8	4 & 9	5 & 10	6 & 11
	NaN	NaN	NaN	NaN	$1{,}07*10^{-6}$	$6{,}98*10^{-6}$

Table 58; Bed load transport per sector [kg/day]

Sector	Upstream	Contraction	Constriction	Expansion	Downstream
	NaN	NaN	0,0	0,2	0,0

Water level

The water levels were measured at locations 1,3,5,6 they are depicted in Table 59. The levels were computed by measuring at 1000 [hz] for 15 seconds, and averaging those results. It is observed that the water level shows a drop of 0,8 [cm]. The water level seems to drop significantly during constriction, while shortly downstream of the constriction the water level seems to increase slightly.

Table 59; Water level [cm]

Location	1	3	5	6
	40,3925	39,7255	39,4026	39,5708

Measurements after 24h

Bed level

A projection of the bed after running for 24 [h] can be observed in Figure 280. The bed shows the development of a very narrow and deep scour hole just upstream of the placed logs. The logs also show to have tilted towards this hole. Furthermore some minor bed forms are observed further upstream of the logs and a small amount of accretion has occurred just downstream of the logs. Near the exit of the experiment a minimal amount of scour has started to occur.

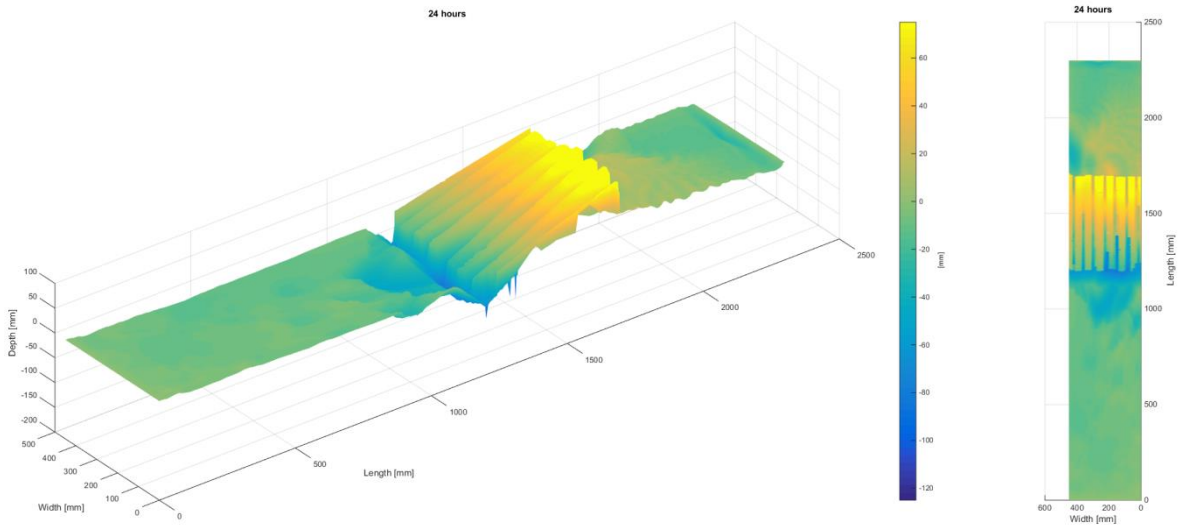

Figure 280; 24[h] bed projection

This can be confirmed with the average transect, observable in Figure 281. It shows a very steep scour hole just upstream of the logs, while also showing a minimal amount of accretion just downstream of the logs which gradually turn into on average scour towards the end of the expansion.

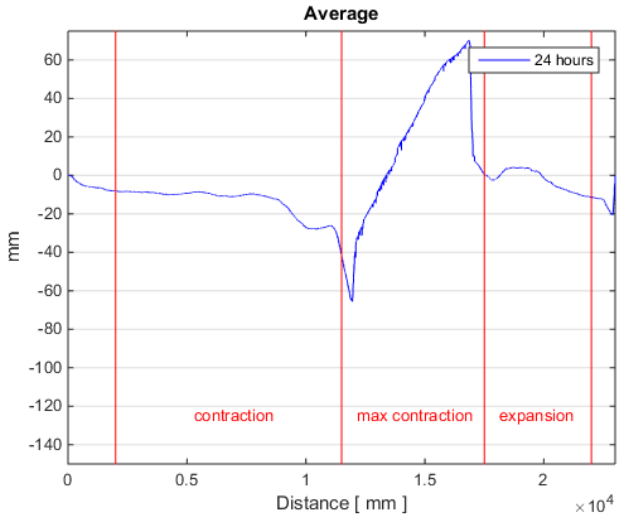

Figure 281; 24[h] average transect

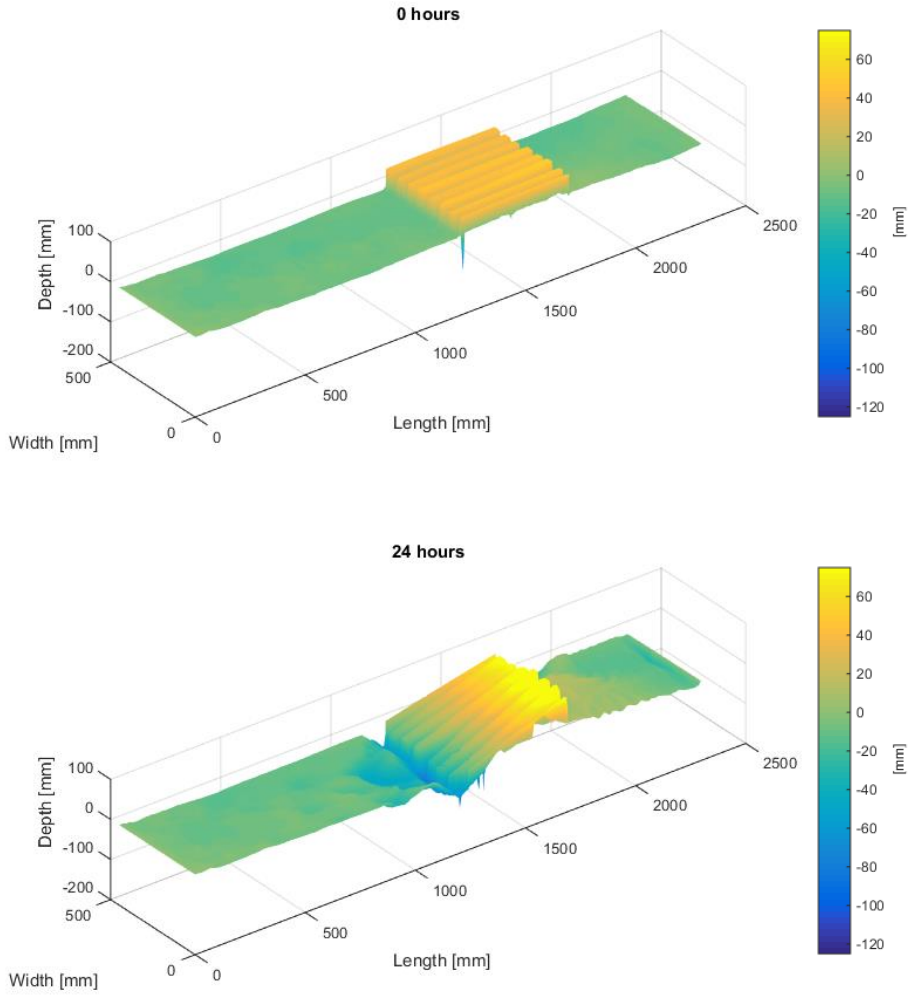

Figure 282; 0[h]-24[h] bed change projection

Table 60; Volume change per sector in [cm^3]

	Upstream	Contraction	Constriction	Expansion	Downstream
Volume	+3	-2097	-2023	+1798	-356

Velocity Profiles

While flow at location 1 remains similar to earlier measurements. At location 3 the flow has accelerated slightly closer to the bed most likely due to the tilting of the logs which has decreased the size of the upstream wake. At location 5 the flow profile has stayed more or less the same as before, although near bed velocities have increased slightly. The same can be said for location 6 with the addition that near the bed flow has now reversed and is on average directed towards the logs. Location 9 does not show any significant difference.

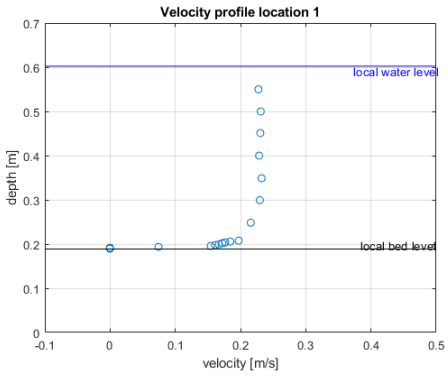

Figure 283; Velocity Profile location 1

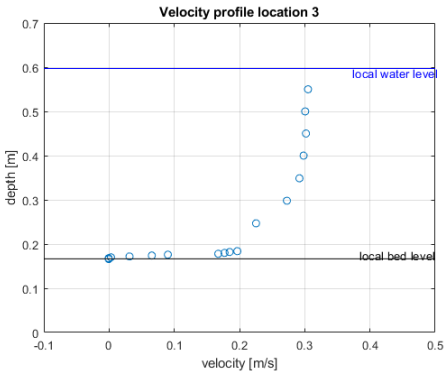

Figure 284; Velocity Profile location 3

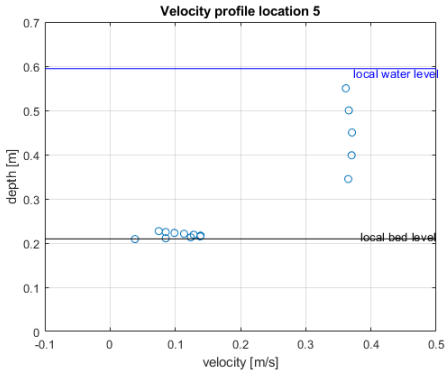

Figure 285; Velocity Profile location 5

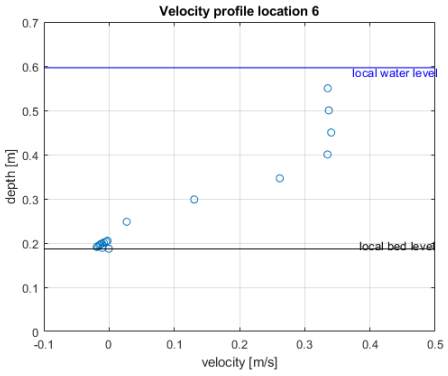

Figure 286; Velocity Profile location 6

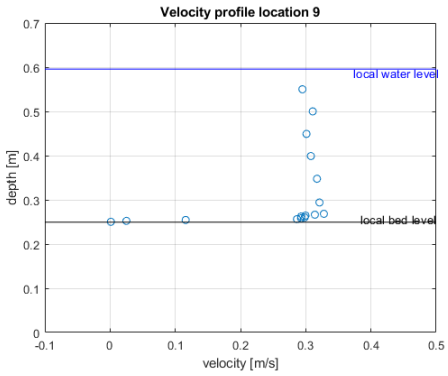

Figure 287; Velocity Profile location 9

Relative fluctuation intensity

Calculated fluctuation intensity shows that during flow contraction, in between location 1 & 2, this fluctuation drops noticeably and strongly increases again towards location 3. This same phenomenon is observed in between locations 7 and 8 although the magnitude of the relative fluctuation intensity is much greater at location 8. At locations 4 and 9 (measured above the logs) the relative fluctuation intensity remains relatively small but especially at location 9 it does show signs of increase with respect to the measurements taken at 0 [h].

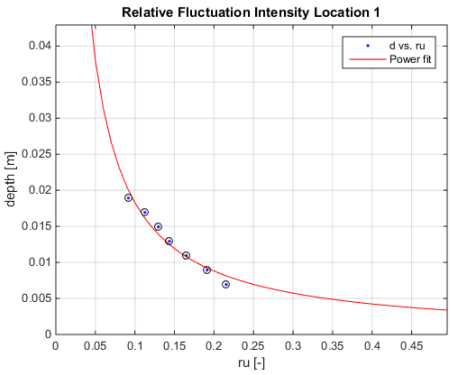

Figure 288; Relative fluctuation intensity location 1

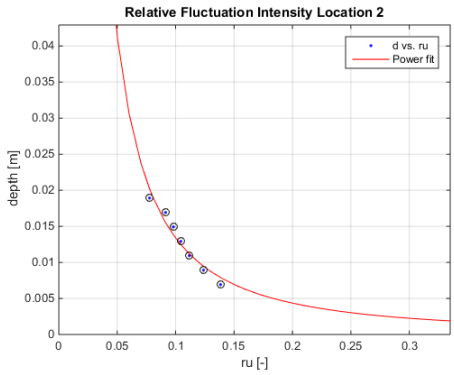

Figure 289; Relative fluctuation intensity location 2

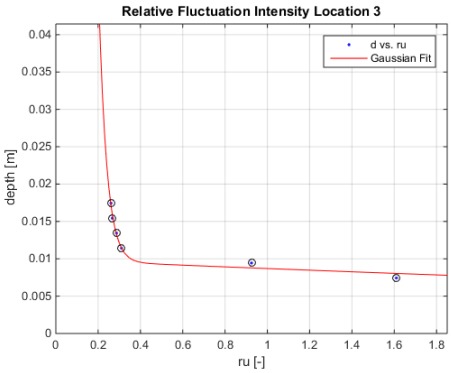

Figure 290; Relative fluctuation intensity location 3

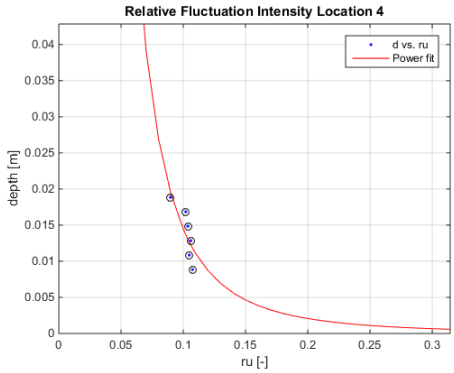

Figure 291; Relative fluctuation intensity location 4

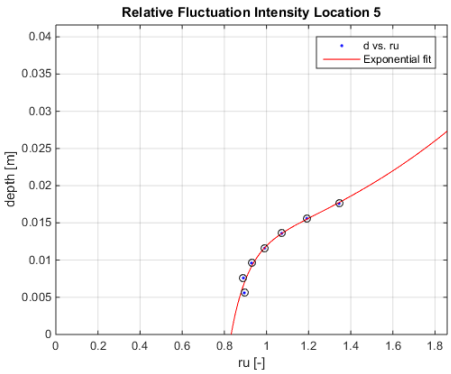

Figure 292; Relative fluctuation intensity location 5

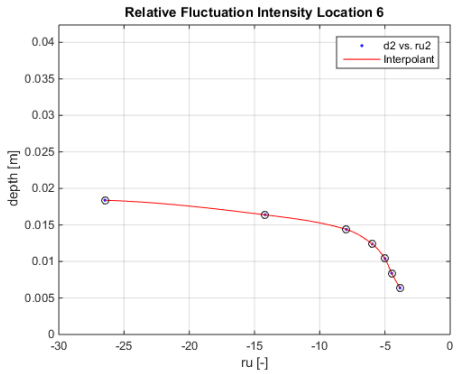

Figure 293; Relative fluctuation intensity location 6

At location 5 the relative fluctuation intensity increases higher up the water column, which is most likely caused due to the measurement being taken within the wake behind the logs, hence fluctuations are most likely stronger higher up the water column where the log is still present. Location 10 shows very strong negative fluctuation intensity; this is however caused by the average velocity in that specific region being close to zero and directed upstream towards the logs. Locations 6 & 11 now also show strong negative fluctuation intensities, indicating an on average very small upstream velocity towards the logs.

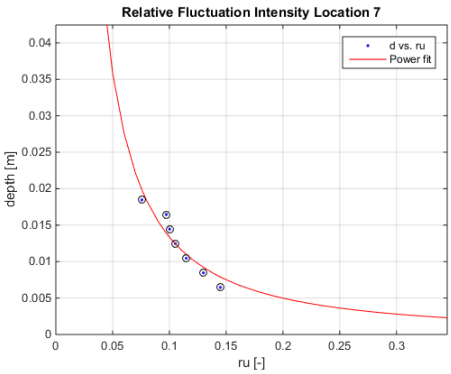

Figure 294; Relative fluctuation intensity location 7

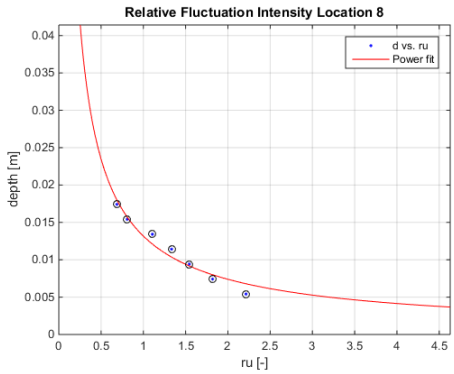

Figure 295; Relative fluctuation intensity location 8

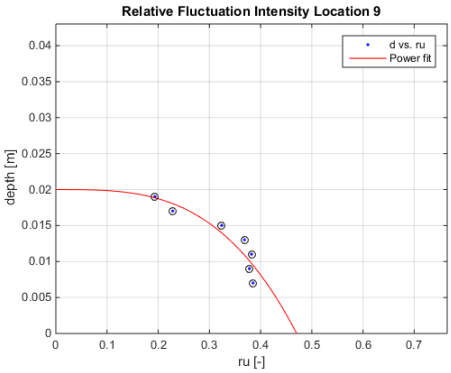

Figure 296; Relative fluctuation intensity location 9

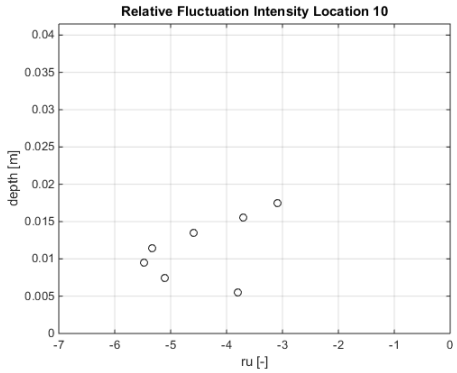

Figure 297; Relative fluctuation intensity location 10

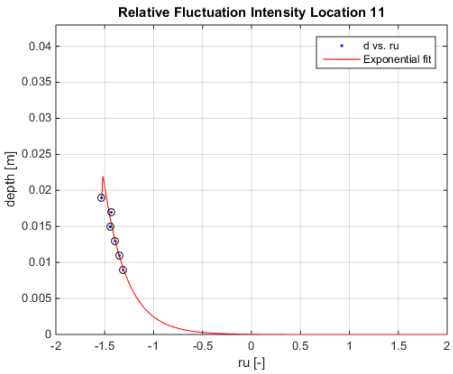

Figure 298; Relative fluctuation intensity location 11

Bed Shear stress

The bed shear stress was determined with Reynolds formula stated in (Schiereck & Verhagen, 2012). Bed shear stresses are determined by averaging the estimation for bed shear stress, over the centimeter measured above the bottom for a time frame of 3 minutes measuring at 50 [hz] per second, excluding all measured values that do not confirm with a signal to noise ratio above 15 and a correlation of 90%.

Observable is that bed shear stresses are highest in the constriction-sector (Locations 4,5,9 & 10). Interesting to note is the strong positive bed shear stresses that occur at these locations. Other locations with show relatively low values which are not directly associated with sediment transport.

Table 61; Bed shear stresses [n/m^2]

Location	1	2	3	4	5	6	7	8	9	10	11
	-0,031	-0,041	0,085	0,455	0,838	-0,046	-0,057	-0,028	0,533	0,438	-0,059

Estimation of transport

Following the formulations of the bed load transport by van Rijn (van Rijn, 2018). The results are represented as such, that locations at the same longitudinal location are coupled and transport is averaged over these locations (Table 62). For the calculations the absolute value was taken of the measured bed shear stresses. The results are also depicted per sector (Table 63) by calculating the area underneath each cross-sectional measurement. In this way it is expected that scour in the constriction and expansion sectors will strongly increase.

Table 62; Bed load transport [kg/m/s]

Location	1	2 & 7	3 & 8	4 & 9	5 & 10	6 & 11
	NaN	NaN	NaN	0,01212	0,02349	NaN

Table 63; Bed load transport per sector [kg/day]

Sector	Upstream	Contraction	Constriction	Expansion	Downstream
	NaN	NaN	321,7	237,5	NaN

Water level

The water levels were measured at locations 1,3,5,6 they are depicted in Table 64. The levels were computed by measuring at 1000 [hz] for 15 seconds, and averaging those results. It is observed that the water level shows a drop of 0,6 [cm]. The water level seems to drop significantly during constriction, while shortly downstream of the constriction the water level seems to increase slightly.

Table 64; Water level [cm]

Location	1	3	5	6
	40,2244	39,6915	39,4415	39,6281

Measurements after 48h

Bed level

As can be seen, the bed shows the largest amount of scour just in front of the logs. This is located at the point of maximum contraction. Furthermore scour now start to prevail just downstream of the logs and a deposition of sediment around 2000 [mm] seems to be moving downstream towards the end of the scanning range. These effects can be observed in Figure 299 & Figure 300.

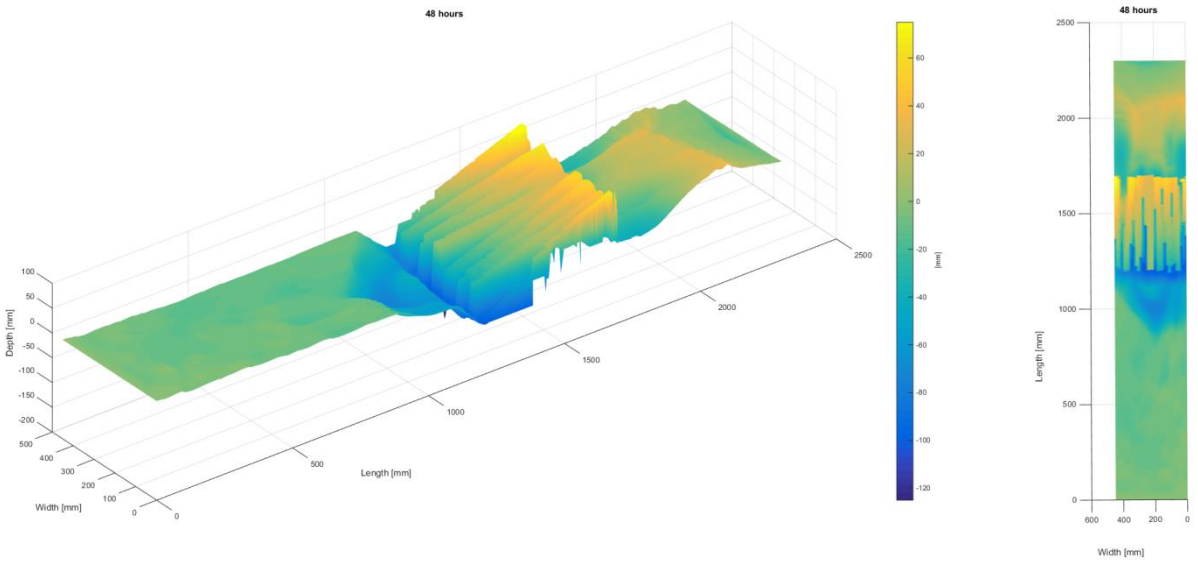

Figure 299; 48[h] bed projection

The average calculated transect observable in Figure 300, shows scour has penetrated up to 90 [mm] just in front of the logs. The bed upstream of the contraction and up till half way of the contracting section still is seemingly unaffected.

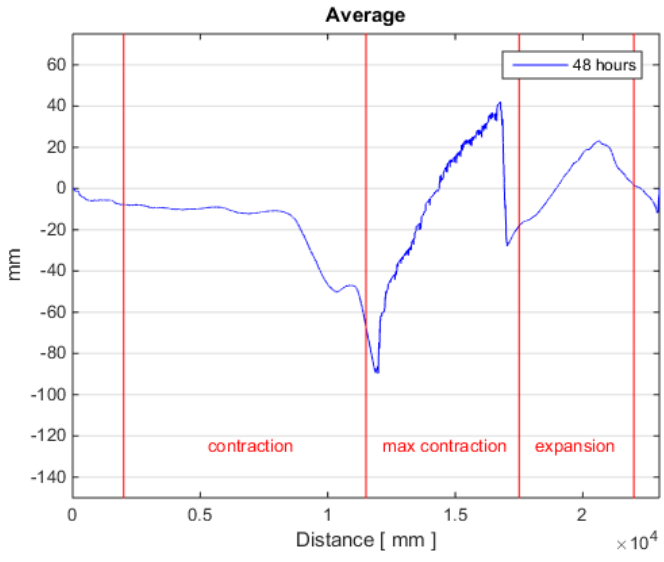

Figure 300; 48[h] average transect

Furthermore Figure 301 shows that erosion is clearly moving upstream, and the logs are starting to erode enough bed material around them to cause them to shift deeper and deeper into the bed. The accretion that had occurred earlier on just downstream of the logs has moved further downstream and scour now also dominates the bed just downstream of the logs. The scour hole upstream of the logs has significantly increased but the bed between 0-1000 [mm] has not been affected noticeably.

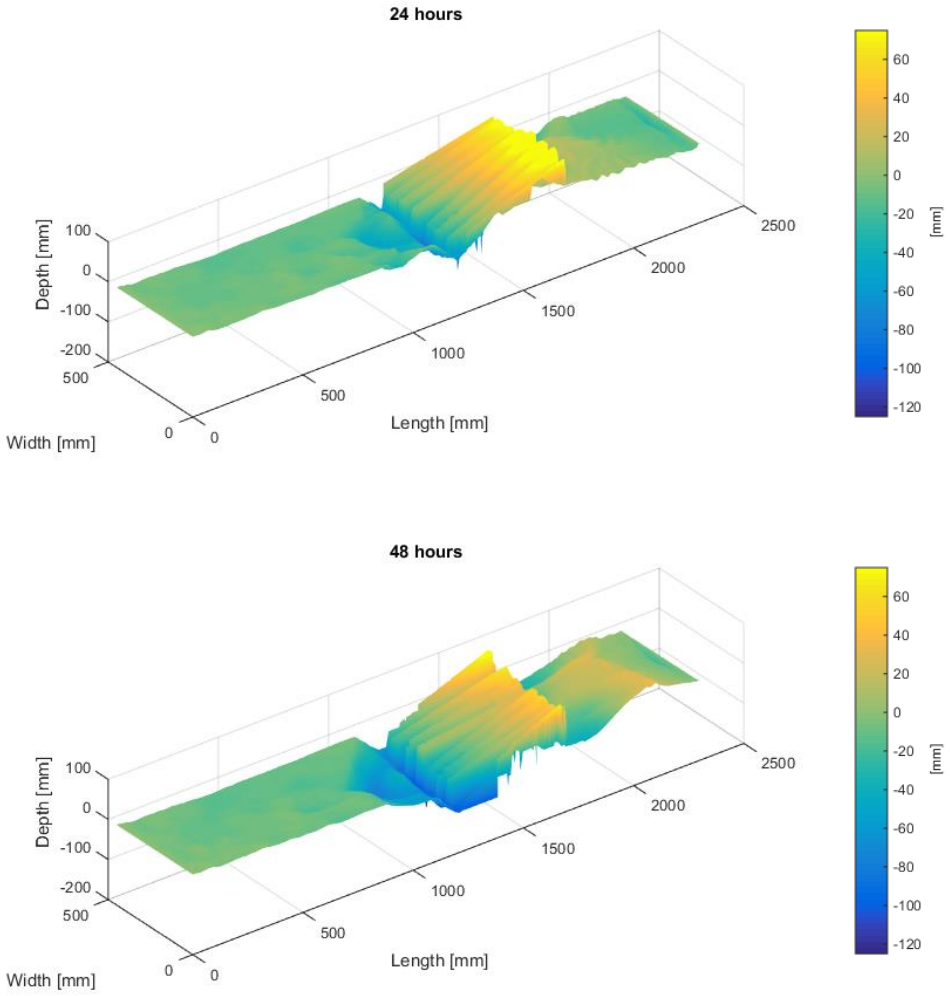

Figure 301; 24[h]-48[h] bed change projection

Table 65; Volume change per sector in [cm^3]

	Upstream	Contraction	Constriction	Expansion	Downstream
Volume	+14	-2380	-7001	+1612	+495

Velocity Profiles

While flow at location 1 & 3 remains similar to earlier measurements. At location 5 the flow profile has stayed more or less the same as before, although near bed flow has reversed. Location 6 now shows positive near bed velocities no longer directed towards the logs. Location 9 does not show any significant difference, except for the local bed level having decreased and the velocities near that bed also having slightly decreased.

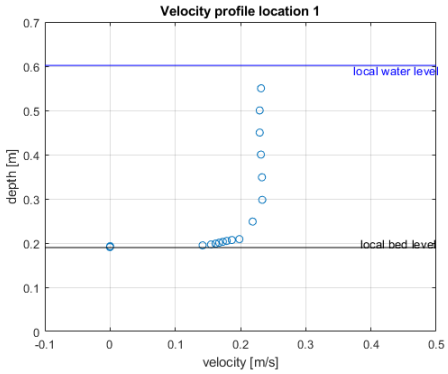

Figure 302; Velocity Profile location 1

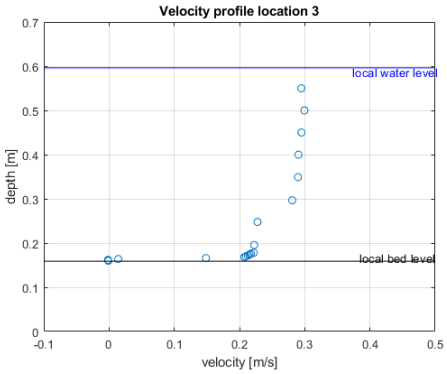

Figure 303; Velocity Profile location 3

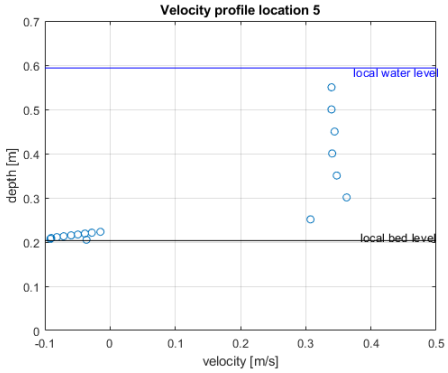

Figure 304; Velocity Profile location 5

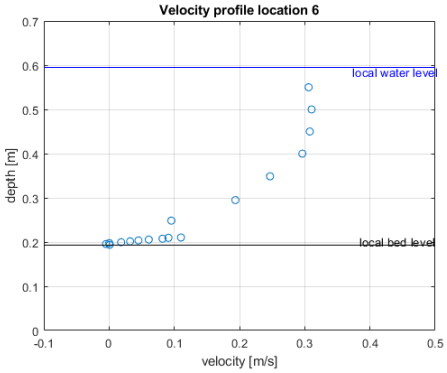

Figure 305; Velocity Profile location 6

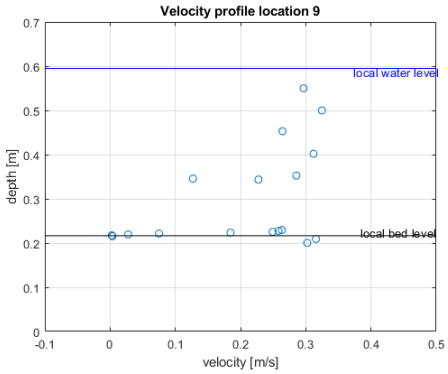

Figure 306; Velocity Profile location 9

Relative fluctuation intensity

Calculated fluctuation intensity shows that during flow contraction, in between location 1 & 2, this fluctuation drops noticeably and variably increases again towards location 3. This same phenomenon is observed in between locations 7 and 8 although the magnitude of the relative fluctuation intensity is much greater at location 8. At locations 4 and 9 (measured above the logs) the relative fluctuation intensity has increased significantly with respect to the measurements taken at 0 [h].

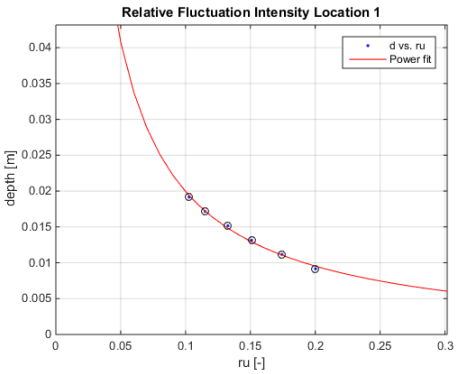

Figure 307; Relative fluctuation intensity location 1

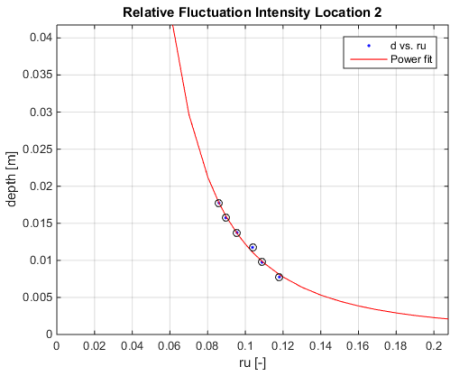

Figure 308; Relative fluctuation intensity location 2

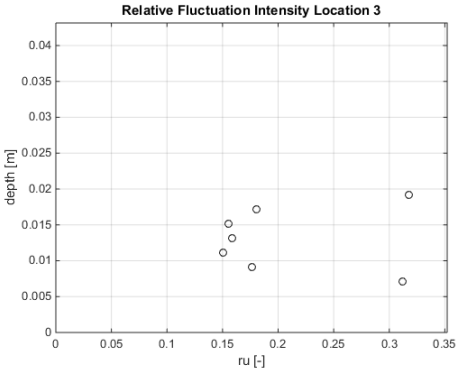

Figure 309; Relative fluctuation intensity location 3

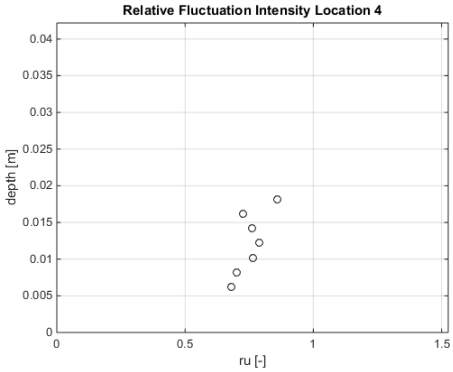

Figure 310; Relative fluctuation intensity location 4

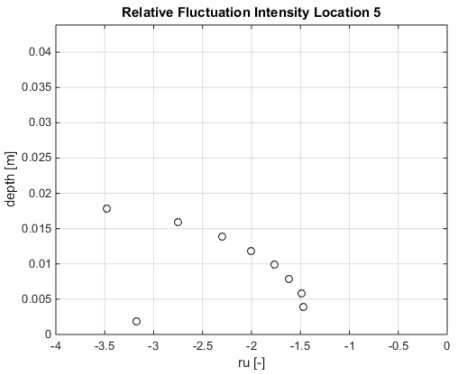

Figure 311; Relative fluctuation intensity location 5

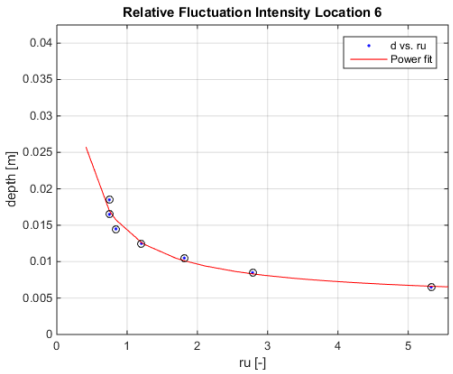

Figure 312; Relative fluctuation intensity location 6

At location 5 the relative fluctuation intensity is negative and increases in absolute sense higher up the water column, which is most likely caused due to the measurement being taken within the wake behind the logs and flow having reversed, hence fluctuations are most likely stronger higher up the water column where the log is still present. Location 10 shows strong positive fluctuation intensity; this is however caused by the average velocity in that specific region being close to zero. Locations 6 & 11 now also show strong no longer negative fluctuation intensities, indicating an on average very small downstream velocity.

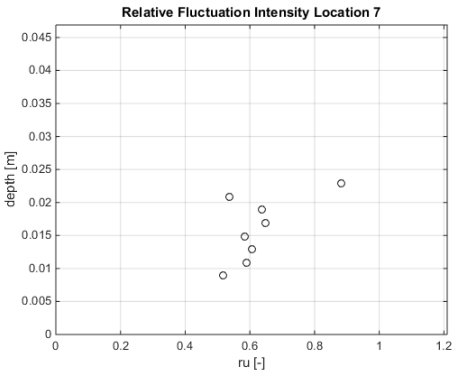

Figure 313; Relative fluctuation intensity location 7

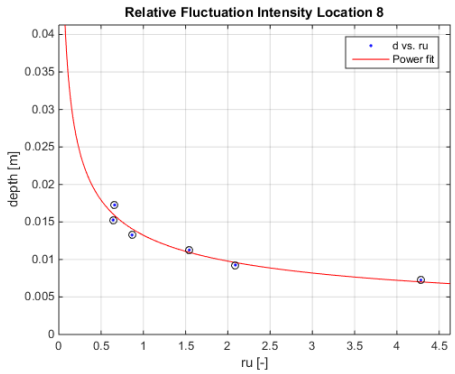

Figure 314; Relative fluctuation intensity location 8

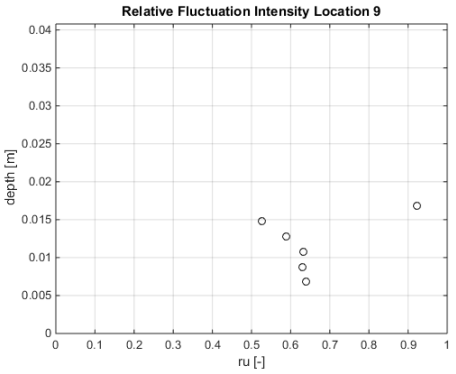

Figure 315; Relative fluctuation intensity location 9

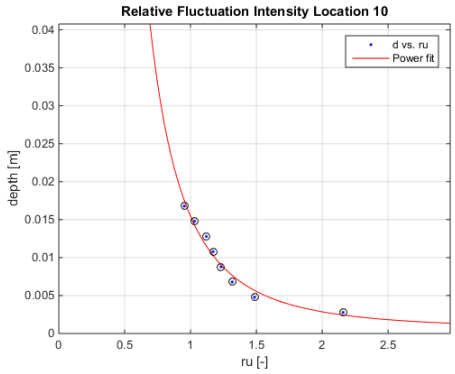

Figure 316; Relative fluctuation intensity location 10

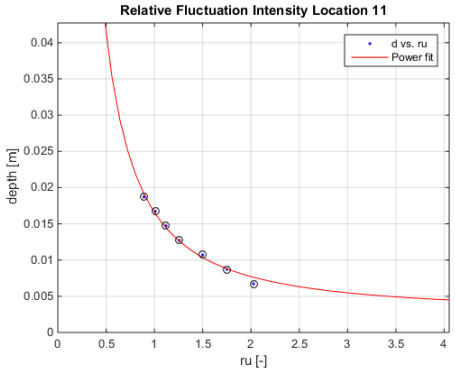

Figure 317; Relative fluctuation intensity location 11

Bed Shear stress

The bed shear stress was determined with Reynolds formula stated in (Schiereck & Verhagen, 2012). Bed shear stresses are determined by averaging the estimation for bed shear stress, over the centimeter measured above the bottom for a time frame of 3 minutes measuring at 50 [hz] per second, excluding all measured values that do not confirm with a signal to noise ratio above 15 and a correlation of 90%.

Bed shear stresses exceed values associated with high level of transport at locations in or downstream of the constriction. Only locations above the logs (4 & 9) show high positive bed shear stresses. Other locations with high bed shear stresses show negative values.

Table 66; Bed shear stresses [n/m^2]

Location	1	2	3	4	5	6	7	8	9	10	11
	-0,049	-0,067	0,096	0,477	-0,170	-0,176	-0,105	-0,042	0,904	-0,252	-0,106

Estimation of transport

Following the formulations of the bed load transport by van Rijn (van Rijn, 2018). The results are represented as such, that locations at the same longitudinal location are coupled and transport is averaged over these locations (Table 67). For the calculations the absolute value was taken of the measured bed shear stresses. The results are also depicted per sector (Table 68) by calculating the area underneath each cross-sectional measurement. The estimation of transport for the constriction-sector is however to be taken with skepticism as the measured bed shear stresses are on top of the logs.

Table 67; Bed load transport [kg/m/s]

Location	1	2 & 7	3 & 8	4 & 9	5 & 10	6 & 11
	NaN	NaN	NaN	0,028304	0,00024	NaN

Table 68; Bed load transport per sector [kg/day]

Sector	Upstream	Contraction	Constriction	Expansion	Downstream
	NaN	NaN	383,1	2,4	NaN

Water level

The water levels were measured at locations 1,3,5,6 they are depicted in Table 69. The levels were computed by measuring at 1000 [hz] for 15 seconds, and averaging those results. It is observed that the water level shows a drop of 0,7 [cm]. The water level seems to drop significantly during constriction, while shortly downstream of the constriction the water level seems to increase slightly.

Table 69; Water level [cm]

Location	1	3	5	6
	40,1663	39,6154	39,3624	39,4816

Measurements after 72h

Bed level

As can be seen, the bed shows the largest amount of scour just in front of the logs. This is located at the point of maximum contraction. Furthermore significant scour now occurs downstream of the logs and a fairly large deposition of sediment around 2000 [mm] seemingly has stopped moving towards the end of the scanning range. These effects can be observed in Figure 318 & Figure 319.

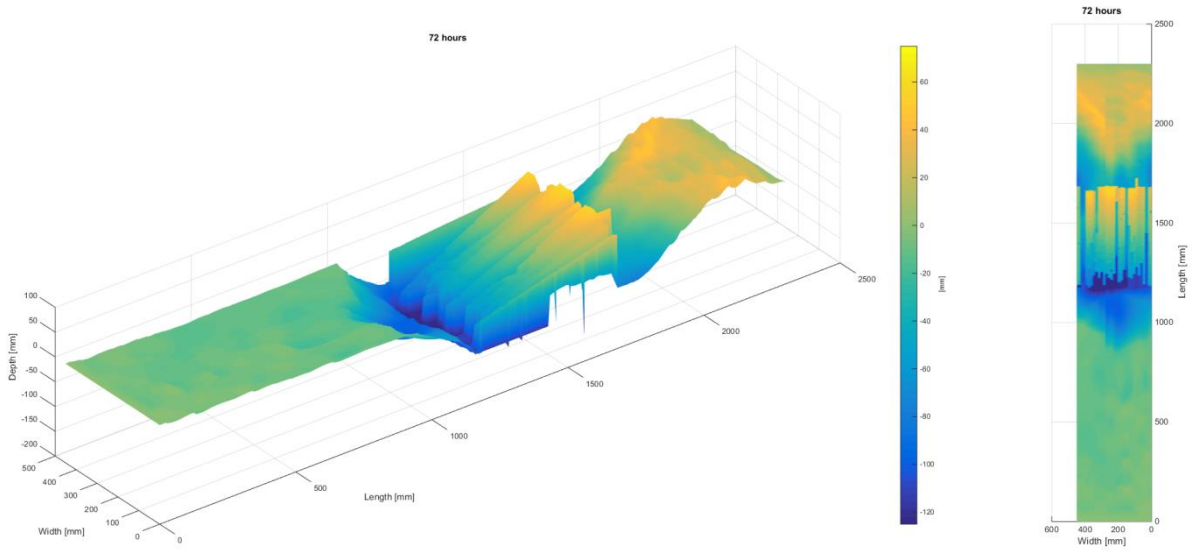

Figure 318; 72[h] bed projection

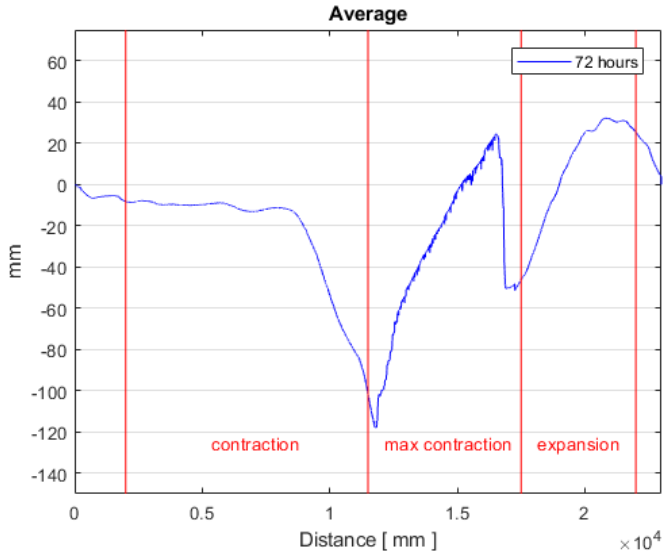

Figure 319; 72[h] average transect

Furthermore Figure 32Figure 320 shows that scour has increased even further in magnitude, and the logs have positioned themselves even deeper than before. Accretion downstream has increased significantly. Furthermore it can be observed that the logs are now for the most part below the original bed level.

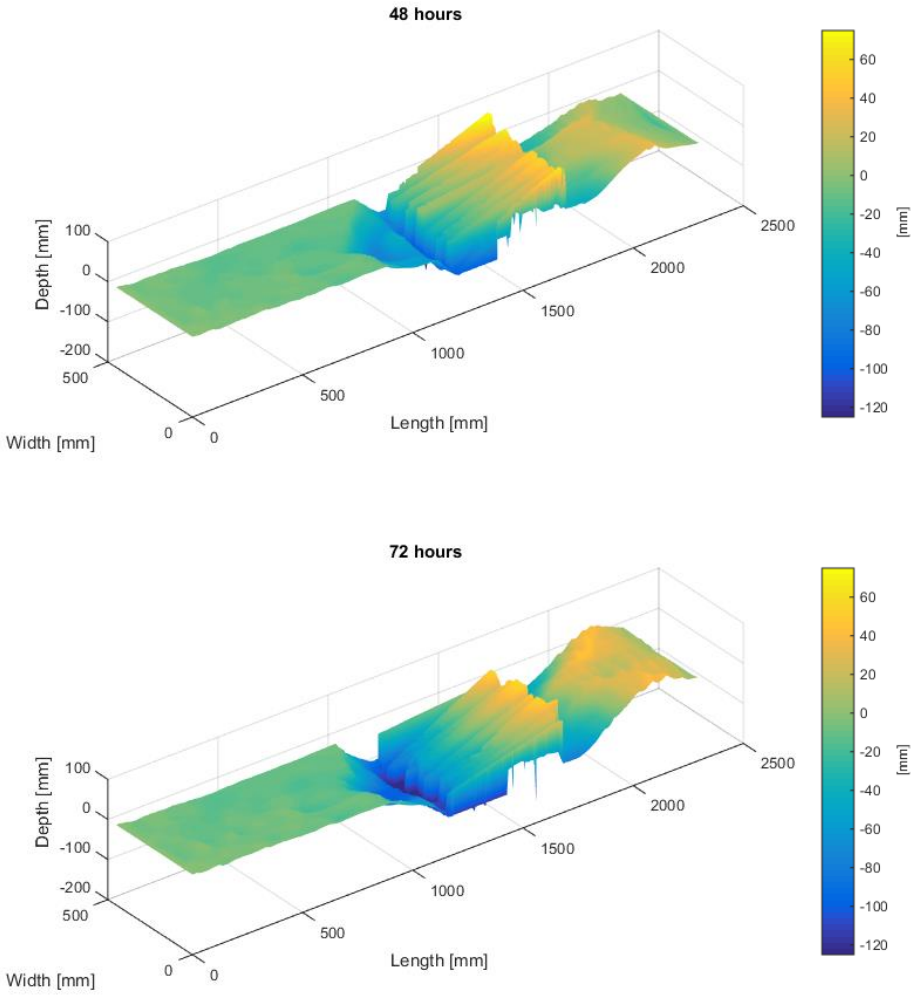

Figure 320; 48[h]-72[h] bed change projection

Table 70; Volume change per sector in [cm^3]

	Upstream	Contraction	Constriction	Expansion	Downstream
Volume [cm^3]	+1	-1886	-5801	+890	+886

Velocity Profiles

While flow at location 1 & 3 remains similar to earlier measurements. At location 5 the flow profile has stayed more or less the same as before, although near bed flow again reversed and are no longer negative. Location 6 still doesn't show a correctly attached flow profile. Location 9 does not show any significant difference, except for the local bed level having decreased even further towards the initial bed level.

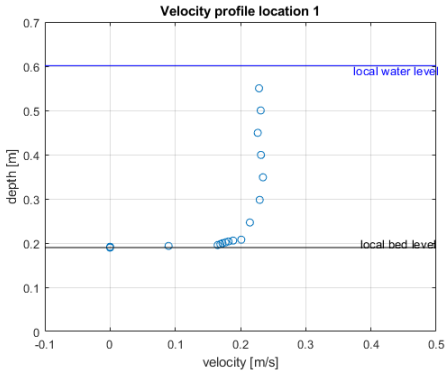

Figure 321; Velocity Profile location 1

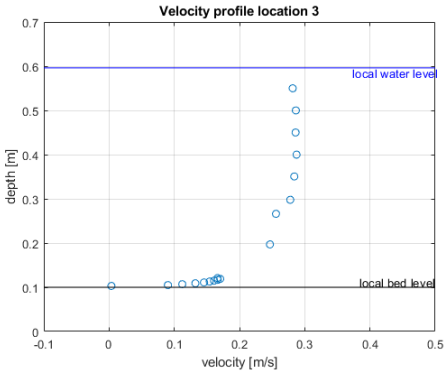

Figure 322; Velocity Profile location 3

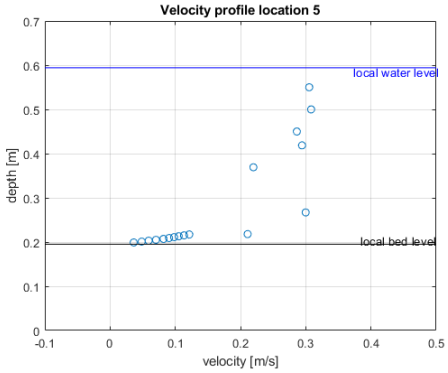

Figure 323; Velocity Profile location 5

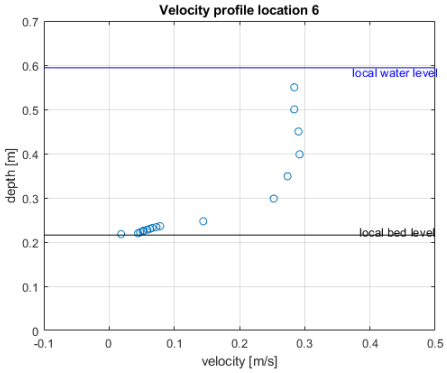

Figure 324; Velocity Profile location 6

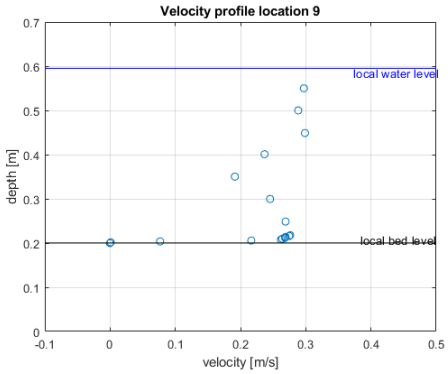

Figure 325; Velocity Profile location 9

Relative fluctuation intensity

Calculated fluctuation intensity shows that during flow contraction, in between location 1 & 2, this fluctuation drops noticeably and variably increases again towards location 3. This same phenomenon is observed in between locations 7 and 8 although the magnitude of the relative fluctuation intensity is much greater at location 8. At locations 4 and 9 (measured above the logs) the relative fluctuation intensity is similar with respect to the measurements taken at 0 [h].

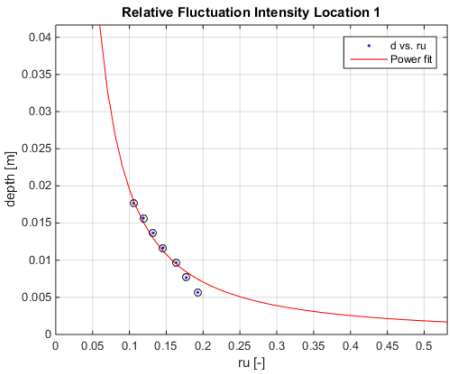

Figure 326; Relative fluctuation intensity location 1

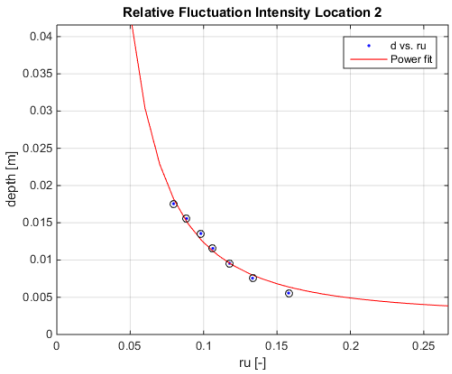

Figure 327; Relative fluctuation intensity location 2

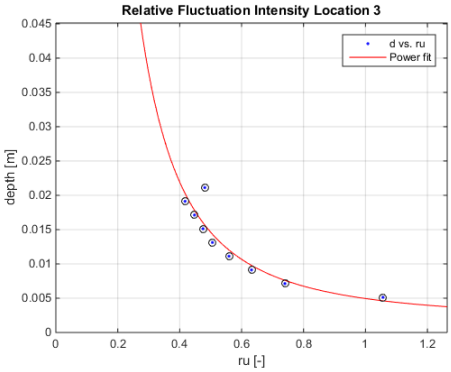

Figure 328; Relative fluctuation intensity location 3

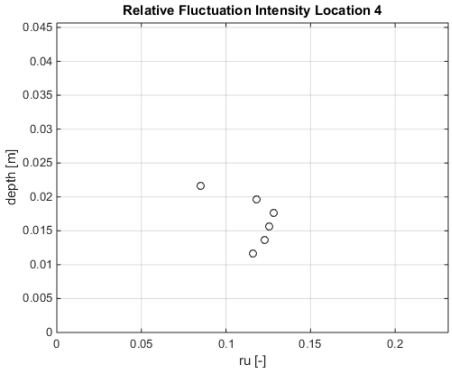

Figure 329; Relative fluctuation intensity location 4

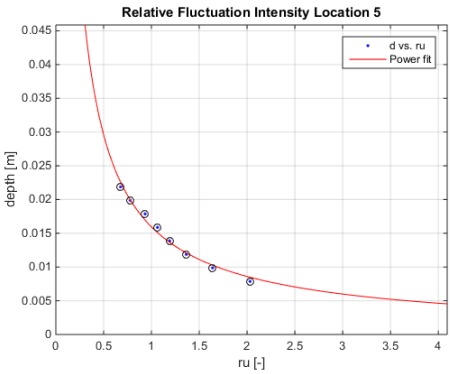

Figure 330; Relative fluctuation intensity location 5

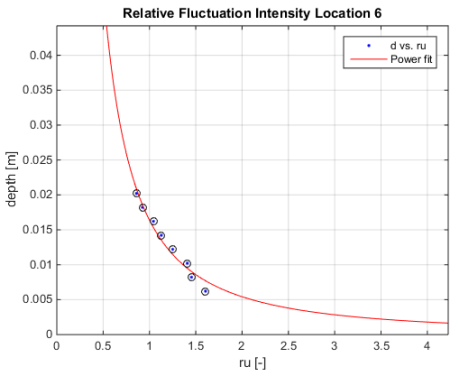

Figure 331; Relative fluctuation intensity location 6

At location 5 the relative fluctuation intensity has now observed a more traditional distribution, although it is relatively large indicating low flow velocities. Location 10 shows very strong positive fluctuation intensity; caused by low flow velocities. Locations 6 & 11 now again show strong positive fluctuation intensities, indicating on average very small downstream directed velocities.

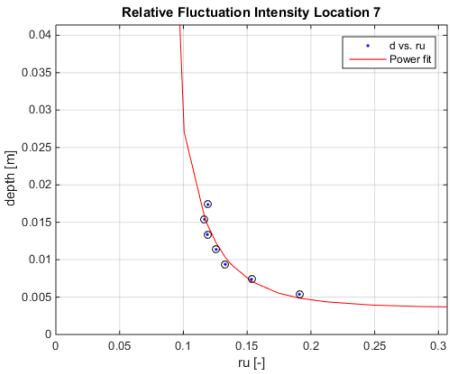

Figure 332; Relative fluctuation intensity location 7

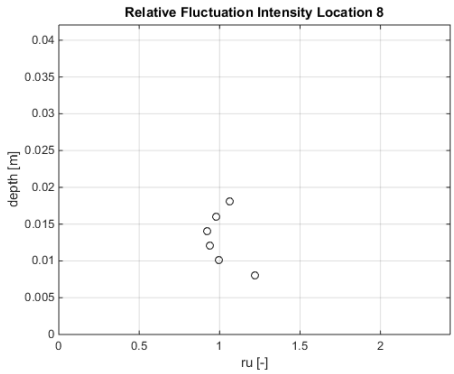

Figure 333; Relative fluctuation intensity location 8

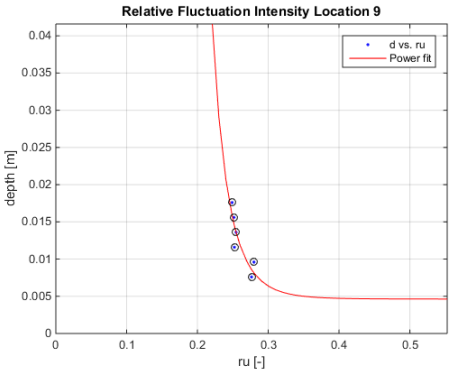

Figure 334; Relative fluctuation intensity location 9

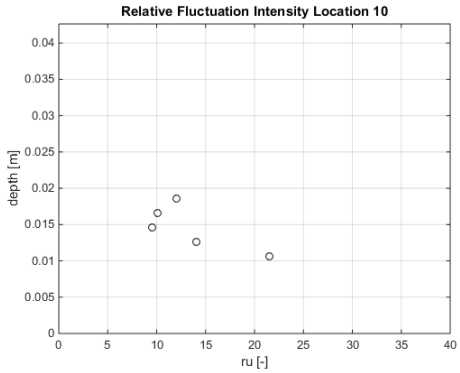

Figure 335; Relative fluctuation intensity location 10

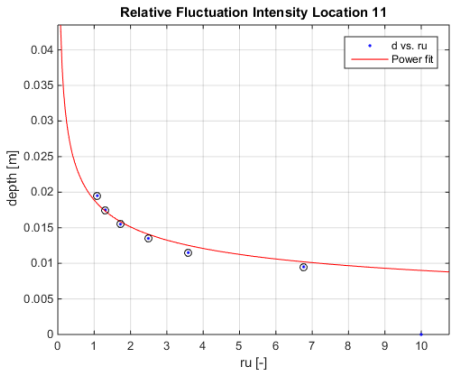

Figure 336; Relative fluctuation intensity location 11

Bed Shear stress

The bed shear stress was determined with Reynolds formula stated in (Schiereck & Verhagen, 2012). Bed shear stresses are determined by averaging the estimation for bed shear stress, over the centimeter measured above the bottom for a time frame of 3 minutes measuring at 50 [hz] per second, excluding all measured values that do not confirm with a signal to noise ratio above 15 and a correlation of 90%.

Bed shear stresses exceed values associated with high level of transport at locations in or downstream of the constriction. Only locations above the logs (4 & 9) show high positive bed shear stresses. Other locations with high bed shear stresses show negative values.

Table 71; Bed shear stresses [n/m^2]

Location	1	2	3	4	5	6	7	8	9	10	11
	-0,054	-0,081	-0,297	0,693	-0,339	-0,114	-0,036	-0,058	0,546	-0,227	-0,192

Estimation of transport

Following the formulations of the bed load transport by van Rijn (van Rijn, 2018). The results are represented as such, that locations at the same longitudinal location are coupled and transport is averaged over these locations (Table 72). For the calculations the absolute value was taken of the measured bed shear stresses. The results are also depicted per sector (Table 73) by calculating the area underneath each cross-sectional measurement. In this way it is expected that scour in the constriction- sector will remain large and the scour in the expansion sector will start to pick up.

Table 72; Bed load transport [kg/m/s]

Location	1	2 & 7	3 & 8	4 & 9	5 & 10	6 & 11
	NaN	NaN	$2{,}078*10^{-5}$	0,02187	0,00165	NaN

Table 73; Bed load transport per sector [kg/day]

Sector	Upstream	Contraction	Constriction	Expansion	Downstream
	NaN	0,2	306,0	16,7	NaN

Water level

The water levels were measured at locations 1,3,5,6 they are depicted in Table 74. The levels were computed by measuring at 1000 [hz] for 15 seconds, and averaging those results. It is observed that the water level shows a drop of 0,7 [cm]. The water level seems to drop significantly during constriction, while shortly downstream of the constriction the water level seems to increase slightly.

Table 74; Water level [cm]

Location	1	3	5	6
	40,1197	39,623	39,406	39,4231

Measurements after 96h

Bed level

The bed after 96 [h] shows an even further intensification of scour, (see Figure 337 & Figure 338). The average transect shows that the logs are now almost fully below the original bed level, and maximum scour average has reached 120 [mm], while locally this is occasionally even stronger.

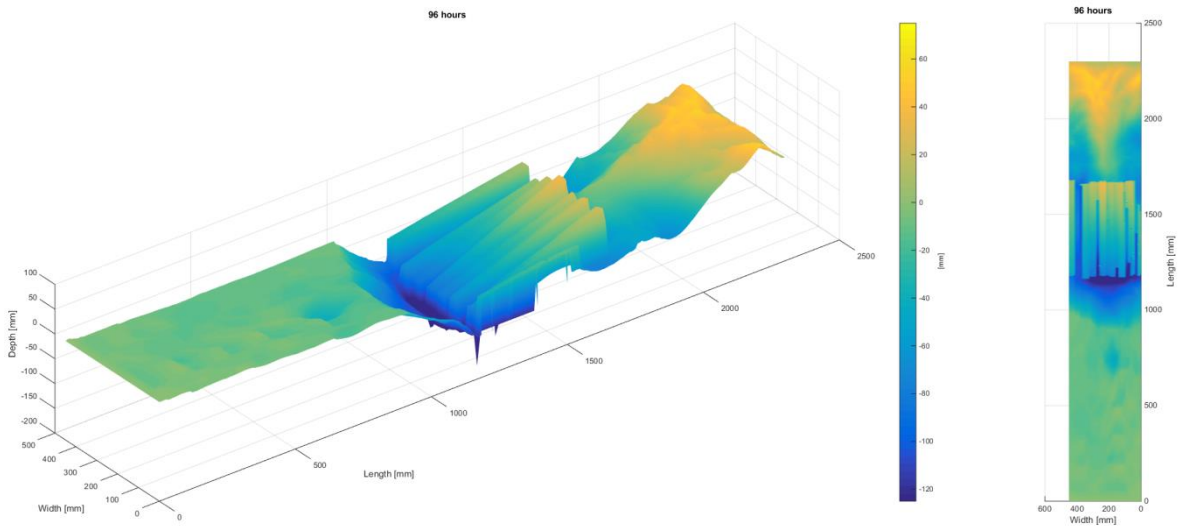

Figure 337; Bed map after 96 [h]

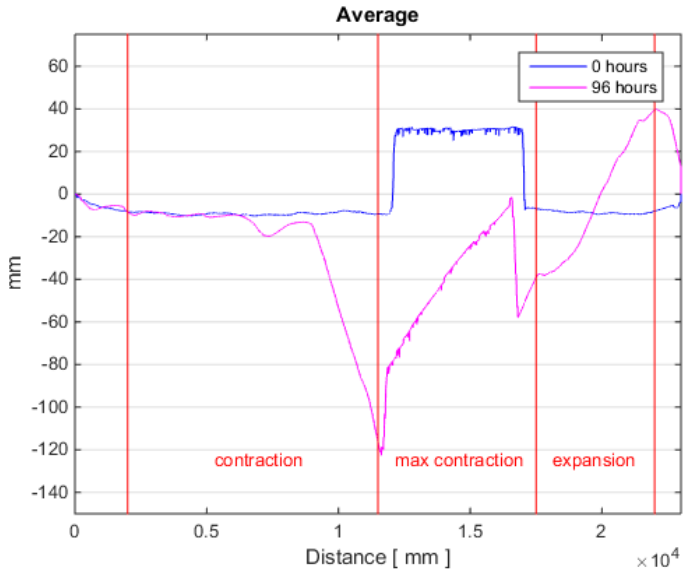

Figure 338; Average transects through time

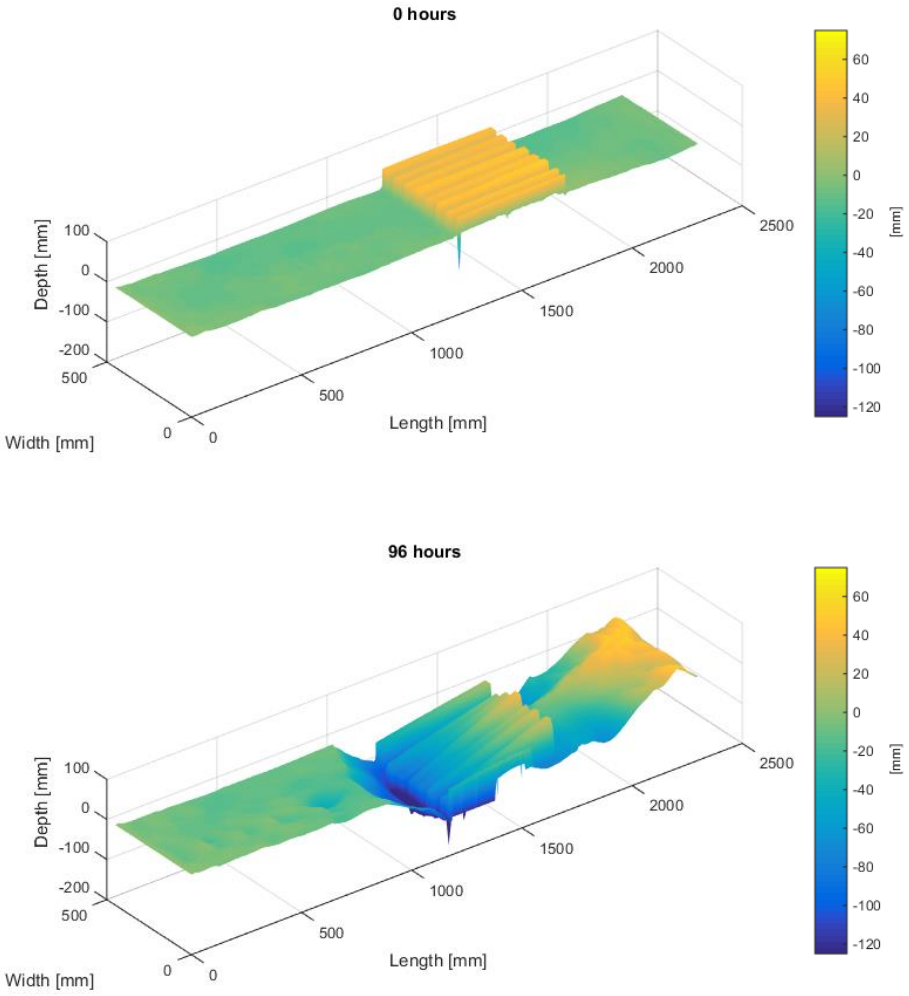

Figure 339; Bed change with respect to 0[h]

Table 75; Volume change per sector in [cm^3]

	Upstream	Contraction	Constriction	Expansion	Downstream
Volume	-14	-686	-2896	-2531	771

Concluding Remarks

This first protected scour does not show any direct positive effects from the placement of logs parallel to the governing flow direction. Comparing the bed after 96 [h] with the bed at 0 [h], shows a dramatic amount of scour has occurred and one could argue scour intensity has even increased in certain areas.

Appendix D II

I Introduction

The protected Scour experiments are considered to be the baseline experiments for the application of wooden logs as a scour protection. The “Protected Scour A” experiments feature a flow parallel placed single layer of logs directly on top of the bed, in the area of maximum contraction. Similar to the basic scour experiments bed, velocity and fluctuation intensity development is measured during a 96 [h] run. This report includes all measured findings during this particular experiment. Conclusions are drawn in the main report on the basis of multiple similarly conducted experiments. A short preliminary conclusion is however included at the end of this report.

Summary

Table 76 represents relevant scour quantities after 96 [h]. Note that the absolute is measured relative to the measurement of the bed at 0 [h], excluding the maximum scour depth which is measured to a reference bed with a 0 [mm] elevation. Measurements of scour volume in the column with respect to reference include missing volume with respect to a reference be of 0 [mm] and corrected for the presence of logs .

Table 76; Summary of quantities (Negative values indicate scour, positive indicate accretion)

	Quantity	With respect to reference
Maximum Scour Depth [mm]	146	146
Total Scoured volume [cm^3]	-22673	-30819
Scoured volume Upstream-sector [cm^3]	-80	-324
Scoured volume Contracting-sector [cm^3]	-11583	-14966
Scoured volume Constricted-sector [cm^3]	-14863	-17593
Scoured volume Expanding-sector [cm^3]	+3311	+1710
Scoured volume Downstream-sector [cm^3]	+542	+1508

Measurements at 0h

Bed level

A projection of the bed at the moment of initiation of flow during the first scour experiment can be seen in Figure 340. Clearly observable are the placed logs on the bed. They are roughly located in between 1200-1700 [mm] from the entry point of flow. The bed further seems to be relatively flat with only minor deformations with respect to the size of the logs.

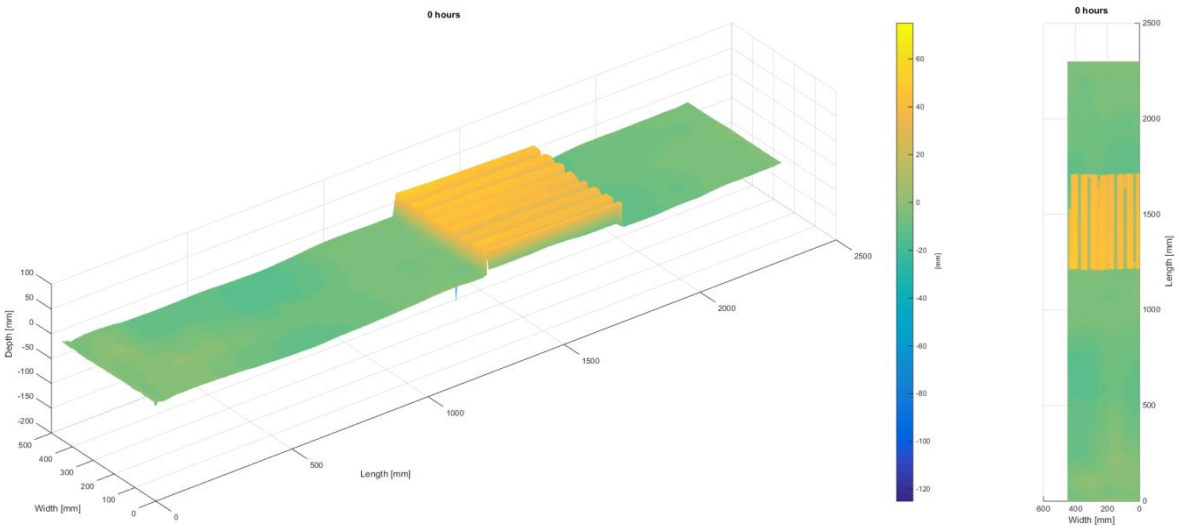

Figure 340; Bed map 0[h]

The average transect, observable in Figure 341, was calculated from the 31 transects taken over the entire length of the laboratory set-up. As can be seen, the bed is on some locations slightly below the target value of 0 [mm] with a maximum deviation of about 10 [mm]. These deformations are located halfway the contraction and at the downstream end of the maximal contracted area.

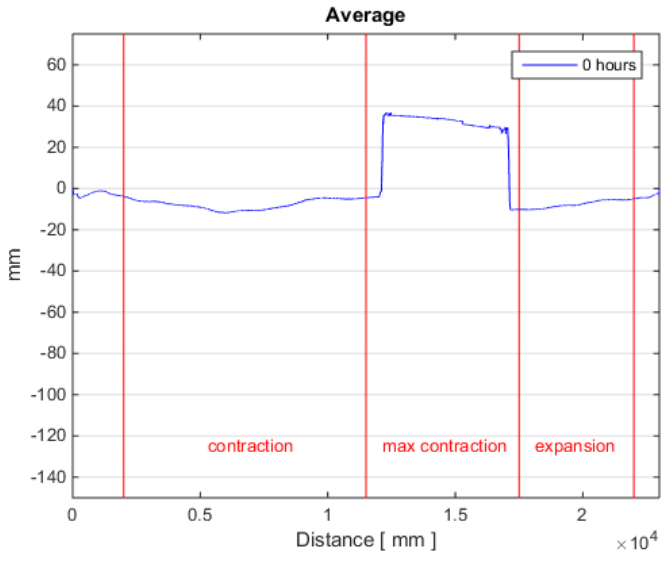

Figure 341; 0 [h] average transect

Velocity Profiles

For the flow profiles at the beginning of the experiment it can be said that for both locations 1 & 3 a typical pattern can be identified with respect to regular turbulent flow. The pattern does increase from location 1 to location 3. For the locations downstream a strong disturbance can be seen close to the bed, where the velocities are very small, this being the effect of the wake of the logs. At location 9 an increase of flow velocity about 10 [cm] above the logs can be seen, which is most likely caused by the presence of the logs. Observing locations 5 & 6 more closely, one can see this local acceleration moving up the water column, and redistributing the log-carpet induced acceleration. Also observable is the attempt of the water column to redistribute the velocity at location 6, where flow is seemingly attempting to reattach to the bottom.

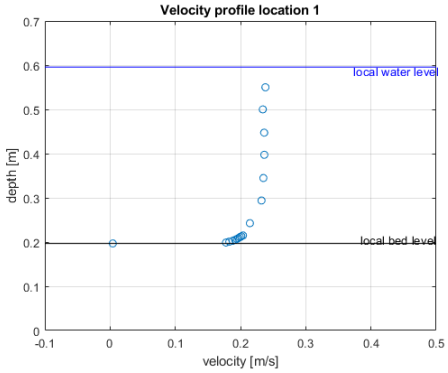

Figure 342; Velocity Profile location 1

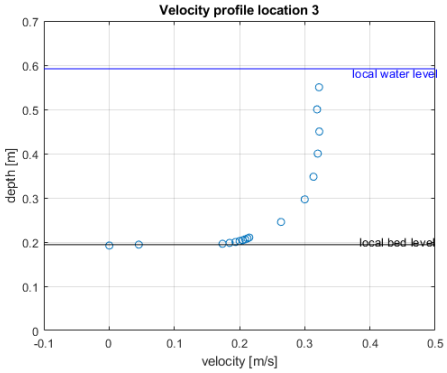

Figure 343; Velocity Profile location 3

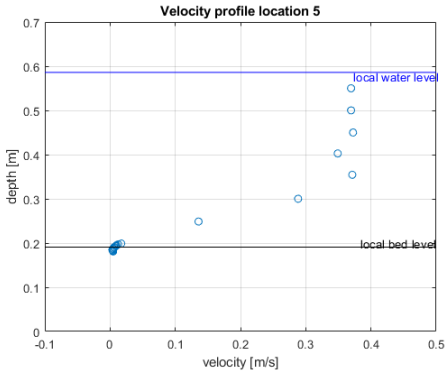

Figure 344; Velocity Profile location 5

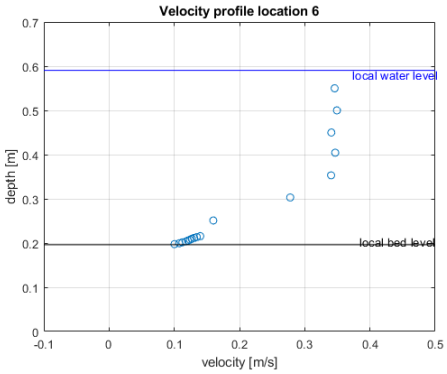

Figure 345; Velocity Profile location 6

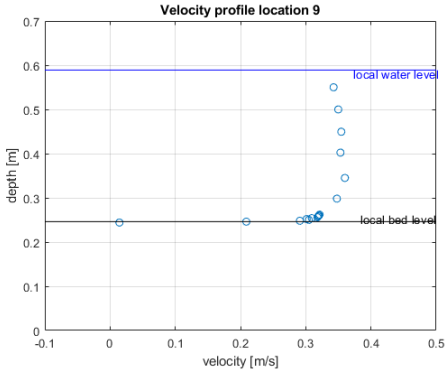

Figure 346; Velocity Profile location 9

Relative fluctuation intensity

It is shown that fluctuation intensity stays proportionally the same during contraction from location 1-3 and location 7-8. At locations on top of the log layer (4 & 9) RFI becomes more uniform and increases with respect to the other locations upstream.

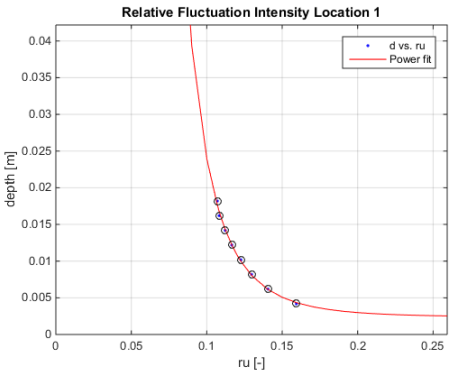

Figure 347; Relative fluctuation intensity location 1

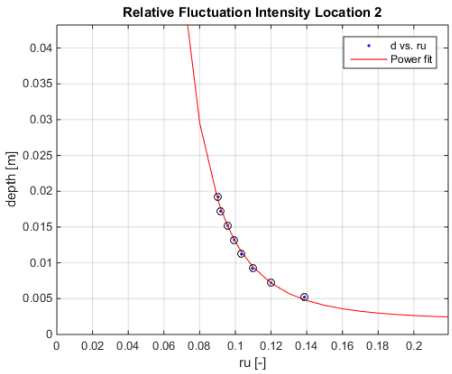

Figure 348; Relative fluctuation intensity location 2

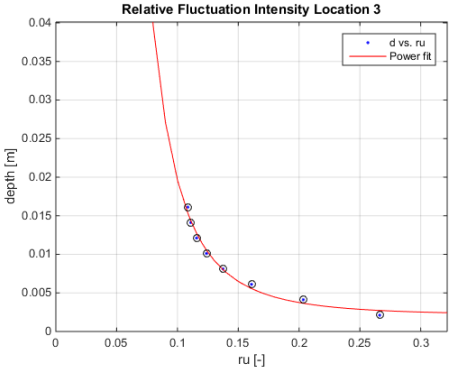

Figure 349; Relative fluctuation intensity location 3

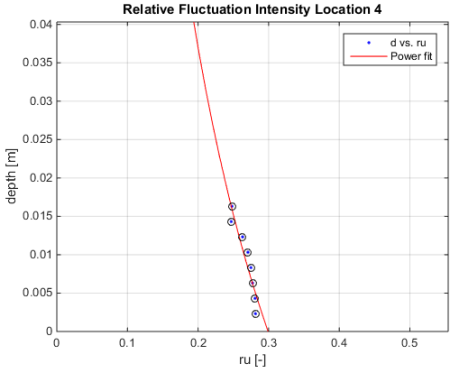

Figure 350; Relative fluctuation intensity location 4

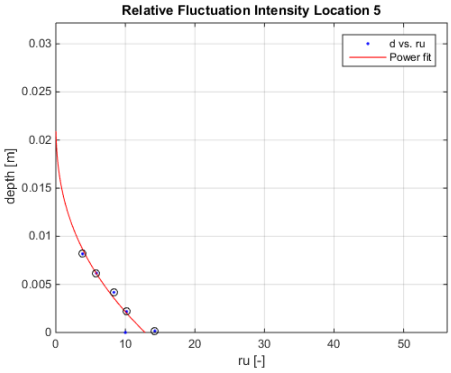

Figure 351; Relative fluctuation intensity location 5

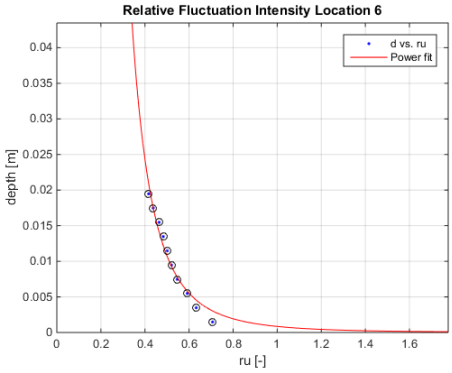

Figure 352; Relative fluctuation intensity location 6

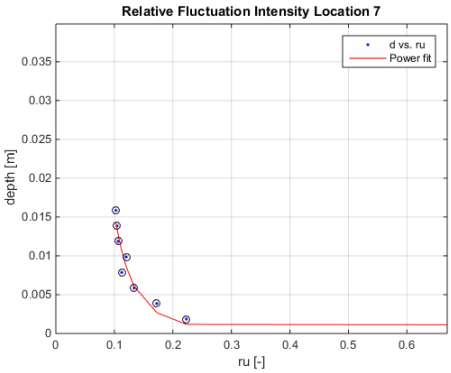

Figure 353; Relative fluctuation intensity location 7

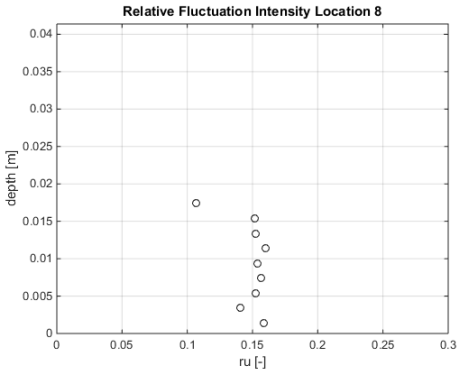

Figure 354; Relative fluctuation intensity location 8

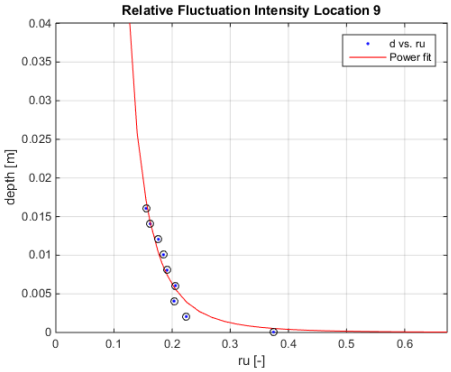

Figure 355; Relative fluctuation intensity location 9

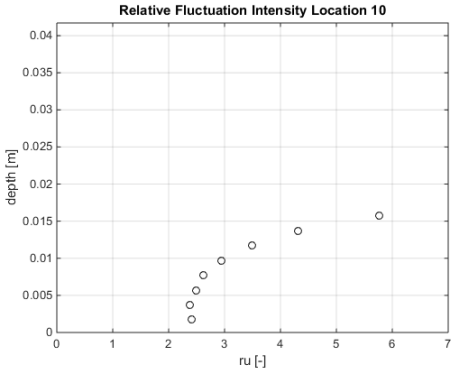

Figure 356; Relative fluctuation intensity location 10

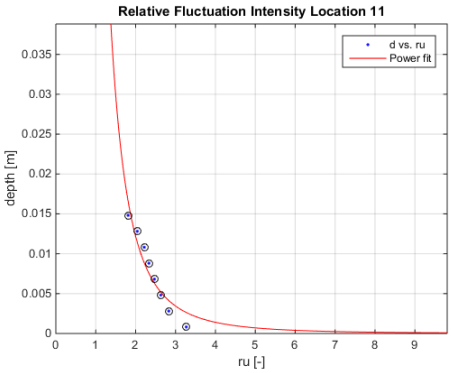

Figure 357; Relative fluctuation intensity location 11

At locations 5 & 10 fluctuation intensity is very high, and caused by the near zero velocities that are present near the bed in the wake of the logs. Further downstream near location 6 & 11 RFI reduces but remains to be fairly high, especially at location 11.

Bed Shear stress

The bed shear stress was determined with Reynolds formula stated in (Schiereck & Verhagen, 2012). Bed shear stresses are determined by averaging the estimation for bed shear stress, over the centimeter measured above the bottom for a time frame of 3 minutes measuring at 50 [hz] per second, excluding all measured values that do not confirm with a signal to noise ratio above 15 and a correlation of 90%.

Bed shear stresses exceed values associated with high level of transport at locations in or downstream of the constriction. Locations in and downstream of the constriction (3,4,5,6,9,10 & 11) immediately show strong bed shear stresses.

Table 77; Bed shear stresses [n/m^2]

Location	1	2	3	4	5	6	7	8	9	10	11
	-0,059	-0,006	-0,101	-0,337	-0,315	-0,117	-0,063	-0,049	-0,231	-0,193	-0,229

Estimation of transport

Following the formulations of the bed load transport by van Rijn (van Rijn, 2018). The results are represented as such, that locations at the same longitudinal location are coupled and transport is averaged over these locations (Table 78). For the calculations the absolute value was taken of the measured bed shear stresses. The results are also depicted per sector (Table 79) by calculating the area underneath each cross-sectional measurement. In this way it is expected that scour will be located in the constriction-sector and the expansion-sector

Table 78; Bed load transport [kg/m/s]

Location	1	2 & 7	3 & 8	4 & 9	5 & 10	6 & 11
	NaN	NaN	NaN	0,00168	0,00093	$1,03*10^{-5}$

Table 79; Bed load transport per sector [kg/day]

Sector	Upstream	Contraction	Constriction	Expansion	Downstream
	NaN	NaN	28,9	19,0	0,0

Water level

The water levels were measured at locations 1,3,5,6 they are depicted in Table 80. The levels were computed by measuring at 1000 [hz] for 15 seconds, and averaging those results. It is observed that the water level shows a drop of 0,5 [cm]. The water level seems to drop significantly during constriction with a cm, while shortly downstream of the constriction the water level seems to increase again with 0,5 cm.

Table 80; Water level [cm]

Location	1	3	5	6
	39,5774	39,1784	38,6068	39,0513

Measurements after 24h

Bed level

A projection of the bed after running for 24 [h] can be observed in Figure 358. The bed shows the development of a very narrow and deep scour hole just upstream of the placed logs. The logs have also tilted slightly towards this hole. Furthermore, small patches of accretion are observed directly downstream of the logs, while further downstream scour seams to appear.

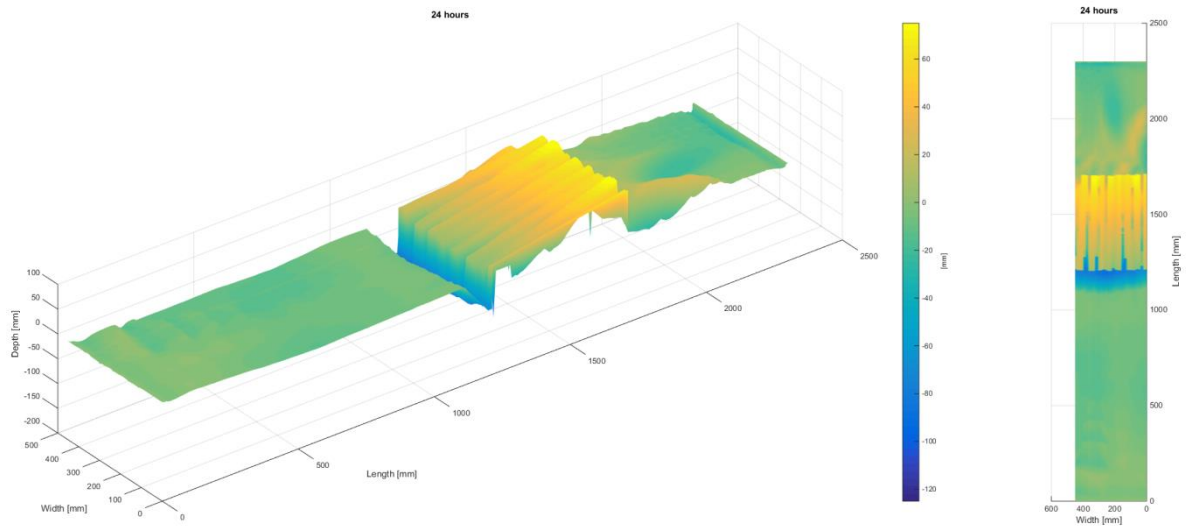

Figure 358; 24[h] bed projection

This can be confirmed with the average transect, observable in Figure 359. It shows a very steep scour hole just upstream of the logs, while also showing a minimal amount of accretion just downstream of the logs which gradually turn into on average scour towards the end of the expansion.

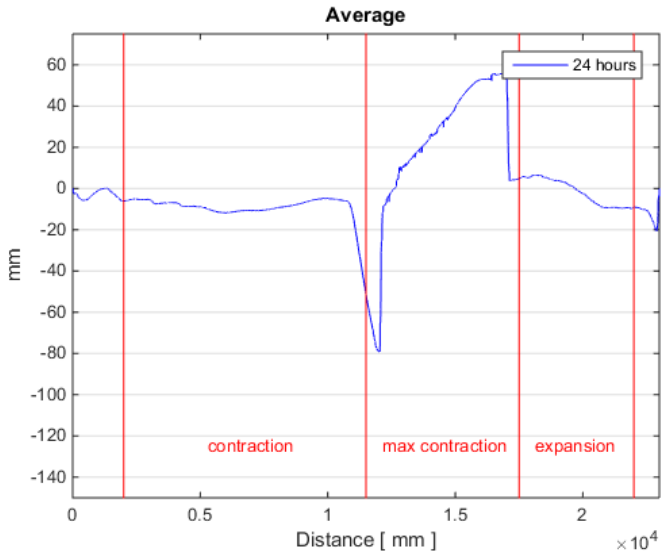

Figure 359; 24[h] average transect

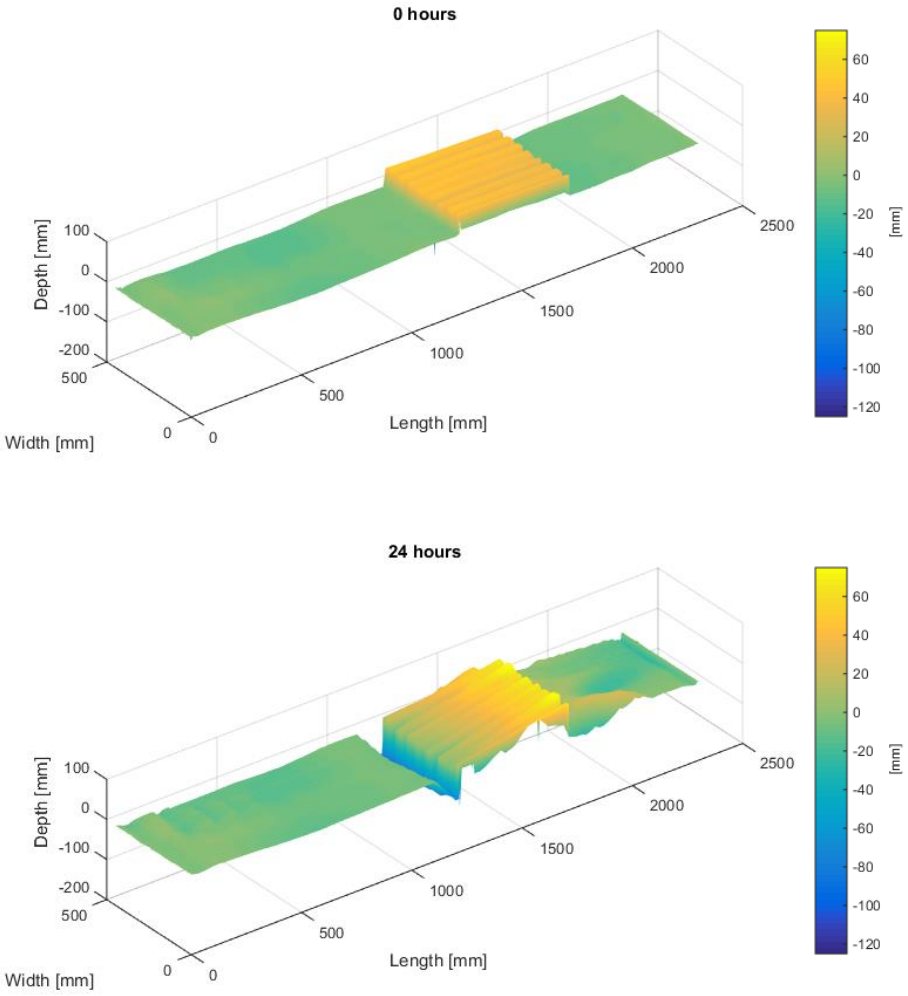

Figure 360; 0[h]-24[h] bed change projection

Table 81; Volume change per sector in [cm^3]

	Upstream	Contraction	Constriction	Expansion	Downstream
Volume	-30	-764	-1875	+1507	-368

Velocity Profiles

For the flow profiles after 24 [h] of the experiment it can be said that for both locations 1 & 3 a typical pattern can be identified with respect to regular turbulent flow. The pattern does increase from location 1 to location 3. For the locations downstream a strong disturbance can be seen close to the bed, where the velocities are very small, this being the effect of the wake of the logs. At location 9 an increase of flow velocity about 10 [cm] above the logs can be seen, which is most likely caused by the presence of the logs. Observing locations 5 & 6 more closely, one can see this local acceleration moving up the water column, and redistributing the log-carpet induced acceleration. Also observable is the attempt of the water column to redistribute the velocity at location 6, where flow is seemingly attempting to reattach to the bottom.

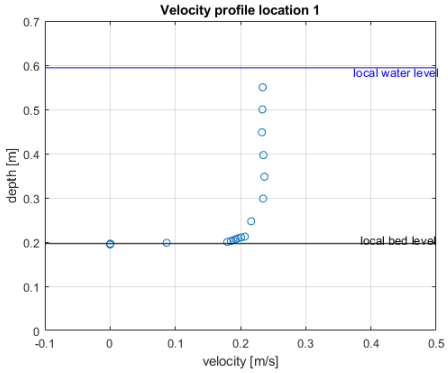

Figure 361; Velocity Profile location 1

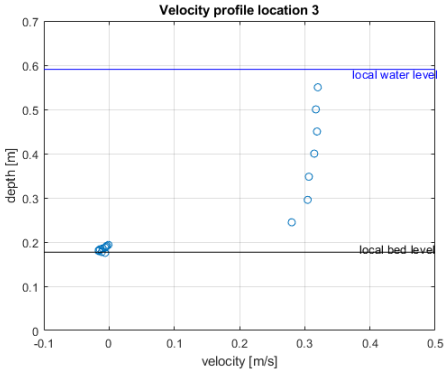

Figure 362; Velocity Profile location 3

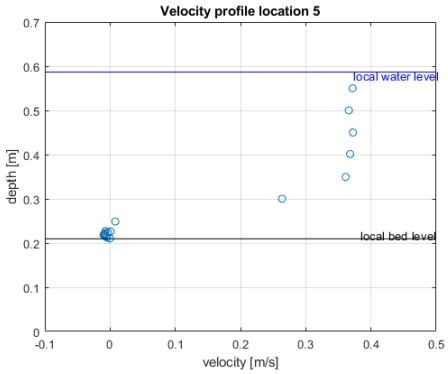

Figure 363; Velocity Profile location 5

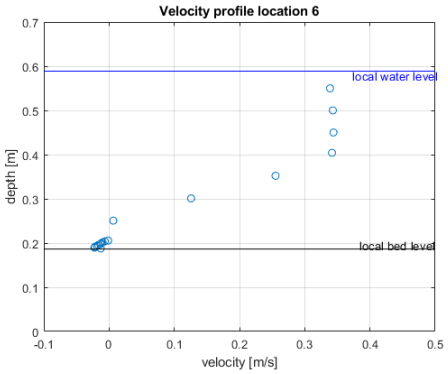

Figure 364; Velocity Profile location 6

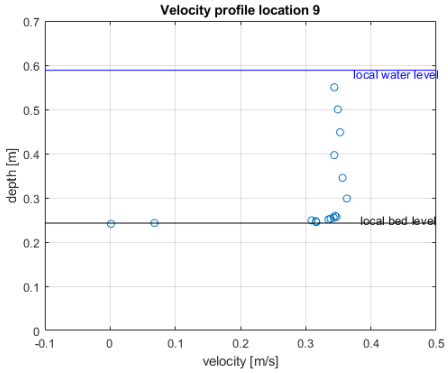

Figure 365; Velocity Profile location 9

Relative fluctuation intensity

It is shown that fluctuation intensity stays proportionally the same during contraction from location 1-2 and location 7-8. At location 3, inside the trench upstream of the logs very large and negative RFI can be observed, indicative of very small velocities and an on average negative flow direction. At locations on top of the log layer (4 & 9) RFI has assumed a more natural distribution with an increase of RFI towards the bottom.

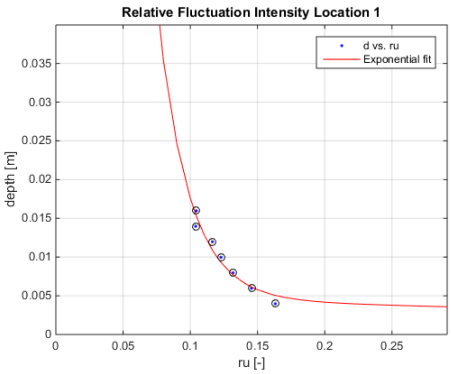

Figure 366; Relative fluctuation intensity location 1

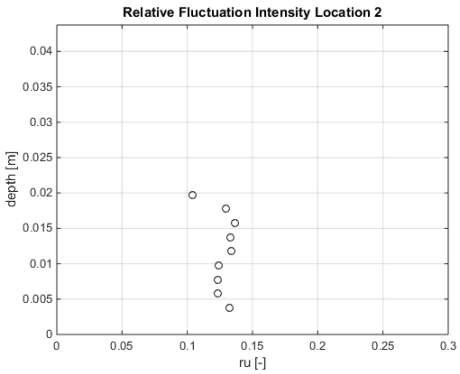

Figure 367; Relative fluctuation intensity location 2

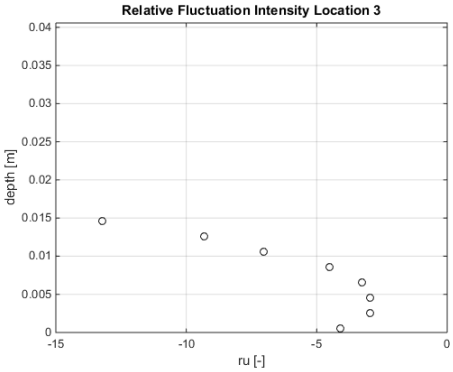

Figure 368; Relative fluctuation intensity location 3

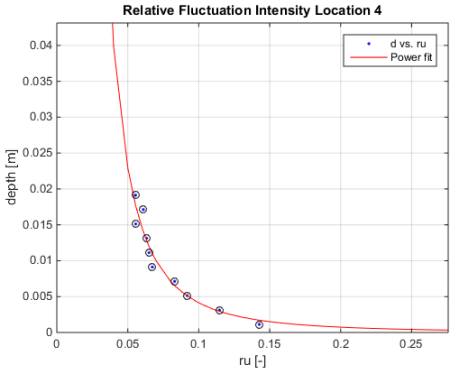

Figure 369; Relative fluctuation intensity location 4

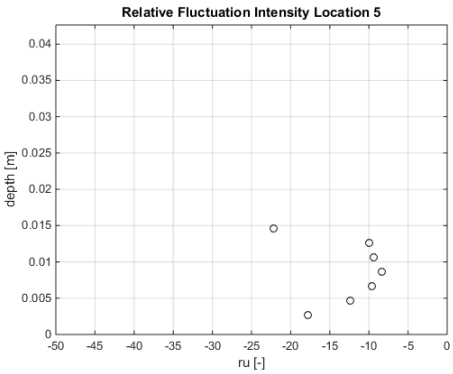

Figure 370; Relative fluctuation intensity location 5

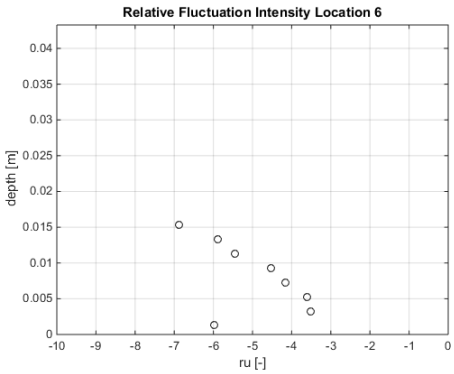

Figure 371; Relative fluctuation intensity location 6

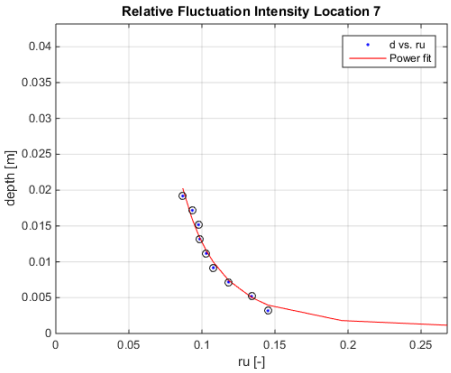

Figure 372; Relative fluctuation intensity location 7

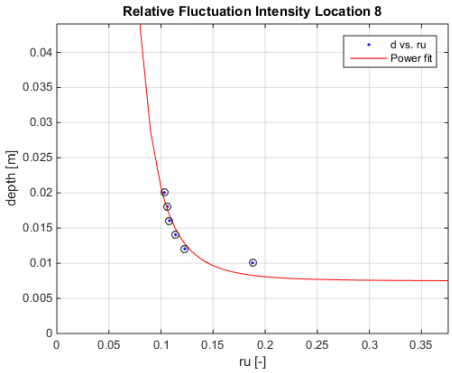

Figure 373; Relative fluctuation intensity location 8

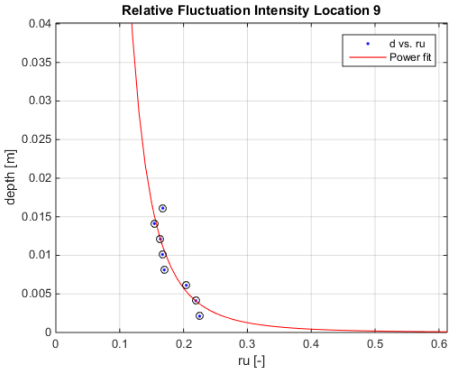

Figure 374; Relative fluctuation intensity location 9

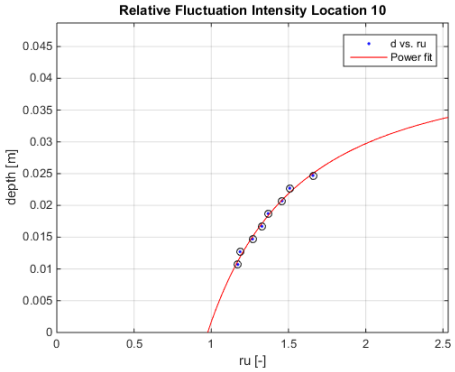

Figure 375; Relative fluctuation intensity location 10

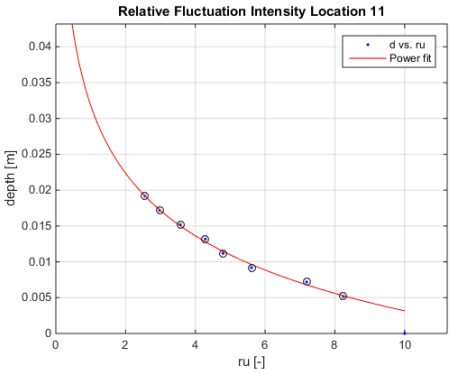

Figure 376; Relative fluctuation intensity location 11

At locations 5 very large negative values are observed. At location 10 fluctuation intensity is still very high, but in contrast to location 5 no negative values are observed. Further downstream near location 6 these negative values are still observed, although the intensity reduces. At location 11 an increase can be observed with respect to location 10.

Bed Shear stress

The bed shear stress was determined with Reynolds formula stated in (Schiereck & Verhagen, 2012). Bed shear stresses are determined by averaging the estimation for bed shear stress, over the centimeter measured above the bottom for a time frame of 3 minutes measuring at 50 [hz] per second, excluding all measured values that do not confirm with a signal to noise ratio above 15 and a correlation of 90%.

Bed shear stresses exceed values associated with high level of transport at locations in or downstream of the constriction. Only locations in the constriction-sector show high bed shear stresses (locations 3,4,9,10)

Table 82; Bed shear stresses [n/m^2]

Location	1	2	3	4	5	6	7	8	9	10	11
	-0,052	-0,039	-0,152	0,190	0,001	-0,081	-0,051	0,061	0,137	0,394	-0,0323

Estimation of transport

Following the formulations of the bed load transport by van Rijn (van Rijn, 2018). The results are represented as such, that locations at the same longitudinal location are coupled and transport is averaged over these locations (Table 83). For the calculations the absolute value was taken of the measured bed shear stresses. The results are also depicted per sector (Table 84) by calculating the area underneath each cross-sectional measurement. In this way it is expected that scour rates will reduce significantly with respect to the first 24 [h].

Table 83; Bed load transport [kg/m/s]

Location	1	2 & 7	3 & 8	4 & 9	5 & 10	6 & 11
	NaN	NaN	NaN	$4,59*10^{-7}$	0,00012	NaN

Table 84; Bed load transport per sector [kg/day]

Sector	Upstream	Contraction	Constriction	Expansion	Downstream
	NaN	NaN	0,8	1,2	NaN

Water level

The water levels were measured at locations 1,3,5,6 they are depicted in Table 85. The levels were computed by measuring at 1000 [hz] for 15 seconds, and averaging those results. It is observed that the water level shows a drop of 0,5 [cm]. The water level seems to drop significantly during constriction with 0,7 cm, while shortly downstream of the constriction the water level seems to increase again with 0,2 cm.

Table 85; Water level [cm]

Location	1	3	5	6
	39,4211	39,0621	38,6663	38,8884

Measurements after 48h

Bed level

A projection of the bed after running for 48 [h] can be observed in (Figure 377). The bed shows the continuation of scour upstream of the logs with the development of bedforms upstream of the logs.

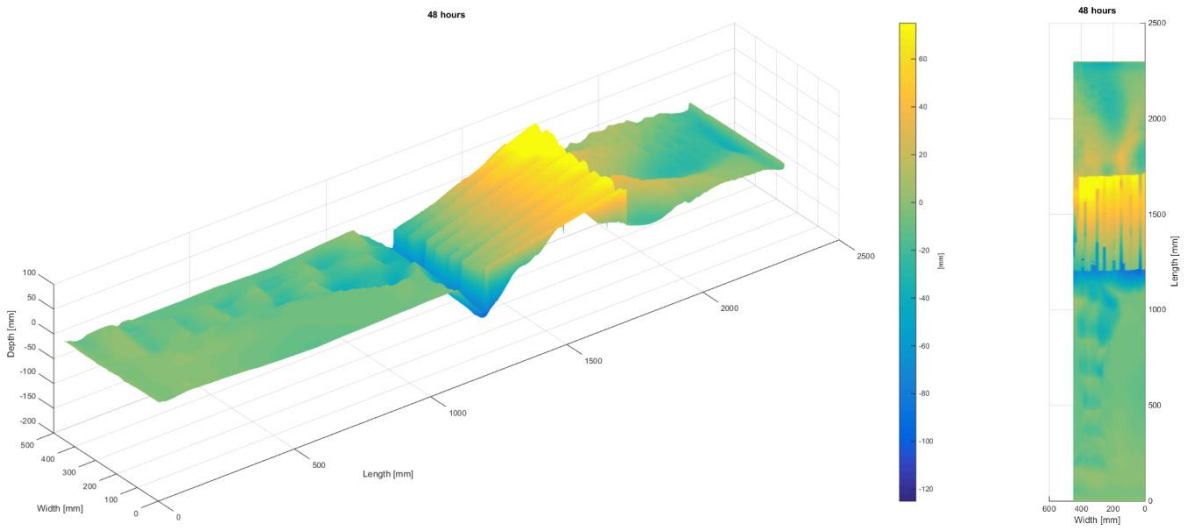

Figure 377; 48[h] bed projection

The average calculated transect observable in Figure 378, shows scour has penetrated up to75 [mm] just in front of the logs and 20 [mm] downstream of the logs.

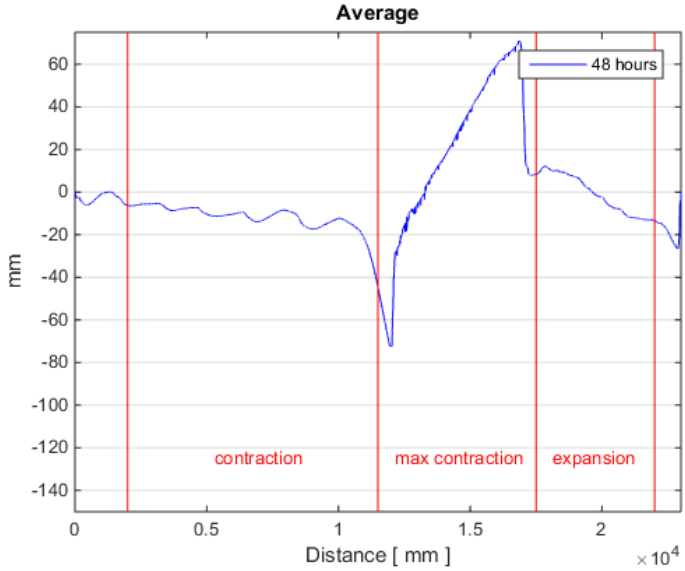

Figure 378; 48[h] average transect

Furthermore Figure 14 shows that the already present scour has increased, meanwhile the logs have tilted even further forward. From this figure it is also clearly observable that the bedforms are generated upstream as minor bedforms were also observable after 24 [h]. Therefore these bedforms might have developed due to turbulence generated by the entry point of the model.

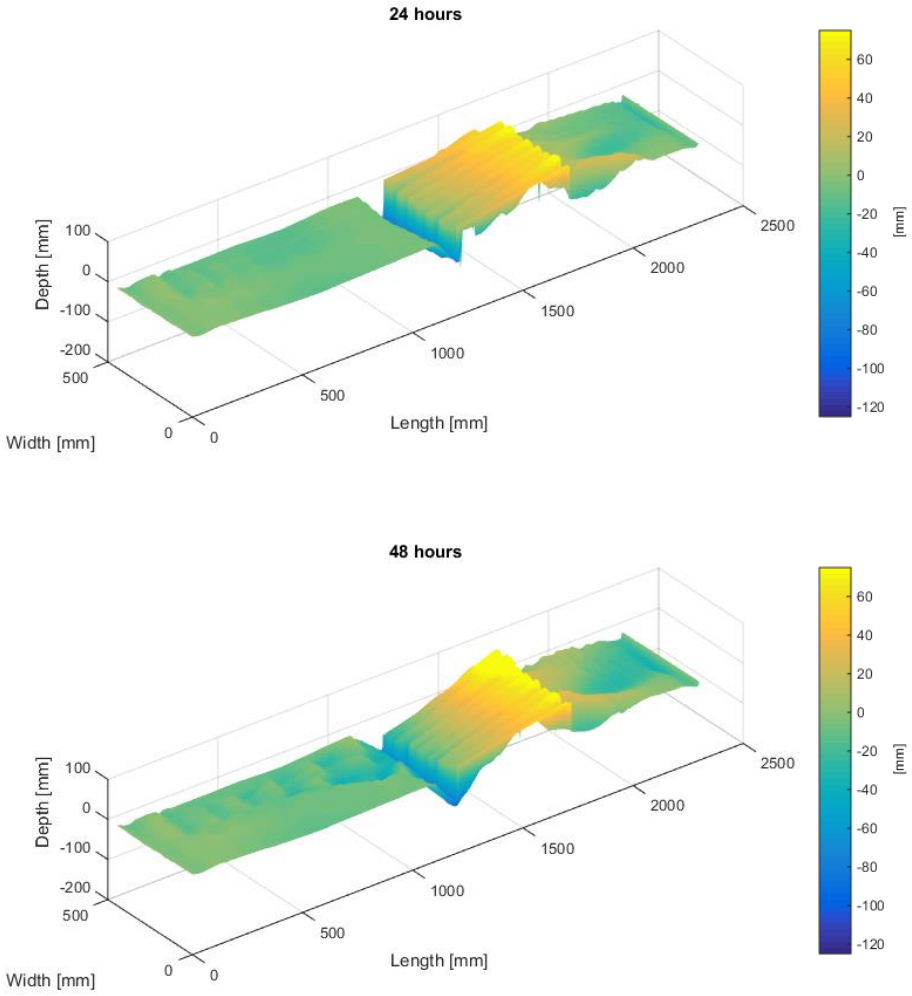

Figure 379; 24[h]-48[h] bed change projection

Table 86; Volume change per sector in [cm^3]

	Upstream	Contraction	Constriction	Expansion	Downstream
Volume	+1	-1152	-610	+1612	-288

Velocity Profiles

For the flow profiles after 48 [h] of the experiment it can be said that for both locations 1 & 3 a typical pattern can be identified with respect to regular turbulent flow. The pattern does increase from location 1 to location 3. For the locations downstream a strong disturbance can be seen close to the bed, where the velocities are very small, this being the effect of the wake of the logs. Location 9 shows acceleration with respect to location 3 although the localized acceleration observable before is no longer directly visible. Locations 5 & 6 show heavy disturbances and in both locations negative velocities near bed.

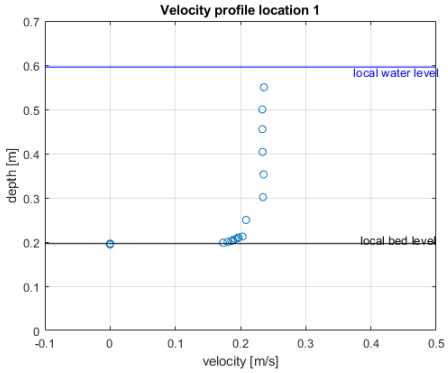

Figure 380; Velocity Profile location 1

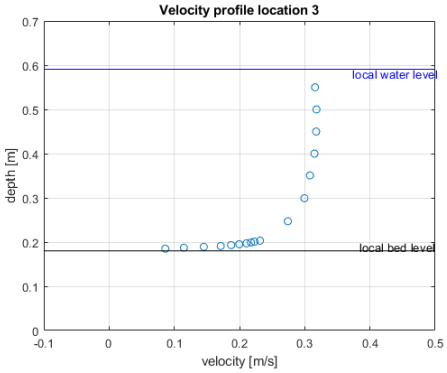

Figure 381; Velocity Profile location 3

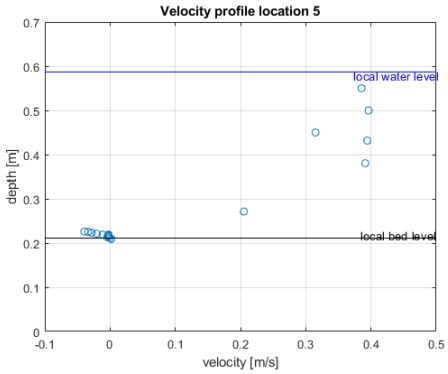

Figure 382; Velocity Profile location 5

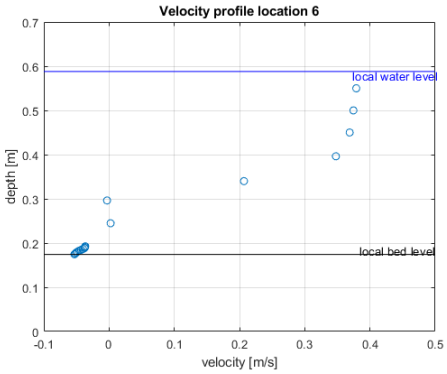

Figure 383; Velocity Profile location 6

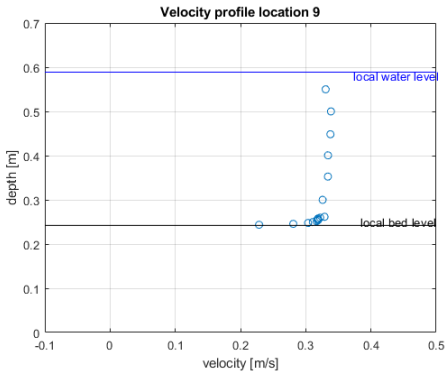

Figure 384; Velocity Profile location 9

Relative fluctuation intensity

Relative fluctuation seemingly increases from location 1-2. Location 3 shows relatively normal RFI while location 8 shows very large negative values. At location 9 above the logs it can be observed that this value is again relatively low and uniform. The measurement at location 4 was dropped due to faulty data

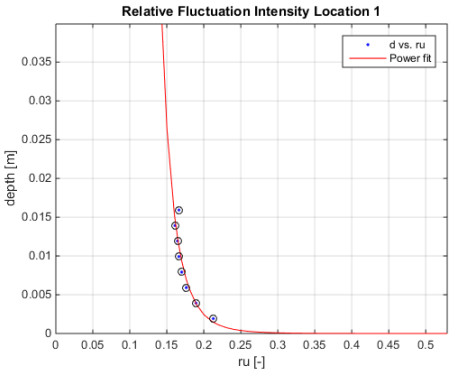

Figure 385; Relative fluctuation intensity location 1

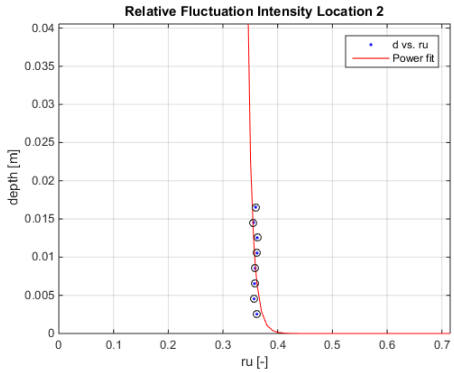

Figure 386; Relative fluctuation intensity location 2

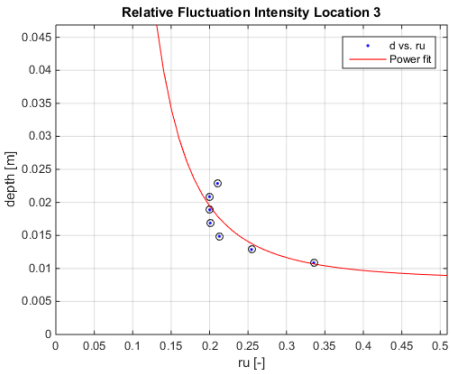

Figure 387; Relative fluctuation intensity location 3

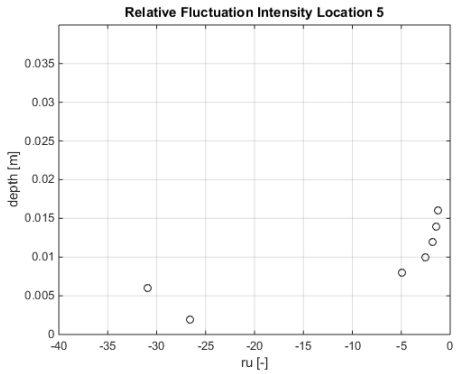

Figure 388; Relative fluctuation intensity location 5

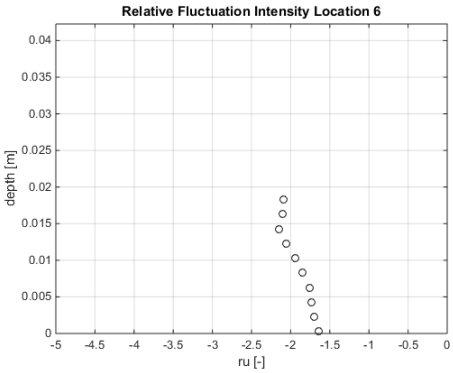

Figure 389; Relative fluctuation intensity location 6

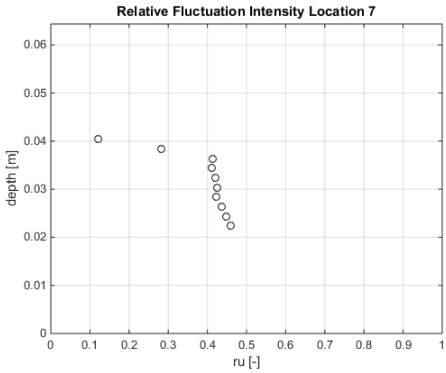

Figure 390; Relative fluctuation intensity location 7

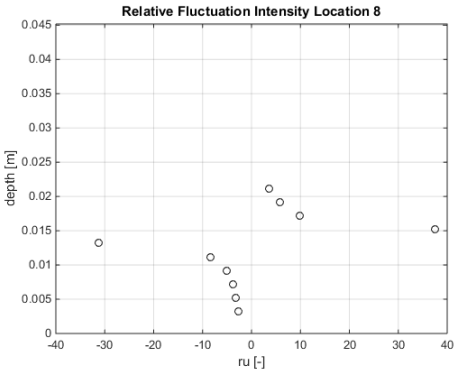

Figure 391; Relative fluctuation intensity location 8

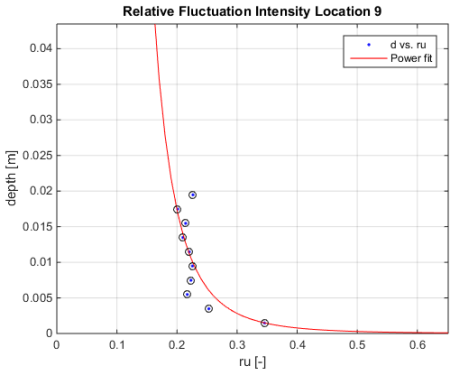

Figure 392; Relative fluctuation intensity location 9

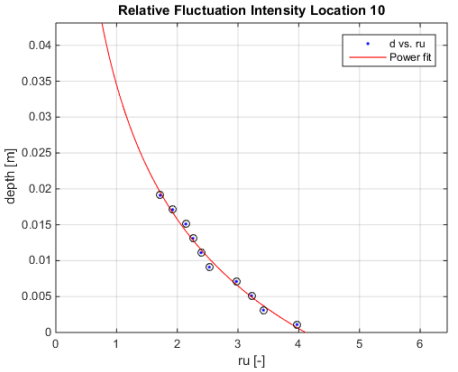

Figure 393; Relative fluctuation intensity location 10

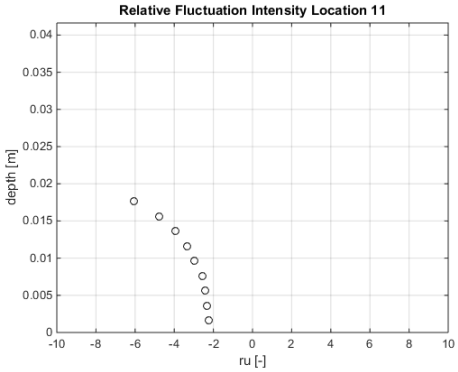

Figure 394; Relative fluctuation intensity location 11

Locations 5 and 10 again high and occasionally negative relative fluctuation intensities, the cause for this is similar to the conditions at start, and is caused by wake formation downstream of the logs. Locations 6 and 11 also show relatively large values of fluctuation intensity which can be explained by the observation that the flow profile has not correctly reattached as is observable in the section regarding flow profiles. Thus flow near bottom is small and on average negative.

Bed Shear stress

The bed shear stress was determined with Reynolds formula stated in (Schiereck & Verhagen, 2012). Bed shear stresses are determined by averaging the estimation for bed shear stress, over the centimeter measured above the bottom for a time frame of 3 minutes measuring at 50 [hz] per second, excluding all measured values that do not confirm with a signal to noise ratio above 15 and a correlation of 90%.

Bed shear stresses exceed values associated with high level of transport at locations 2,3,5,6,8,9,10 & 11. At location 5 & 9 this bed shear stress is positive.

Table 87; Bed shear stresses [n/m^2]

Location	1	2	3	4	5	6	7	8	9	10	11
	-0,091	0,151	-0,280	-0,027	0,403	-0,197	-0,035	-0,910	0,659	-0,154	-0,137

Estimation of transport

Following the formulations of the bed load transport by van Rijn (van Rijn, 2018). The results are represented as such, that locations at the same longitudinal location are coupled and transport is averaged over these locations (Table 88) For the calculations the absolute value was taken of the measured bed shear stresses. The results are also depicted per sector (Table 89) by calculating the area underneath each cross-sectional measurement. In this way it is expected that scour will be located in contraction/constriction & expansion sectors and will increase significantly with respect to the earlier measurements.

Table 88; Bed load transport [kg/m/s]

Location	1	2 & 7	3 & 8	4 & 9	5 & 10	6 & 11
	NaN	NaN	0,01980	0,00375	0,00152	$2,39*10^{-6}$

Table 89; Bed load transport per sector [kg/day]

Sector	Upstream	Contraction	Constriction	Expansion	Downstream
	NaN	222,4	194,2	30,8	0,0

Water level

The water levels were measured at locations 1,3,5,6 they are depicted in Table 90. The levels were computed by measuring at 1000 [hz] for 15 seconds, and averaging those results. It is observed that the water level shows a drop of 0,7 [cm]. The water level seems to drop significantly during constriction with 0,9 cm, while shortly downstream of the constriction the water level seems to increase again with 0,2 cm.

Table 90; Water level [cm]

Location	1	3	5	6
	39,5631	39,0825	38,6877	38,8851

Measurements after 72h

Bed level

A projection of the bed after running for 72 [h] can be observed in Figure 395. The bed shows upstream bedforms, severely titled logs and large patches of erosion and accretion around the logs.

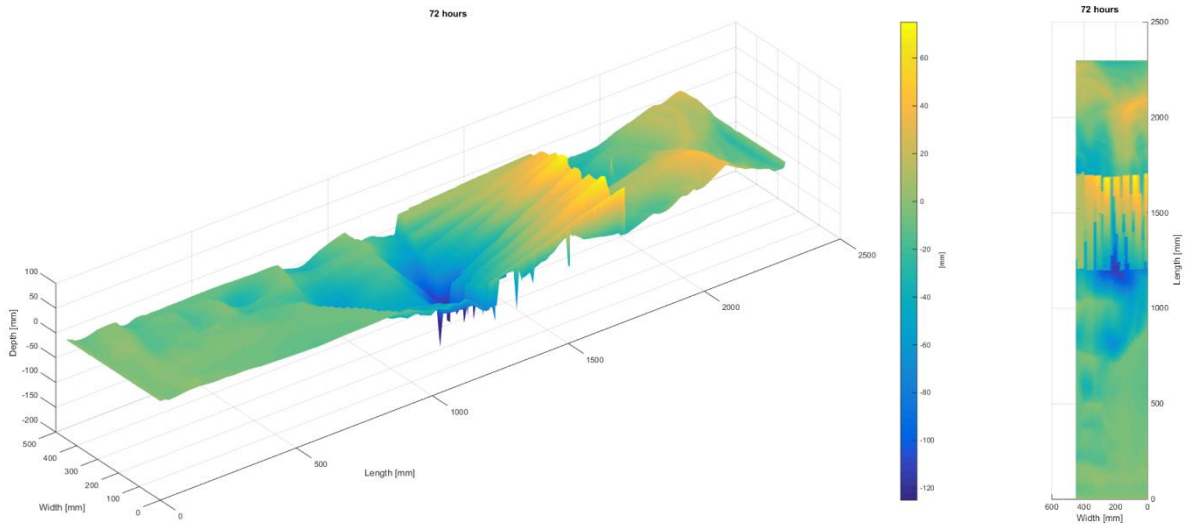

Figure 395; 72[h] bed projection

The average calculated transect observable in Figure 396, shows scour has penetrated up to 80 [mm] just in front of the logs and 30 [mm] downstream of the logs.

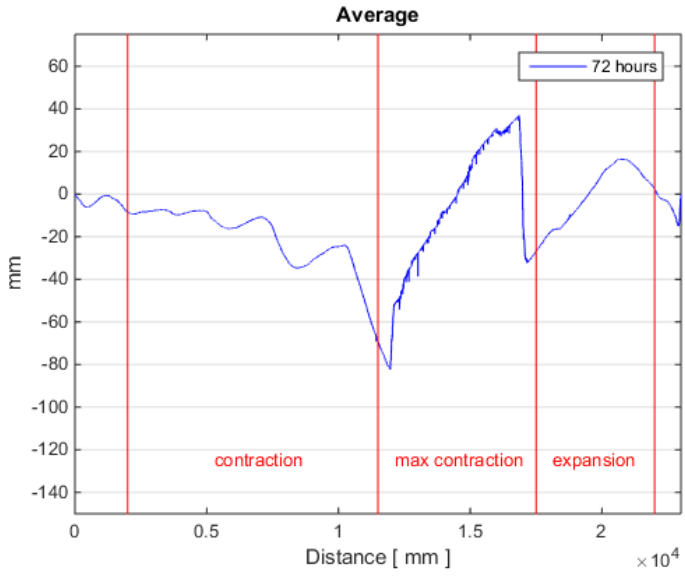

Figure 396; 72[h] average transect

Furthermore Figure 397 that the bedforms originating from upstream have increased in size and might have caused the slope of the scour hole upstream of the logs to collapse. This instability has caused all logs to tilt differently, which is causing a complex pattern of hills and valleys downstream of the logs.

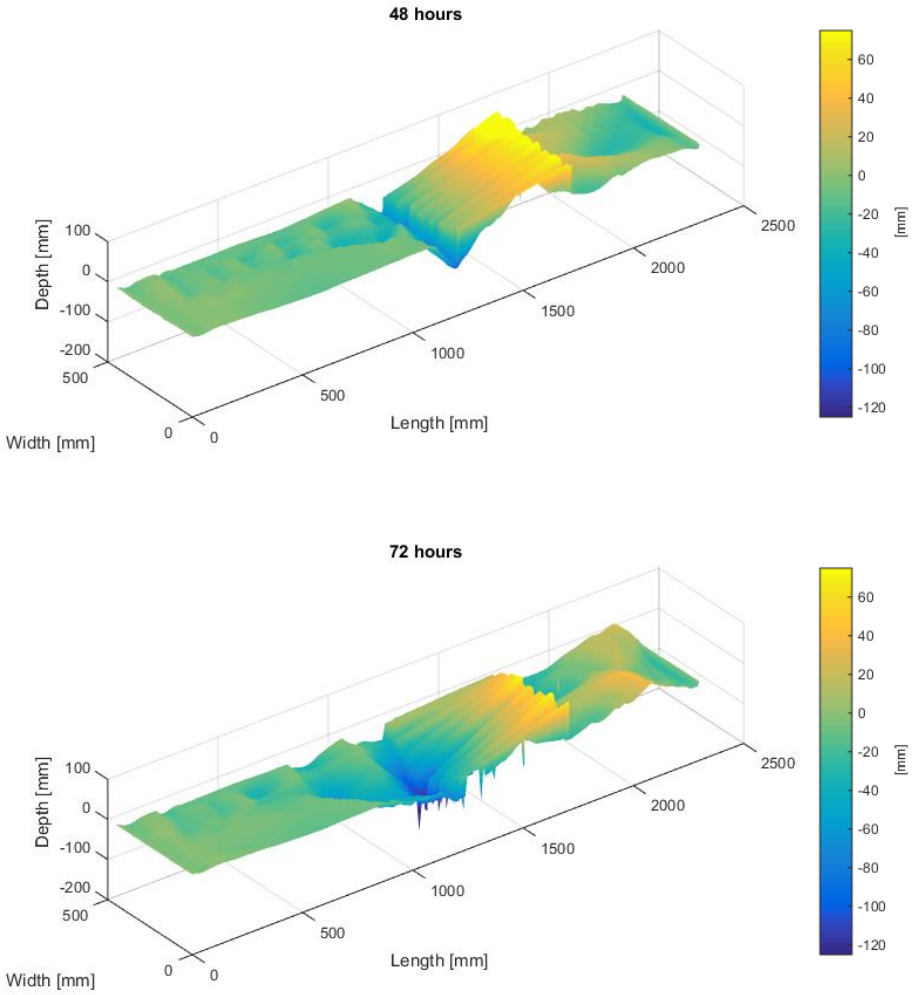

Figure 397; 48[h]-72[h] bed change projection

Table 91; Volume change per sector in [cm^3]

	Upstream	Contraction	Constriction	Expansion	Downstream
Volume	-52	-3715	-7587	+199	+608

Velocity Profiles

For the flow profiles after 72 [h] of the experiment it can be said that for both locations 1 & 3 a typical pattern can be identified with respect to regular turbulent flow. The pattern does increase from location 1 to location 3. For the locations downstream a strong disturbance can be seen close to the bed, where the velocities are very small, this being the effect of the wake of the logs. Location 9 shows acceleration with respect to location 3 localized about 10 [cm] above the logs. Locations 5 & 6 show heavy disturbances and at location 5 near bed velocities are on average negative.

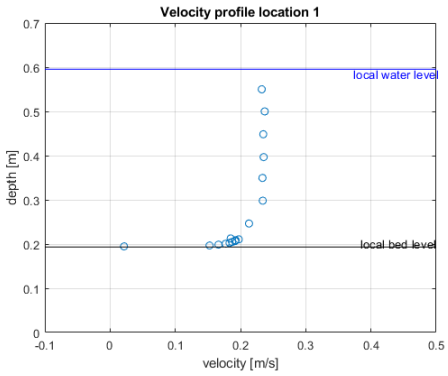

Figure 398; Velocity Profile location 1

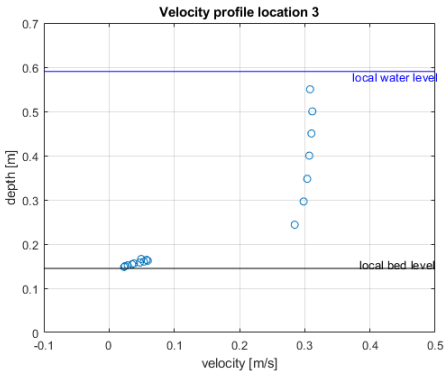

Figure 399; Velocity Profile location 3

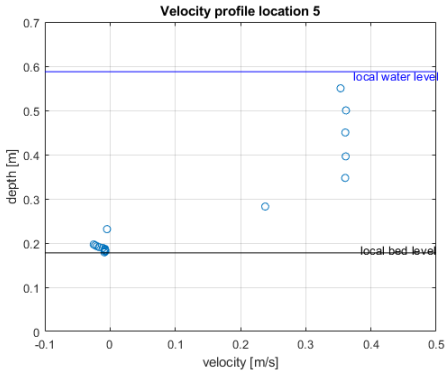

Figure 400; Velocity Profile location 5

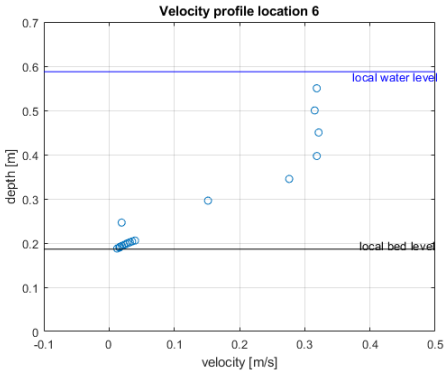

Figure 401; Velocity Profile location 6

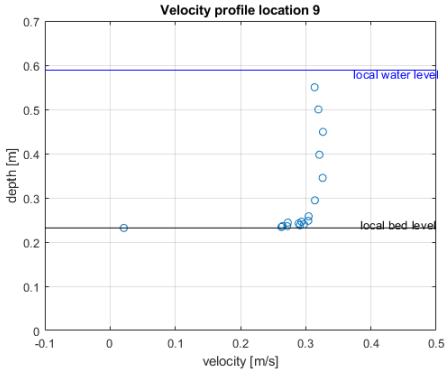

Figure 402; Velocity Profile location 9

Relative fluctuation intensity

It is shown that fluctuation intensity stays proportionally the same during contraction from location 1-2 and location 7-8. At location 3, just upstream of the logs, the RFI is large but no longer negative. The collapse of the scour hole can be a cause for this, as the point of detachment no longer exists as before.. At locations on top of the log layer (4 & 9) RFI is small however it is stronger near the wall.

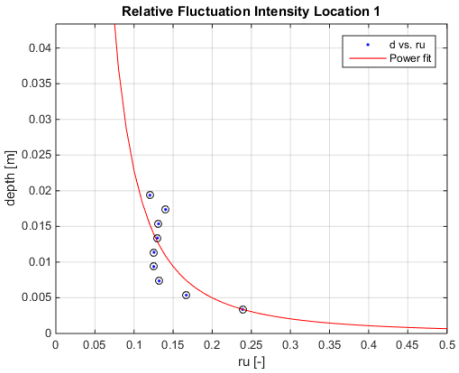

Figure 403; Relative fluctuation intensity location 1

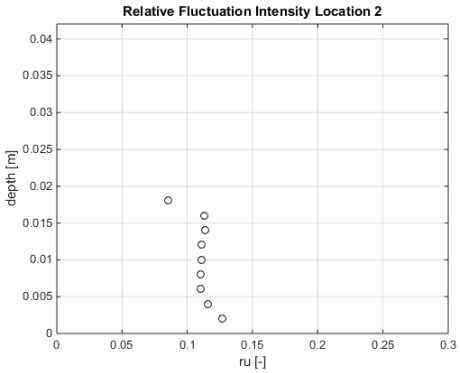

Figure 404; Relative fluctuation intensity location 2

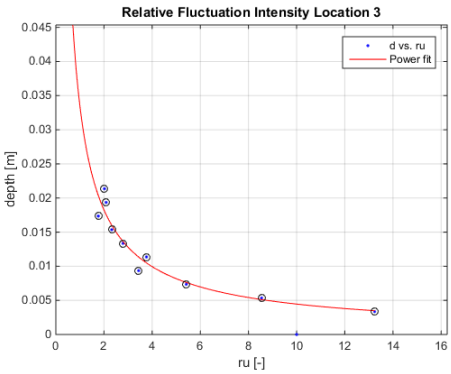

Figure 405; Relative fluctuation intensity location 3

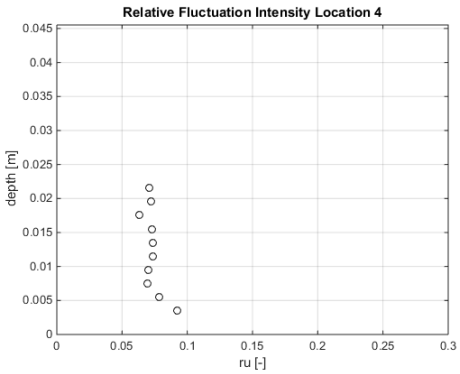

Figure 406; Relative fluctuation intensity location 4

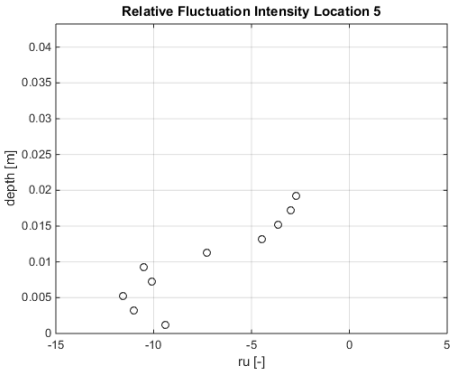

Figure 407; Relative fluctuation intensity location 5

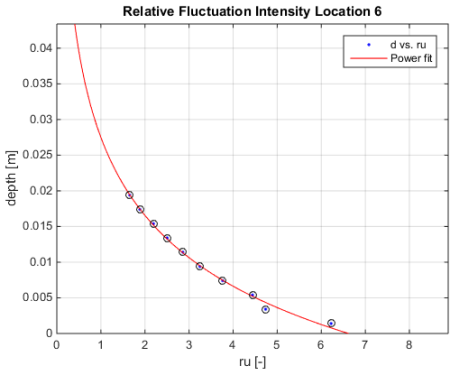

Figure 408; Relative fluctuation intensity location 6

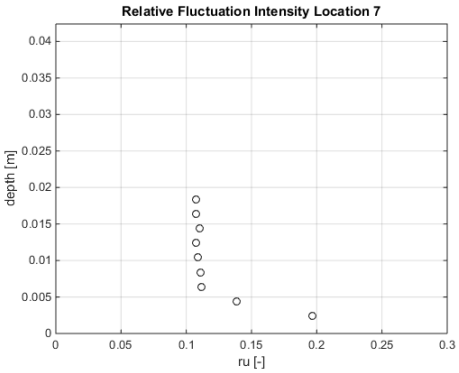

Figure 409; Relative fluctuation intensity location 7

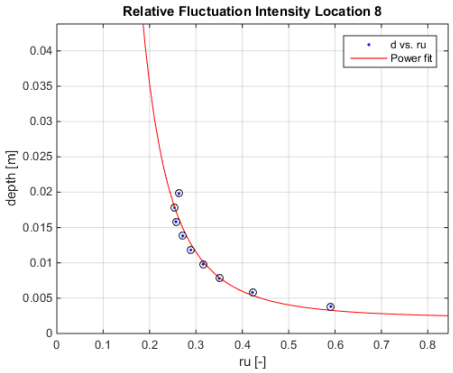

Figure 410; Relative fluctuation intensity location 8

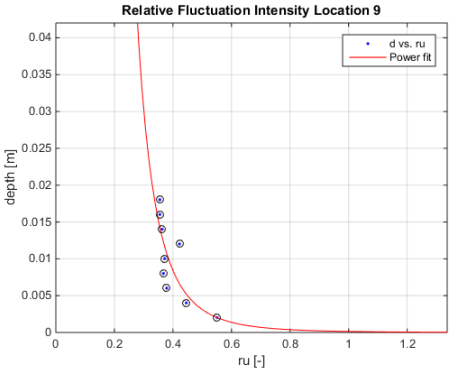

Figure 411; Relative fluctuation intensity location 9

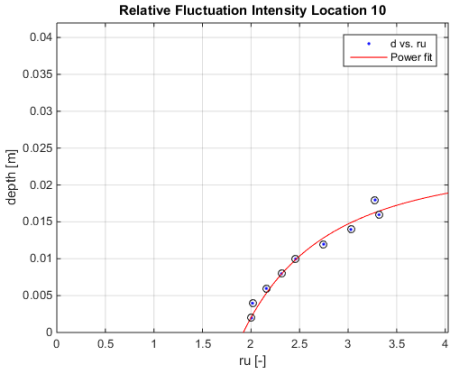

Figure 412; Relative fluctuation intensity location 10

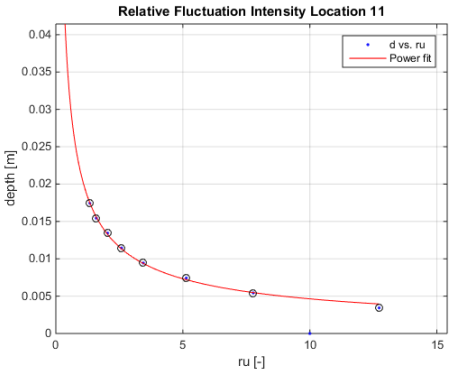

Figure 413; Relative fluctuation intensity location 11

Locations 5 and 10 again high and occasionally negative relative fluctuation intensities, the cause for this is similar to the conditions at start, and is caused by wake formation downstream of the logs. Locations 6 and 11 also show relatively large values of fluctuation intensity which can be explained by the observation that the flow profile has not correctly reattached as is observable in the section regarding flow profiles.

Bed Shear stress

The bed shear stress was determined with Reynolds formula stated in (Schiereck & Verhagen, 2012). Bed shear stresses are determined by averaging the estimation for bed shear stress, over the centimeter measured above the bottom for a time frame of 3 minutes measuring at 50 [hz] per second, excluding all measured values that do not confirm with a signal to noise ratio above 15 and a correlation of 90%.

Bed shear stresses exceed values associated with high level of transport at locations 3,4,5,6,8,9,10 & 11. At location 4,5 & 9 this bed shear stress is positive.

Table 92; Bed shear stresses [n/m^2]

Location	1	2	3	4	5	6	7	8	9	10	11
	-0,078	-0,059	-0,616	0,501	0,172	-0,366	-0,055	-0,333	1,339	-0,367	-0,562

Estimation of transport

Following the formulations of the bed load transport by van Rijn (van Rijn, 2018). The results are represented as such, that locations at the same longitudinal location are coupled and transport is averaged over these locations (Table 93) For the calculations the absolute value was taken of the measured bed shear stresses. The results are also depicted per sector (Table 94) by calculating the area underneath each cross-sectional measurement. The estimations now predict scour rates that vastly exceed the amount of sand available in the model.

Table 93; Bed load transport [kg/m/s]

Location	1	2 & 7	3 & 8	4 & 9	5 & 10	6 & 11
	NaN	NaN	0,0108	0,0529	0,0013	0,0102

Table 94; Bed load transport per sector [kg/day]

Sector	Upstream	Contraction	Constriction	Expansion	Downstream
	NaN	121,3	794,6	232,5	45,8

Water level

The water levels were measured at locations 1,3,5,6 they are depicted in Table 95. The levels were computed by measuring at 1000 [hz] for 15 seconds, and averaging those results. It is observed that the water level shows a drop of 0,8 [cm]. The water level seems to drop significantly during constriction with 0,8 cm and does not show an increase downstream of the constriction.

Table 95; Water level [cm]

Location	1	3	5	6
	39,5470	39,0175	38,7613	38,7531

Measurements after 96h

Bed level

The bed after 96 [h] shows a continuation of the existing scour formation, (see Figure 414 & Figure 415). At the end of the experiment scour is strongest and focused just upstream of the logs. Large patches of accretion are seen downstream of the logs.

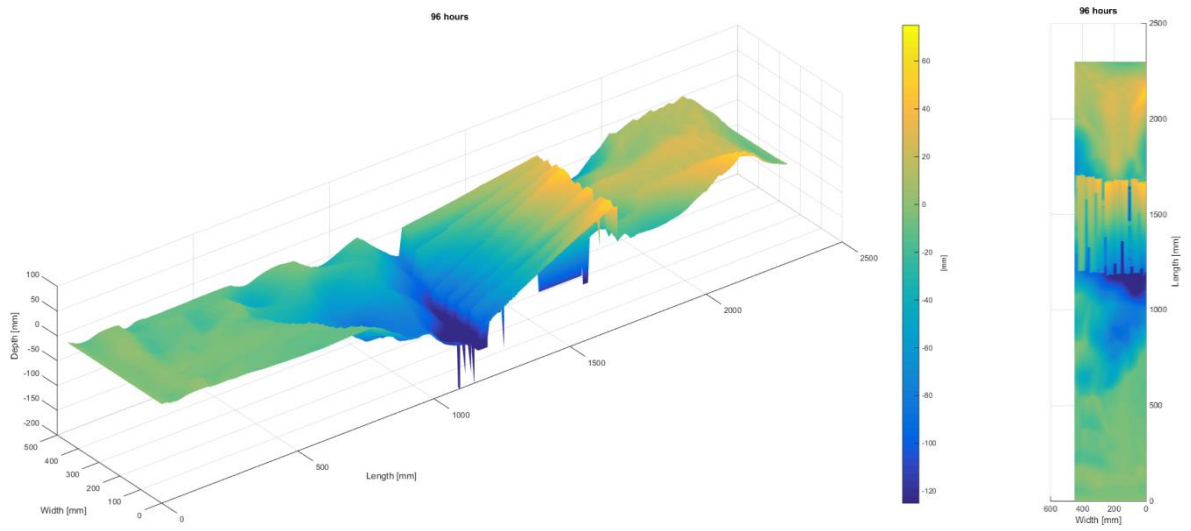

Figure 414; Bed map after 96 [h]

The average calculated transect, shows scour has penetrated up to 115 [mm] just in front of the logs and 25 [mm] downstream of the logs, although there is significantly more accretion than there to be scour downstream of the logs.

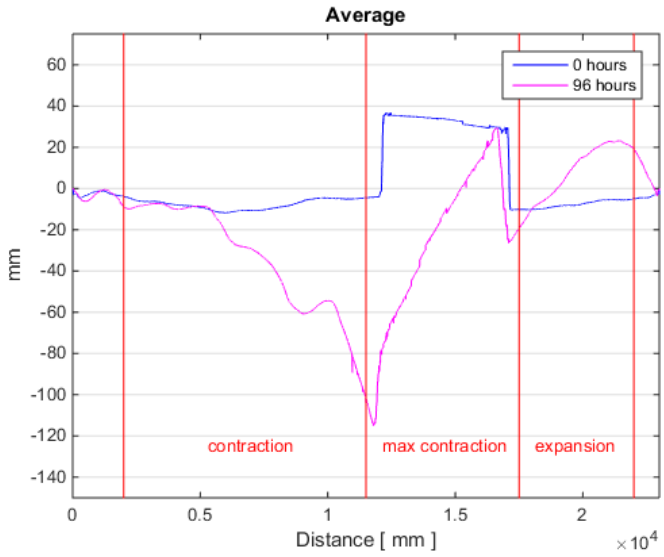

Figure 415; Average transects through time

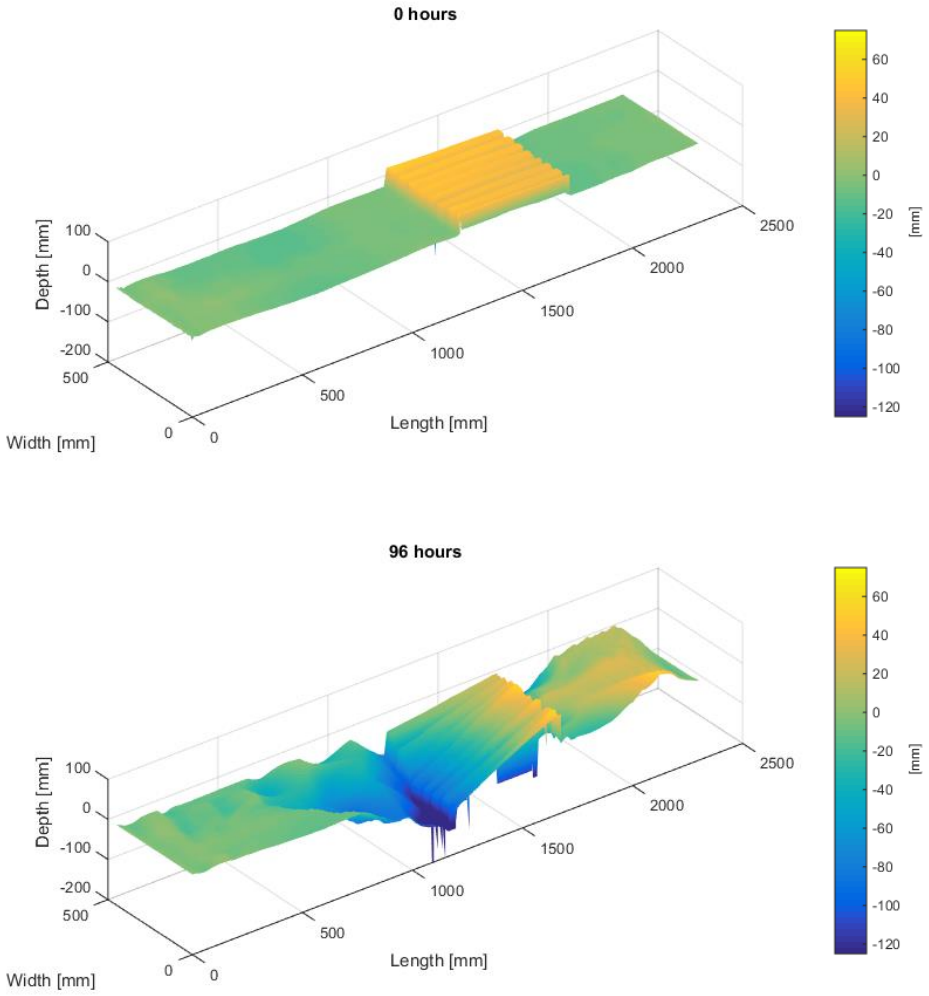

Figure 416; Bed change with respect to 0[h]

Table 96; Volume change per sector in [cm^3]

	Upstream	Contraction	Constriction	Expansion	Downstream
Volume	+1	-5967	-4791	+2029	+590

Concluding Remarks

The second experiment conducted with flow parallel placed logs has shown little improvement with respect to basic scour experiments. Scour depths are relatively deep reaching to depths up to 15 [cm]. Meanwhile scour quantities show little improvement in the constriction-sector.

Appendix D III

I Introduction

The protected Scour experiments are considered to be the baseline experiments for the application of wooden logs as a scour protection. The “Protected Scour A” experiments feature a flow parallel placed single layer of logs directly on top of the bed, in the area of maximum contraction. Similar to the basic scour experiments bed, velocity and fluctuation intensity development is measured during a 96 [h] run. This report includes all measured findings during this particular experiment. Conclusions are drawn in the main report on the basis of multiple similarly conducted experiments. A short preliminary conclusion is however included at the end of this report.

Summary

Table 97 represents relevant scour quantities after 96 [h]. Note that the absolute is measured relative to the measurement of the bed at 0 [h], excluding the maximum scour depth which is measured to a reference bed with a 0 [mm] elevation. Measurements of scour volume in the column with respect to reference include missing volume with respect to a reference be of 0 [mm] and corrected for the presence of logs .

Table 97; Summary of quantities (Negative values indicate scour, positive indicate accretion)

	Quantity	With respect to reference
Maximum Scour Depth [mm]	109	109
Total Scoured volume [cm^3]	-4642	-9607
Scoured volume Upstream-sector [cm^3]	+1	-327
Scoured volume Contracting-sector [cm^3]	-1384	-3342
Scoured volume Constricted-sector [cm^3]	-2682	-3894
Scoured volume Expanding-sector [cm^3]	+788	-536
Scoured volume Downstream-sector [cm^3]	-1364	-1508

Measurements at 0h

Bed level

A projection of the bed at the moment of initiation of flow during the first scour experiment can be seen in Figure 417. Clearly observable are the placed logs on the bed. They are roughly located in between 1200-1700 [mm] from the entry point of flow. The bed further seems to be relatively flat with only minor deformations with respect to the size of the logs.

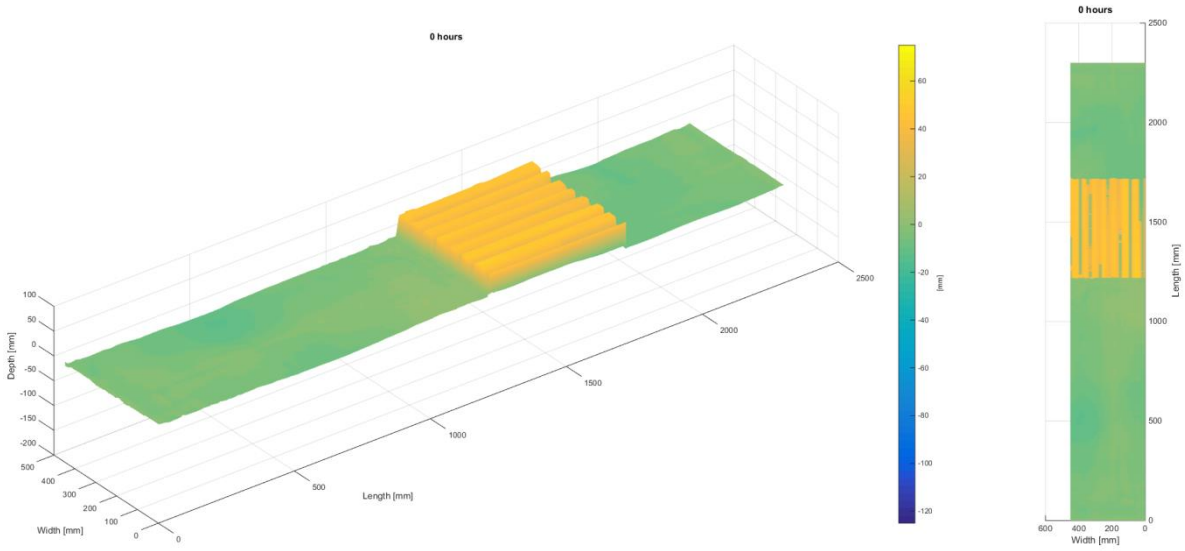

Figure 417; Bed map 0[h]

The average transect, observable in Figure 418, was calculated from the 31 transects taken over the entire length of the laboratory set-up. As can be seen, the bed is on some locations slightly below the target value of 0 [mm] with a maximum deviation of about 10 [mm]. The position of the logs is also clearly observable within the area of maximum contraction.

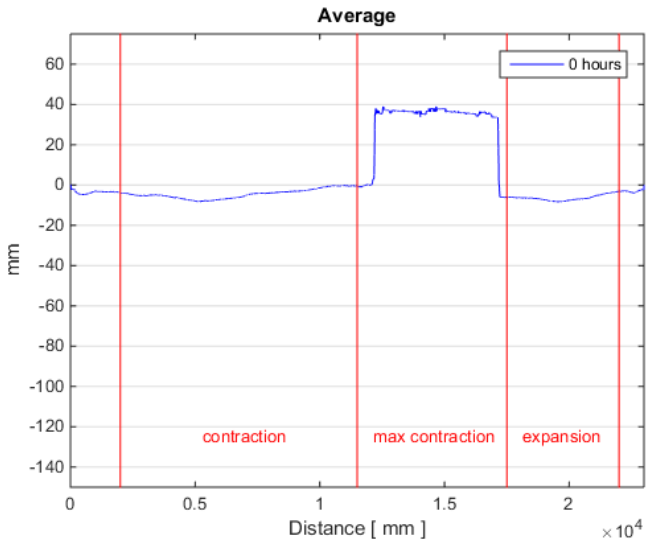

Figure 418; 0 [h] average transect

Velocity Profiles

In this section, individual flow profiles of locations marked above are shown. It can be observed that upon arrival the flow profile shows the characteristic profile for turbulent flow (location 1). At location 3 the flow has accelerated significantly, while close to the bottom flow is accelerated only slightly, skewing the flow profile. The flow velocity at location 5 increases further higher up the water column, but reduces to zero/near zero in the wake of the logs. At location 6 it can be observed that the flow profile is attempting to redistribute to the original flow profile (location 1) but has yet been successful at obtaining this distribution. The flow profile at location 9 above the logs shows an intensification of flow about 10 [cm] above the logs while the flow directly on top of the logs is almost uniform.

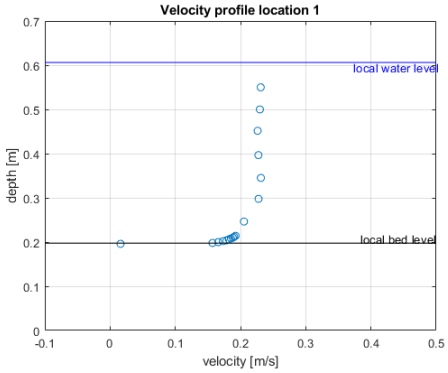

Figure 419; Velocity Profile location 1

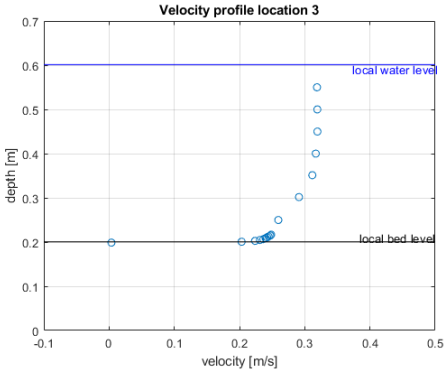

Figure 420; Velocity Profile location 3

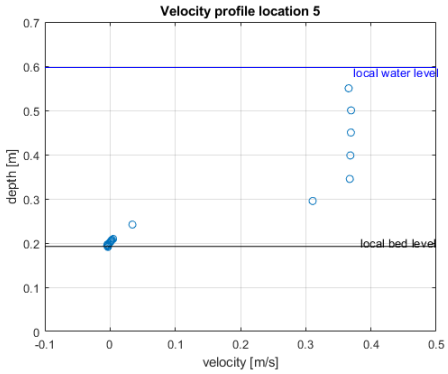

Figure 421; Velocity Profile location 5

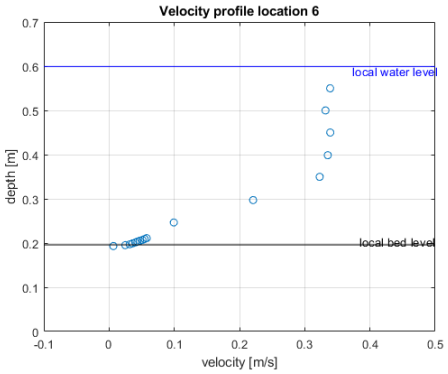

Figure 422; Velocity Profile location 6

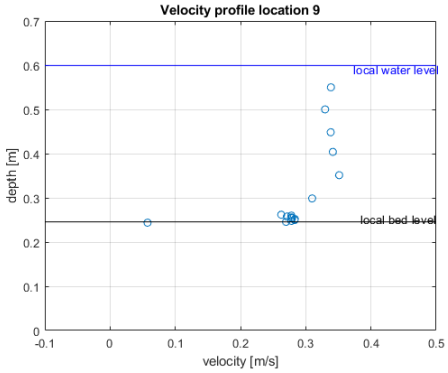

Figure 423; Velocity Profile location 9

Relative fluctuation intensity

It is shown that fluctuation intensity reduces during flow contraction, in between location 1-2-3, this is not the case for measurement between location 7-8, which shows no reduction. At locations 4 and 9 (measured above the logs) the relative fluctuation intensity remains small and more uniform. Wherever possible, curve fitting has been applied.

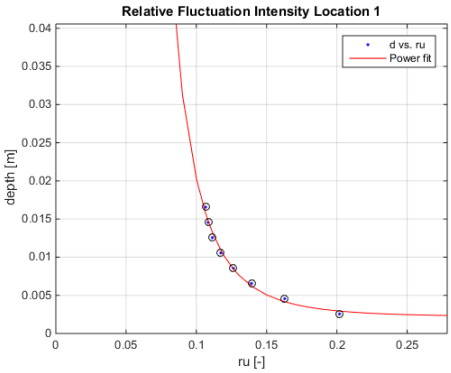

Figure 424; Relative fluctuation intensity location 1

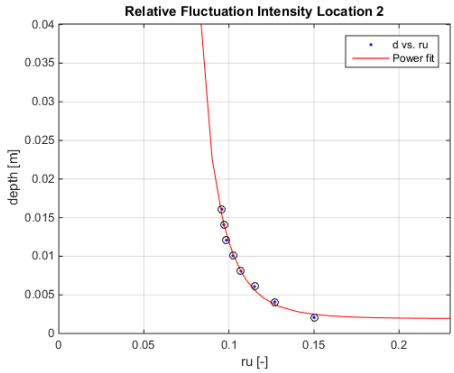

Figure 425; Relative fluctuation intensity location 2

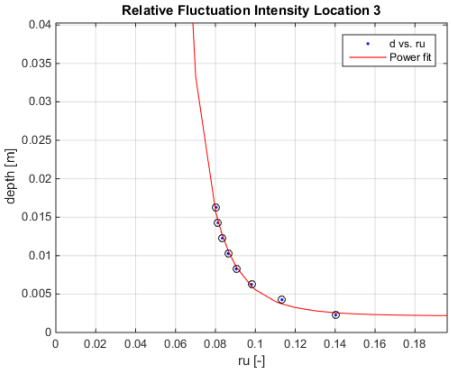

Figure 426; Relative fluctuation intensity location 3

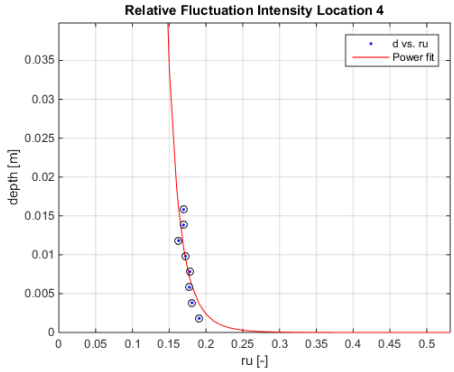

Figure 427; Relative fluctuation intensity location 4

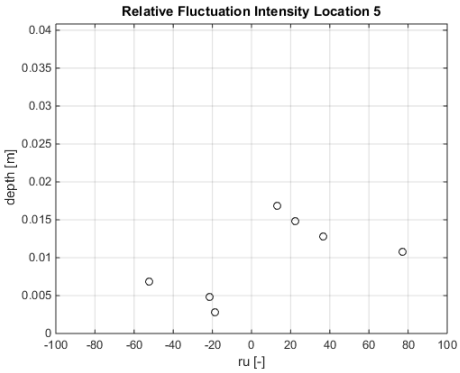

Figure 428; Relative fluctuation intensity location 5

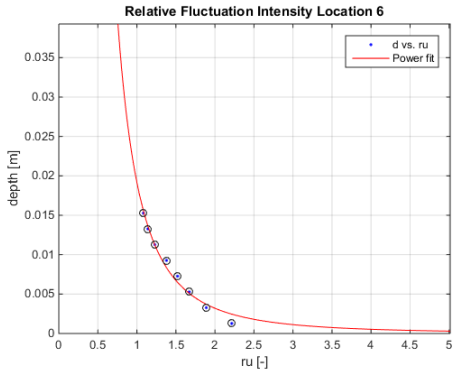

Figure 429; Relative fluctuation intensity location 6

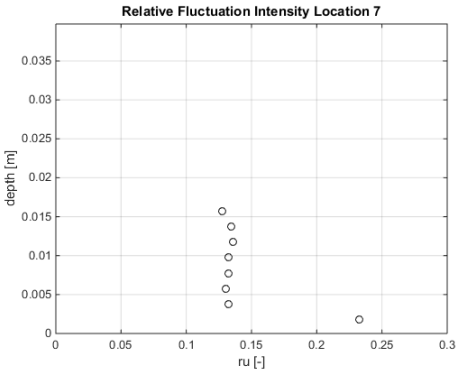

Figure 430; Relative fluctuation intensity location 7

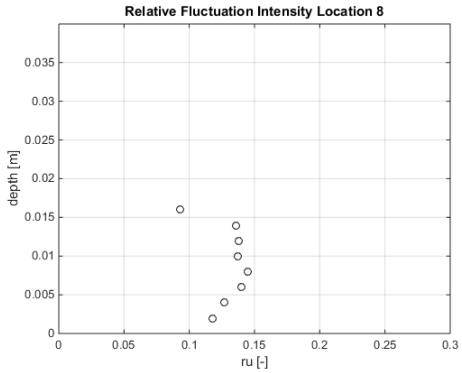

Figure 431; Relative fluctuation intensity location 8

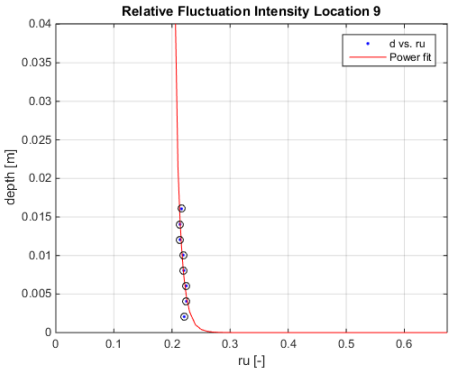

Figure 432; Relative fluctuation intensity location 9

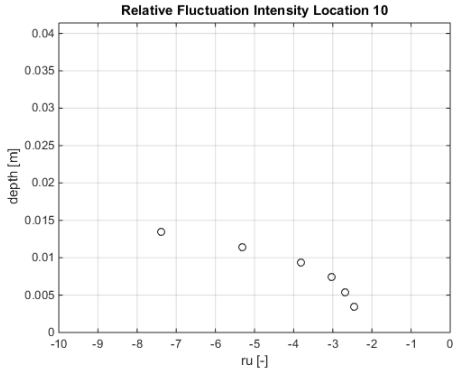

Figure 433; Relative fluctuation intensity location 10

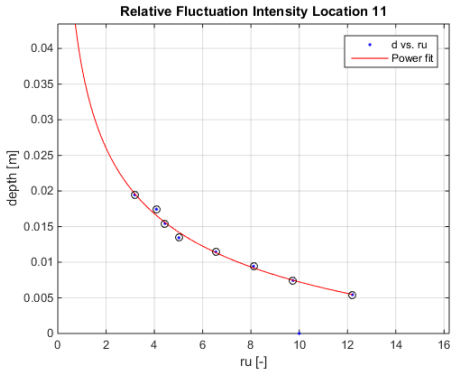

Figure 434; Relative fluctuation intensity location 11

At locations 5 & 10 fluctuation intensity is high and negative, indicative of upstream velocities. The relatively high fluctuation intensity can be explained by pointing out that this location is located within the wake of the logs, and thus average velocity is small, and the vortex formation causes relatively intense fluctuations with respect to the average flow velocity. Locations 6 & 11 which are located close to the exit point show strong fluctuations with respect to average flow, caused by the flow not having reattached to the bottom yet.

Bed Shear stress

The bed shear stress was determined with Reynolds formula stated in (Schiereck & Verhagen, 2012). Bed shear stresses are determined by averaging the estimation for bed shear stress, over the centimeter measured above the bottom for a time frame of 3 minutes measuring at 50 [hz] per second, excluding all measured values that do not confirm with a signal to noise ratio above 15 and a correlation of 90%.

Bed shear stresses exceed values associated with high level of transport at locations 4,5,6 & 10. At location 5 & 9 this bed shear stress is positive.

Table 98; Bed shear stresses [n/m^2]

Location	1	2	3	4	5	6	7	8	9	10	11
	-0,065	-0,044	-0,071	-0,150	-0,188	-0,124	-0,062	-0,048	-0,071	-0,309	-0,045

Estimation of transport

Following the formulations of the bed load transport by van Rijn (van Rijn, 2018). The results are represented as such, that locations at the same longitudinal location are coupled and transport is averaged over these locations (Table 99) For the calculations the absolute value was taken of the measured bed shear stresses. The results are also depicted per sector (Table 100) by calculating the area underneath each cross-sectional measurement. In this way it is expected that scour will mainly occur at the interface between the Constriction & Expansion Sectors.

Table 99; Bed load transport [kg/m/s]

Location	1	2 & 7	3 & 8	4 & 9	5 & 10	6 & 11
	NaN	NaN	NaN	NaN	0,00082	NaN

Table 100; Bed load transport per sector [kg/day]

Sector	Upstream	Contraction	Constriction	Expansion	Downstream
	NaN	NaN	5,5	8,3	NaN

Water level

The water levels were measured at locations 1,3,5,6 they are depicted in Table 101. The levels were computed by measuring at 1000 [hz] for 15 seconds, and averaging those results. It is observed that the water level shows a drop of 0,7 [cm]. The water level seems to drop significantly during constriction with 1 cm, while shortly downstream of the constriction the water level seems to increase again with 0,3 cm.

Table 101; Water level [cm]

Location	1	3	5	6
	40,6205	40,1361	39,6909	39,9155

Measurements after 24h

Bed level

A projection of the bed after running for 24 [h] can be observed in Figure 435. The bed shows the development of a very narrow and deep scour hole just upstream of the placed logs. The logs have also tilted slightly towards this hole. Furthermore, small patches of accretion are observed directly downstream of the logs, while further downstream scour seams to appear.

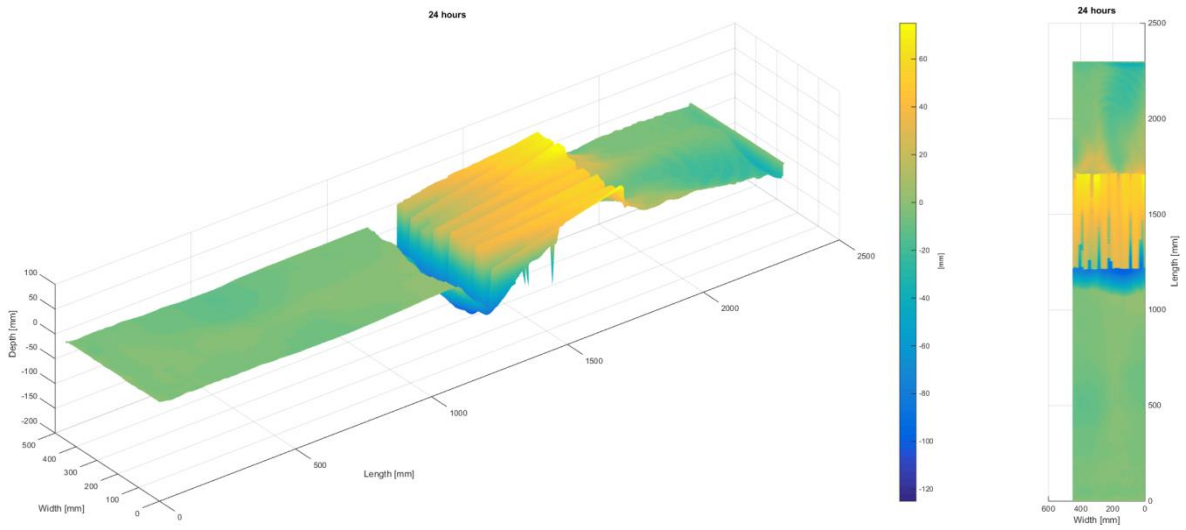

Figure 435; 24[h] bed projection

This can be confirmed with the average transect, observable in Figure 436. It shows a very steep scour hole just upstream of the logs, while also showing a minimal amount of accretion just downstream of the logs which gradually turn into on average scour towards the end of the expansion.

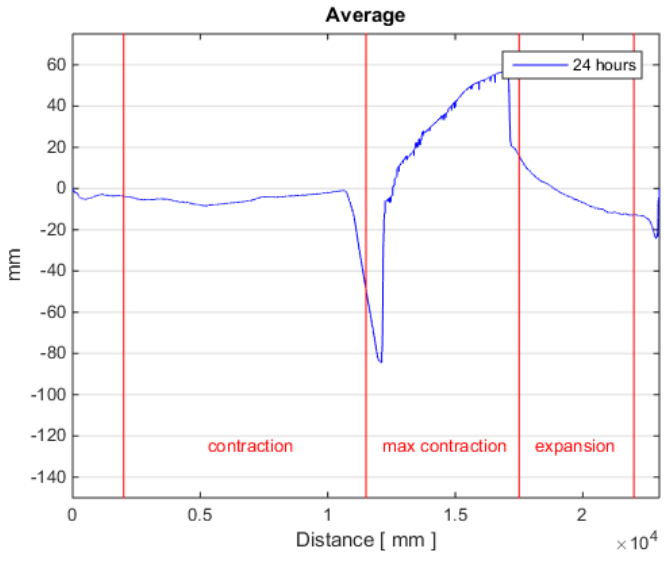

Figure 436; 24[h] average transect

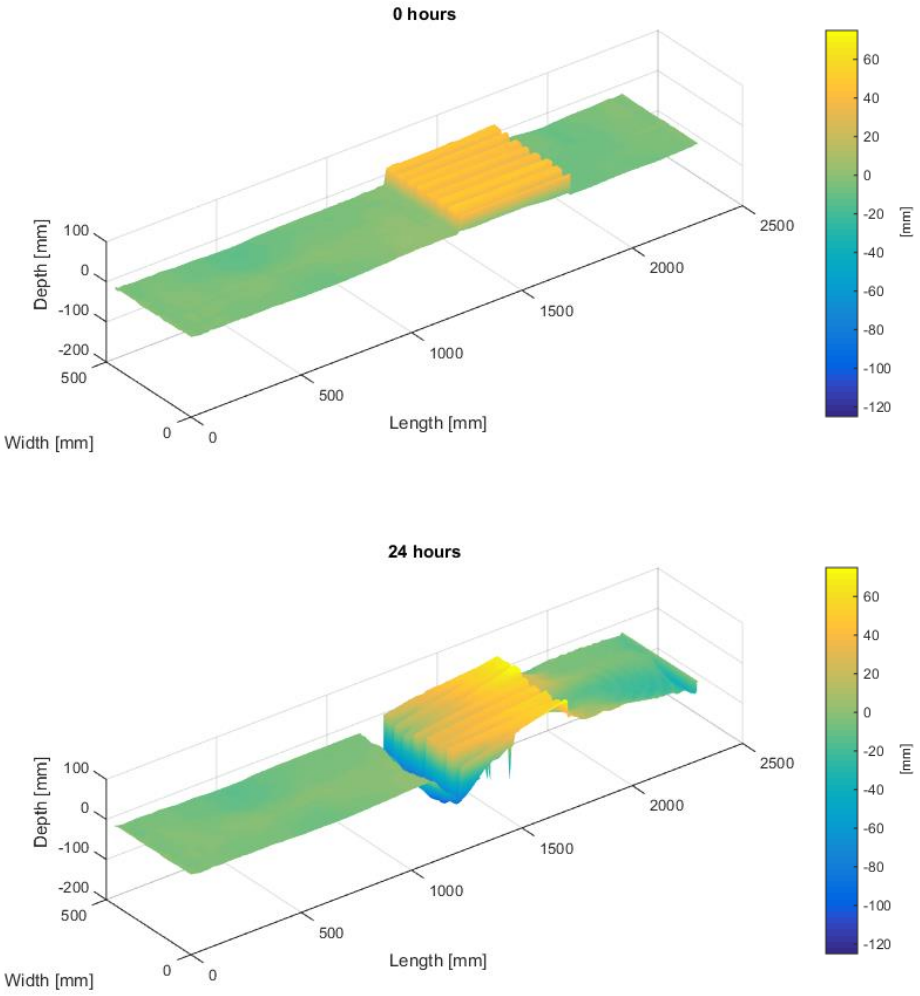

Figure 437; 0[h]-24[h] bed change projection

Table 102; Volume change per sector in [cm^3]

	Upstream	Contraction	Constriction	Expansion	Downstream
Volume	-5	-853	-2345	+541	-573

Velocity Profiles

From the velocity profiles it can be concluded that the situation does not change much most locations. Location 1 still holds the same distribution, also still observable are negative near bed velocities at locations 3 and 5. Location 6 shows an incomplete reattachment and location 9 shows a more equally distributed flow pattern in contrast with the local acceleration measured about 10 [cm] above the logs right after the start of the experiment.

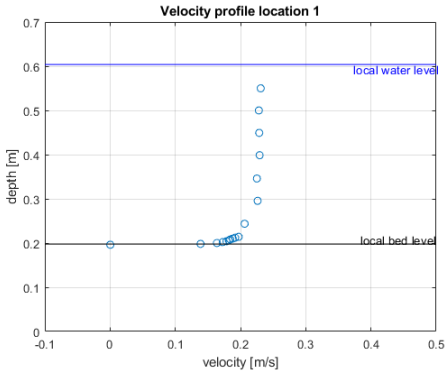

Figure 438; Velocity Profile location 1

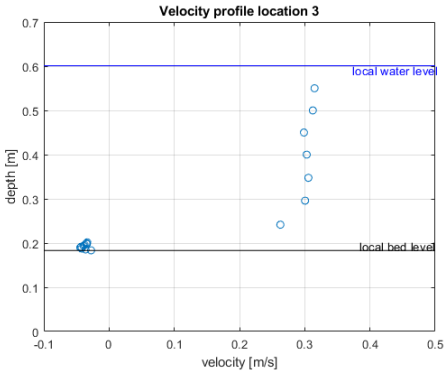

Figure 439; Velocity Profile location 3

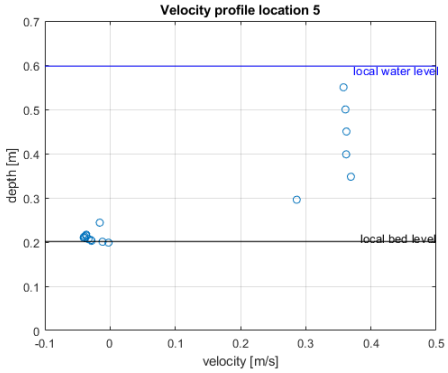

Figure 440; Velocity Profile location 5

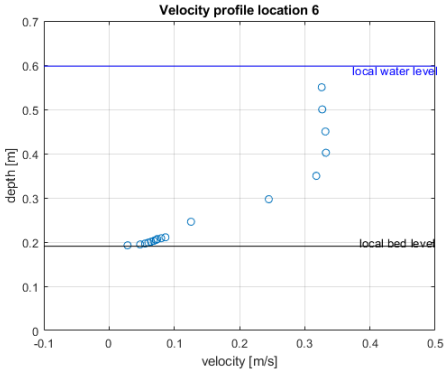

Figure 441; Velocity Profile location 6

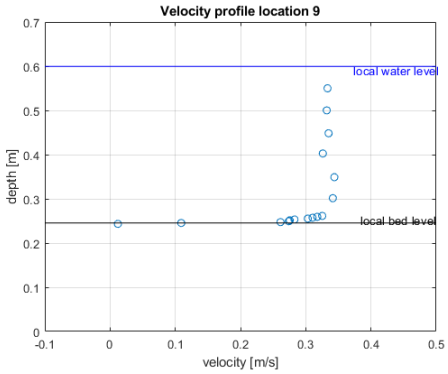

Figure 442; Velocity Profile location 9

Relative fluctuation intensity

Relative fluctuation development shows familiar patterns with a reduction during contraction from locations 1-2. At location 3 & 8 these values are strongly negative, indicative of negative velocities. This is caused by the measurements being taken within the trench that has developed just upstream of the logs where flow is on very small and upstream directed. At locations 4 and 9 above the logs it can be observed that this value is again relatively low and uniform, although it shows to be slightly stronger at location 9, which is close to the wall.

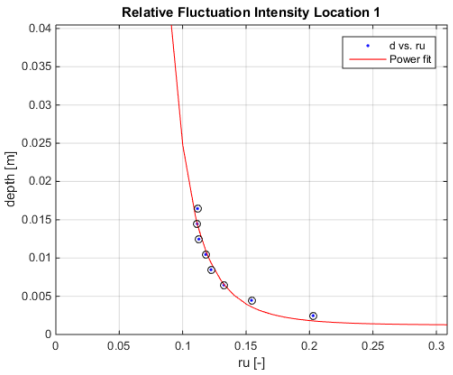

Figure 443; Relative fluctuation intensity location 1

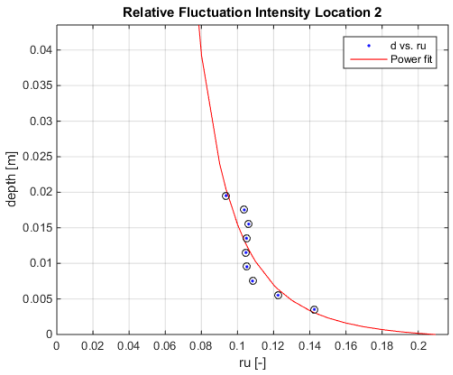

Figure 444; Relative fluctuation intensity location 2

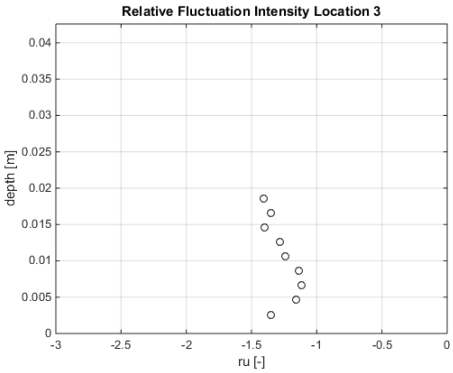

Figure 445; Relative fluctuation intensity location 3

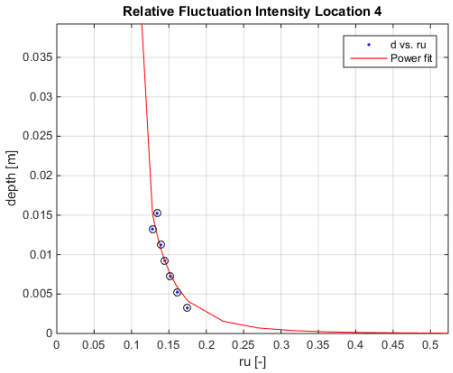

Figure 446; Relative fluctuation intensity location 4

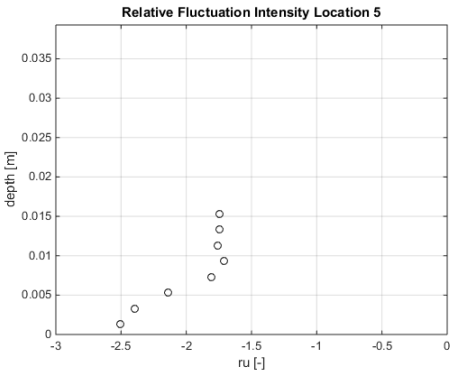

Figure 447; Relative fluctuation intensity location 5

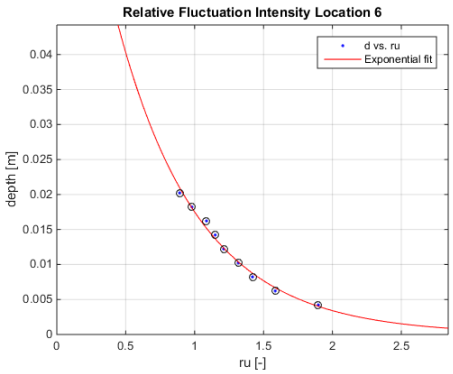

Figure 448; Relative fluctuation intensity location 6

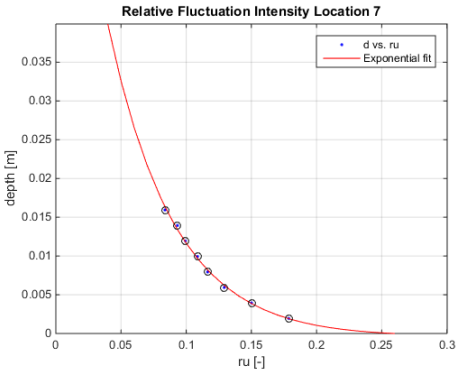

Figure 449; Relative fluctuation intensity location 7

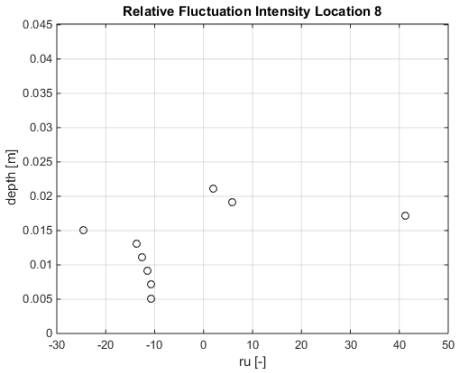

Figure 450; Relative fluctuation intensity location 8

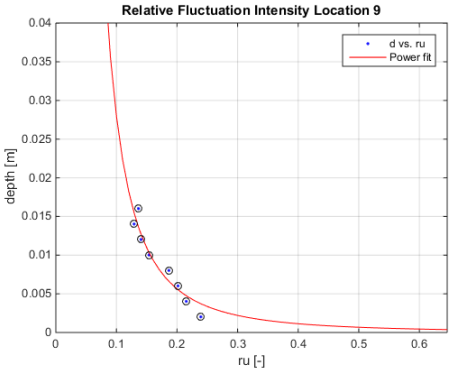

Figure 451; Relative fluctuation intensity location 9

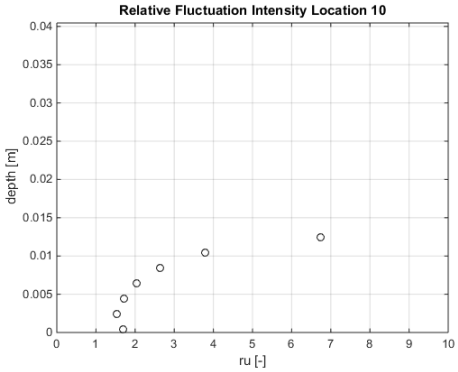

Figure 452; Relative fluctuation intensity location 10

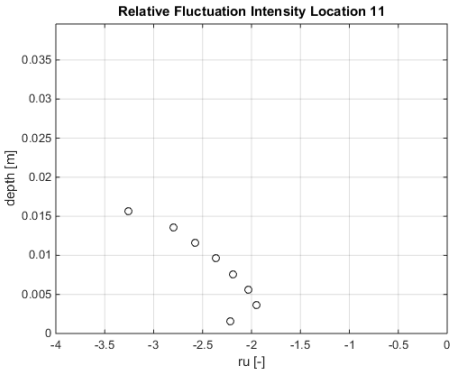

Figure 453; Relative fluctuation intensity location 11

Locations 5 and 10 again high relative fluctuation intensities, the cause for this is similar to the conditions at start, and is caused by wake formation downstream of the logs. Locations 6 and 11 also show relatively large values of fluctuation intensity which can be explained by the observation that the flow profile has net correctly reattached as is observable in the section regarding flow profiles. Thus flow near bottom is small and occasionally negative.

Bed Shear stress

The bed shear stress was determined with Reynolds formula stated in (Schiereck & Verhagen, 2012). Bed shear stresses are determined by averaging the estimation for bed shear stress, over the centimeter measured above the bottom for a time frame of 3 minutes measuring at 50 [hz] per second, excluding all measured values that do not confirm with a signal to noise ratio above 15 and a correlation of 90%.

Bed shear stresses exceed values associated with high level of transport at locations 3,6,10 & 11. At location 10 this bed shear stress is positive.

Table 103; Bed shear stresses [n/m^2]

Location	1	2	3	4	5	6	7	8	9	10	11
	-0,058	-0,043	-0,314	-0,807	-0,044	-0,279	-0,067	-0,078	-0,067	0,463	-0,129

Estimation of transport

Following the formulations of the bed load transport by van Rijn (van Rijn, 2018). The results are represented as such, that locations at the same longitudinal location are coupled and transport is averaged over these locations (Table 104) For the calculations the absolute value was taken of the measured bed shear stresses. The results are also depicted per sector (Table 105) by calculating the area underneath each cross-sectional measurement. In this way it is expected scour will accelerate mainly in the constriction & expansion sectors.

Table 104; Bed load transport [kg/m/s]

Location	1	2 & 7	3 & 8	4 & 9	5 & 10	6 & 11
	NaN	NaN	0,00011	0,0085	0,0009	0,00017

Table 105; Bed load transport per sector [kg/day]

Sector	Upstream	Contraction	Constriction	Expansion	Downstream
	NaN	1,2	121,4	21,6	0,8

Water level

The water levels were measured at locations 1,3,5,6 they are depicted in Table 106. The levels were computed by measuring at 1000 [hz] for 15 seconds, and averaging those results. It is observed that the water level shows a drop of 0,6 [cm]. The water level seems to drop during constriction with 0,6 [cm], and then remains constant

Table 106; Water level [cm]

Location	1	3	5	6
	40,3860	40,1111	39,7793	39,777

Measurements after 48h

Bed level

A projection of the bed after running for 48 [h] can be observed in Figure 454. The bed shows the continued development of a very narrow and deep scour hole just upstream of the placed logs. The logs have also tilted slightly towards this hole. Furthermore, small patches of accretion are observed directly downstream of the logs, while further downstream scour seams to appear.

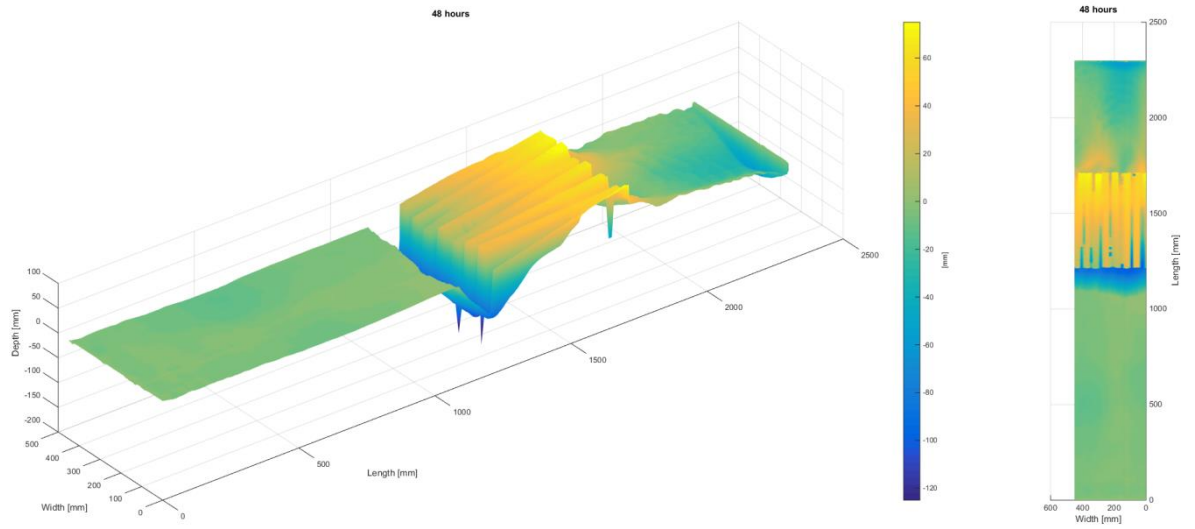

Figure 454; 48[h] bed projection

The average calculated transect observable in Figure 455, shows scour has penetrated up to 90 [mm] just in front of the logs and 40 [m] downstream of the logs.

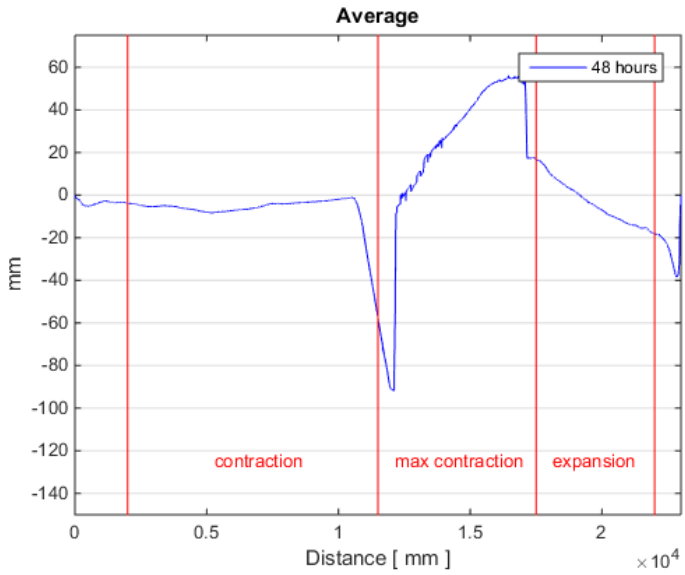

Figure 455; 48[h] average transect

Furthermore Figure 456 shows that scour downstream of the logs has intensified, but the logs have been generally unaffected during this specific time interval, with none of the logs tilting significantly, and the upstream scour hole showing no further growth.

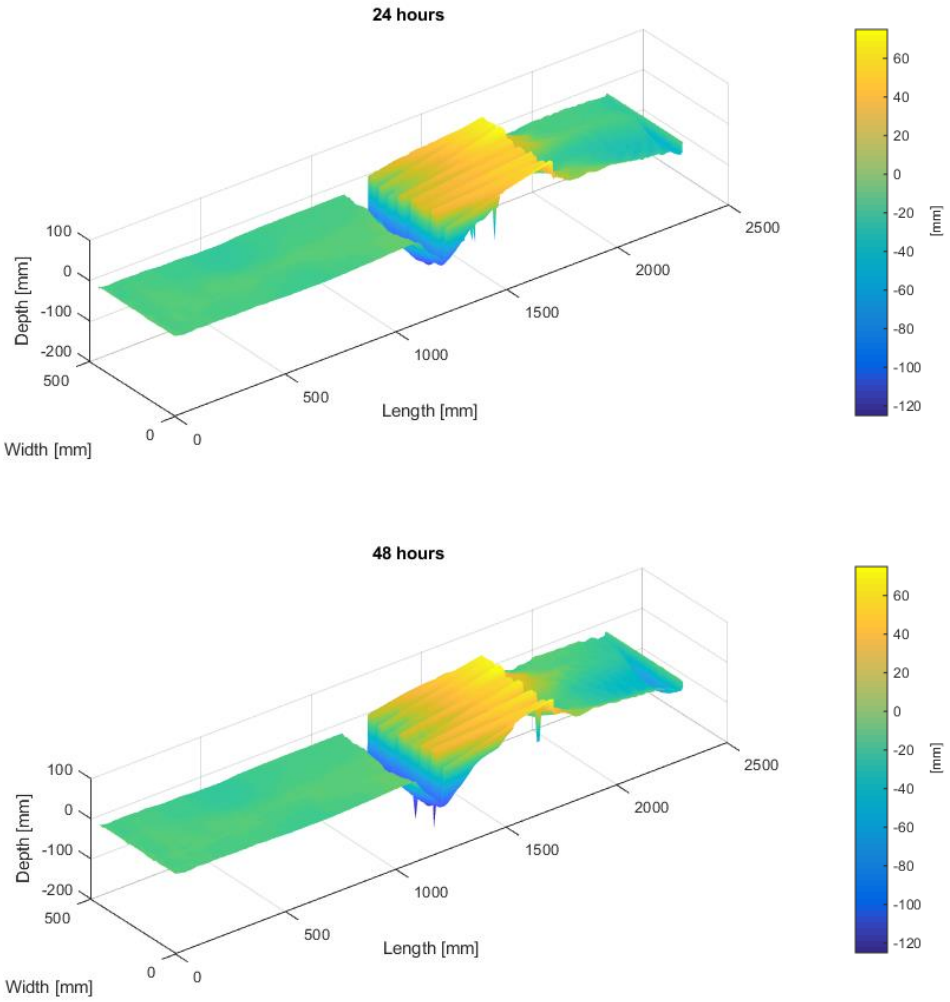

Figure 456; 24[h]-48[h] bed change projection

Table 107; Volume change per sector in [cm^3]

	Upstream	Contraction	Constriction	Expansion	Downstream
Volume	+2	-269	-520	+142	-288

Velocity Profiles

Flow profiles after 48 show no change for location 1. Locations 3 shows a bolstered version of the flow profile at location 1 with the exception of near zero/zero velocity near the bottom just upstream of the logs. Locations 5, 6 & 9 have remained roughly the same as before.

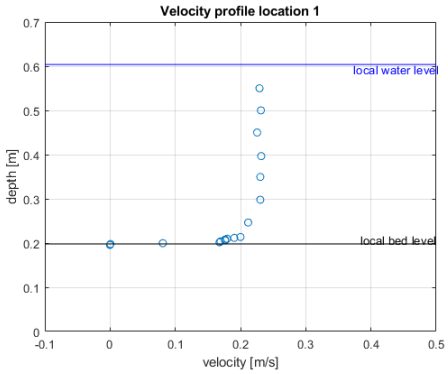

Figure 457; Velocity Profile location 1

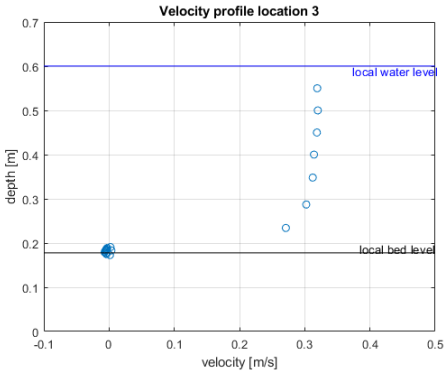

Figure 458; Velocity Profile location 3

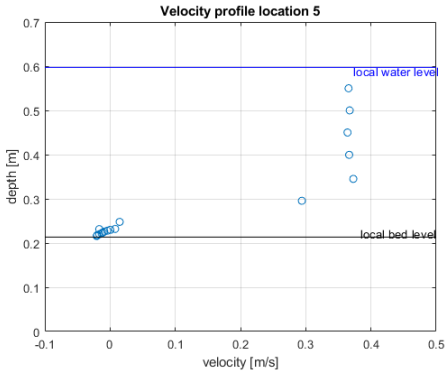

Figure 459; Velocity Profile location 5

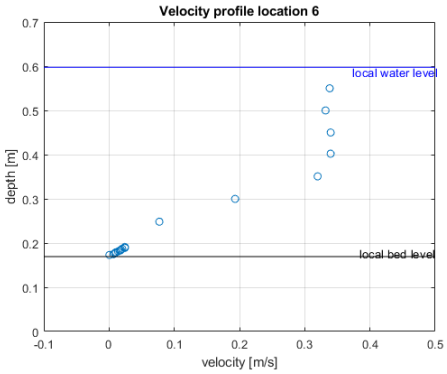

Figure 460; Velocity Profile location 6

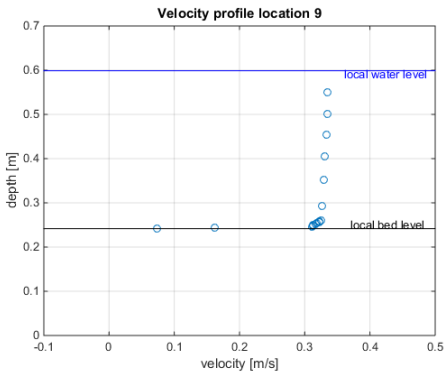

Figure 461; Velocity Profile location 9

Relative fluctuation intensity

Relative fluctuation seemingly increases from location 1-2. At location 3 & 8 these values large and occasionally negative, indicative of near zero velocities. This is caused by the measurements being taken within the trench that has developed just upstream of the log. At locations 4 and 9 above the logs it can be observed that this value is again relatively low and uniform, although it shows to be significantly stronger at location 9, which is close to the wall.

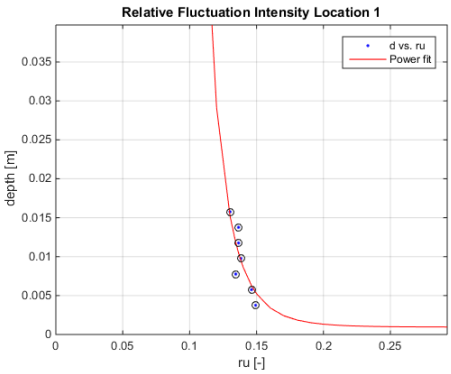

Figure 462; Relative fluctuation intensity location 1

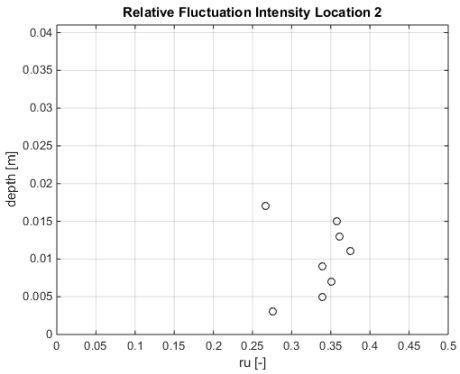

Figure 463; Relative fluctuation intensity location 2

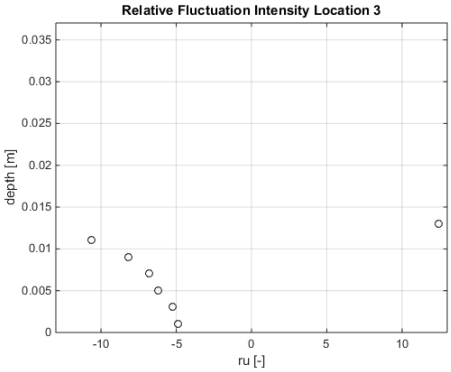

Figure 464; Relative fluctuation intensity location 3

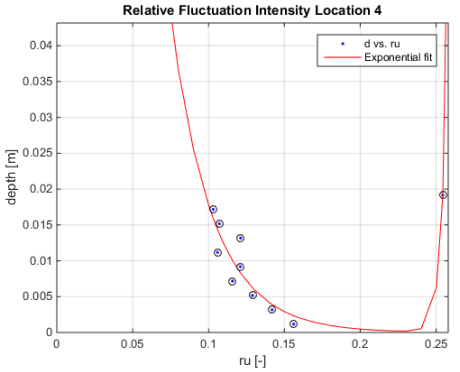

Figure 465; Relative fluctuation intensity location 4

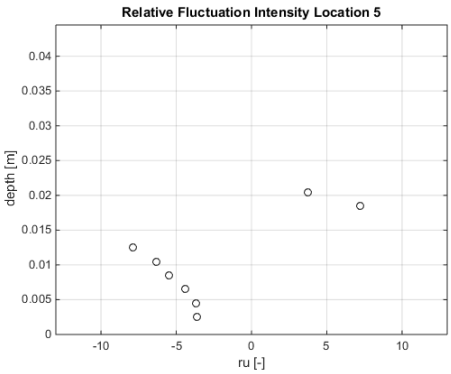

Figure 466; Relative fluctuation intensity location 5

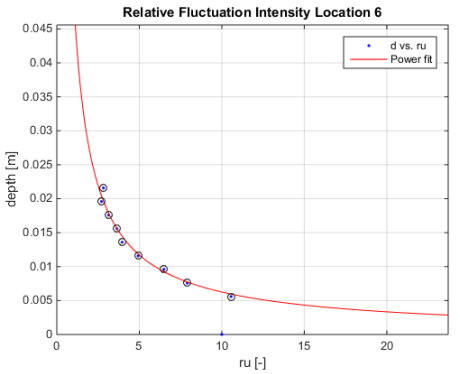

Figure 467; Relative fluctuation intensity location 6

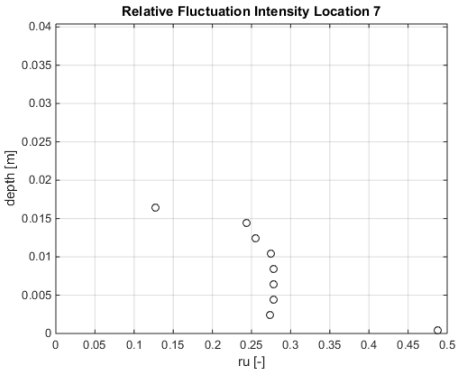

Figure 468; Relative fluctuation intensity location 7

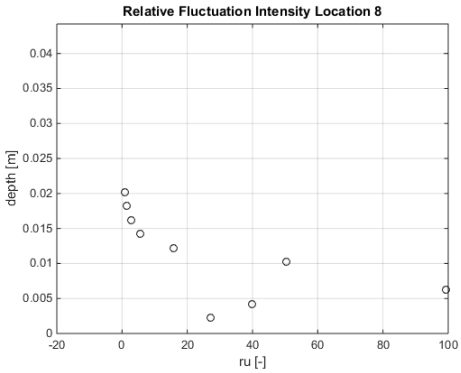

Figure 469; Relative fluctuation intensity location 8

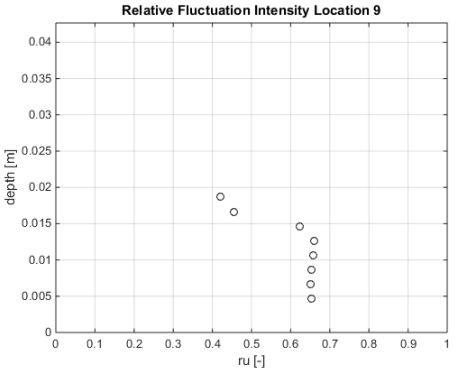

Figure 470; Relative fluctuation intensity location 9

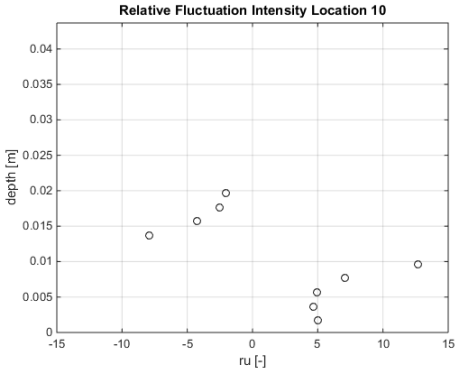

Figure 471; Relative fluctuation intensity location 10

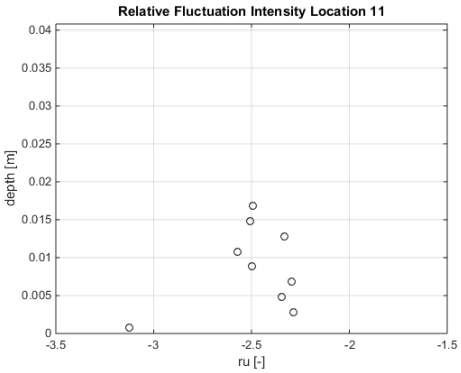

Figure 472; Relative fluctuation intensity location 11

Locations 5 and 10 again high and occasionally negative relative fluctuation intensities, the cause for this is similar to the conditions at start, and is caused by wake formation downstream of the logs. Locations 6 and 11 also show relatively large values of fluctuation intensity which can be explained by the observation that the flow profile has net correctly reattached as is observable in the section regarding flow profiles. Thus flow near bottom is small and occasionally negative.

Bed Shear stress

The bed shear stress was determined with Reynolds formula stated in (Schiereck & Verhagen, 2012). Bed shear stresses are determined by averaging the estimation for bed shear stress, over the centimeter measured above the bottom for a time frame of 3 minutes measuring at 50 [hz] per second, excluding all measured values that do not confirm with a signal to noise ratio above 15 and a correlation of 90%.

Bed shear stresses exceed values associated with high level of transport at locations 4,6,9 & 10. At locations 9 & 10 this bed shear stress is positive.

Table 108; Bed shear stresses [n/m^2]

Location	1	2	3	4	5	6	7	8	9	10	11
	-0,067	-0,090	-0,008	0,251	-0,075	-0,278	-0,065	-0,030	0,459	0,288	-0,021

Estimation of transport

Following the formulations of the bed load transport by van Rijn (van Rijn, 2018). The results are represented as such, that locations at the same longitudinal location are coupled and transport is averaged over these locations (Table 109) For the calculations the absolute value was taken of the measured bed shear stresses. The results are also depicted per sector (Table 110) by calculating the area underneath each cross-sectional measurement. In this way it is expected scour to mainly to continue in the constriction-sector.

Table 109; Bed load transport [kg/m/s]

Location	1	2 & 7	3 & 8	4 & 9	5 & 10	6 & 11
	NaN	NaN	NaN	0,0043	$3{,}36*10^{-5}$	NaN

Table 110; Bed load transport per sector [kg/day]

Sector	Upstream	Contraction	Constriction	Expansion	Downstream
	NaN	NaN	58,0	0,3	NaN

Water level

The water levels were measured at locations 1,3,5,6 they are depicted in Table 111. The levels were computed by measuring at 1000 [hz] for 15 seconds, and averaging those results. It is observed that the water level shows a drop of 0,6 [cm]. The water level seems to drop during constriction with 0,6 [cm], and then remains constant

Table 111; Water level [cm]

Location	1	3	5	6
	40,3639	40,0192	39,7257	39,7318

Measurements after 72h

Bed level

A projection of the bed after running for 72 [h] can be observed in Figure 473. The bed shows the continued development of a very narrow and deep scour hole just upstream of the placed logs. The logs have also tilted slightly towards this hole. Furthermore, small patches of accretion are observed directly downstream of the logs, while further downstream scour seams to appear.

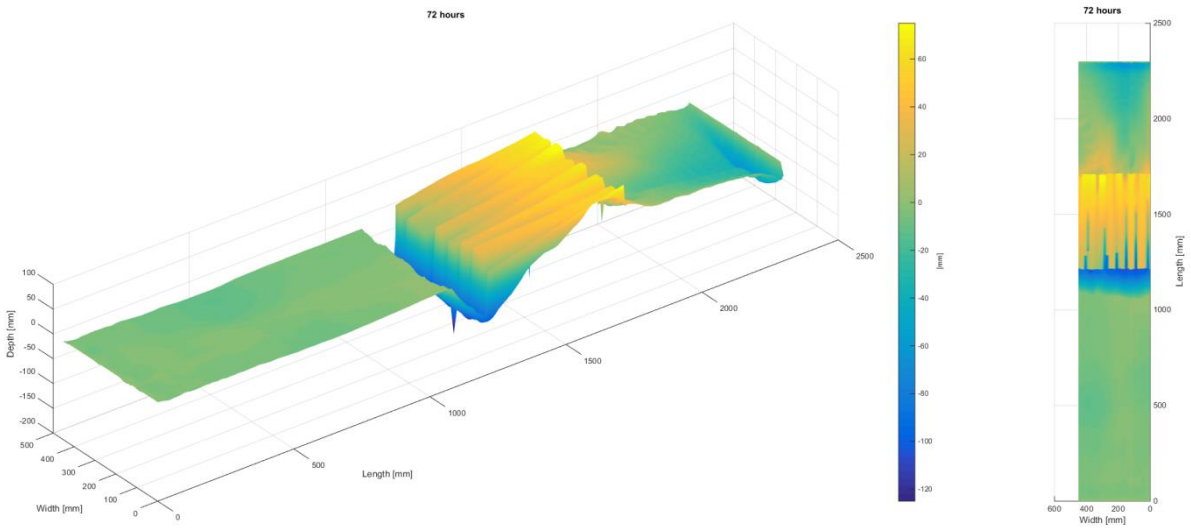

Figure 473; 72[h] bed projection

The average calculated transect observable in Figure 474, shows scour has penetrated up to 95 [mm] just in front of the logs and 45 [m] downstream of the logs.

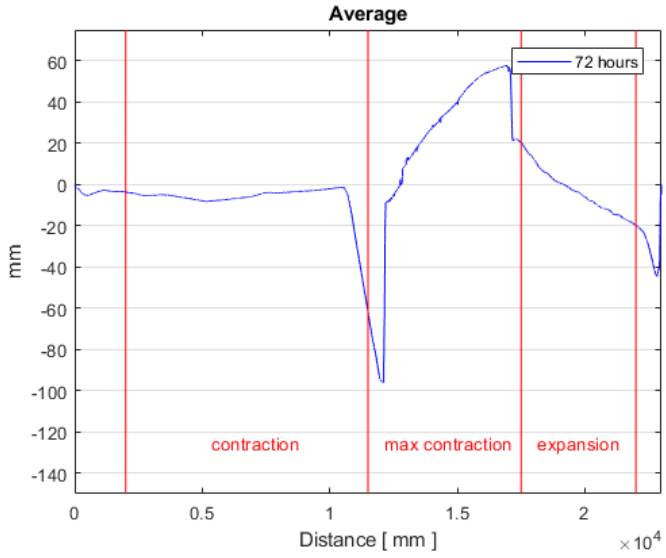

Figure 474; 72[h] average transect

Furthermore Figure 475 shows that scour downstream of the logs has not changed noticeably and the same goes for the scour hole upstream of the logs.

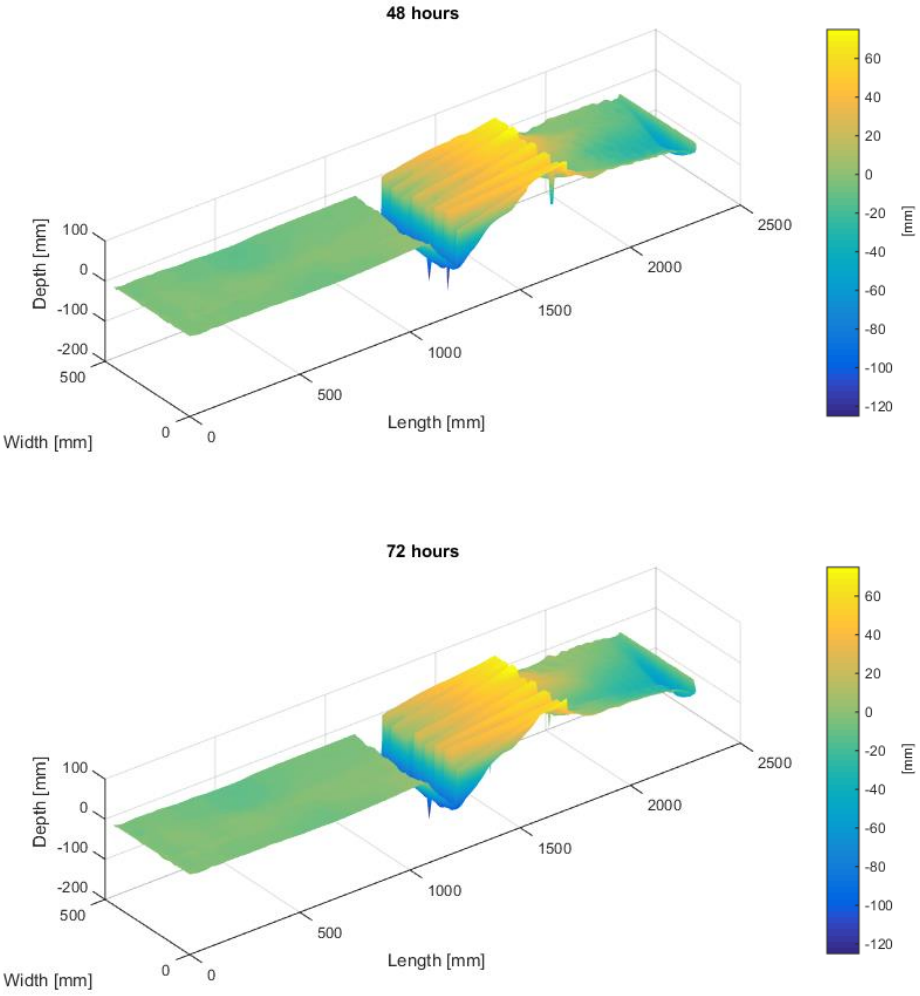

Figure 475; 48[h]-72[h] bed change projection

Table 112; Volume change per sector in [cm^3]

	Upstream	Contraction	Constriction	Expansion	Downstream
Volume	+3	-139	-63	+64	-207

Velocity Profiles

Flow profiles after 72 [h] Fin shows little to no change for location 1. Locations 3 shows a bolstered version of the flow profile at location 1 with the exception of near zero/zero velocity near the bottom just upstream of the logs. Locations 5, 6 & 9 have remained roughly the same as before.

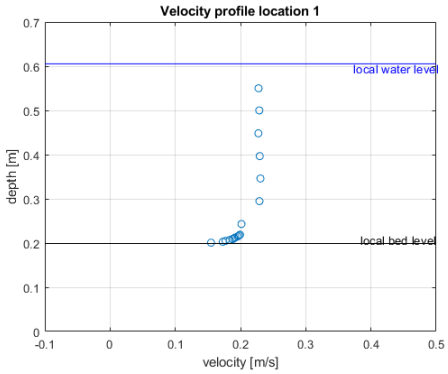

Figure 476; Velocity Profile location 1

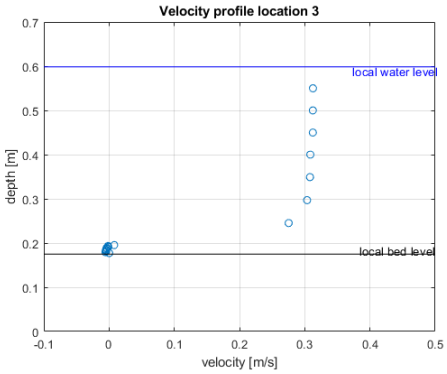

Figure 477; Velocity Profile location 3

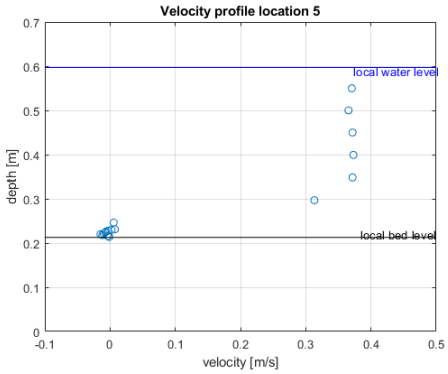

Figure 478; Velocity Profile location 5

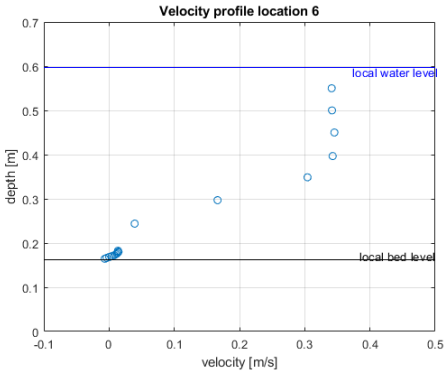

Figure 479; Velocity Profile location 6

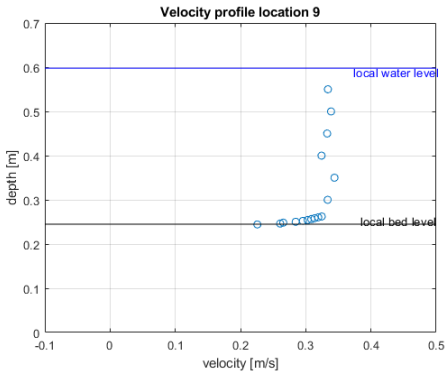

Figure 480; Velocity Profile location 9

Relative fluctuation intensity

Relative fluctuation seemingly reduces from location 1-2. At location 3 & 8 these values large and only occasionally positive, indicative of near zero velocities. This is caused by the measurements being taken within the trench that has developed just upstream of the log. At locations 4 and 9 above the logs it can be observed that this value is again relatively low and uniform, although it shows to be significantly stronger at location 9.

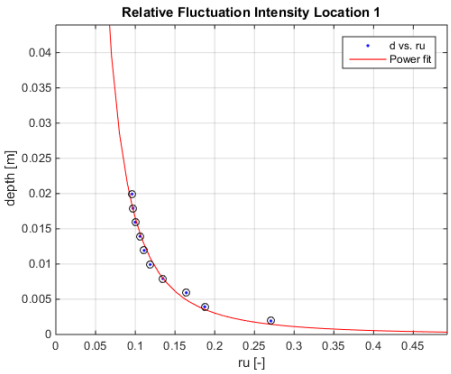

Figure 481; Relative fluctuation intensity location 1

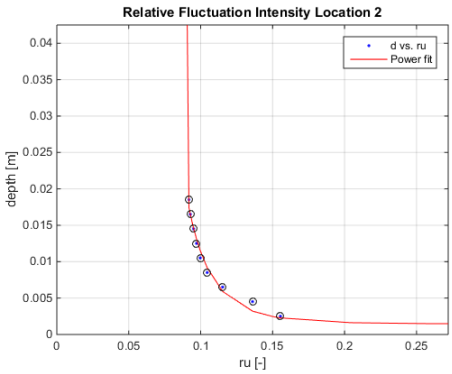

Figure 482; Relative fluctuation intensity location 2

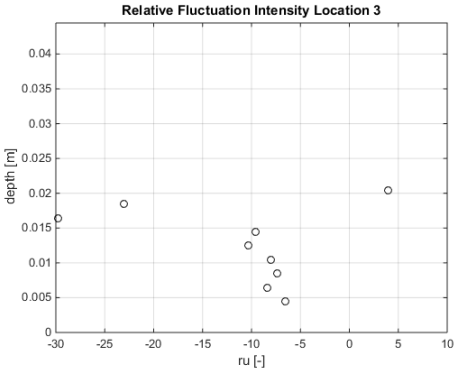

Figure 483; Relative fluctuation intensity location 3

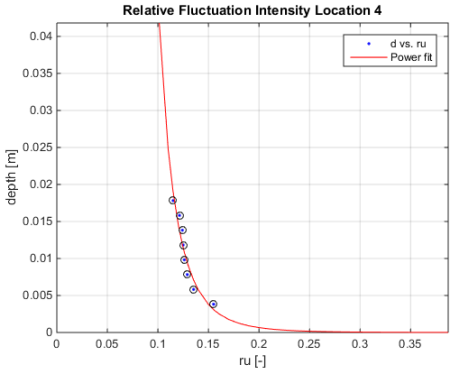

Figure 484; Relative fluctuation intensity location 4

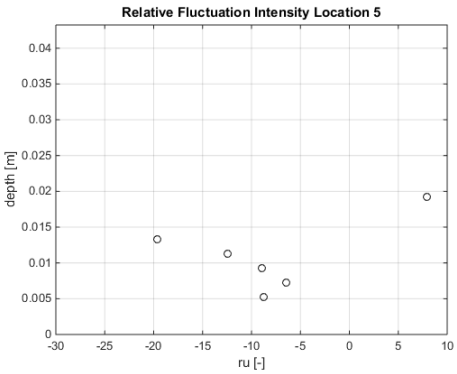

Figure 485; Relative fluctuation intensity location 5

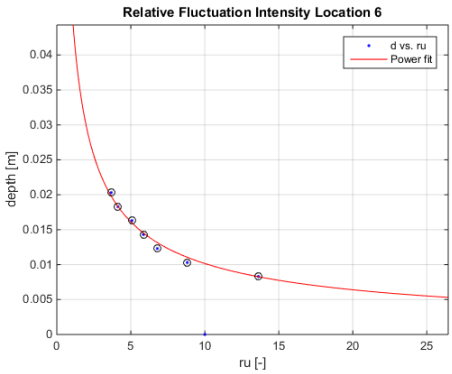

Figure 486; Relative fluctuation intensity location 6

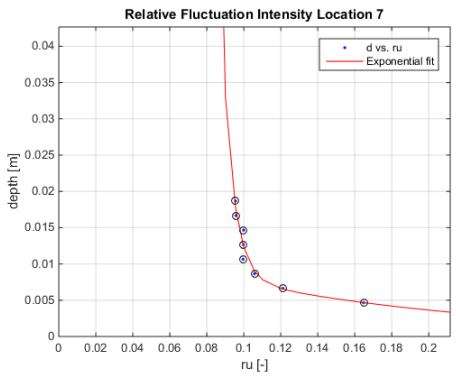

Figure 487; Relative fluctuation intensity location 7

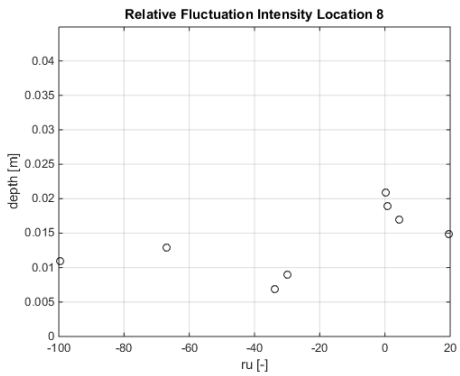

Figure 488; Relative fluctuation intensity location 8

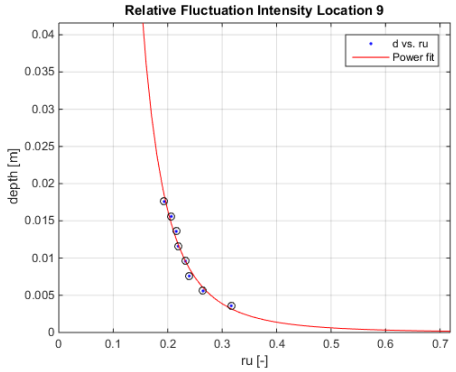

Figure 489; Relative fluctuation intensity location 9

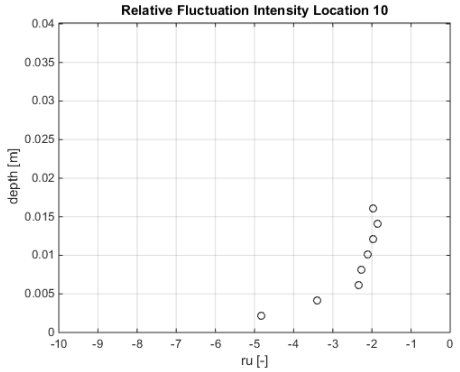

Figure 490; Relative fluctuation intensity location 10

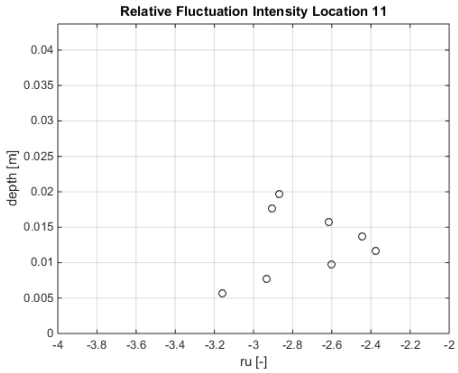

Figure 491; Relative fluctuation intensity location 11

At location 5 & 10 again negative and large values are found, indicative of small velocities and near the bed upstream directed net flow. Locations further downstream (6 & 11) also still show relatively large fluctuations and negative values.

Bed Shear stress

The bed shear stress was determined with Reynolds formula stated in (Schiereck & Verhagen, 2012). Bed shear stresses are determined by averaging the estimation for bed shear stress, over the centimeter measured above the bottom for a time frame of 3 minutes measuring at 50 [hz] per second, excluding all measured values that do not confirm with a signal to noise ratio above 15 and a correlation of 90%.

Bed shear stresses exceed values associated with high level of transport at locations 6. Locations 4,9,10,11 show positive bed shear stresses.

Table 113; Bed shear stresses [n/m^2]

Location	1	2	3	4	5	6	7	8	9	10	11
	-0,061	-0,047	-0,037	0,040	-0,031	-0,110	-0,049	-0,010	0,048	0,022	0,030

Estimation of transport

Following the formulations of the bed load transport by van Rijn (van Rijn, 2018). The results are represented as such, that locations at the same longitudinal location are coupled and transport is averaged over these locations (Table 114) For the calculations the absolute value was taken of the measured bed shear stresses. The results are also depicted per sector (Table 115) by calculating the area underneath each cross-sectional measurement. In this way it is expected scour to stop, or in any case reduce significantly.

Table 114; Bed load transport [kg/m/s]

Location	1	2 & 7	3 & 8	4 & 9	5 & 10	6 & 11
	NaN	NaN	NaN	NaN	NaN	NaN

Table 115; Bed load transport per sector [kg/day]

Sector	Upstream	Contraction	Constriction	Expansion	Downstream
	NaN	NaN	NaN	NaN	NaN

Water level

The water levels were measured at locations 1,3,5,6 they are depicted in Table 116. The levels were computed by measuring at 1000 [hz] for 15 seconds, and averaging those results. It is observed that the water level shows a drop of 0,8 [cm]. The water level seems to drop during constriction with 0,8 [cm], and then remains constant

Table 116; Water level [cm]

Location	1	3	5	6
	40,5259	39,8418	39,6953	39,6979

Measurements after 96h

Bed level

The bed after 96 [h] shows a continuation of the existing scour formation, (see Figure 492 & Figure 493). At the end of the experiment 2 areas of scour can be clearly identified, namely the region just upstream of the logs and the region downstream of the logs near the edge of the model. A quick observation shows a clear reduction of scour with respect

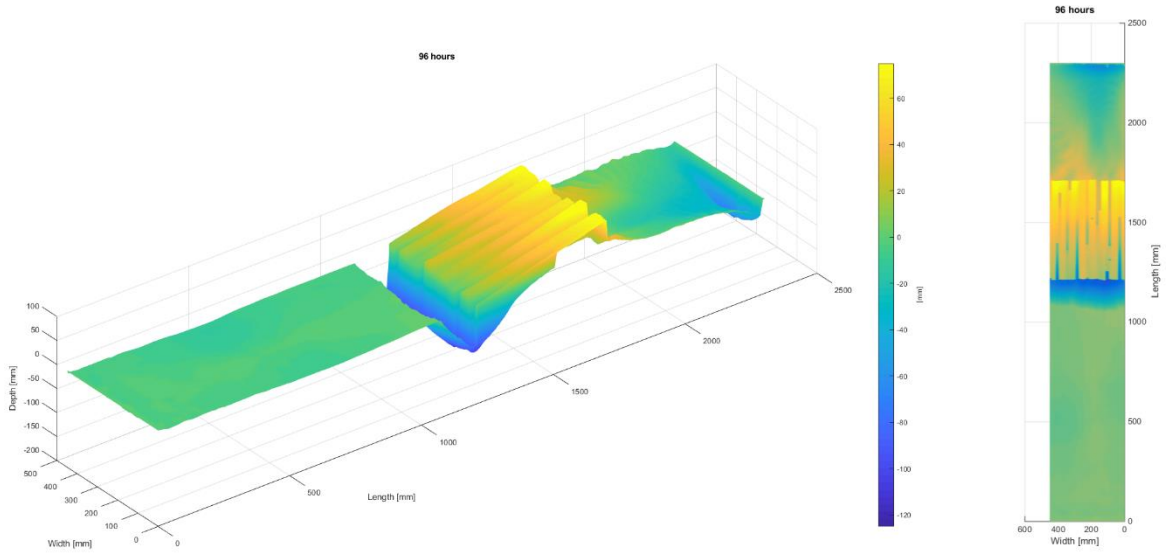

Figure 492; Bed map after 96 [h]

The average transect Figure 493 clearly shows these two regions, it also shows that the logs have tilted inwards to the upstream scour hole, and just downstream of the logs a small area of accretion has developed.

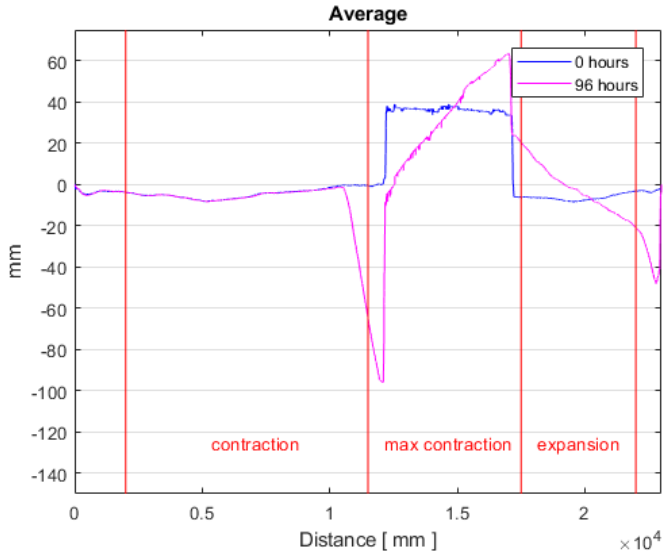

Figure 493; Average transects through time

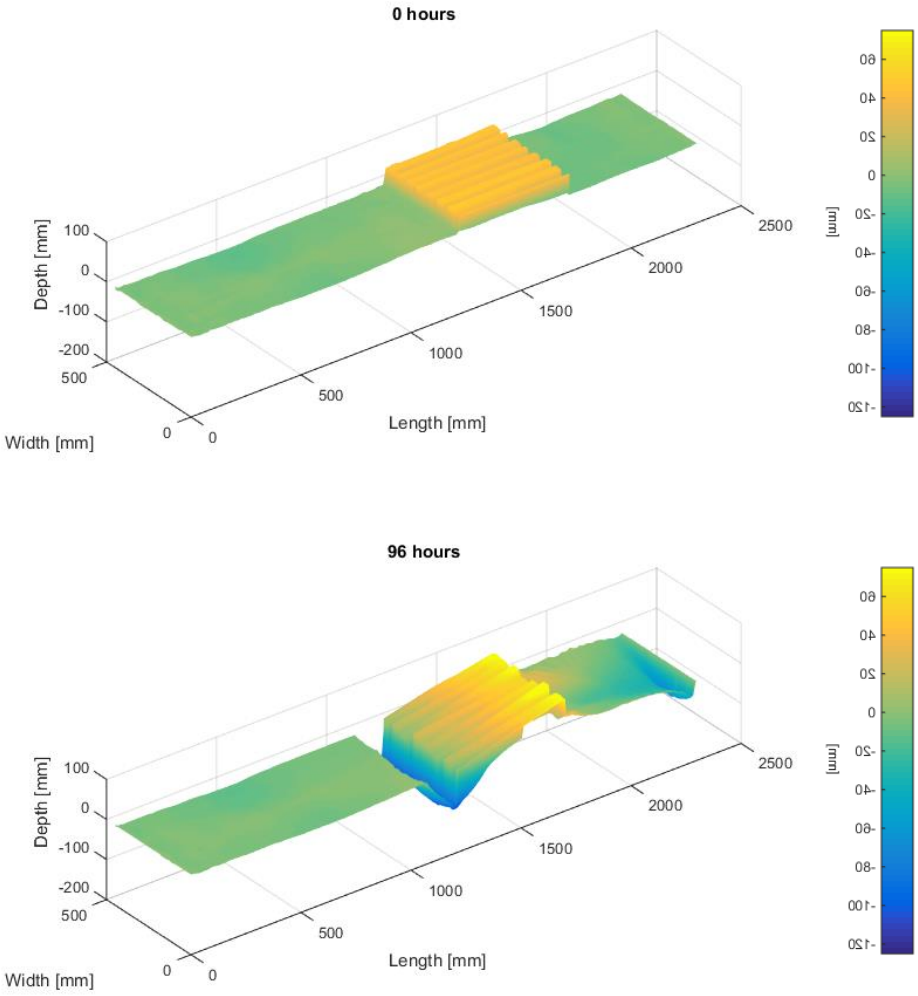

Figure 494; Bed change with respect to 0[h]

Table 117; Volume change per sector in [cm^3]

	Upstream	Contraction	Constriction	Expansion	Downstream
Volume	+1	-123	+246	+139	-143

Concluding Remarks

The third experiment conducted with flow parallel placed logs has shown a significant improvement compared to all basic scour tests. A reduction of scoured bed material of … percent was achieved. This is however somewhat countered by the fact that the maximum scour depth is still relatively high with almost 100 [mm], and thus being as high or higher with respect to all the basic scour experiments.

Appendix E I

I Introduction

The protected Scour experiments are considered to be the baseline experiments for the application of wooden logs as a scour protection. The “Protected Scour B” experiments feature a flow perpendicular placed single layer of logs directly on top of the bed, in the area of maximum contraction. Similar to the basic scour experiments bed, velocity and fluctuation intensity development is measured during a 96 [h] run. This report includes all measured findings during this particular experiment. Conclusions are drawn in the main report on the basis of multiple similarly conducted experiments. A short preliminary conclusion is however included at the end of this report.

Summary

Table 118 represents relevant scour quantities after 96 [h]. Note that the absolute is measured relative to the measurement of the bed at 0 [h], excluding the maximum scour depth which is measured to a reference bed with a 0 [mm] elevation. Measurements of scour volume in the column with respect to reference include missing volume with respect to a reference be of 0 [mm] and corrected for the presence of logs .

Table 118; Summary of quantities (Negative values indicate scour, positive indicate accretion)

	Quantity	With respect to reference
Maximum Scour Depth [mm]	93	93
Total Scoured volume [cm^3]	-6117	-18734
Scoured volume Upstream-sector [cm^3]	+3	-232
Scoured volume Contracting-sector [cm^3]	-668	-5598
Scoured volume Constricted-sector [cm^3]	-927	-6479
Scoured volume Expanding-sector [cm^3]	-2077	-4013
Scoured volume Downstream-sector [cm^3]	-2448	-2413

Measurements at 0h

Bed level

A projection of the bed at the moment of initiation of flow during the first scour experiment can be seen in Figure 495 Clearly observable are the placed logs on the bed. They are roughly located in between 1200-1700 [mm] from the entry point of flow, and are spaced about 1 [cm] from each other. This spacing was however lost due to the logs shifting into each other immediately after initiation of flow. The bed further appears to be again relatively flat, although colors indicate that the bed level is somewhat lower near the logs.

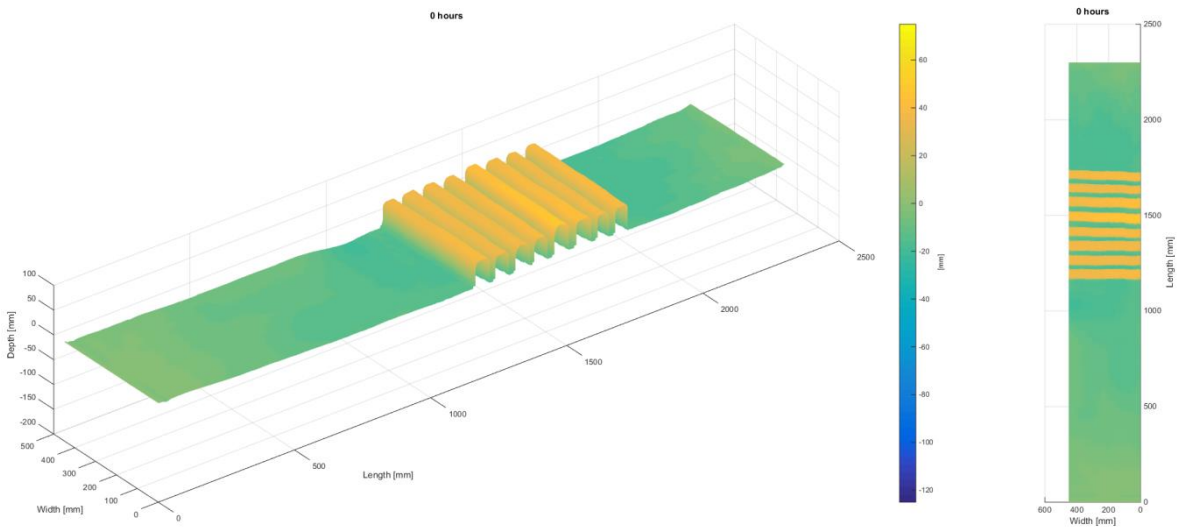

Figure 495; Bed map 0[h]

The average transect, observable in Figure 496, was calculated from the 31 transects taken over the entire length of the laboratory set-up. As can be seen, the bed is slightly below the target value of 0 [mm] with about 20 [mm] in the area of maximum contraction.

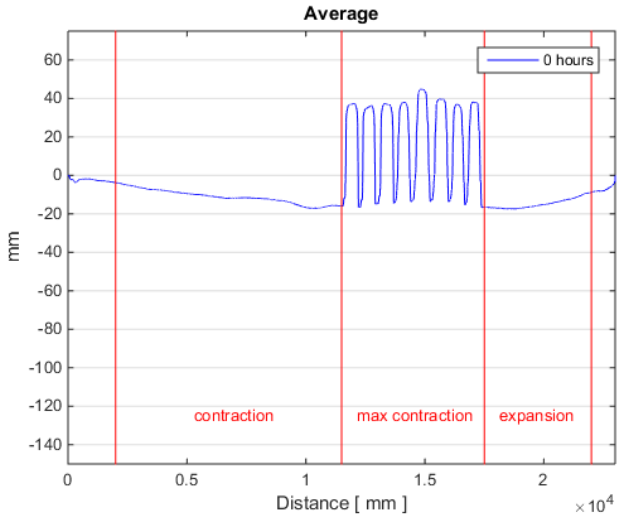

Figure 496; 0 [h] average transect

Velocity Profiles

In this section, individual flow profiles of locations specified earlier are shown. At location 3, which is located at the point of maximum contraction, the flow profile is distributed differently and flow accelerates especially higher up the water Colum. At location 5, just downstream of the log layer, it can be seen flow is reversed near the bottom in the wake of the logs, while higher up the water Colum, flow is accelerated even further with respect to location 3. At location 6, flow near the bottom is again directed downstream, but flow has seemingly not completely reattached, as the flow does not compare to the velocity profile at location 1 (which has the same cross-sectional dimension). Location 9 shows measured values similar to location 5 higher up the water column, and flow near the bed (top log layer) is seemingly very strong very close to the bed.

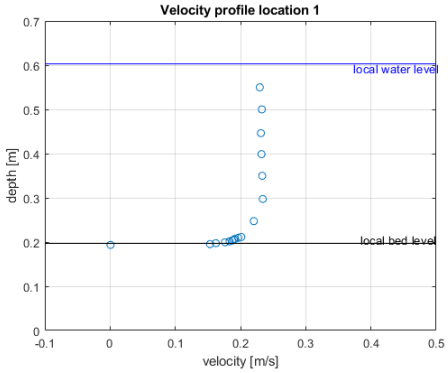

Figure 497; Velocity Profile location 1

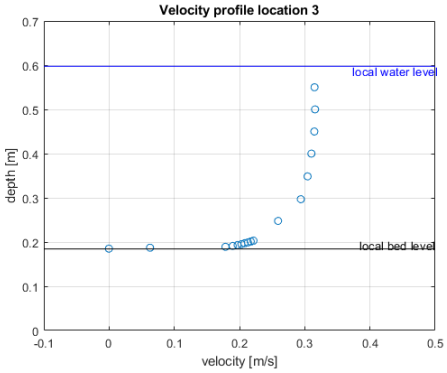

Figure 498; Velocity Profile location 3

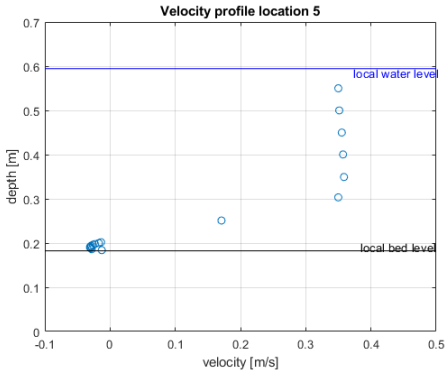

Figure 499; Velocity Profile location 5

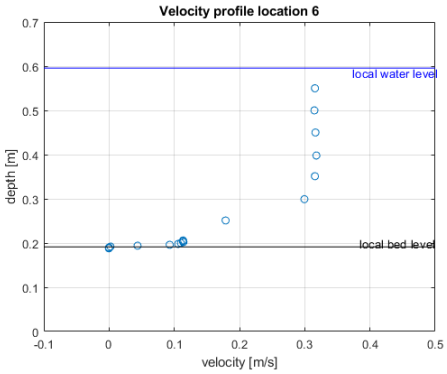

Figure 500; Velocity Profile location 6

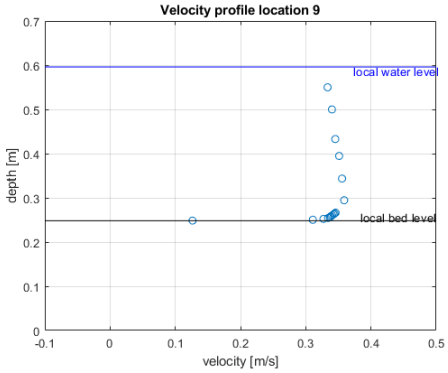

Figure 501; Velocity Profile location 9

Relative fluctuation intensity

Calculated fluctuation intensity shows that during flow contraction, in between location 1 & 2, this fluctuation drop now slightly increases again towards location 3. In between locations 7&8 this property remains about the same. At locations 4 and 9 (measured above the logs) we can see a slight increase especially at location 4, but nonetheless the relative fluctuation intensity remains small. Wherever possible, curve fitting has been applied to make interpretation easier.

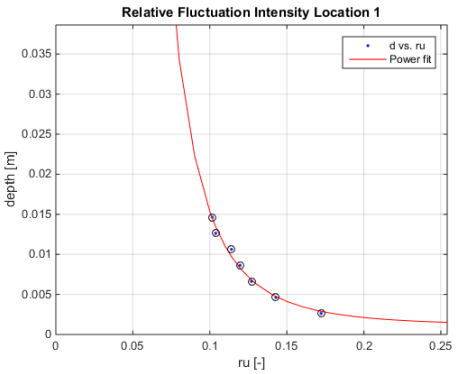

Figure 502; Relative fluctuation intensity location 1

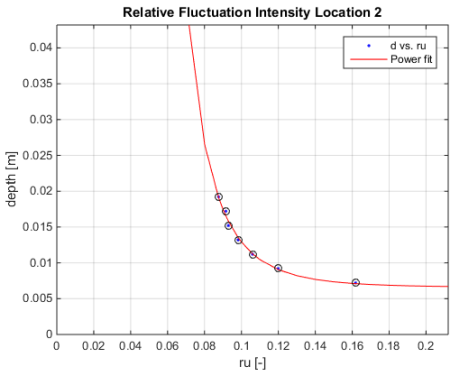

Figure 503 ; Relative fluctuation intensity location2

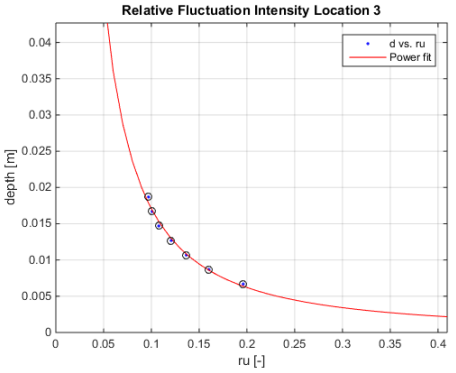

Figure 504; Relative fluctuation intensity location 3

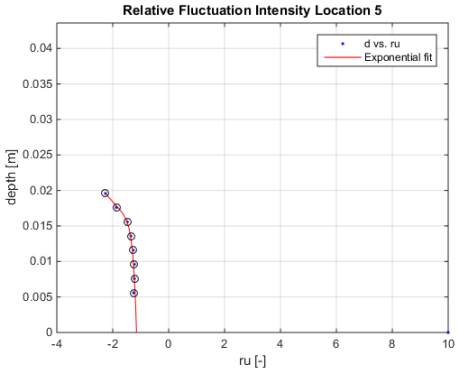

Figure 506; Relative fluctuation intensity location 4

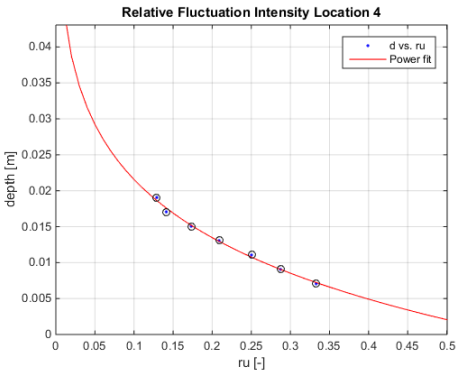

Figure 505; Relative fluctuation intensity location 5

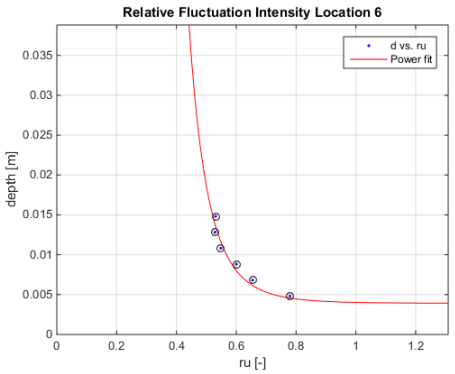

Figure 507; Relative fluctuation intensity location 6

Location 5& 10 both show negative fluctuation intensity, indication of flow upstream. The magnitude of the relative fluctuation intensity is high at both locations, but this is explained through average flow velocities being rather small. Lastly, near location 6 & 11 the relative fluctuation intensity is yet again positive and within a more reasonable range, even though location 11 is still a bit high.

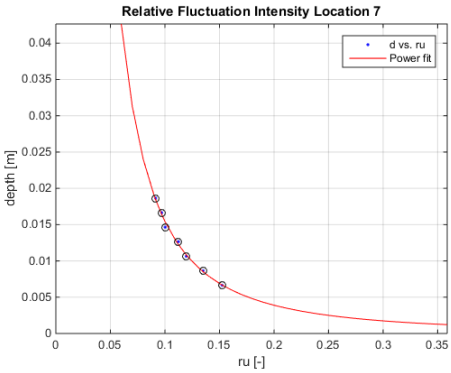

Figure 508; Relative fluctuation intensity location 7

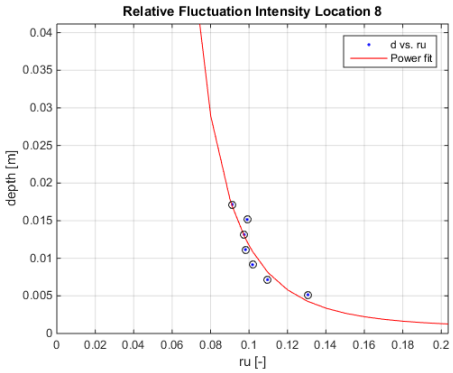

Figure 509; Relative fluctuation intensity location 8

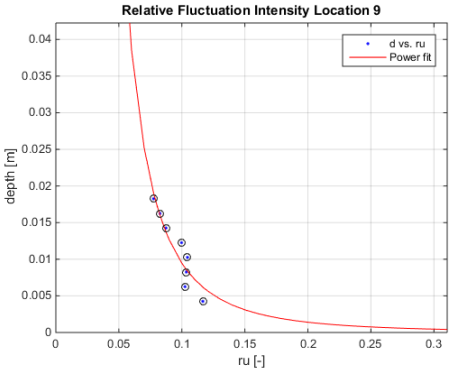

Figure 510; Relative fluctuation intensity location 9

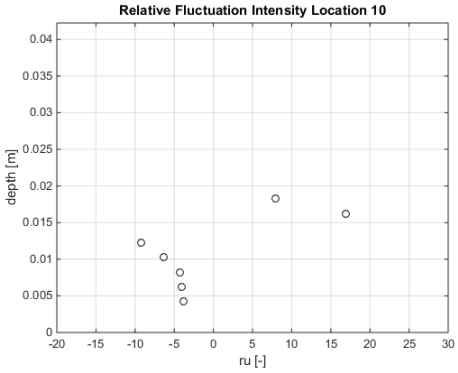

Figure 511; Relative fluctuation intensity location 10

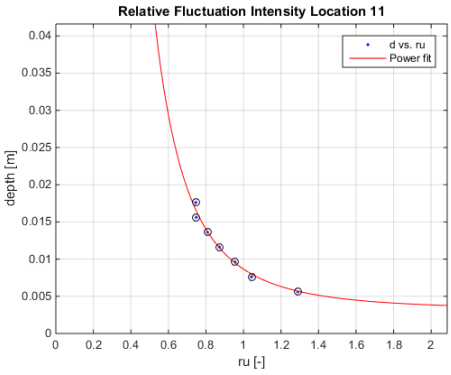

Figure 512; Relative fluctuation intensity location 11

Bed Shear stress

The bed shear stress was determined with Reynolds formula stated in (Schiereck & Verhagen, 2012). Bed shear stresses are determined by averaging the estimation for bed shear stress, over the centimeter measured above the bottom for a time frame of 3 minutes measuring at 50 [hz] per second, excluding all measured values that do not confirm with a signal to noise ratio above 15 and a correlation of 90%.

Bed shear stresses exceed values associated with high level of transport at locations 4,6,10 & 11. At all locations bed shear stresses were negative.

Table 119; Bed shear stresses [n/m^2]

Location	1	2	3	4	5	6	7	8	9	10	11
	-0,066	-0,071	-0,011	-0,282	-0,022	-0,133	-0,057	-0,059	-0,089	-0,105	-0,220

Estimation of transport

Following the formulations of the bed load transport by van Rijn (van Rijn, 2018). The results are represented as such, that locations at the same longitudinal location are coupled and transport is averaged over these locations (Table 120) For the calculations the absolute value was taken of the measured bed shear stresses. The results are also depicted per sector (Table 121) by calculating the area underneath each cross-sectional measurement. In this way it is expected that scour will be small and mainly located downstream of the logs.

Table 120; Bed load transport [kg/m/s]

Location	1	2 & 7	3 & 8	4 & 9	5 & 10	6 & 11
	NaN	NaN	NaN	$4{,}99*10^{-5}$	NaN	$1{,}81*10^{-5}$

Table 121; Bed load transport per sector [kg/day]

Sector	Upstream	Contraction	Constriction	Expansion	Downstream
	NaN	NaN	0,67	0,2	0,1

Water level

The water levels were measured at locations 1,3,5,6 they are depicted in Table 122. The levels were computed by measuring at 1000 [hz] for 15 seconds, and averaging those results. It is observed that the water level shows a drop of 0,7 [cm]. The water level seems to drop during constriction with 0,8 [cm], and then slightly increases again with 0,1 [cm].

Table 122; Water level [cm]

Location	1	3	5	6
	40,2952	39,7448	39,4323	39,5584

Measurements after 24h

Bed level

A projection of the bed after running for 24 [h] can be observed in Figure 513. The bed shows to have developed a small and narrow scour hole in front of the upstream located log. It can also be seen that this specific log has rolled into the scour hole, and the second and third log located from the upstream face have also moved towards this scour hole. Near the downstream end of the scanned area (2300 [mm]) minor scour has occurred.

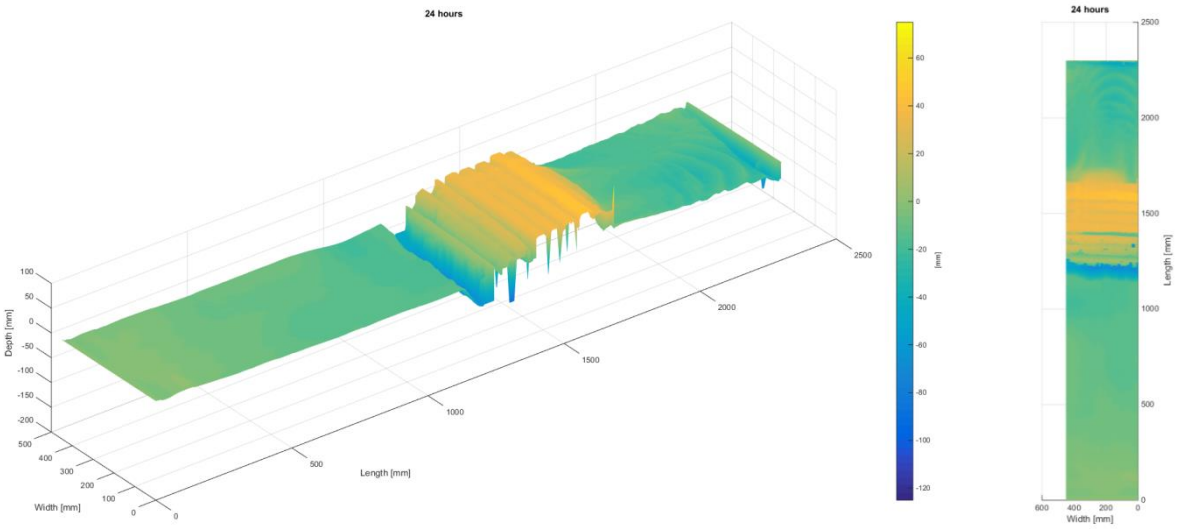

Figure 513; 24[h] bed projection

This can be confirmed with the average transect, observable in Figure 514. It shows a steep and narrow scour hole just upstream of the logs, with an average maximum of about 60 [mm]. Downstream the bed has started to accrete to the logs and near the end another smaller scour hole has developed.

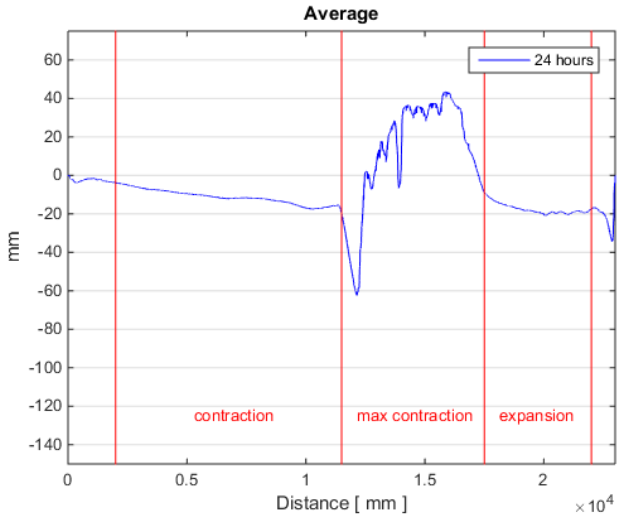

Figure 514; 24[h] average transect

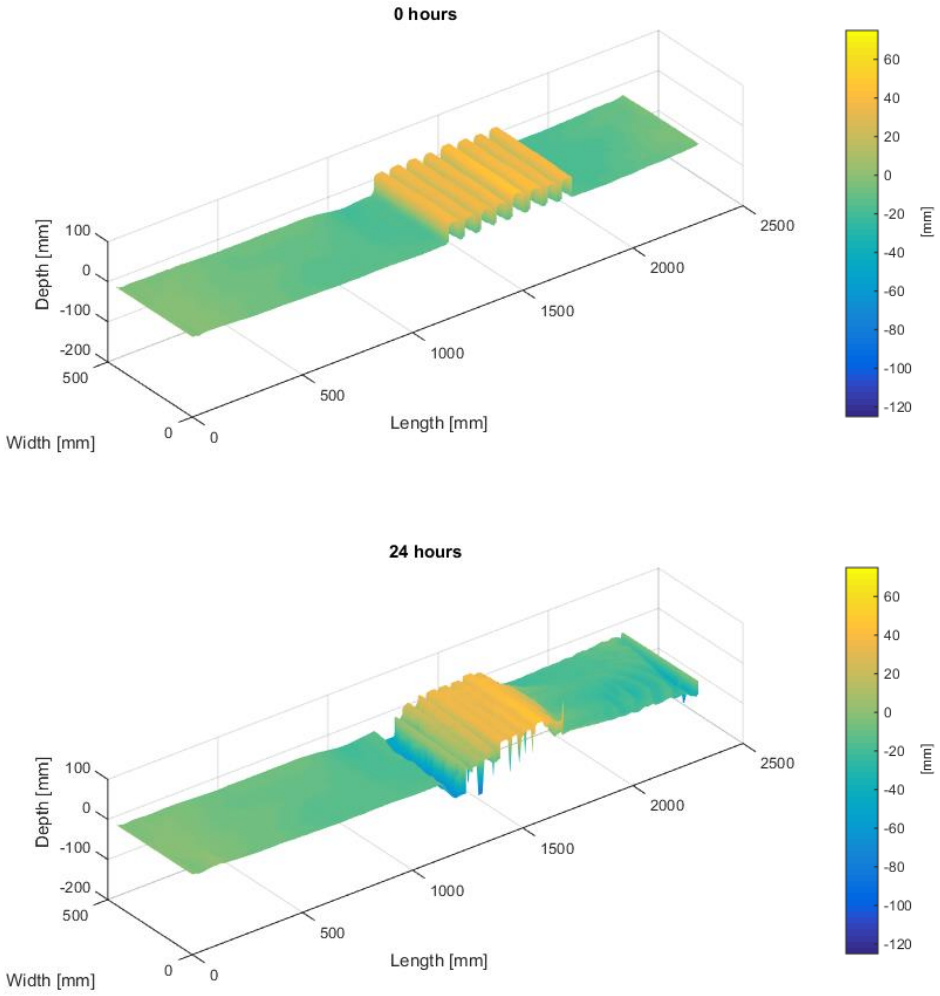

Figure 515; 0[h]-24[h] bed change projection

Table 123; Volume change per sector in [cm^3]

	Upstream	Contraction	Constriction	Expansion	Downstream
Volume	+2	-66	-1990	+63	-487

Velocity Profiles

Observably, the flow profiles do not seem to change much at all locations except for the negative velocity near the bed located at location 5. This has become positive, which can be explained through the accretion of the bed on the downstream face of the log layer no longer allowing the wake to fully develop.

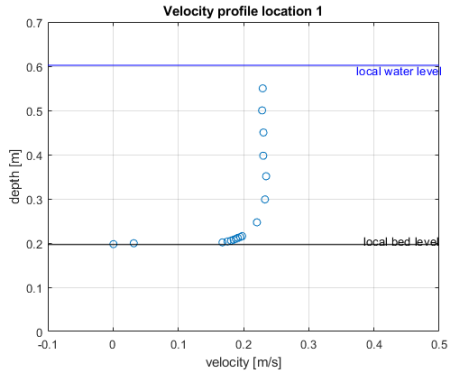

Figure 516; Velocity Profile location 1

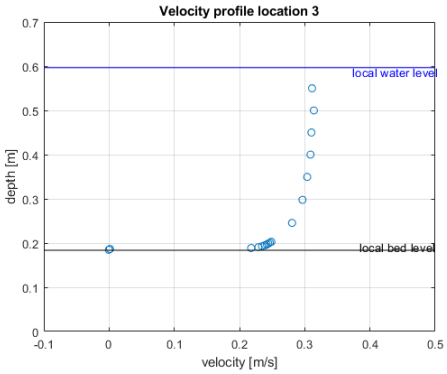

Figure 517; Velocity Profile location 3

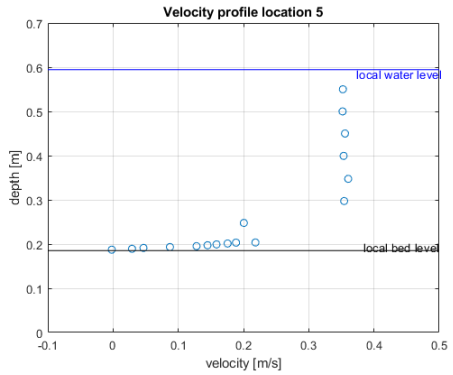

Figure 518; Velocity Profile location 5

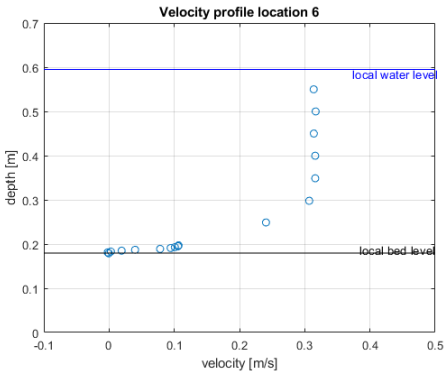

Figure 519; Velocity Profile location 6

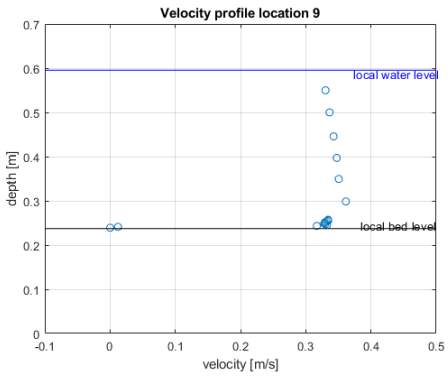

Figure 520; Velocity Profile location 9

Relative fluctuation intensity

Calculated fluctuation intensity shows that during flow contraction, in between location 1 & 2, this fluctuation drops slightly and hence stays of similar towards location 3. This is also observed in between locations 7 and 8. At locations 4 and 9 (measured above the logs) the relative fluctuation intensity becomes even smaller.

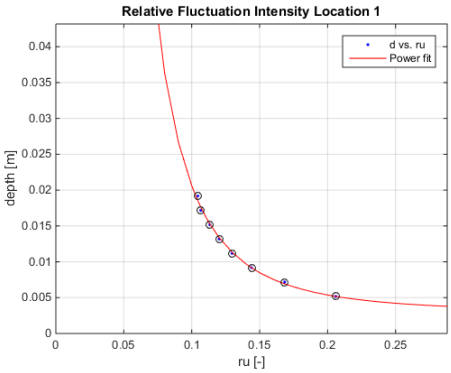

Figure 521; Relative fluctuation intensity location 1

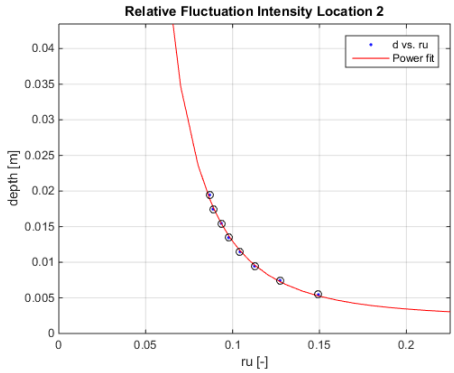

Figure 522; Relative fluctuation intensity location 2

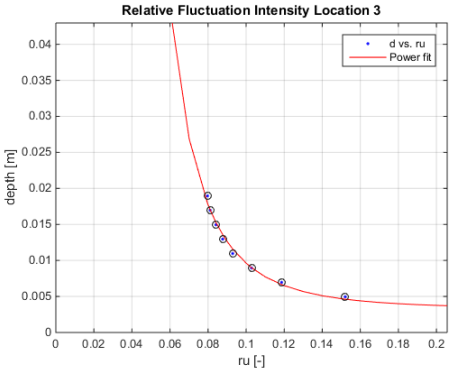

Figure 523; Relative fluctuation intensity location 3

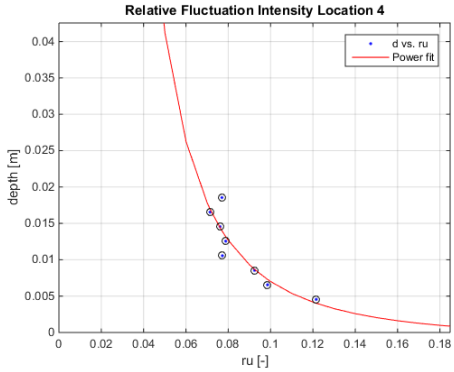

Figure 524; Relative fluctuation intensity location 4

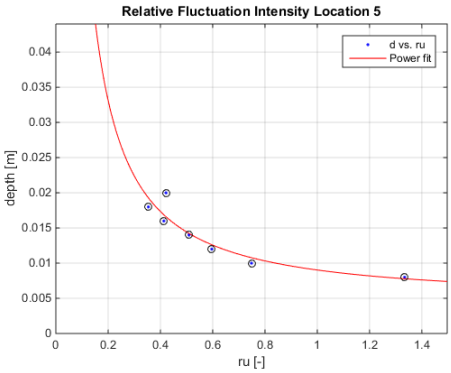

Figure 525; Relative fluctuation intensity location 5

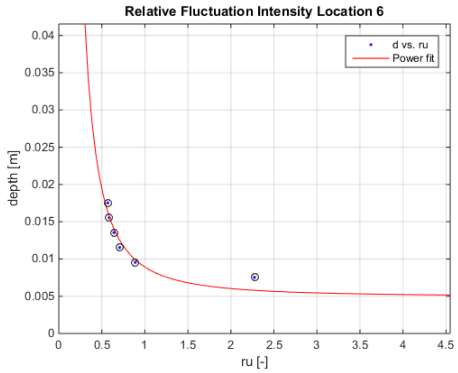

Figure 526; Relative fluctuation intensity location 6

At location 5 the relative fluctuation intensity increases, this location is however still within the wake of the logs, thus flow velocities are relatively small thus relatively the fluctuation intensity becomes larger. Location 10 also shows strong positive fluctuation intensity for the same reason. Location 6 is similar to location 5 and location 11 is similar to location 10.

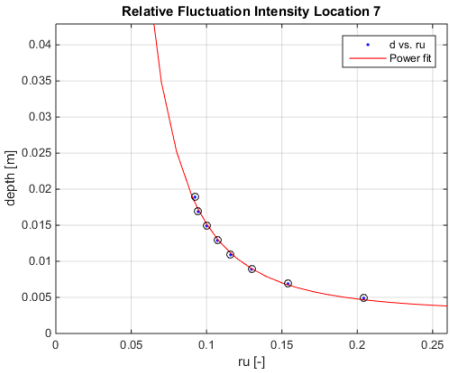

Figure 527; Relative fluctuation intensity location 7

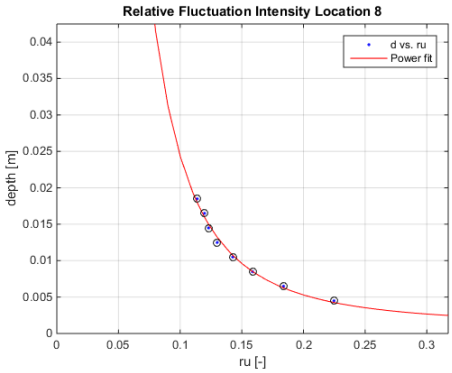

Figure 528; Relative fluctuation intensity location 8

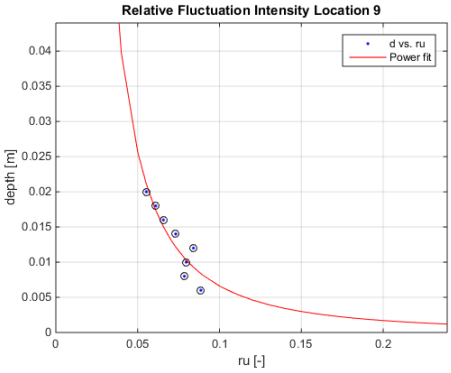

Figure 529; Relative fluctuation intensity location 9

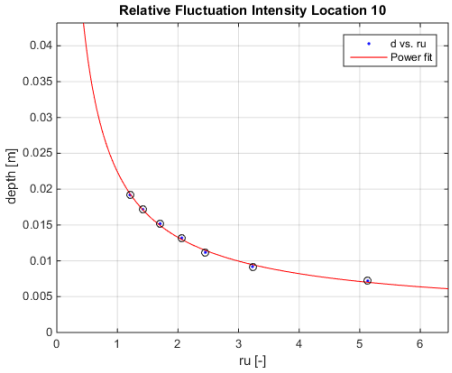

Figure 530; Relative fluctuation intensity location 10

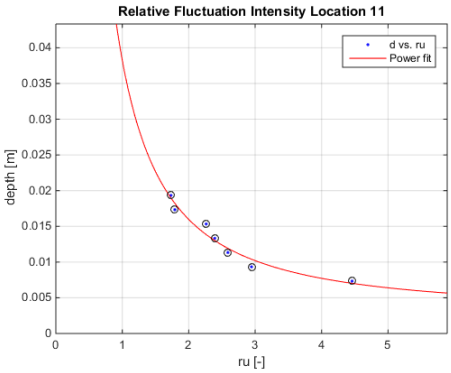

Figure 531; Relative fluctuation intensity location 11

Bed Shear stress

The bed shear stress was determined with Reynolds formula stated in (Schiereck & Verhagen, 2012). Bed shear stresses are determined by averaging the estimation for bed shear stress, over the centimeter measured above the bottom for a time frame of 3 minutes measuring at 50 [hz] per second, excluding all measured values that do not confirm with a signal to noise ratio above 15 and a correlation of 90%.

Bed shear stresses exceed values associated with high level of transport at locations 4,6,10 & 11. At all locations bed shear stresses were negative.

Table 124; Bed shear stresses [n/m^2]

Location	1	2	3	4	5	6	7	8	9	10	11
	-0,027	-0,051	-0,045	0,593	-0,443	-0,020	-0,037	-0,042	-0,100	-0,765	-0,144

Estimation of transport

Following the formulations of the bed load transport by van Rijn (van Rijn, 2018). The results are represented as such, that locations at the same longitudinal location are coupled and transport is averaged over these locations (Table 125) For the calculations the absolute value was taken of the measured bed shear stresses. The results are also depicted per sector (Table 126) by calculating the area underneath each cross-sectional measurement. The scour rates predict strong scour near the interface of the constriction and expansion sectors.

Table 125; Bed load transport [kg/m/s]

Location	1	2 & 7	3 & 8	4 & 9	5 & 10	6 & 11
	NaN	NaN	NaN	0,0039	0,021	NaN

Table 126; Bed load transport per sector [kg/day]

Sector	Upstream	Contraction	Constriction	Expansion	Downstream
	NaN	NaN	194,1	212,3	NaN

Water level

The water levels were measured at locations 1,3,5,6 they are depicted in Table 127. The levels were computed by measuring at 1000 [hz] for 15 seconds, and averaging those results. It is observed that the water level shows a drop of 0,7 [cm]. The water level seems to drop during constriction with 0,8 [cm], and then slightly increases again with 0,1 [cm].

Table 127; Water level [cm]

Location	1	3	5	6
	40,2952	39,7448	39,4323	39,5584

Measurements after 48h

Bed level

A projection of the bed after running for 48 [h] can be observed in Figure 532.The logs have apparently not moved significantly and only the scour near the downstream end has slightly increased in size. Furthermore it can be seen that sand has accreted directly downstream of the logs.

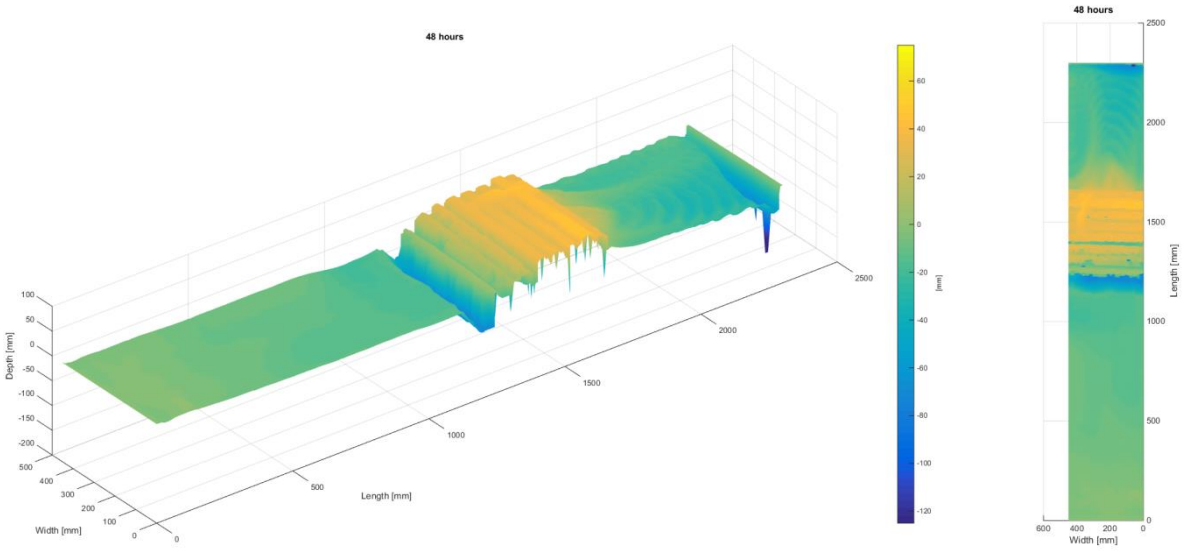

Figure 532; 48[h] bed projection

The average calculated transect observable in Figure 533, shows scour has penetrated up to 65 [mm] just in front of the logs. The bed upstream and within the contraction are not affected while the bed in the expansion seems erode near the outer edge of the transect while accreting behind the logs.

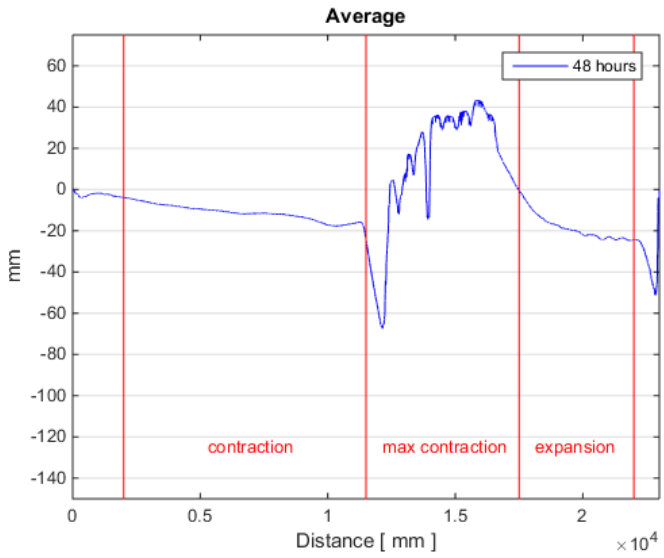

Figure 533; 48[h] average transect

Furthermore Figure 534 confirms that the placement of the logs perpendicular to the governing flow direction does seem to prevent acceleration of scour in the area of maximum contraction. The presence of scour near the downstream end was not observed in any other experiment, yet it is completely possible that this was until now not noticeable due to strong erosion and scour in the area of maximum contraction and downstream transport of this material.

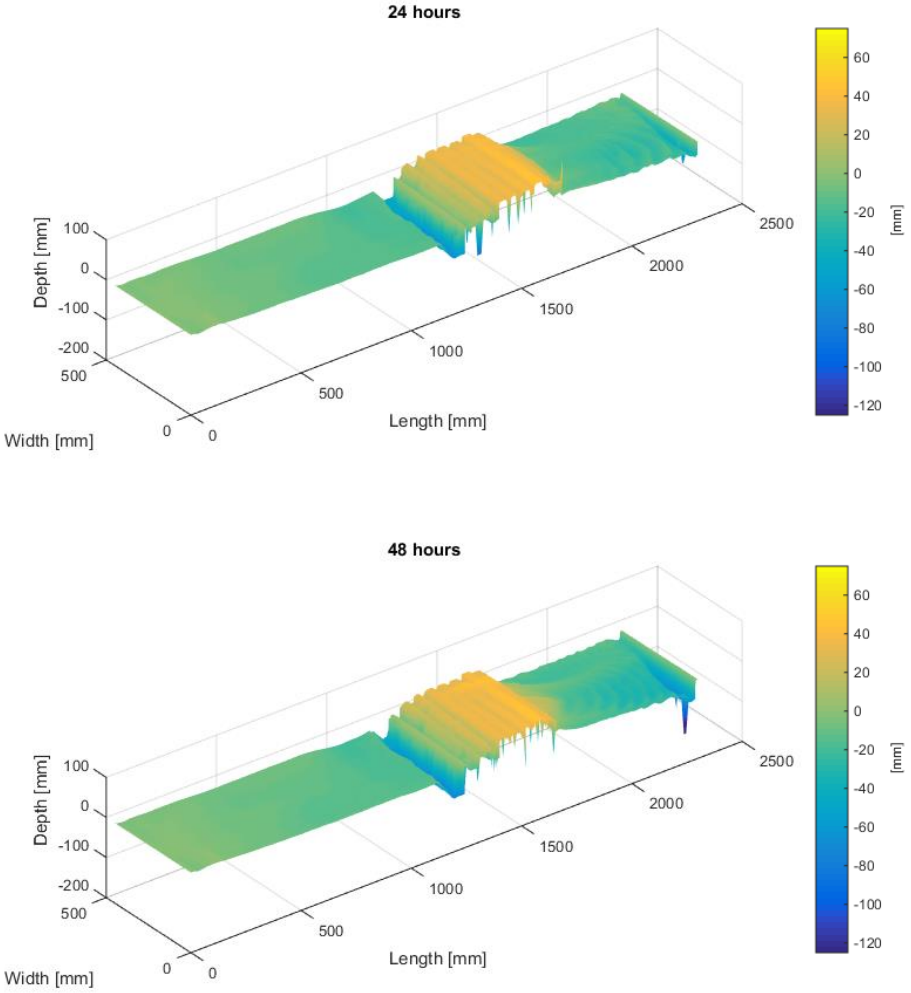

Figure 534; 24[h]-48[h] bed change projection

Table 128; Volume change per sector in [cm^3]

	Upstream	Contraction	Constriction	Expansion	Downstream
Volume	-8	-1	-169	-199	-514

Velocity Profiles

Observably, the flow profiles do not seem to change much at all locations. One should note that the flow near the bed at location 5 is close to zero and even negative very close to the bed. All other locations do not experience significant changes, which is in agreement with the bed not having conditions not having changed.

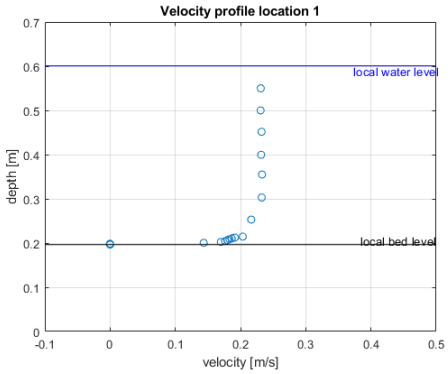

Figure 535; Velocity Profile location 1

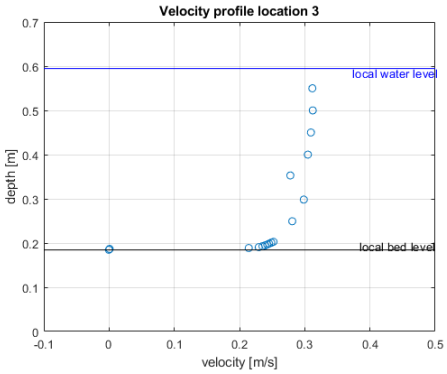

Figure 536; Velocity Profile location 3

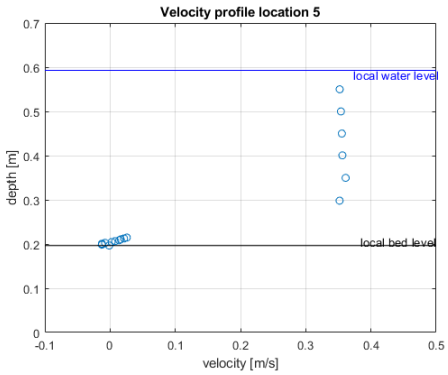

Figure 537; Velocity Profile location 5

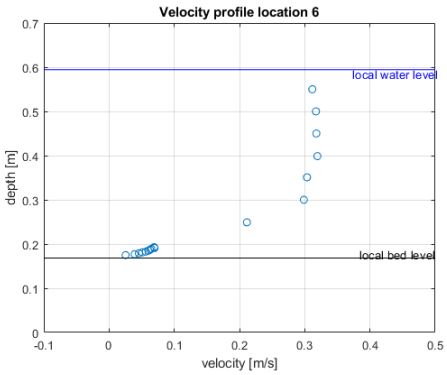

Figure 538; Velocity Profile location 6

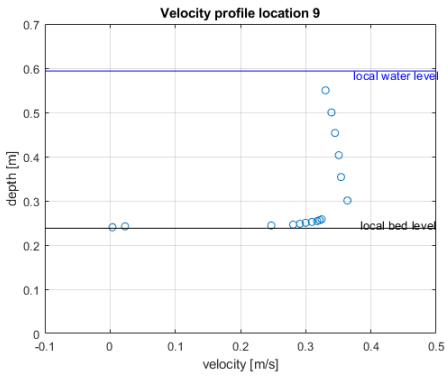

Figure 539; Velocity Profile location9

Relative fluctuation intensity

Fluctuation intensity does not vary much with respect to the measurements taken at 24 [h]. The intensity reduces from location 1 to 3 due to the contraction, and only slightly increases towards location 4 directly above the logs. This can also be observed between locations 7-8-9.

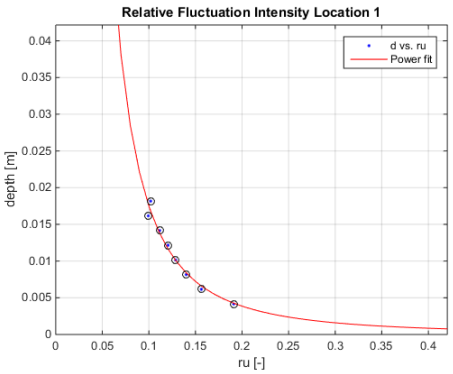

Figure 540; Relative fluctuation intensity location 1

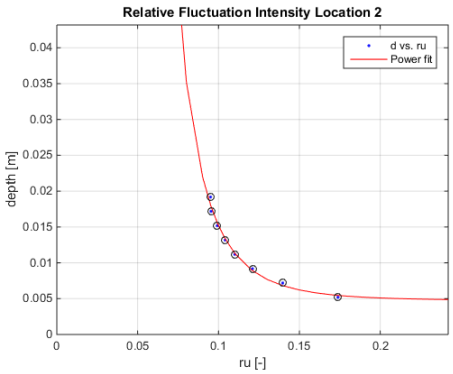

Figure 541; Relative fluctuation intensity location 2

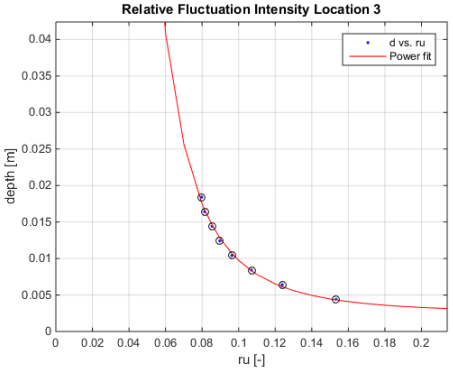

Figure 542; Relative fluctuation intensity location 3

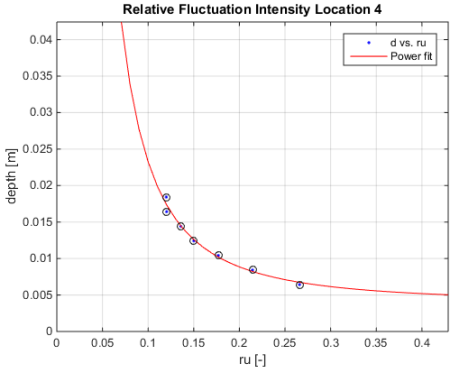

Figure 543; Relative fluctuation intensity location 4

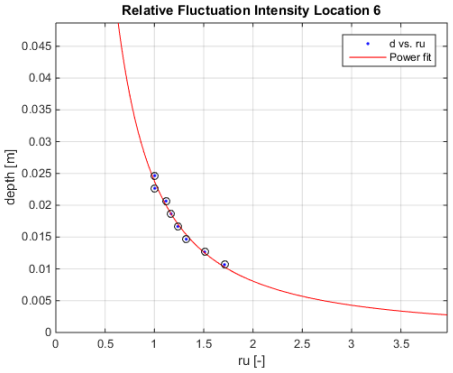

Figure 544; Relative fluctuation intensity location 6

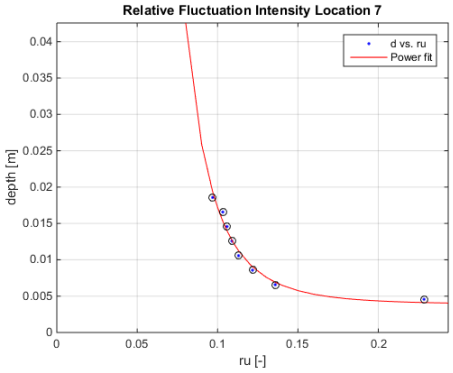

Figure 545; Relative fluctuation intensity location 7

For locations 5 no measurement was possible and at location 10 just behind the downstream face of the log layer very strong negative and very strong positive fluctuation intensities were computed, this was caused by flow velocities almost approaching zero. For locations 6-11 strong positive values were obtained. These measurements were now taken in well within the scouring hole formed on the downstream end, thus flow velocities were small and vortex formation therefor causes the velocity fluctuations therefor to dominate.

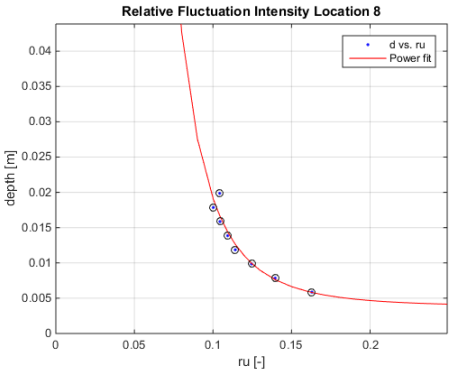

Figure 546; Relative fluctuation intensity location 8

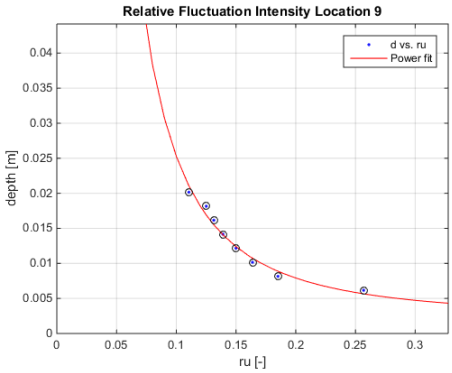

Figure 547; Relative fluctuation intensity location 9

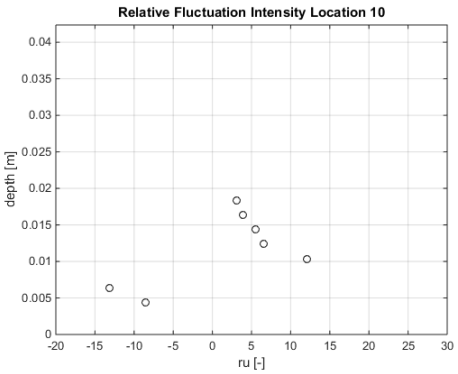

Figure 548; Relative fluctuation intensity location 10

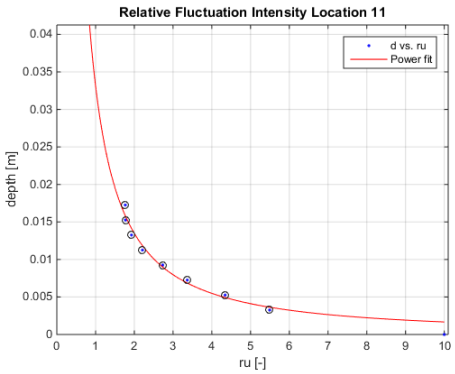

Figure 549; Relative fluctuation intensity location 11

Bed Shear stress

The bed shear stress was determined with Reynolds formula stated in (Schiereck & Verhagen, 2012). Bed shear stresses are determined by averaging the estimation for bed shear stress, over the centimeter measured above the bottom for a time frame of 3 minutes measuring at 50 [hz] per second, excluding all measured values that do not confirm with a signal to noise ratio above 15 and a correlation of 90%.

Bed shear stresses exceed values associated with high level of transport at locations 4,5,6,10 & 11. At location 7 this bed shear stress was observed to be positive.

Table 129; Bed shear stresses [n/m^2]

Location	1	2	3	4	5	6	7	8	9	10	11
	-0,019	-0,037	-0,050	-0,218	-0,192	-0,380	0,041	-0,059	-0,049	-0,192	-0,140

Estimation of transport

Following the formulations of the bed load transport by van Rijn (van Rijn, 2018). The results are represented as such, that locations at the same longitudinal location are coupled and transport is averaged over these locations (Table 130) For the calculations the absolute value was taken of the measured bed shear stresses. The results are also depicted per sector (Table 131) by calculating the area underneath each cross-sectional measurement. In this way it is expected that scour will again mainly occur downstream of the logs in the expansion and downstream sectors.

Table 130; Bed load transport [kg/m/s]

Location	1	2 & 7	3 & 8	4 & 9	5 & 10	6 & 11
	NaN	NaN	NaN	NaN	$8{,}42*10^{-5}$	0,0011

Table 131; Bed load transport per sector [kg/day]

Sector	Upstream	Contraction	Constriction	Expansion	Downstream
	NaN	NaN	0,6	11,6	4,9

Water level

The water levels were measured at locations 1,3,5,6 they are depicted in Table 132. The levels were computed by measuring at 1000 [hz] for 15 seconds, and averaging those results. It is observed that the water level shows a drop of 0,6 [cm]. The water level seems to drop during constriction with 0,8 [cm], and then slightly increases again with 0,2 [cm].

Table 132; Water level [cm]

Location	1	3	5	6
	40,0659	39,4595	39,2763	39,4443

Measurements after 72h

Bed level

A projection of the bed after running for 72[h] can be observed in Figure 550. The logs have again shown no significant movement. Downstream scour seems to have increased, which can be confirmed with the average transect.

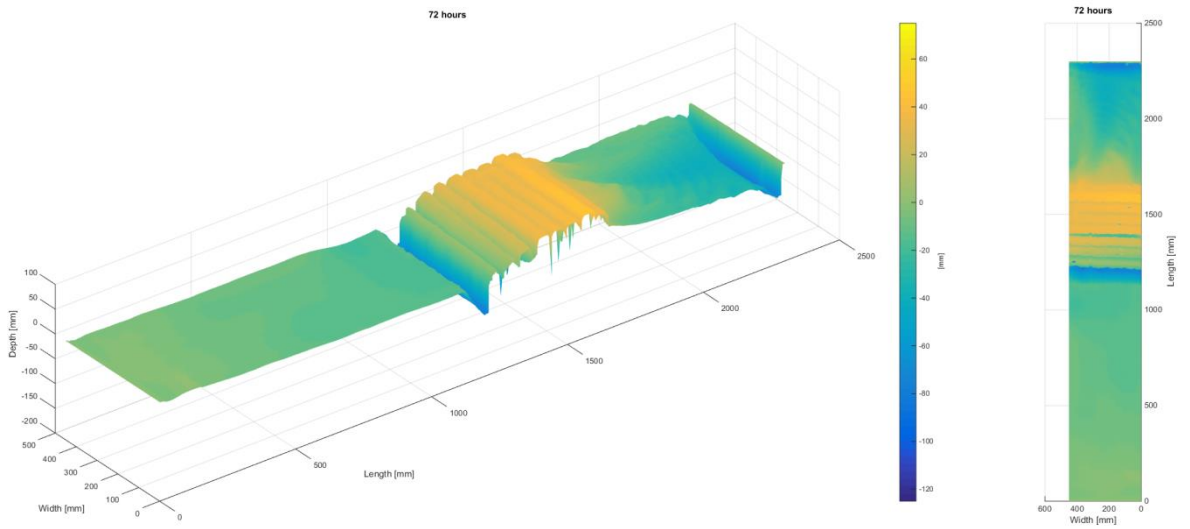

Figure 550; 72[h] bed projection

From the average transect (Figure 551) it can be observed that scour has reached approximately 70 [mm] in front of the log layer. The scour downstream has reached up to on average 65 [m]. The bed upstream still seems un-afflicted while the bed downstream of the logs shows accretion to the logs.

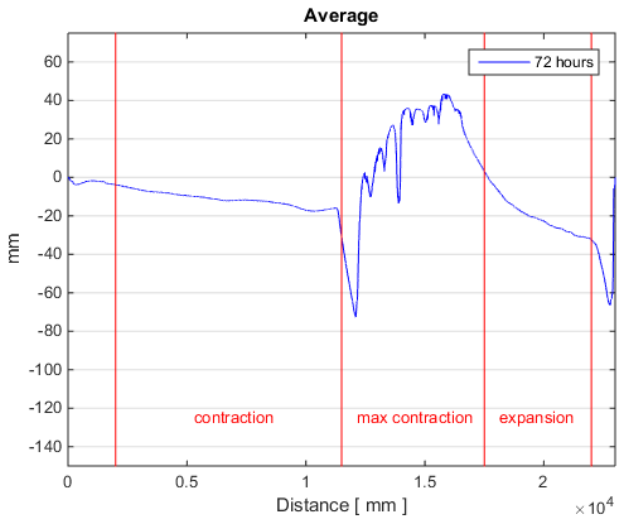

Figure 551; 72[h] average transect

Furthermore Figure 552 shows that compared with the measurement taken at 48 hours scour does not seem to have increased significantly, although a clear trench can be seen to have formed at the edge of the model. Other than that no observable changes can be distinguished.

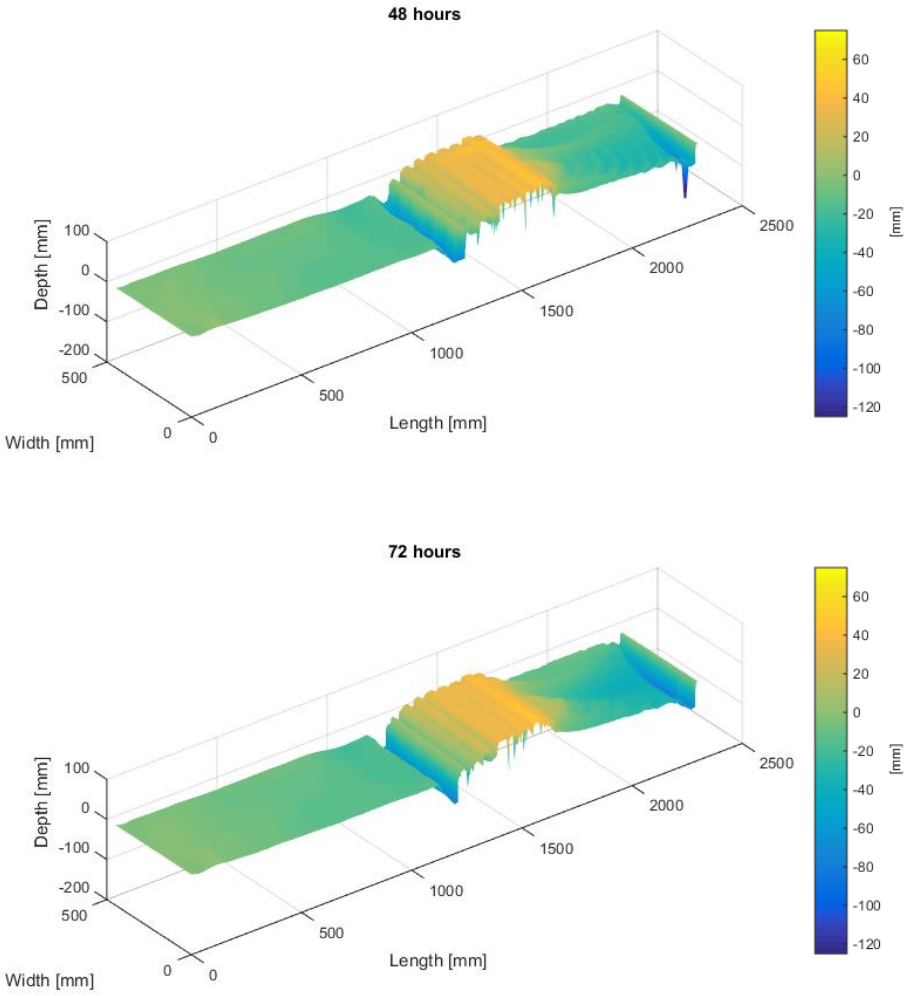

Figure 552; 48[h]-72[h] bed change projection

Table 133; Volume change per sector in [cm^3]

	Upstream	Contraction	Constriction	Expansion	Downstream
Volume	+7	-87	+215	-299	-596

Velocity Profiles

Observably, the flow profiles do not seem to change much at all locations although at location 6 it can now be seen that flow is nearly stagnant near the bottom, due the fact that this location is located within the scour hole at the downstream end of the flume, located near a hard barrier. Also the velocities near the bed at location 9 above the log layer have reduced slightly, but this is attributable to the geometry of the logs and the difficulty measuring at the exact same position as earlier.

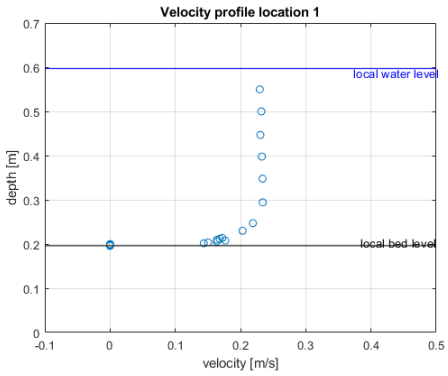

Figure 553; Velocity Profile location 1

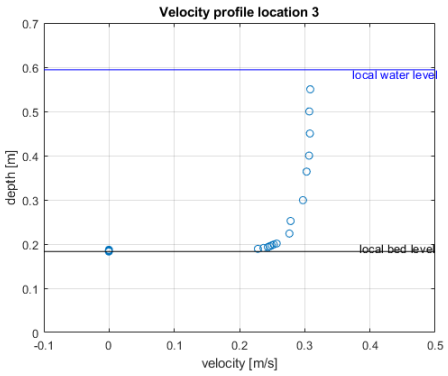

Figure 554; Velocity Profile location 3

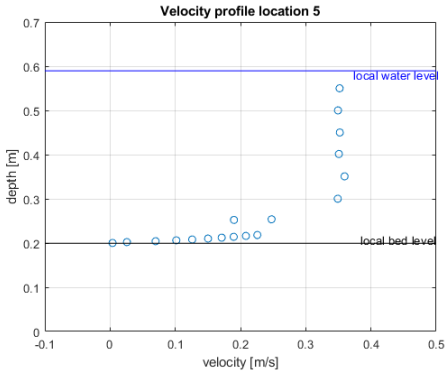

Figure 555; Velocity Profile location 5

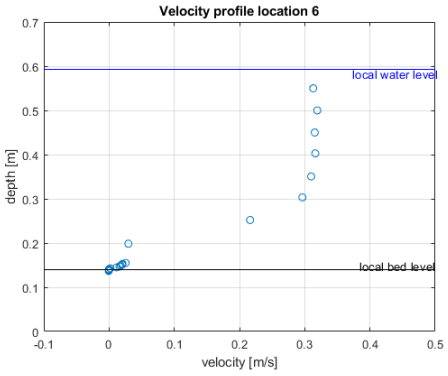

Figure 556; Velocity Profile location 6

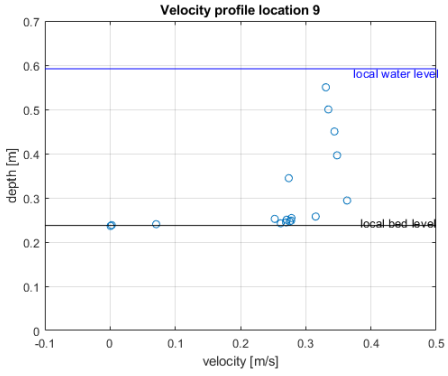

Figure 557; Velocity Profile location 9

Relative fluctuation intensity

The magnitude of relative fluctuation intensity again does not vary much with respect to the measurements taken at 48 [h]. The intensity reduces from location 1 to 3 due to the contraction, and only slightly increases towards location 4 directly above the logs. In between locations 7-8 it slightly increases and decreases again, directly above the log layer (Location 9).

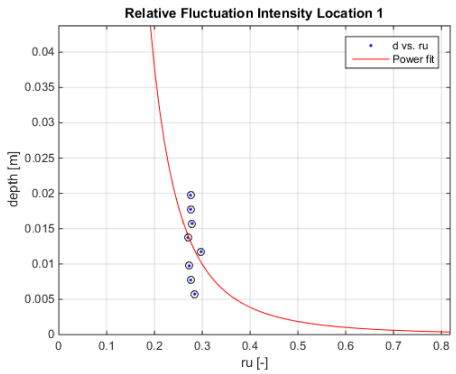

Figure 558; Relative fluctuation intensity location 1

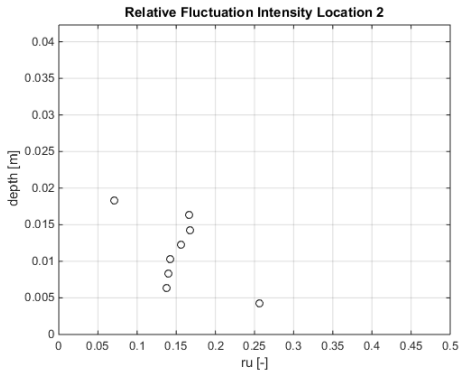

Figure 559; Relative fluctuation intensity location 2

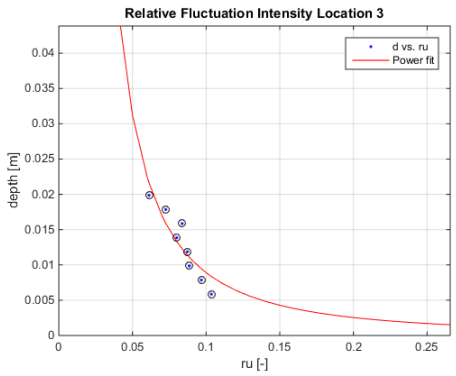

Figure 560; Relative fluctuation intensity location 3

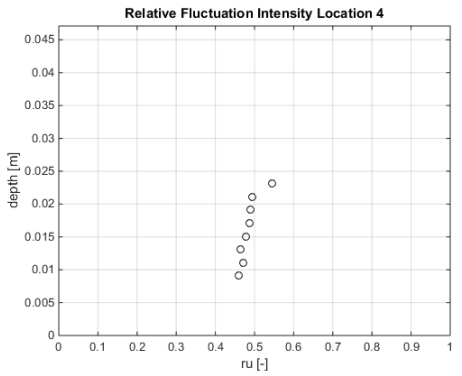

Figure 561; Relative fluctuation intensity location 4

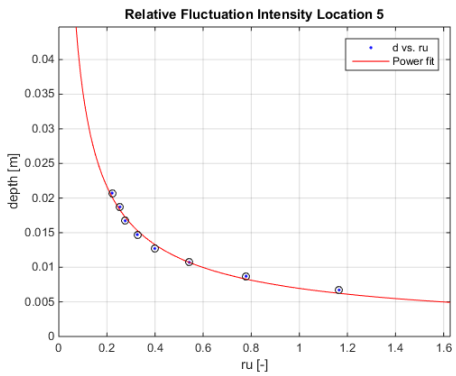

Figure 562; Relative fluctuation intensity location 5

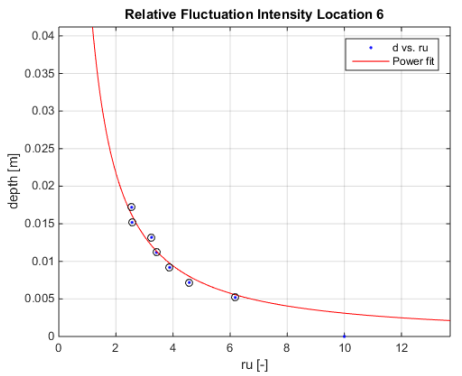

Figure 563; Relative fluctuation intensity location 6

Location 5 has moderate Relative fluctuation intensity while location 10 experiences heavy fluctuations, most likely caused by the logs still forming a wake with relative low average flow velocities behind it. For location 6 & 11 the same conclusion holds as stated earlier after 48 [h].

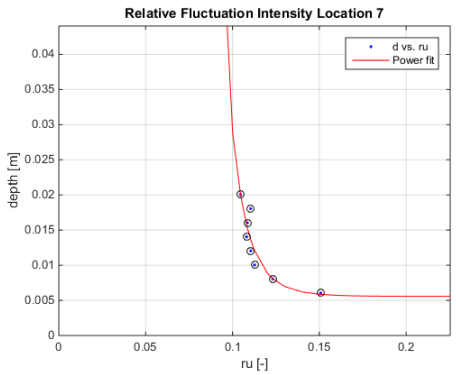

Figure 564; Relative fluctuation intensity location 7

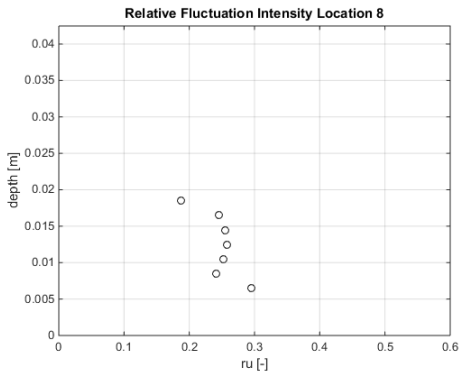

Figure 565; Relative fluctuation intensity location 8

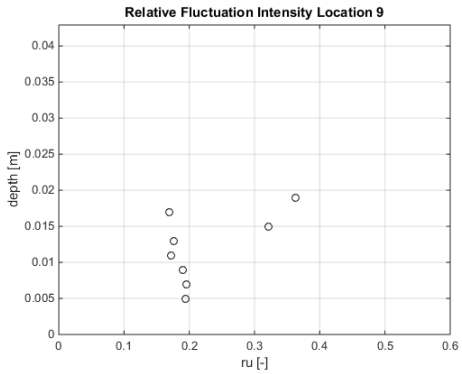

Figure 566; Relative fluctuation intensity location 9

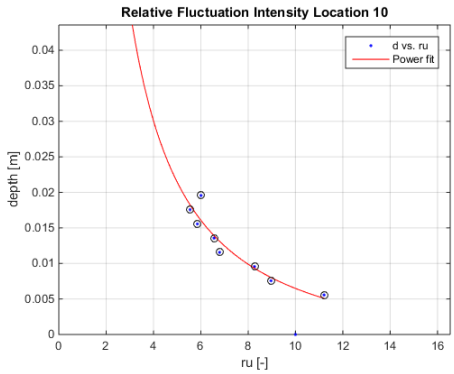

Figure 567; Relative fluctuation intensity location 10

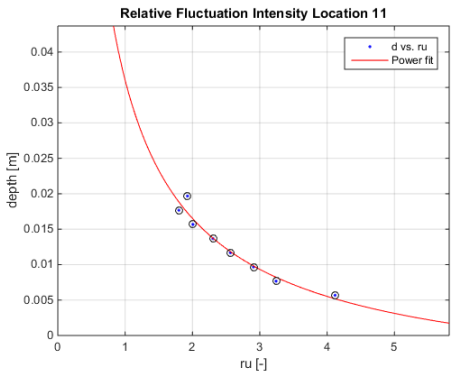

Figure 568; Relative fluctuation intensity location 11

Bed Shear stress

The bed shear stress was determined with Reynolds formula stated in (Schiereck & Verhagen, 2012). Bed shear stresses are determined by averaging the estimation for bed shear stress, over the centimeter measured above the bottom for a time frame of 3 minutes measuring at 50 [hz] per second, excluding all measured values that do not confirm with a signal to noise ratio above 15 and a correlation of 90%.

Bed shear stresses exceed values associated with high level of transport at locations 4,5, 9, 10 & 11. At all locations bed shear stresses were negative.

Table 134; Bed shear stresses [n/m^2]

Location	1	2	3	4	5	6	7	8	9	10	11
	-0,048	-0,011	-0,036	-0,299	-0,342	-0,086	-0,015	0,011	0,256	-0,403	-0,101

Estimation of transport

Following the formulations of the bed load transport by van Rijn (van Rijn, 2018). The results are represented as such, that locations at the same longitudinal location are coupled and transport is averaged over these locations (Table 135). For the calculations the absolute value was taken of the measured bed shear stresses. The results are also depicted per sector (Table 136) by calculating the area underneath each cross-sectional measurement. In this way it is expected that scour will accelerate in the constriction and expansion sectors.

Table 135; Bed load transport [kg/m/s]

Location	1	2 & 7	3 & 8	4 & 9	5 & 10	6 & 11
	NaN	NaN	NaN	0,0015	0,005	NaN

Table 136; Bed load transport per sector [kg/day]

Sector	Upstream	Contraction	Constriction	Expansion	Downstream
	NaN	NaN	54,3	51,2	NaN

Water level

The water levels were measured at locations 1,3,5,6 they are depicted in Table 137. The levels were computed by measuring at 1000 [hz] for 15 seconds, and averaging those results. It is observed that the water level shows a drop of 0,4 [cm]. The water level seems to drop during constriction with 0,7 [cm], and then slightly increases again with 0,3 [cm].

Table 137; Water level [cm]

Location	1	3	5	6
	39,6594	39,4012	38,9478	39,2766

Measurements after 96h

Bed level

A projection of the bed after running for 96[h] can be observed in Figure 569. The logs don't seem to have moved any further. Beside the downstream scour having increased ever so slightly no other significant observations can be made.

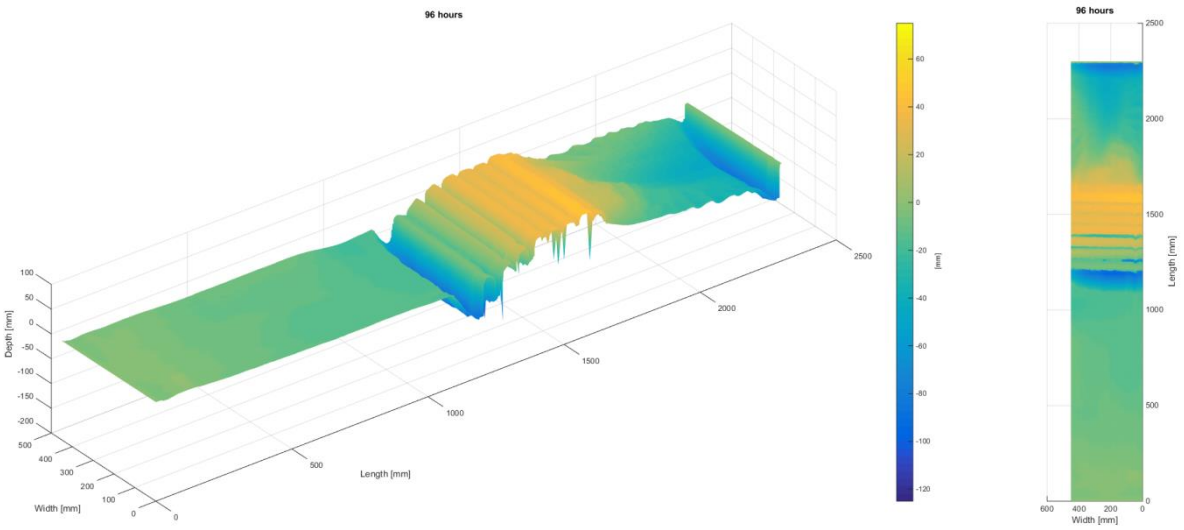

Figure 569; Bed map after 96 [h]

Comparing the average transect with the average transect taken at 0 [h], it can clearly be seen that the bed in the contraction is almost completely unaffected. Furthermore the logs have retained there postion and even caused accretion on their downstream face. Also a significant scour hole has developed further downstream of the logs (see Figure 570).

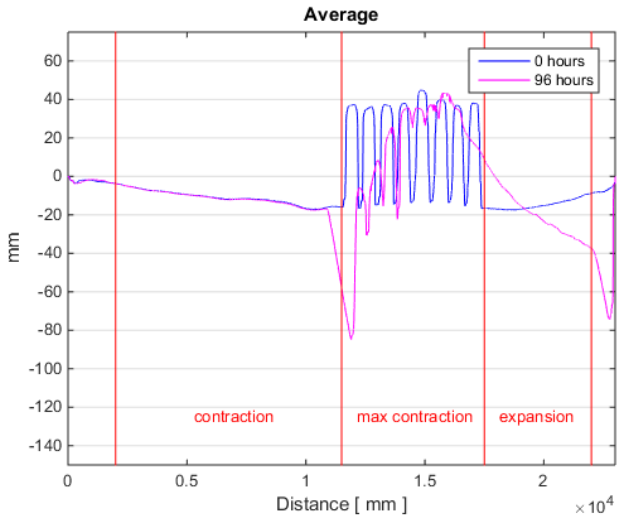

Figure 570; Average transects through time

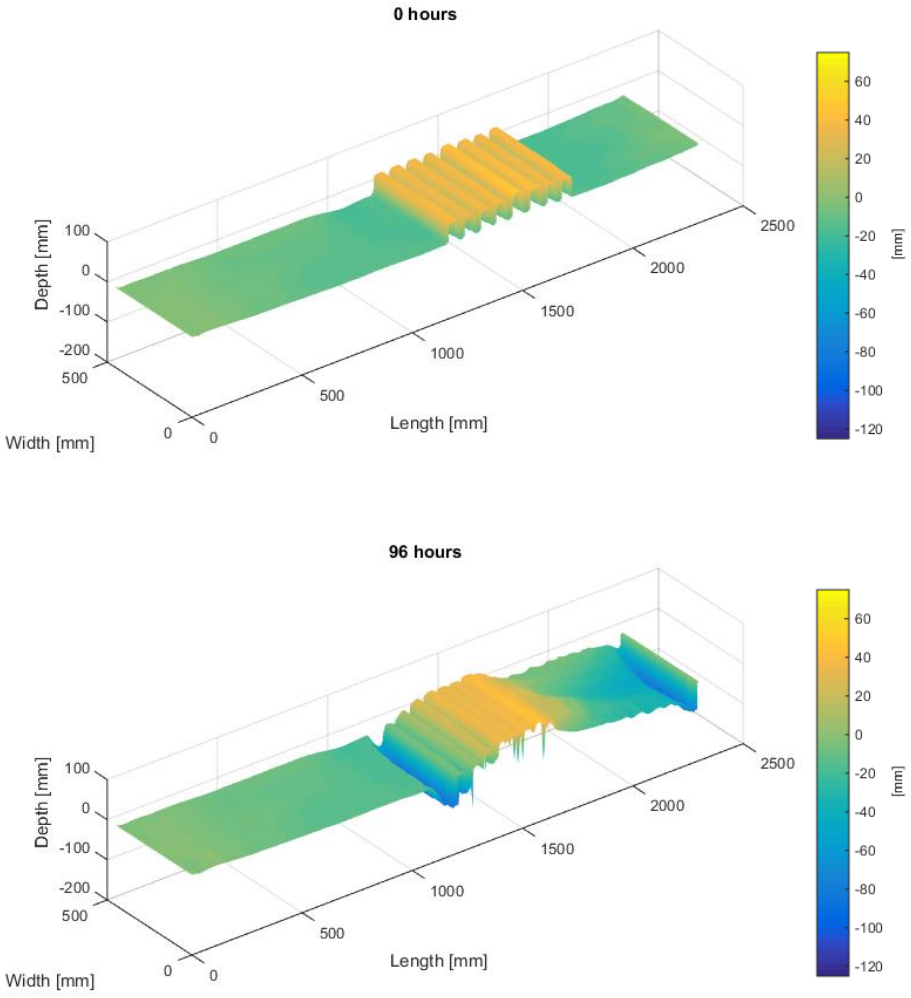

Figure 571; Bed change with respect to 0[h]

Table 138; Volume change per sector in [cm^3]

	Upstream	Contraction	Constriction	Expansion	Downstream
Volume	+6	-513	-504	146	-310

Concluding Remarks

This first protected scour B experiment has shown some promising results. At the point of highest flow velocities, located above the logs, scour has significantly reduced with respect to the basic scour experiments. Other than that the logs have shown typical pipeline scour patterns, creating a small trench in front of the first log causing it to roll in and activate the logs behind it. This effect was anticipated. The scour formation downstream of the logs was not expected, and it has yet to be determined if this particular phenomenon occurs because of the logs, or due to the design of the laboratory model.

Appendix E II

I Introduction

The protected Scour experiments are considered to be the baseline experiments for the application of wooden logs as a scour protection. The “Protected Scour B” experiments feature a flow perpendicular placed single layer of logs directly on top of the bed, in the area of maximum contraction. Similar to the basic scour experiments bed, velocity and fluctuation intensity development is measured during a 96 [h] run. This report includes all measured findings during this particular experiment. Conclusions are drawn in the main report on the basis of multiple similarly conducted experiments. A short preliminary conclusion is however included at the end of this report.

Summary

Table 139 represents relevant scour quantities after 96 [h]. Note that the absolute is measured relative to the measurement of the bed at 0 [h], excluding the maximum scour depth which is measured to a reference bed with a 0 [mm] elevation. Measurements of scour volume in the column with respect to reference include missing volume with respect to a reference be of 0 [mm] and corrected for the presence of logs .

Table 139; Summary of quantities (Negative values indicate scour, positive indicate accretion)

	Quantity	With respect to reference
Maximum Scour Depth [mm]	127	127
Total Scoured volume [cm^3]	-19885	-26414
Scoured volume Upstream-sector [cm^3]	-17	-292
Scoured volume Contracting-sector [cm^3]	-3446	-7372
Scoured volume Constricted-sector [cm^3]	-8027	-8754
Scoured volume Expanding-sector [cm^3]	-4282	-5705
Scoured volume Downstream-sector [cm^3]	-4113	-4292

Measurements at 0h

Bed level

A projection of the bed at the moment of initiation of flow during the first scour experiment can be seen in Figure 572. Clearly observable are the placed logs on the bed. They are roughly located in between 1200-1700 [mm] from the entry point of flow, and are placed without spacing to prevent the logs from rolling.

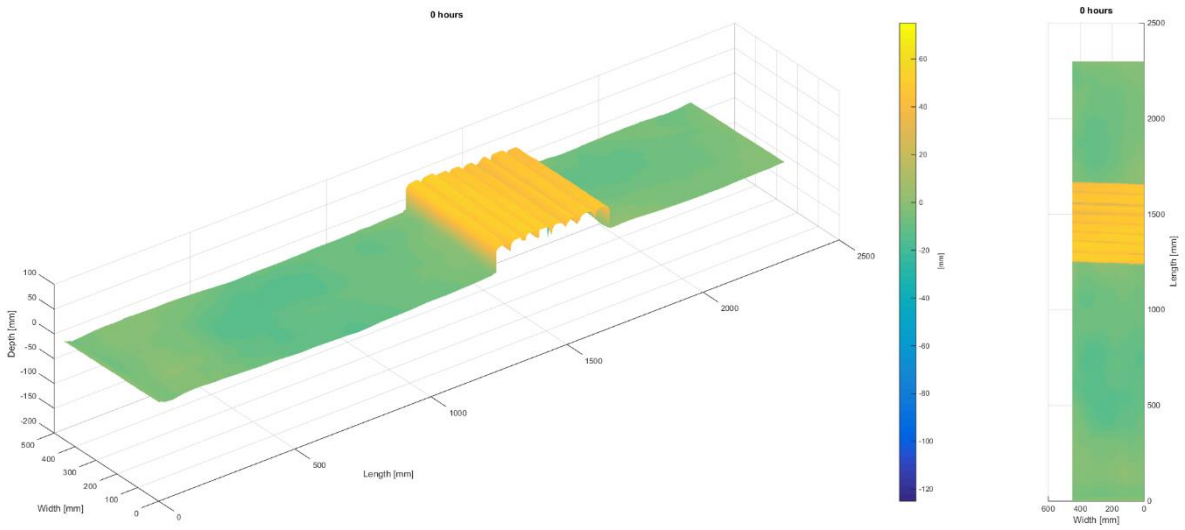

Figure 572; Bed map 0[h]

The average transect, observable in Figure 573, was calculated from the 31 transects taken over the entire length of the laboratory set-up. As can be seen, the bed is slightly below the target value of 0 [mm] with about 15 [mm] halfway contraction. Also observable is a small indenture at the upstream entry point of about 7 [mm].

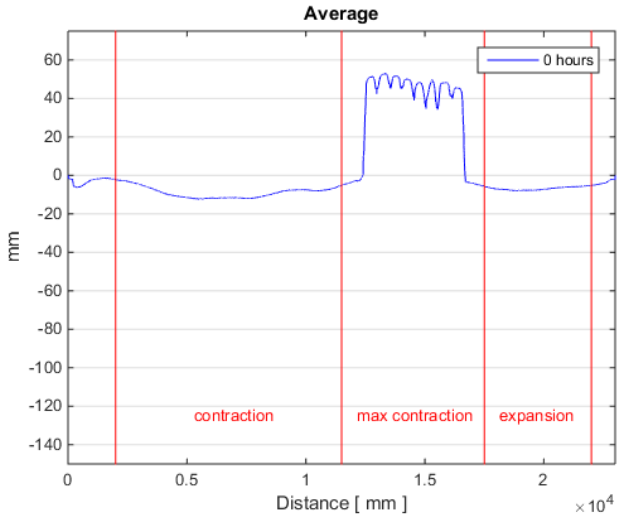

Figure 573; 0 [h] average transect

Velocity Profiles

In this section, individual flow profiles of locations marked above are shown. It can be observed that upon arrival the flow profile shows the characteristic profile for turbulent flow (location 1). At location 3 the flow has accelerated significantly, while close to the bottom flow is accelerated only slightly, thereby skewing the flow profile. The flow velocity at location 5 increases even further higher up the water column, but reduces to zero/near zero in the wake of the logs. At location 6 it can be observed that the flow profile is attempting to redistribute to the original flow profile (location 1) but has yet been successful at obtaining this distribution and thus flow velocities are much higher, higher up the water column. The flow profile at location 9 above the logs shows an intensification of flow about 10 [cm] above the logs.

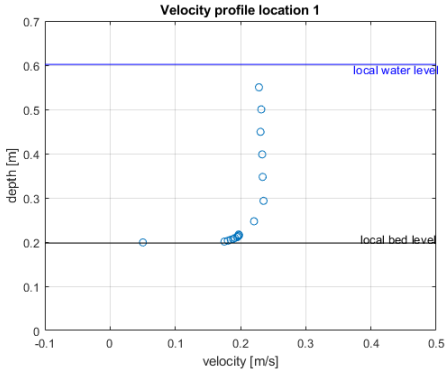

Figure 574; Velocity Profile location 1

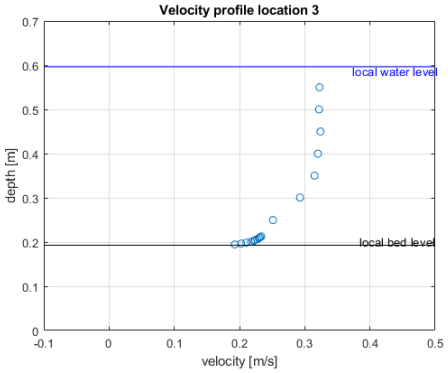

Figure 575; Velocity Profile location 3

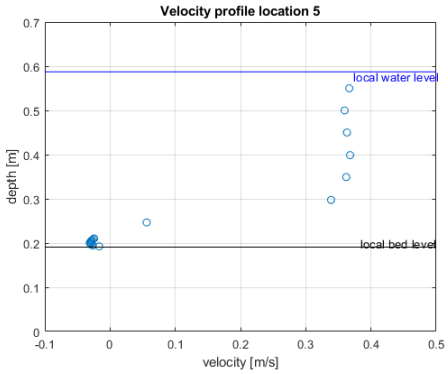

Figure 576; Velocity Profile location 5

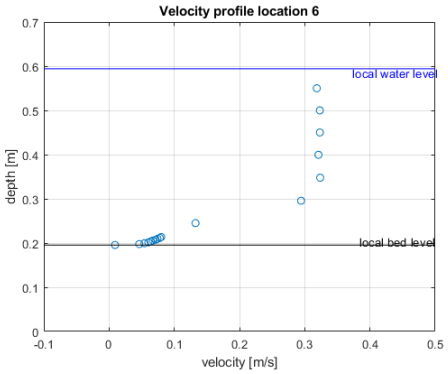

Figure 577; Velocity Profile location 6

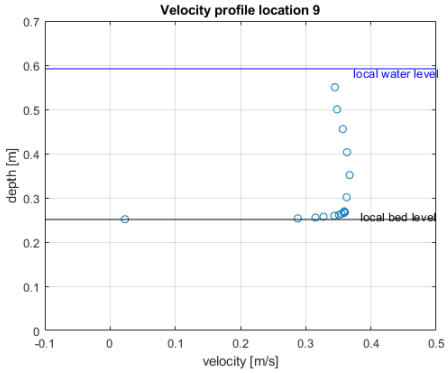

Figure 578; Velocity Profile location 9

Relative fluctuation intensity

It is shown that fluctuation intensity reduces slightly during flow contraction, in between location 1-2-3, this is not the case for measurement between location 7-8, which shows no reduction. At locations 4 and 9 (measured above the logs) the relative fluctuation intensity remains small but does retain a traditional shape. Wherever possible, curve fitting has been applied. Location 5 & 10 both show negative fluctuation intensity, indication of flow upstream. The magnitude of the relative fluctuation intensity is high at both locations, but this is explained through average flow velocities being rather small. Lastly, near location 6 & 11 the relative fluctuation intensity is yet again positive but still very high with respect to normal flow.

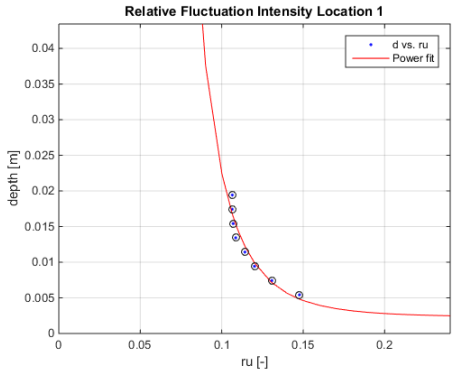

Figure 579; Relative fluctuation intensity location 1

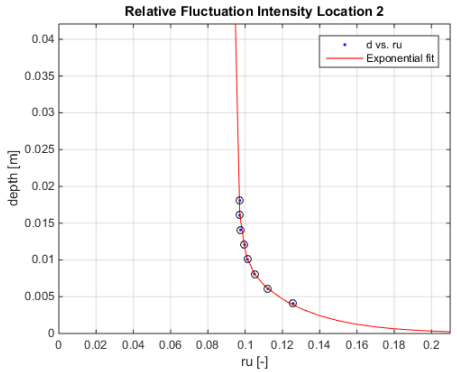

Figure 580; Relative fluctuation intensity location 2

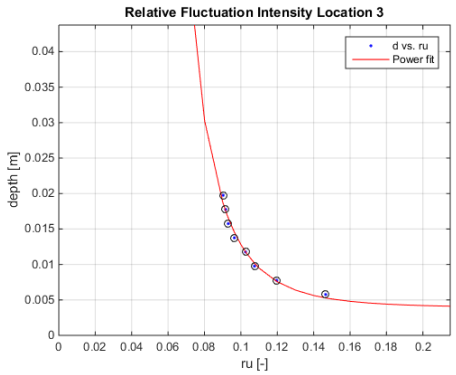

Figure 581; Relative fluctuation intensity location 3

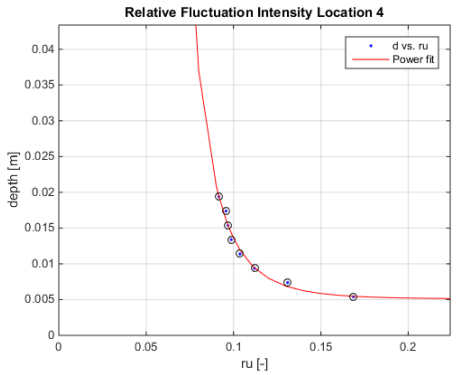

Figure 582; Relative fluctuation intensity location 4

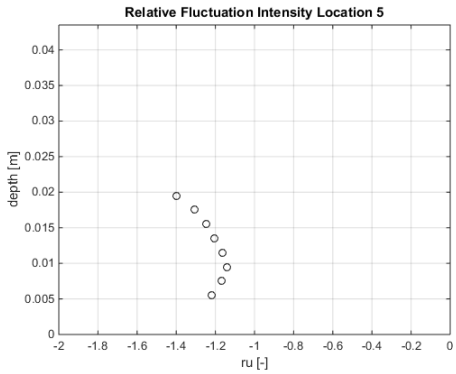

Figure 583; Relative fluctuation intensity location 5

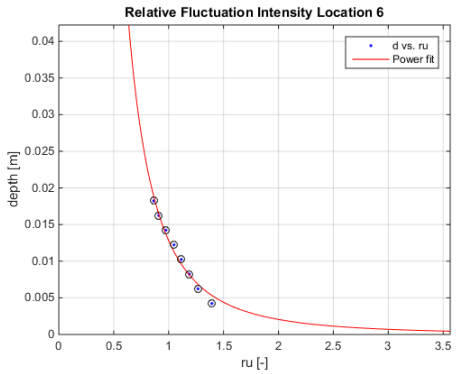

Figure 584; Relative fluctuation intensity location 6

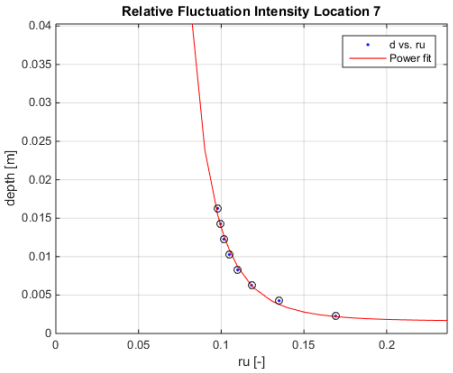

Figure 585; Relative fluctuation intensity location 7

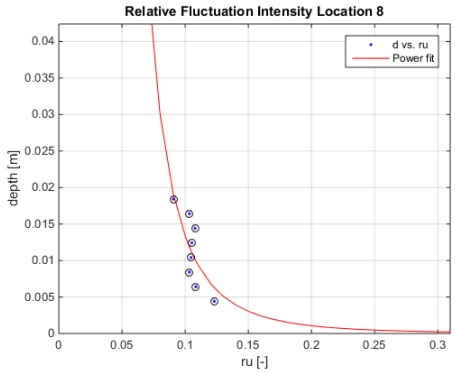

Figure 586; Relative fluctuation intensity location 8

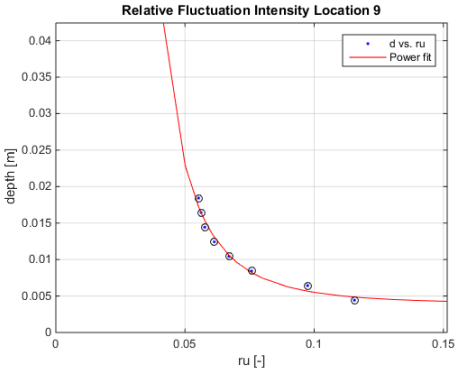

Figure 587; Relative fluctuation intensity location 9

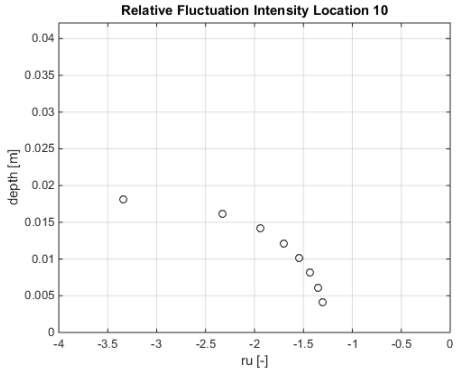

Figure 588; Relative fluctuation intensity location 10

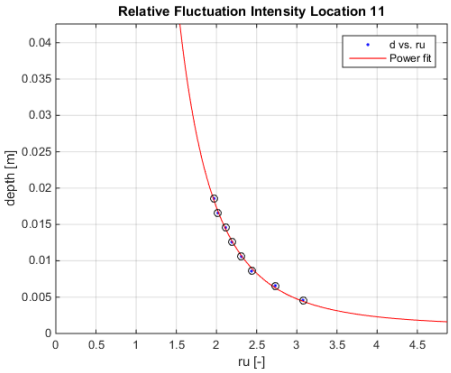

Figure 589; Relative fluctuation intensity location 11

Bed Shear stress

The bed shear stress was determined with Reynolds formula stated in (Schiereck & Verhagen, 2012). Bed shear stresses are determined by averaging the estimation for bed shear stress, over the centimeter measured above the bottom for a time frame of 3 minutes measuring at 50 [hz] per second, excluding all measured values that do not confirm with a signal to noise ratio above 15 and a correlation of 90%.

Bed shear stresses exceed values associated with high level of transport at locations 4,6,9, & 11. At all locations bed shear stresses were negative.

Table 140; Bed shear stresses [n/m^2]

Location	1	2	3	4	5	6	7	8	9	10	11
	-0,053	-0,065	-0,077	-0,288	-0,040	-0,203	-0,062	-0,035	-0,122	-0,142	-0,171

Estimation of transport

Following the formulations of the bed load transport by van Rijn (van Rijn, 2018). The results are represented as such, that locations at the same longitudinal location are coupled and transport is averaged over these locations (Table 141) For the calculations the absolute value was taken of the measured bed shear stresses. The results are also depicted per sector (Table 142) by calculating the area underneath each cross-sectional measurement. In this way it is expected that scour rates will be low throughout the set-up.

Table 141; Bed load transport [kg/m/s]

Location	1	2 & 7	3 & 8	4 & 9	5 & 10	6 & 11
	NaN	NaN	NaN	0,0002	NaN	$5{,}70*10^{-5}$

Table 142; Bed load transport per sector [kg/day]

Sector	Upstream	Contraction	Constriction	Expansion	Downstream
	NaN	NaN	2,7	0,6	0,3

Water level

The water levels were measured at locations 1,3,5,6 they are depicted in Table 143. The levels were computed by measuring at 1000 [hz] for 15 seconds, and averaging those results. It is observed that the water level shows a drop of 0,8 [cm]. The water level seems to drop during constriction with 1,5 [cm], and then increases again with 0,7 [cm].

Table 143; Water level [cm]

Location	1	3	5	6
	40,1816	39,6212	38,7315	39,4001

Measurements after 24h

Bed level

A projection of the bed after running for 24 [h] can be observed in Figure 590. The bed shows to have developed both a small and narrow scour hole upstream of the log carpet as well as a scour hole upstream of the exit point of the model. It can be seen that the most upstream located logs have rolled into the upstream located scour hole while the logs located in the center have somewhat unexpectedly tilted towards one side.

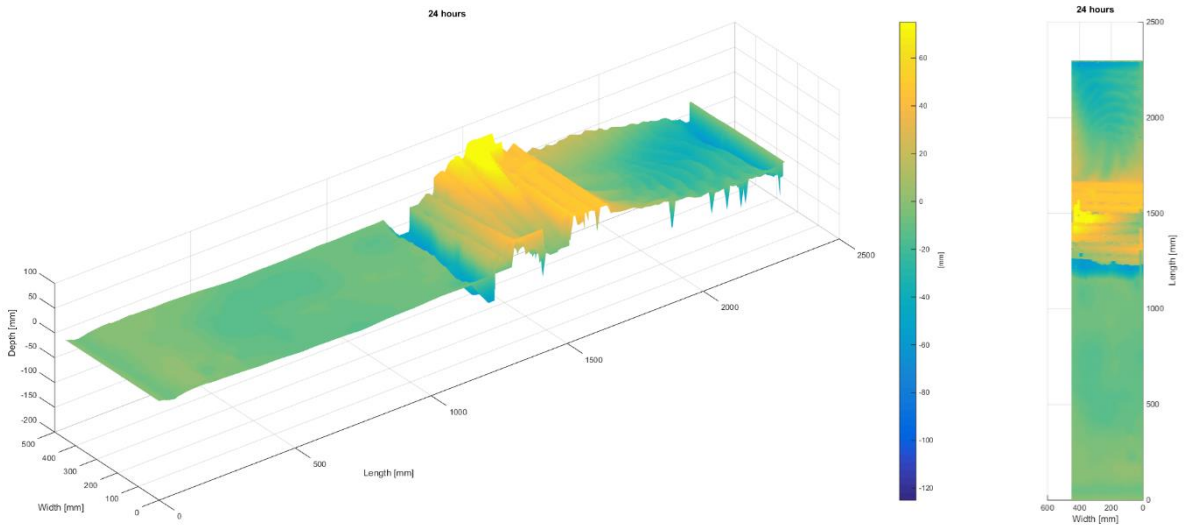

Figure 590; 24[h] bed projection

It can be seen in clearly seen in Figure 591 that two scour holes have developed. Both of these scour holes are approximately 50 [mm] deep. On average only the upstream logs have clearly moved into the scour hole while the others stay relatively at the same level, even though they may have tilted.

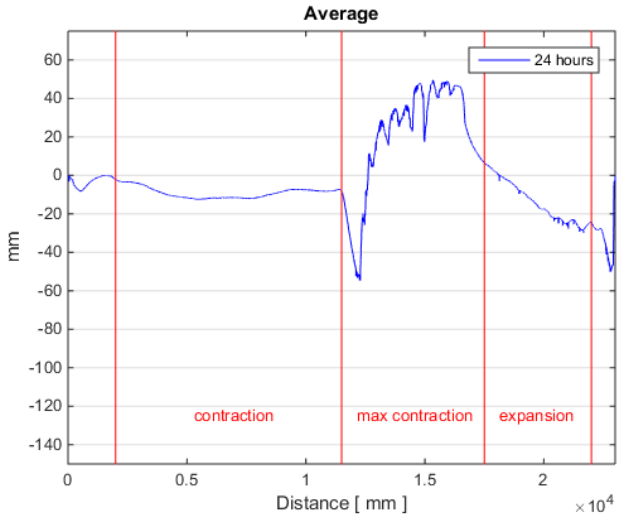

Figure 591; 24[h] average transect

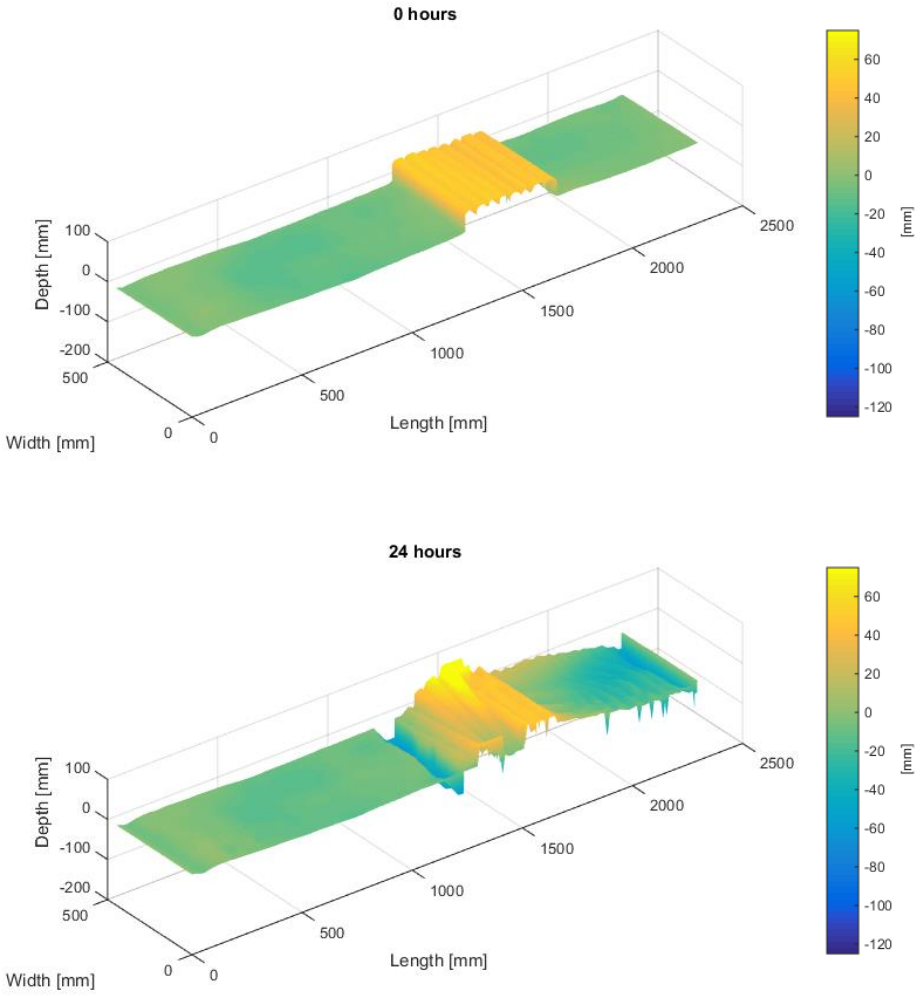

Figure 592; 0[h]-24[h] bed change projection

Table 144; Volume change per sector in [cm^3]

	Upstream	Contraction	Constriction	Expansion	Downstream
Volume	+2	-64	-3200	-1427	-1325

Velocity Profiles

In this section, individual flow profiles of locations marked above are shown. It can be observed that upon arrival the flow profile shows the characteristic profile for turbulent flow (location 1). At location 3 the flow has accelerated significantly, while close to the bottom flow is accelerated only slightly, thereby skewing the flow profile. The flow velocity at location 5 increases even further higher up the water column, but reduces to zero/near zero in the wake of the logs. At location 6 it can be observed that the flow profile is attempting to redistribute to the original flow profile (location 1) but has yet been successful at obtaining this distribution and thus flow velocities are much higher, higher up the water column. The flow profile at location 9 shows a strong disturbance near the bed, caused by this location being located in between logs.

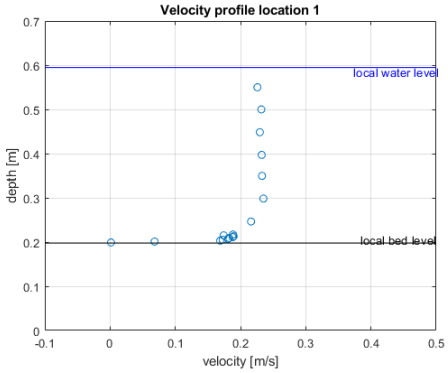

Figure 593; Velocity Profile location 1

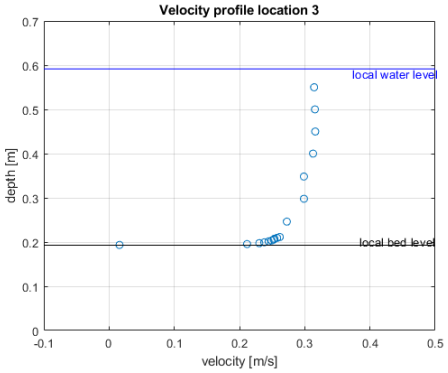

Figure 594; Velocity Profile location 3

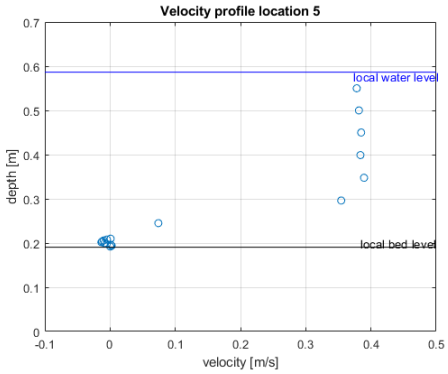

Figure 595; Velocity Profile location 5

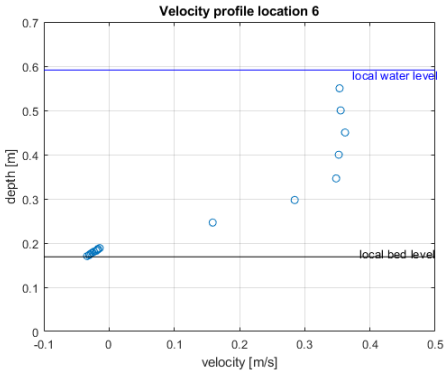

Figure 596; Velocity Profile location 6

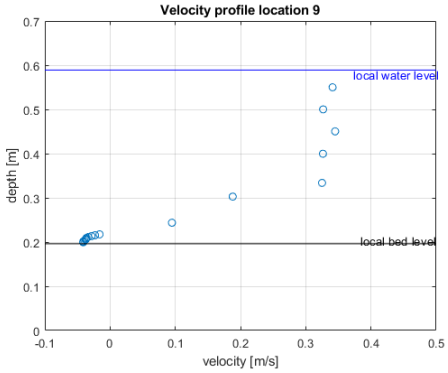

Figure 597; Velocity Profile location 9

Relative fluctuation intensity

It is shown that fluctuation intensity reduces slightly during flow contraction, in between location 1-2-3 and stays approximately the same between locations 7-8. At location 4 traditional values are observed while at location 9 negative values are measured. This is caused by the tilted logs. Locations 5 & 6 show large and negative RFI, indicative of upstream directed velocities. Location 10 shows larger than average positive values and location 11 shows a more traditional magnitude of RFI.

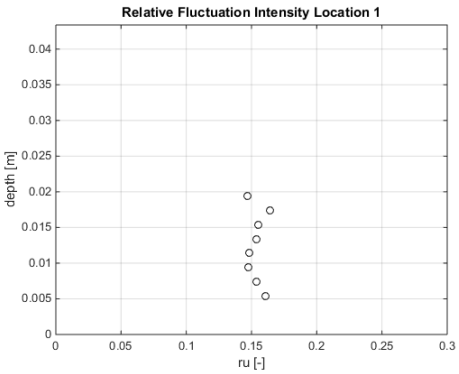

Figure 598; Relative fluctuation intensity location 1

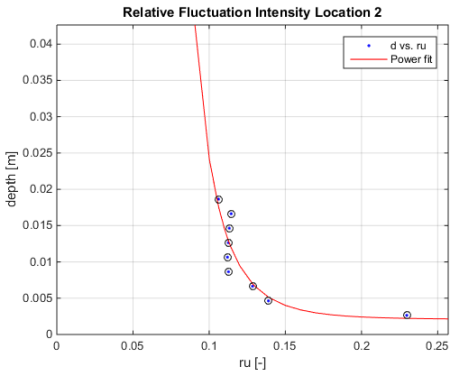

Figure 599; Relative fluctuation intensity location 2

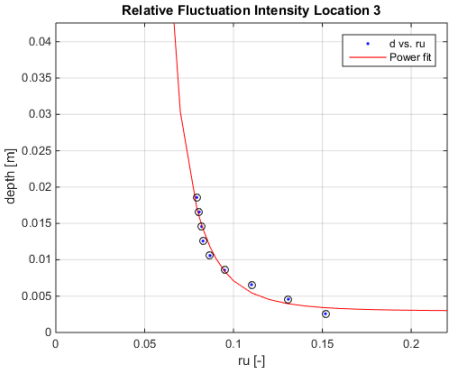

Figure 600; Relative fluctuation intensity location 3

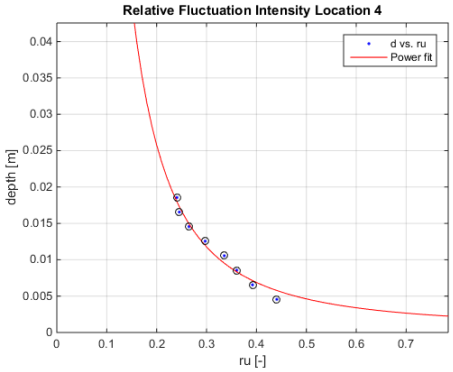

Figure 601; Relative fluctuation intensity location 4

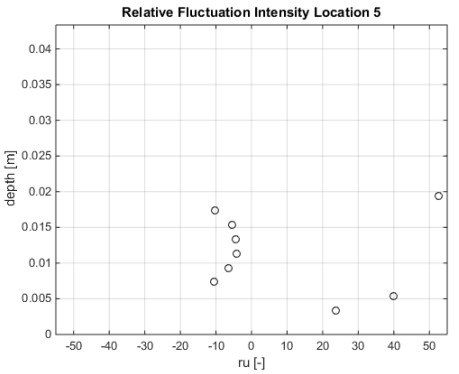

Figure 602; Relative fluctuation intensity location 5

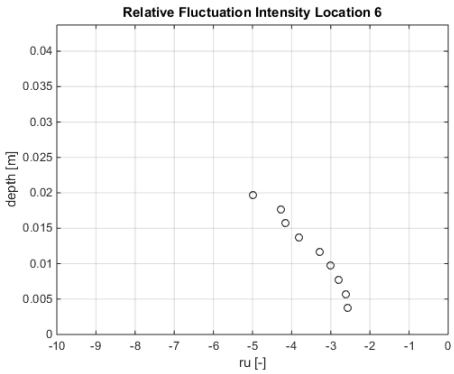

Figure 603; Relative fluctuation intensity location 6

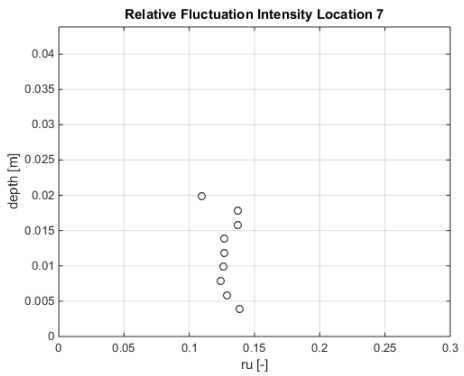

Figure 604; Relative fluctuation intensity location 7

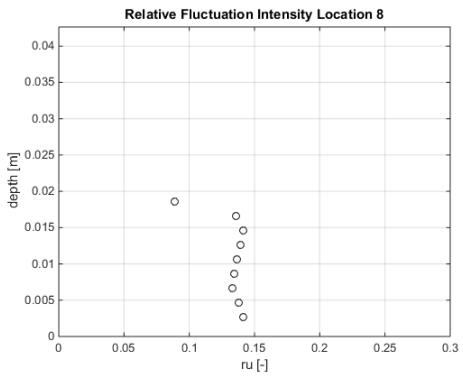

Figure 605; Relative fluctuation intensity location 8

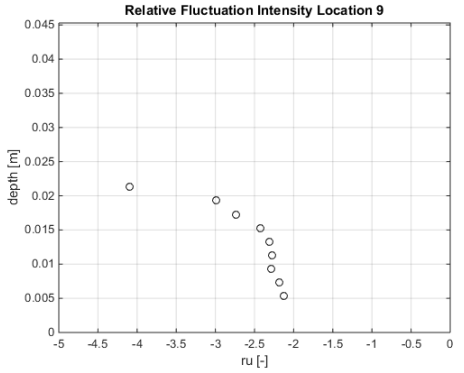

Figure 606; Relative fluctuation intensity location 9

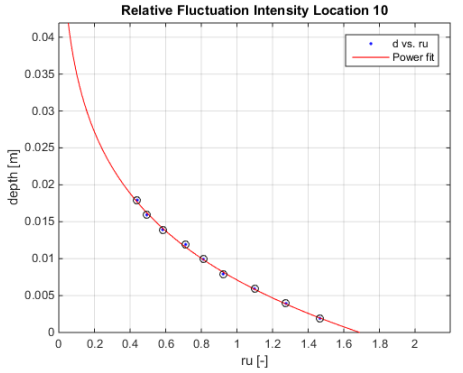

Figure 607; Relative fluctuation intensity location 10

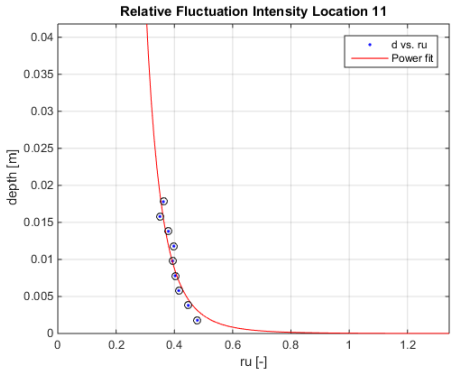

Figure 608; Relative fluctuation intensity location 11

Bed Shear stress

The bed shear stress was determined with Reynolds formula stated in (Schiereck & Verhagen, 2012). Bed shear stresses are determined by averaging the estimation for bed shear stress, over the centimeter measured above the bottom for a time frame of 3 minutes measuring at 50 [hz] per second, excluding all measured values that do not confirm with a signal to noise ratio above 15 and a correlation of 90%.

Bed shear stresses exceed values associated with high level of transport at locations 6,9,10 & 11. At locations 4 & 5 bed shear stresses were observed to be positive

Table 145; Bed shear stresses [n/m^2]

Location	1	2	3	4	5	6	7	8	9	10	11
	-0,043	-0,019	-0,047	0,031	0,034	-0,260	-0,069	-0,044	-0,166	-1,339	-0,182

Estimation of transport

Following the formulations of the bed load transport by van Rijn (van Rijn, 2018). The results are represented as such, that locations at the same longitudinal location are coupled and transport is averaged over these locations (Table 146) For the calculations the absolute value was taken of the measured bed shear stresses. The results are also depicted per sector (Table 147) by calculating the area underneath each cross-sectional measurement. In this way it is expected that scour will primarily occur in the constriction and expansion sectors.

Table 146; Bed load transport [kg/m/s]

Location	1	2 & 7	3 & 8	4 & 9	5 & 10	6 & 11
	NaN	NaN	NaN	NaN	0,028	0,0004

Table 147; Bed load transport per sector [kg/day]

Sector	Upstream	Contraction	Constriction	Expansion	Downstream
	NaN	NaN	188,7	323,5	1,8

Water level

The water levels were measured at locations 1,3,5,6 they are depicted in Table 148. The levels were computed by measuring at 1000 [hz] for 15 seconds, and averaging those results. It is observed that the water level shows a drop of 0,3 [cm]. The water level seems to drop during constriction with 0,8 [cm], and then increases again with 0,5 [cm].

Table 148; Water level [cm]

Location	1	3	5	6
	39,4560	39,1535	38,6594	39,1256

Measurements after 48h

Bed level

A projection of the bed after running for 48 [h] can be observed in Figure 609. The downstream scour hole has now become the largest scour hole and has clustered around the right side of the model.

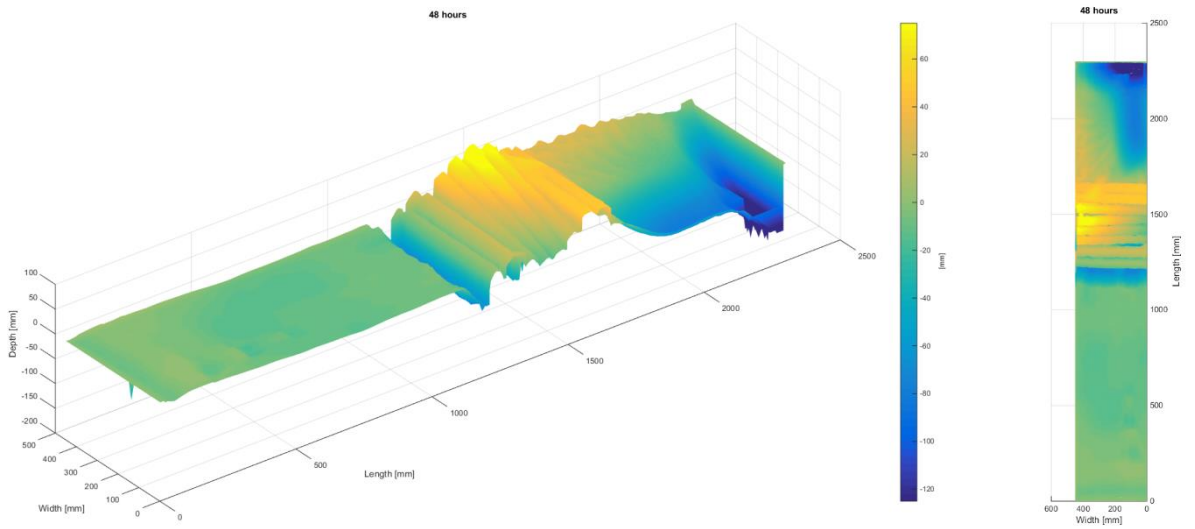

Figure 609; 48[h] bed projection

The average calculated transect observable in Figure 610, shows scour has penetrated up to 65 [mm] just in front of the logs and almost 100 [mm] at the downstream located scour. The bed upstream of the contraction and in the contraction seems fairly unaffected.

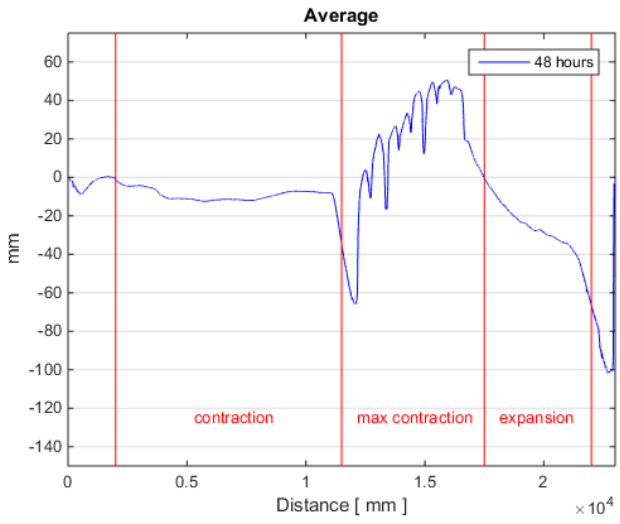

Figure 610; 48[h] average transect

Furthermore Figure 611 shows that the location of the logs has only changed slightly, with the third log located from downstream now also having tilted. The bed upstream is indeed unaffected, as is the scour hole upstream of the logs. The scour hole downstream of the logs has however grown significantly.

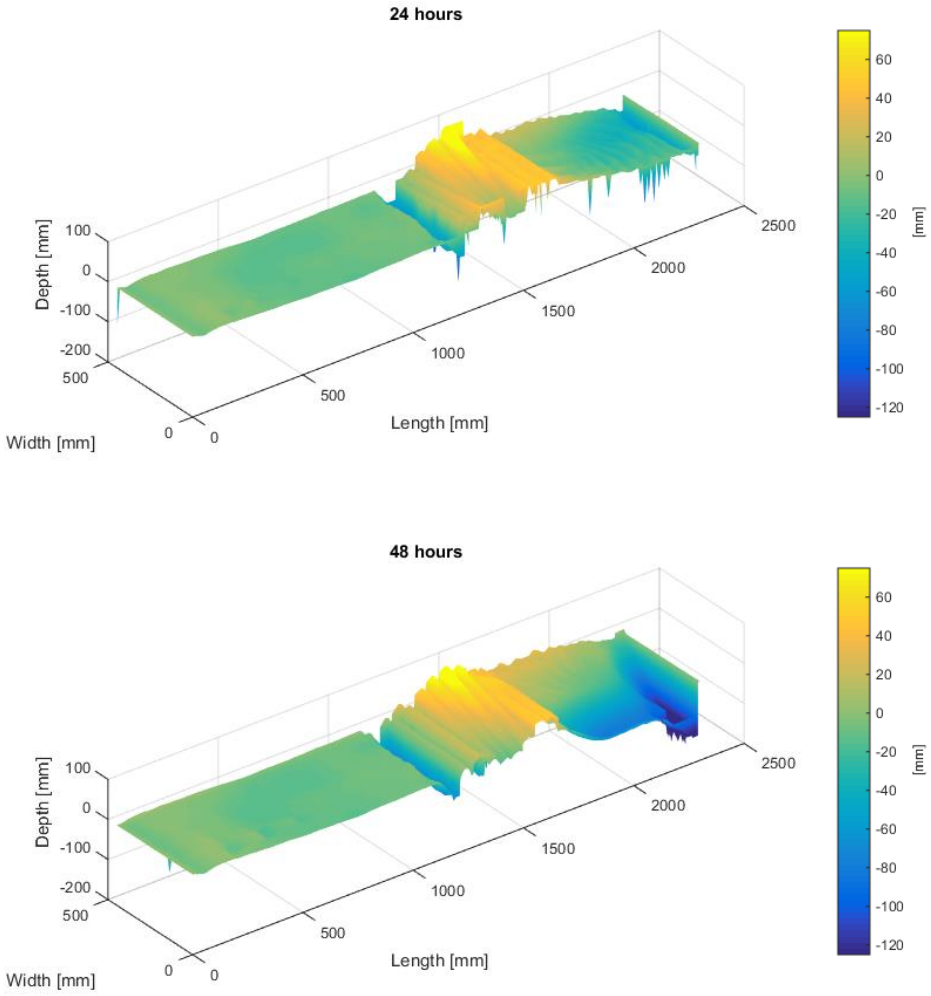

Figure 611; 24[h]-48[h] bed change projection

Table 149; Volume change per sector in [cm^3]

	Upstream	Contraction	Constriction	Expansion	Downstream
Volume	+14	-174	-1166	-2909	-2351

Velocity Profiles

In this section, individual flow profiles of locations marked above are shown. It can be observed that upon arrival the flow profile shows the characteristic profile for turbulent flow (location 1). At location 3 the flow has accelerated significantly, while close to the bottom flow is accelerated only slightly, thereby slightly skewing the flow profile. The flow velocity at location 5 increases even further higher up the water column, but reduces to zero/near zero in the wake of the logs. At location 6 it can be observed that the flow profile is attempting to redistribute to the original flow profile (location 1) but has yet been successful at obtaining this distribution and thus flow velocities are much higher, higher up the water column. The flow profile at location 9 shows a strong disturbance near the bed, caused by this location being located in between logs.

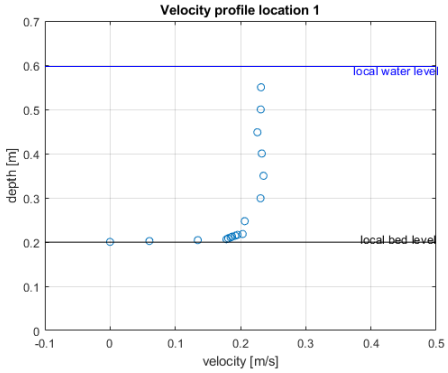

Figure 612; Velocity Profile location 1

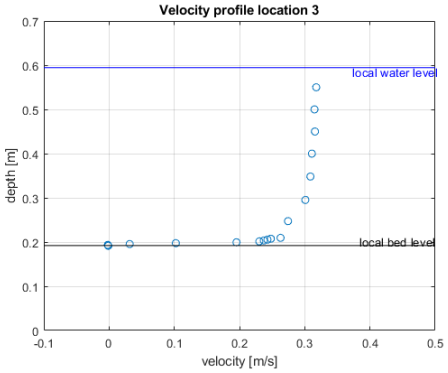

Figure 613; Velocity Profile location 3

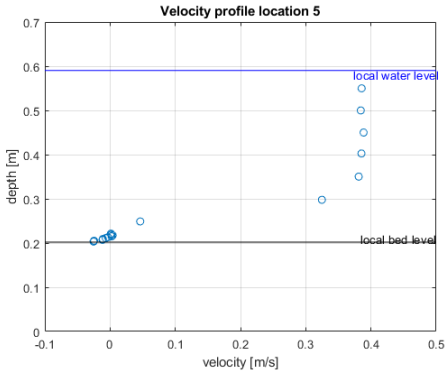

Figure 614; Velocity Profile location 5

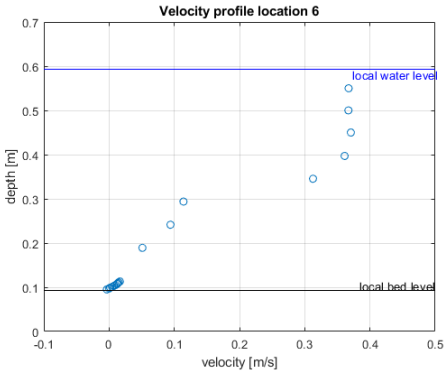

Figure 615; Velocity Profile location 6

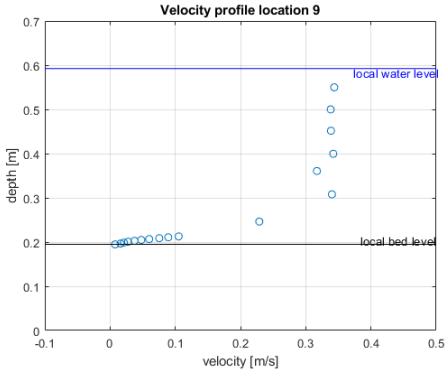

Figure 616; Velocity Profile location 9

Relative fluctuation intensity

It is shown that fluctuation intensity reduces slightly during flow contraction, in between location 1-2-3 and strongly in between locations 7 -8. At location 4 traditional values are observed while at location 9 RFI is very large. Locations 5 & 6 show large and negative RFI, indicative of upstream directed velocities. Location 10 shows larger than average positive values and location 11 shows a more traditional magnitude of RFI.

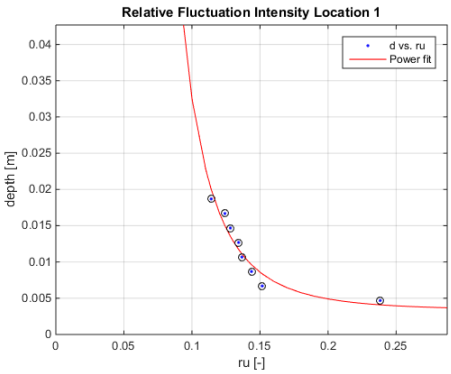

Figure 617; Relative fluctuation intensity location 1

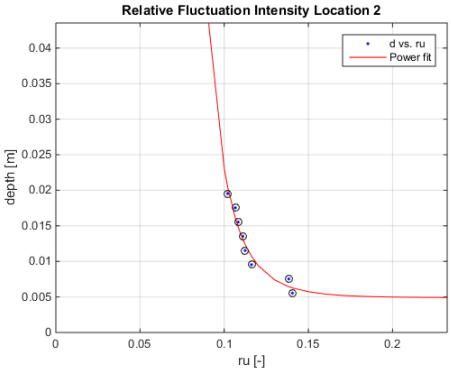

Figure 618; Relative fluctuation intensity location 3

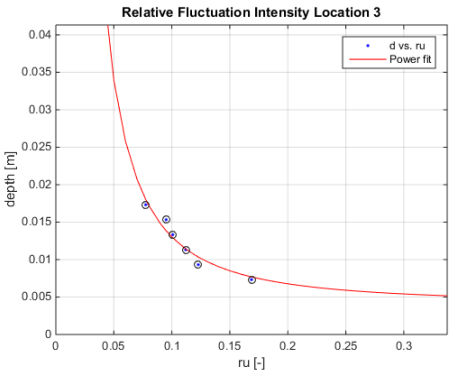

Figure 619; Relative fluctuation intensity location 5

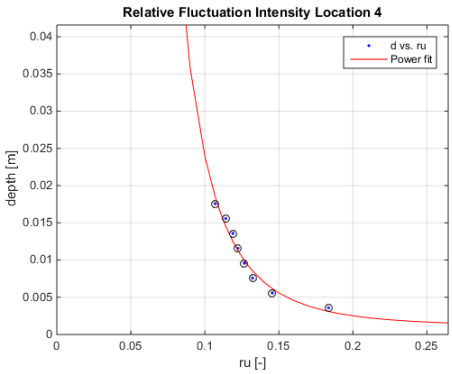

Figure 620; Relative fluctuation intensity location 2

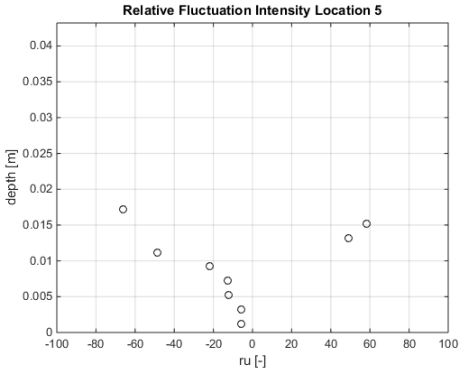

Figure 621; Relative fluctuation intensity location 4

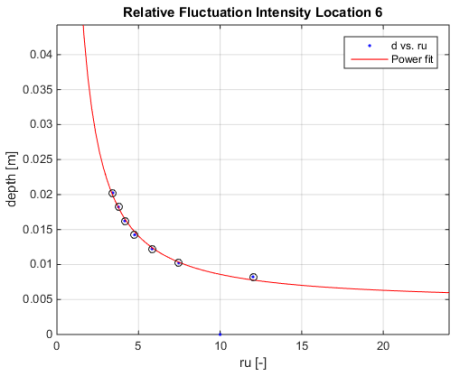

Figure 622; Relative fluctuation intensity location 6

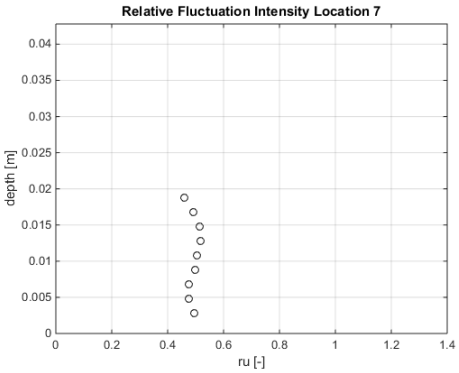

Figure 623; Relative fluctuation intensity location 7

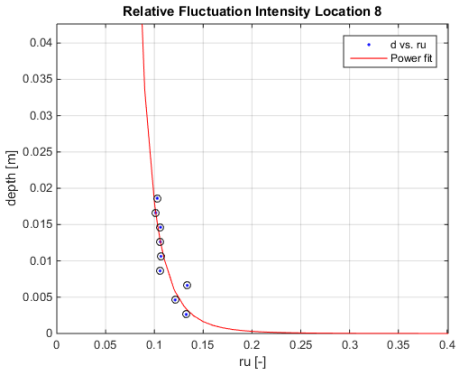

Figure 624; Relative fluctuation intensity location 8

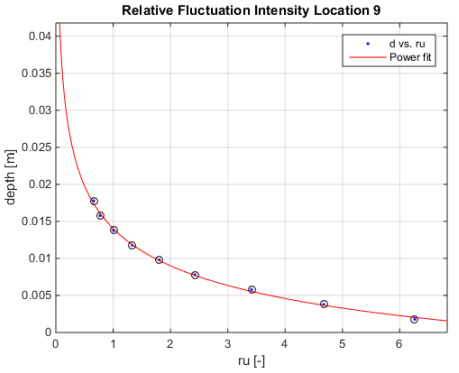

Figure 625; Relative fluctuation intensity location 9

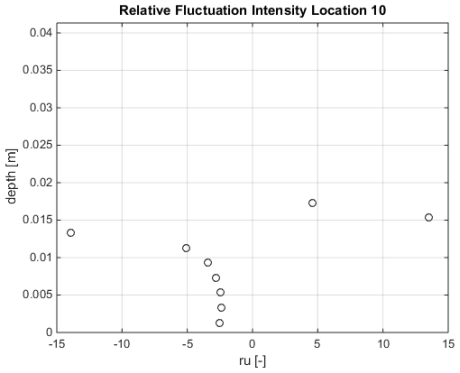

Figure 626; Relative fluctuation intensity location 10

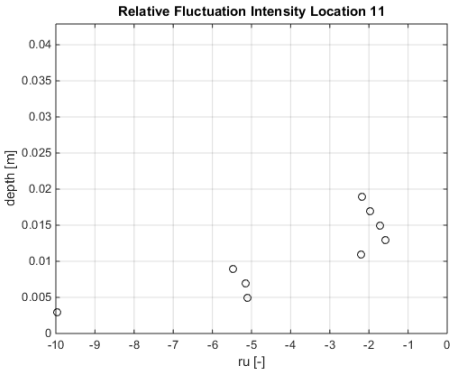

Figure 627; Relative fluctuation intensity location 11

Bed Shear stress

The bed shear stress was determined with Reynolds formula stated in (Schiereck & Verhagen, 2012). Bed shear stresses are determined by averaging the estimation for bed shear stress, over the centimeter measured above the bottom for a time frame of 3 minutes measuring at 50 [hz] per second, excluding all measured values that do not confirm with a signal to noise ratio above 15 and a correlation of 90%.

Bed shear stresses exceed values associated with high level of transport at locations 4,5,6,9,10 & 11. At all location 3,4 & 8 the measured bed shear stresses were positive.

Table 150; Bed shear stresses [n/m^2]

Location	1	2	3	4	5	6	7	8	9	10	11
	-0,089	-0,094	0,01	0,157	-0,377	-0,188	-0,048	0,019	-0,304	-0,172	-0,235

Estimation of transport

Following the formulations of the bed load transport by van Rijn (van Rijn, 2018). The results are represented as such, that locations at the same longitudinal location are coupled and transport is averaged over these locations (Table 151) For the calculations the absolute value was taken of the measured bed shear stresses. The results are also depicted per sector (Table 152) by calculating the area underneath each cross-sectional measurement. In this way it is expected that scour will mainly occur at the interface between the Constriction & Expansion Sectors at reduced rates with respect to the previous 24 [h].

Table 151; Bed load transport [kg/m/s]

Location	1	2 & 7	3 & 8	4 & 9	5 & 10	6 & 11
	NaN	NaN	NaN	0,0005	0,0014	0,0003

Table 152; Bed load transport per sector [kg/day]

Sector	Upstream	Contraction	Constriction	Expansion	Downstream
	NaN	NaN	16,2	17,2	1,3

Water level

The water levels were measured at locations 1,3,5,6 they are depicted in Table 153. The levels were computed by measuring at 1000 [hz] for 15 seconds, and averaging those results. It is observed that the water level shows a drop of 0,5 [cm]. The water level seems to drop during constriction with 0,4 [cm], and then decrease again with 0,1 [cm] in the expansion-sector.

Table 153; Water level [cm]

Location	1	3	5	6
	39,6857	39,4294	39,3003	39,2348

Measurements after 72h

Bed level

A projection of the bed after running for 72[h] can be observed in Figure 628. Strong scour is still clearly present near the downstream barrier. Meanwhile upstream minor bedforms are visible and at the location of the placed logs it can be seen the logs are still relatively in place.

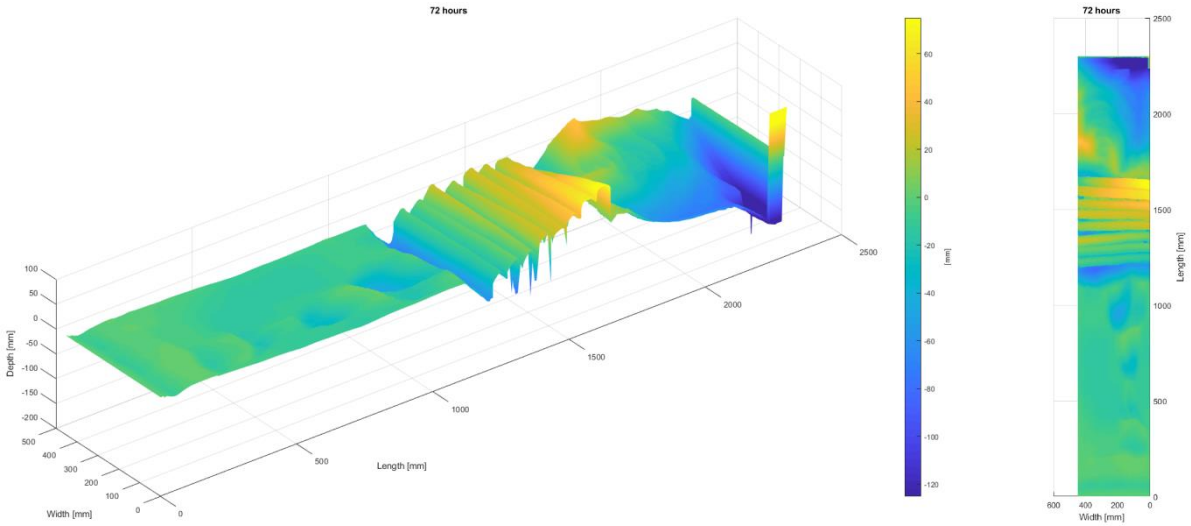

Figure 628; 72[h] bed projection

From the average transect (Figure 629) it can be observed that scour has reached approximately 60 [mm] in front of the log layer. The scour downstream has reached up to on average 100 [mm]. The bed upstream now shows minor bedforms developing.

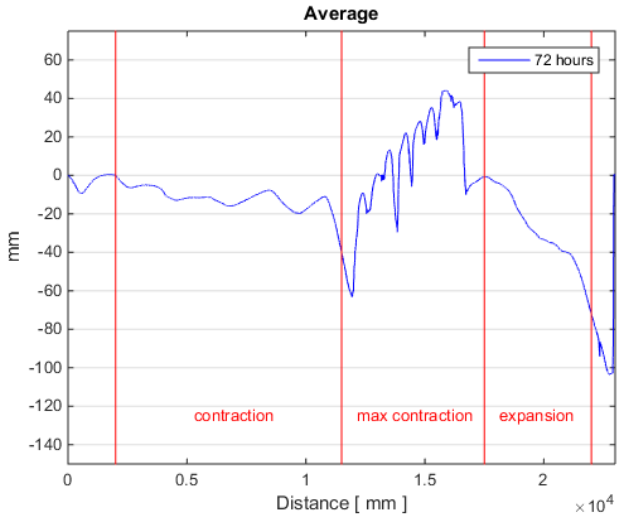

Figure 629; 72[h] average transect

Furthermore Figure 630 shows that compared with the measurement taken at 48 hours scour does not seem to have increased significantly, although it is visible that the logs are eroding bed material and are sinking in deeper ever so slightly.

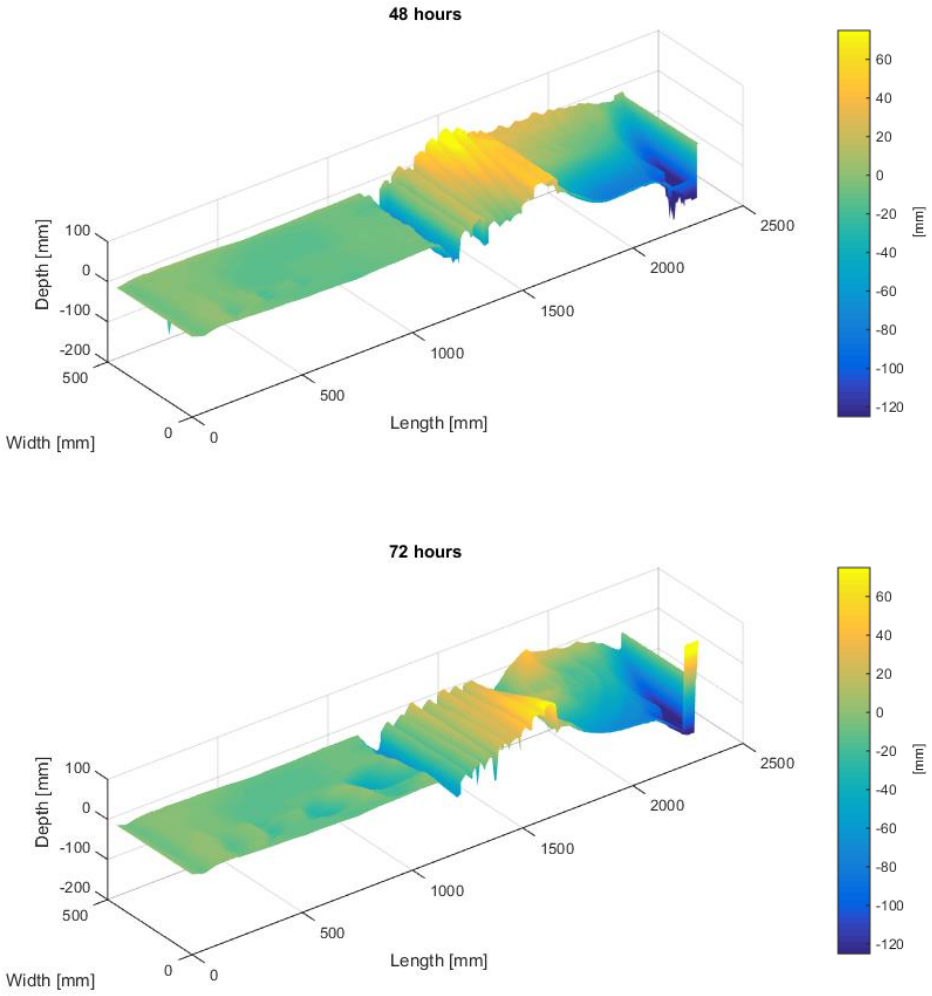

Figure 630; 48[h]-72[h] bed change projection

Table 154; Volume change per sector in [cm^3]

	Upstream	Contraction	Constriction	Expansion	Downstream
Volume	-21	-1186	-3059	-155	-69

Velocity Profiles

With respect to earlier measurements the flow profiles do not seem to change much. Noticeable is the local acceleration near bed at location 3 and 9. Locations 5-6 still show detached flow with negative near bed velocities.

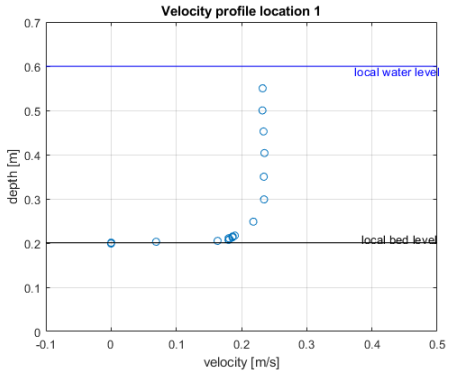

Figure 631; Velocity Profile location 1

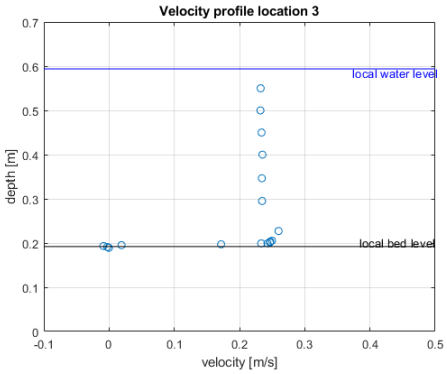

Figure 632; Velocity Profile location 3

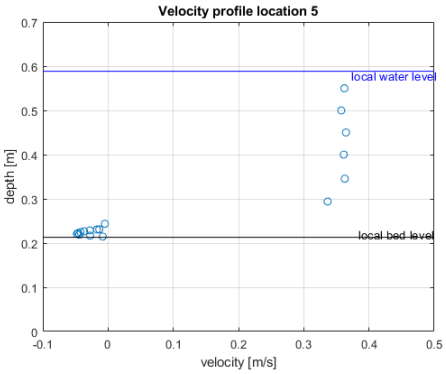

Figure 633; Velocity Profile location 5

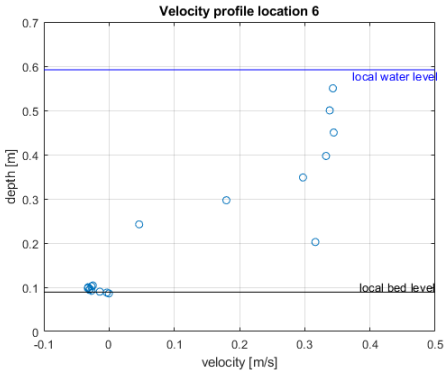

Figure 634; Velocity Profile location 6

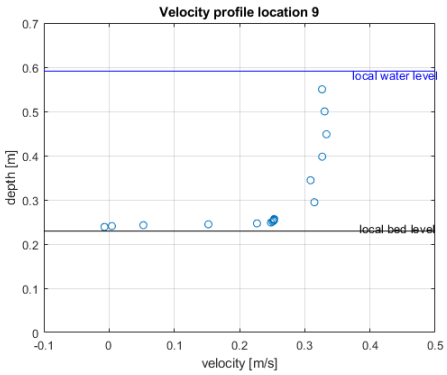

Figure 635; Velocity Profile location 9

Relative fluctuation intensity

It is shown that fluctuation intensity increases during flow contraction, in between location 1-2 and 7-8. At location 4 and 9 RFI does not exceed on average 40% average flow velocity. Locations 5,6,10 and 11 show large negative values in the wake of the logs and the scour hole that has developed downstream.

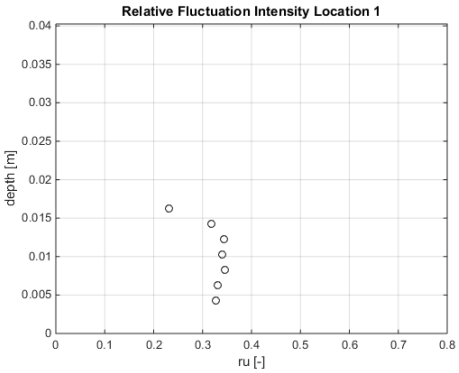

Figure 636; Relative fluctuation intensity location 1

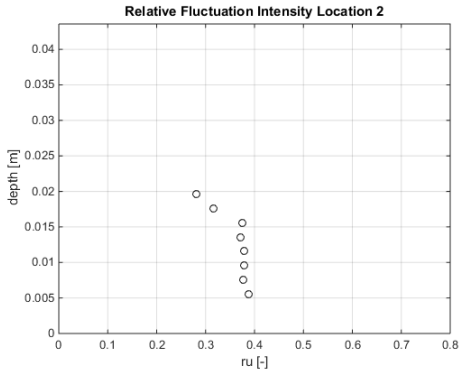

Figure 637; Relative fluctuation intensity location 2

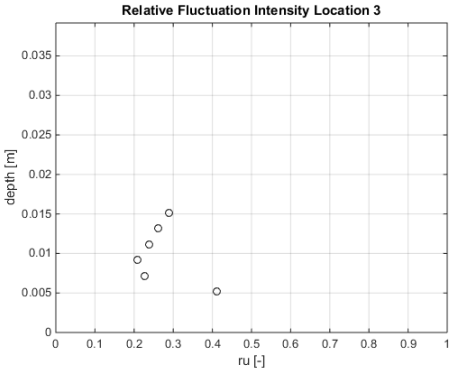

Figure 638; Relative fluctuation intensity location 3

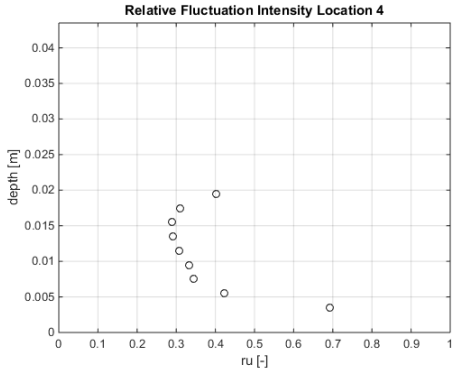

Figure 639; Relative fluctuation intensity location 4

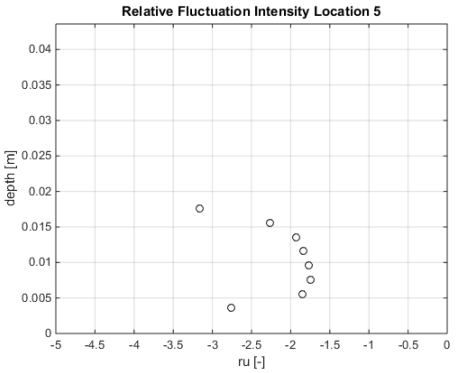

Figure 640; Relative fluctuation intensity location 5

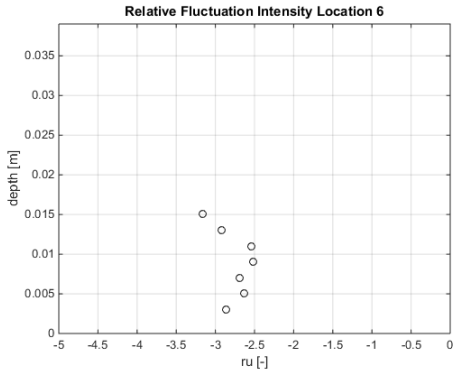

Figure 641; Relative fluctuation intensity location 6

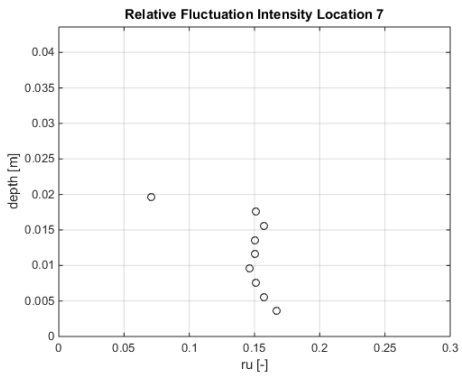

Figure 642; Relative fluctuation intensity location 7

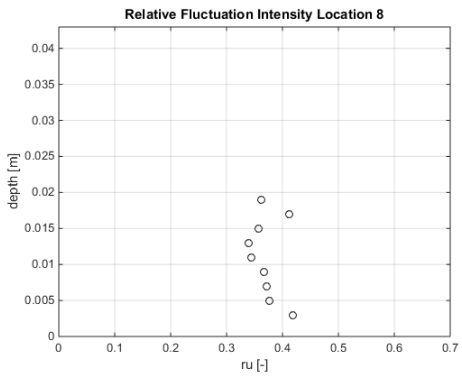

Figure 643; Relative fluctuation intensity location 8

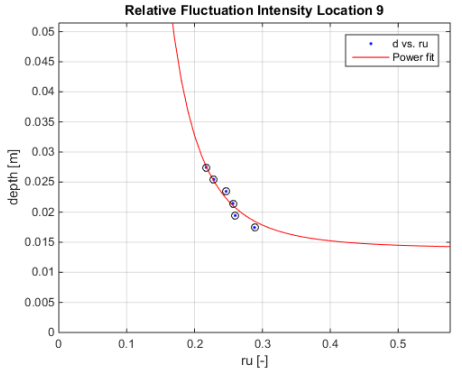

Figure 644; Relative fluctuation intensity location 9

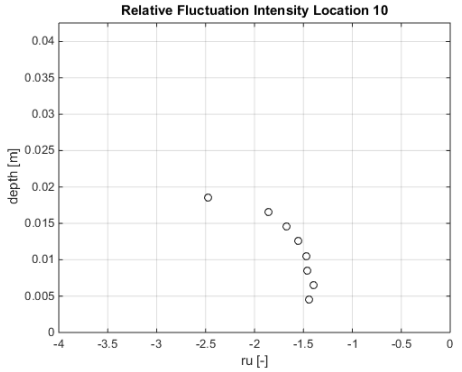

Figure 645; Relative fluctuation intensity location 10

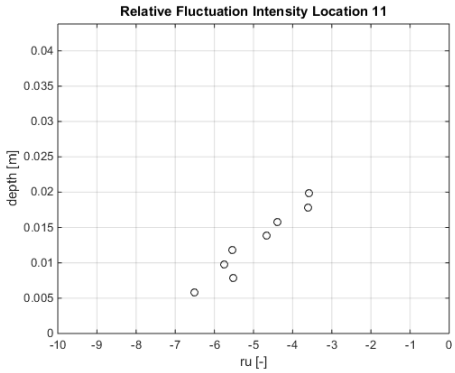

Figure 646; Relative fluctuation intensity location 11

Bed Shear stress

The bed shear stress was determined with Reynolds formula stated in (Schiereck & Verhagen, 2012). Bed shear stresses are determined by averaging the estimation for bed shear stress, over the centimeter measured above the bottom for a time frame of 3 minutes measuring at 50 [hz] per second, excluding all measured values that do not confirm with a signal to noise ratio above 15 and a correlation of 90%.

Bed shear stresses exceed values associated with high level of transport at locations 2,3,6,8 & 9. At locations 3 this bed shear stress was observed to be positive.

Table 155; Bed shear stresses [n/m^2]

Location	1	2	3	4	5	6	7	8	9	10	11
	-0,033	-0,106	0,325	-0,058	-0,040	-0,321	-0,055	-0,124	-0,198	-0,055	-0,004

Estimation of transport

Following the formulations of the bed load transport by van Rijn (van Rijn, 2018). The results are represented as such, that locations at the same longitudinal location are coupled and transport is averaged over these locations (Table 156) For the calculations the absolute value was taken of the measured bed shear stresses. The results are also depicted per sector (Table 157) by calculating the area underneath each cross-sectional measurement. In this way it is expected that scour will mainly occur upstream of the logs, location 6 however shows locally high bed shear stresses which could indicate higher transport rates at this specific location.

Table 156; Bed load transport [kg/m/s]

Location	1	2 & 7	3 & 8	4 & 9	5 & 10	6 & 11
	NaN	NaN	0,0004	NaN	NaN	$2,05*10^{-7}$

Table 157; Bed load transport per sector [kg/day]

Sector	Upstream	Contraction	Constriction	Expansion	Downstream
	NaN	4,5	2,7	0,0	0,0

Water level

The water levels were measured at locations 1,3,5,6 they are depicted in Table 158. The levels were computed by measuring at 1000 [hz] for 15 seconds, and averaging those results. It is observed that the water level shows a drop of 0,8 [cm]. The water level seems to drop during constriction with 1,1[cm], and then increases again with 0,3 [cm].

Table 158; Water level [cm]

Location	1	3	5	6
	39,9614	39,3771	38,8517	39,1924

Measurements after 96h

Bed level

A projection of the bed after running for 96[h] can be observed in Figure 647. The largest scour hole is still located at the downstream barrier. The logs have started to form a clear slope and visual estimations would suggest that in the area of maximum contraction scour has been reduced.

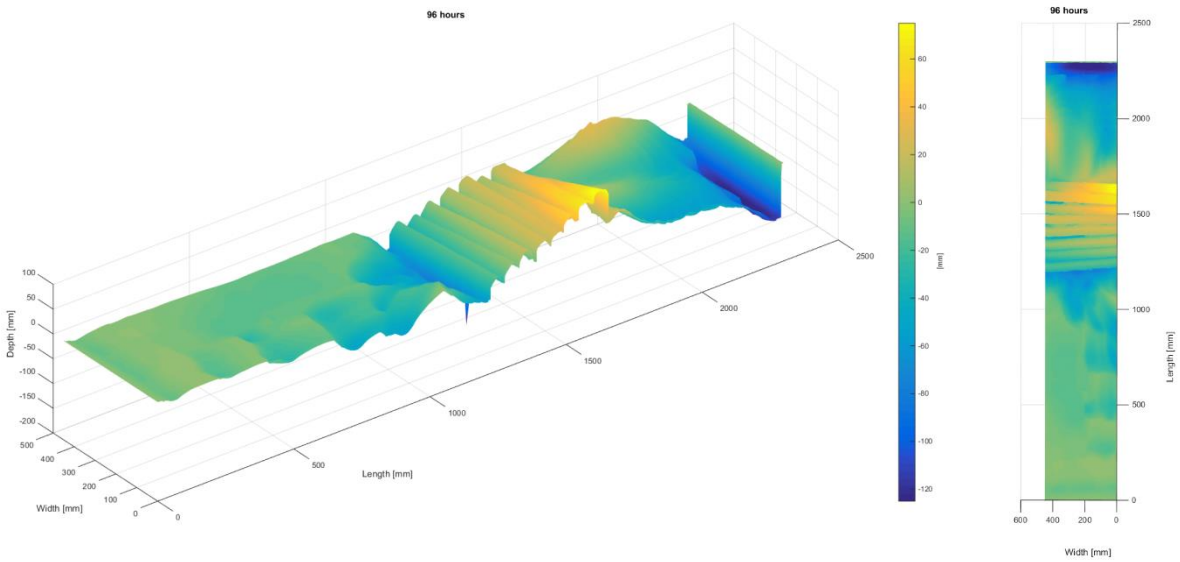

Figure 647; Bed map after 96 [h]

Comparing the average transect (Figure 648) with the average transect taken at 0 [h], it can clearly be seen that the bed in the area of max contraction is affected but the effect is relatively small. The scour hole that has developed downstream has Cleary become the larger scour hole with a penetration of 120 [mm] into the bed.

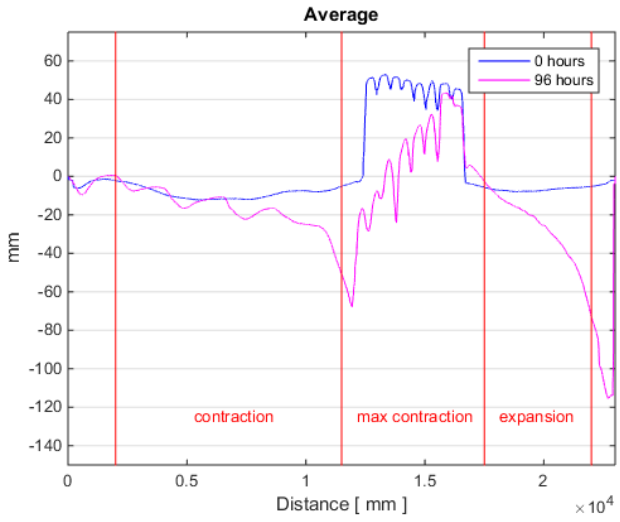

Figure 648; Average transects through time

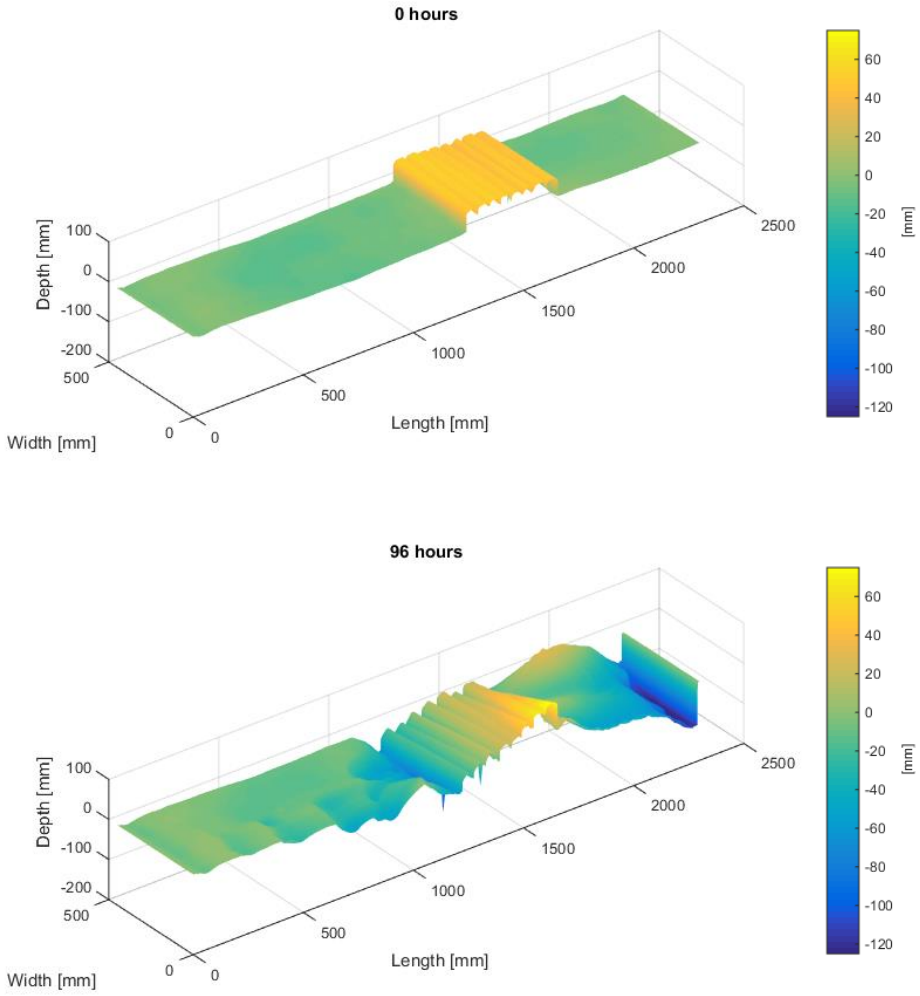

Figure 649; Bed change with respect to 0[h]

Table 159; Volume change per sector in [cm^3]

	Upstream	Contraction	Constriction	Expansion	Downstream
Volume	-12	-2023	-602	+209	-364

Concluding Remarks

This Second protected scour B experiment has shown some promising results. At the point of highest flow velocities, located above the logs, scour has significantly reduced with respect to the basic scour experiments. Other than that the logs have shown typical pipeline scour patterns, creating a small trench in front of the first log causing it to roll in and activate the logs behind it. This effect was anticipated. The scour formation downstream of the logs was not expected, and it has yet to be determined if this particular phenomenon occurs because of the logs, or due to the design of the laboratory model.

Appendix E III

I Introduction

The protected Scour experiments are considered to be the baseline experiments for the application of wooden logs as a scour protection. The "Protected Scour B" experiments feature a flow perpendicular placed single layer of logs directly on top of the bed, in the area of maximum contraction. Similar to the basic scour experiments bed, velocity and fluctuation intensity development is measured during a 96 [h] run. This report includes all measured findings during this particular experiment. Conclusions are drawn in the main report on the basis of multiple similarly conducted experiments. A short preliminary conclusion is however included at the end of this report.

Summary

Table 160 represents relevant scour quantities after 96 [h]. Note that the absolute is measured relative to the measurement of the bed at 0 [h], excluding the maximum scour depth which is measured to a reference bed with a 0 [mm] elevation. Measurements of scour volume in the column with respect to reference include missing volume with respect to a reference be of 0 [mm] and corrected for the presence of logs.

Table 160; Summary of quantities (Negative values indicate scour, positive indicate accretion)

	Quantity	With respect to reference
Maximum Scour Depth [mm]	100	100
Total Scoured volume [cm^3]	-4328	-23875
Scoured volume Upstream-sector [cm^3]	-318	-358
Scoured volume Contracting-sector [cm^3]	-1536	-13956
Scoured volume Constricted-sector [cm^3]	-8192	-10011
Scoured volume Expanding-sector [cm^3]	+1673	+1281
Scoured volume Downstream-sector [cm^3]	+338	-831

Measurements at 0h

Bed level

A projection of the bed at the moment of initiation of flow during the first scour experiment can be seen in Figure 650. Clearly observable are the placed logs on the bed. They are roughly located in between 1200-1700 [mm] from the entry point of flow, and have no spacing in between each other.

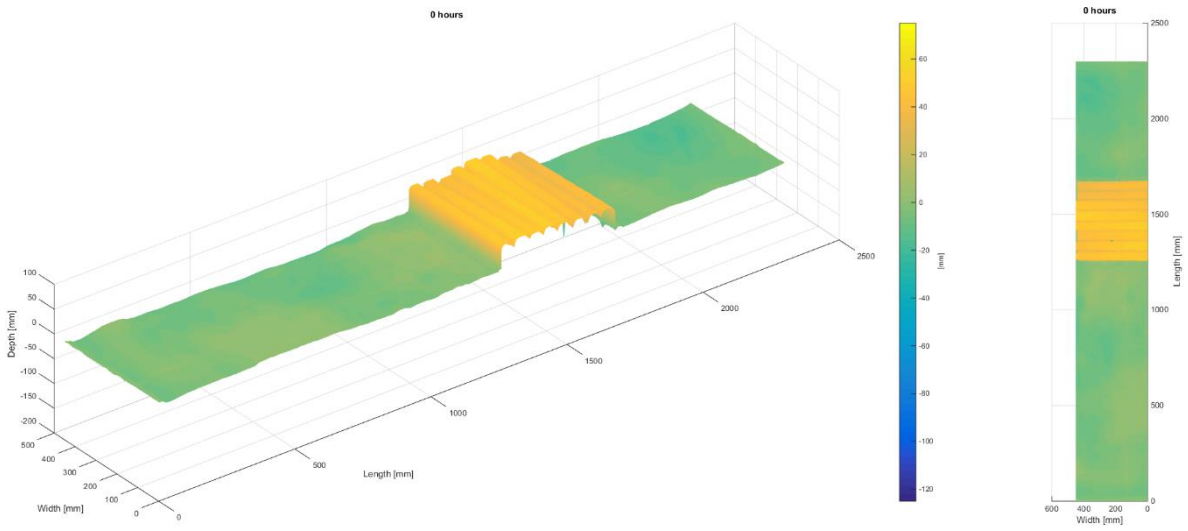

Figure 650; Bed map 0[h]

The average transect, observable in Figure 651 show the bed is incidentally below target value with a maximum deviation of about 13 [mm] downstream of the logs.

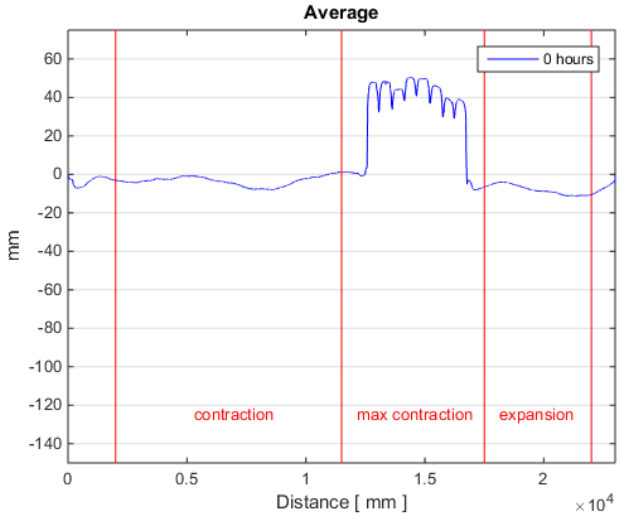

Figure 651; 0 [h] average transect

Velocity Profiles

Velocity profiles in Figure 652 - Figure 656 show that flow accelerates and transforms into a more turbulent distribution in the contraction sector (1-3). Flow above the logs is locally strongly accelerated (9), and flow downstream of the logs in the expansion-sector is detached and close to the bed at location 5 upstream directed.

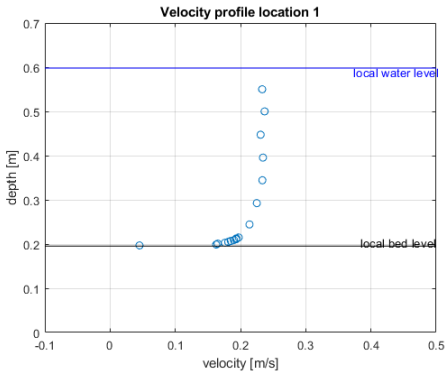

Figure 652; Velocity Profile location 1

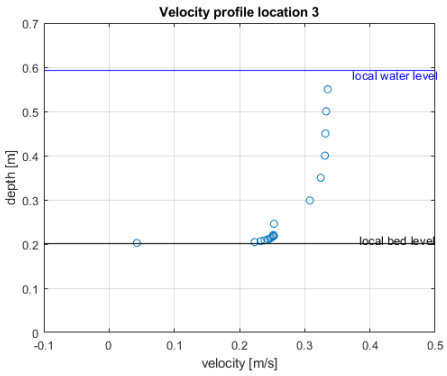

Figure 653; Velocity Profile location 3

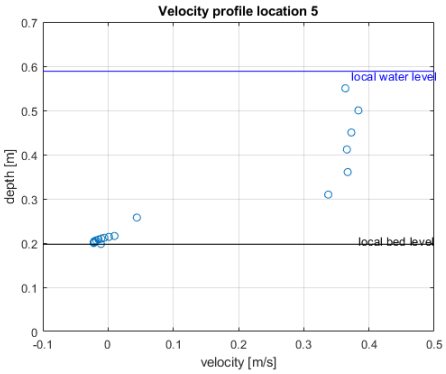

Figure 654; Velocity Profile location 5

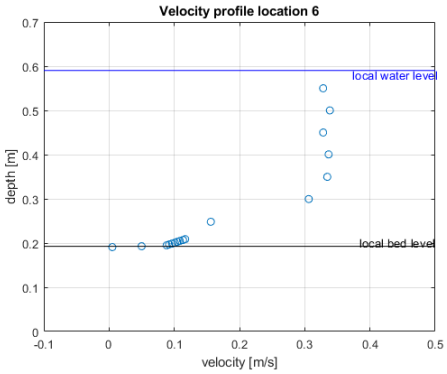

Figure 655; Velocity Profile location 6

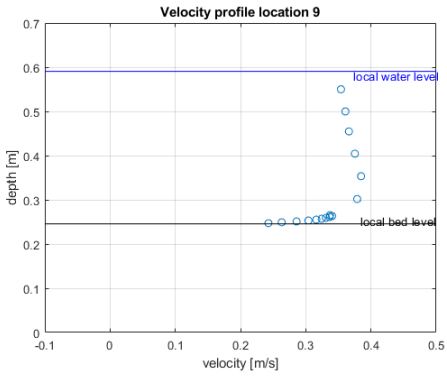

Figure 656; Velocity Profile location 9

Relative fluctuation intensity

Fluctuation intensity follows traditional patterns for the locations upstream of the logs (1-2-3). RFU increases from location 7-8. Above the logs measured RFU at locations 4-9 is relatively small with respect to the basic scour experiments. Locations downstream of the logs (5-10) show large but negative RFU which indicates near bed upstream directed velocities. Further downstream at locations 6-11 where the flow is attempting to reattach, fluctuations are large and positive, thus flow is again downstream directed.

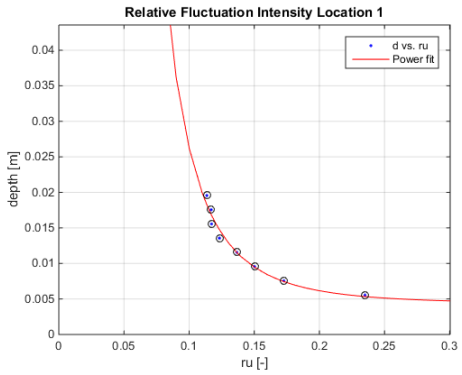

Figure 657; Relative fluctuation intensity location 1

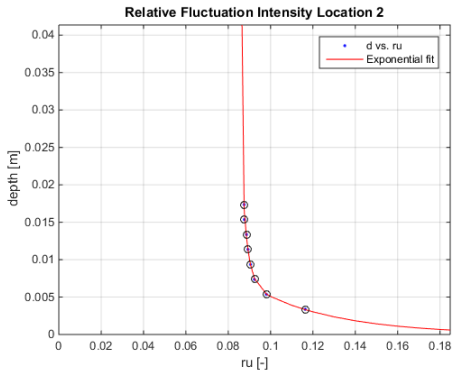

Figure 658; Relative fluctuation intensity location 2

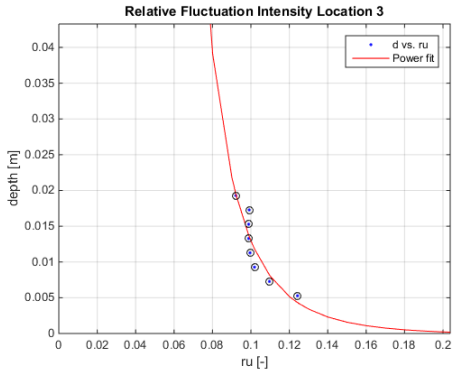

Figure 659; Relative fluctuation intensity location 3

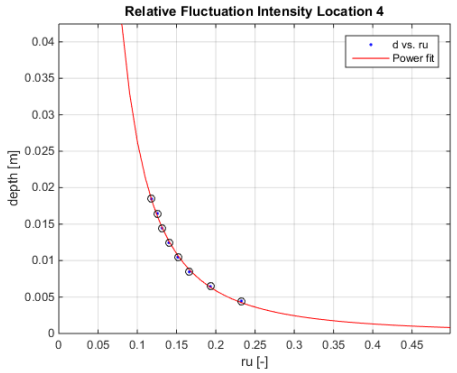

Figure 660; Relative fluctuation intensity location 4

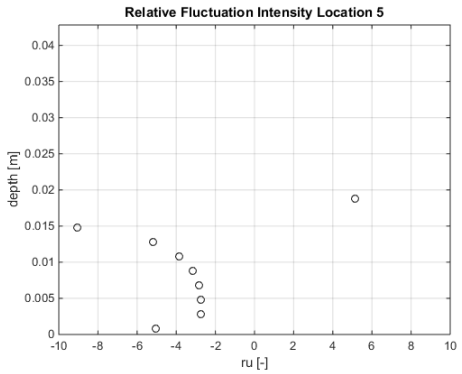

Figure 661; Relative fluctuation intensity location 5

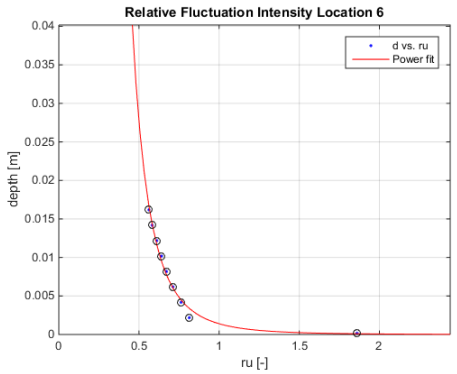

Figure 662; Relative fluctuation intensity location 6

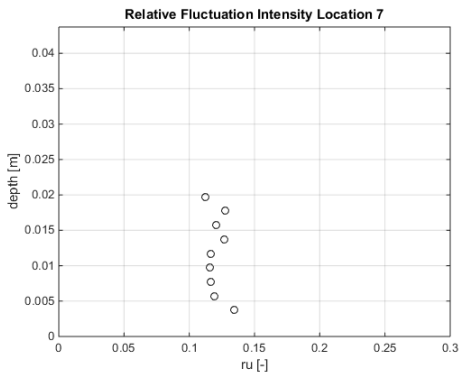

Figure 663; Relative fluctuation intensity location 7

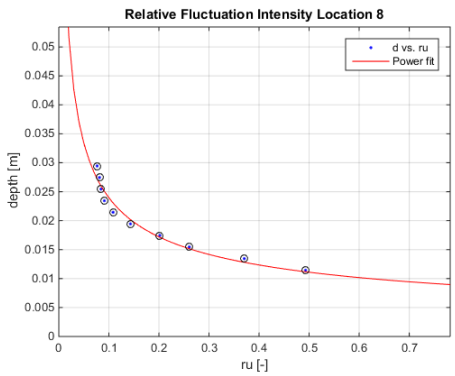

Figure 664; Relative fluctuation intensity location 8

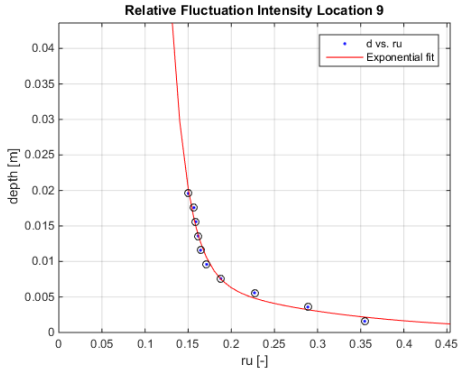

Figure 665; Relative fluctuation intensity location 9

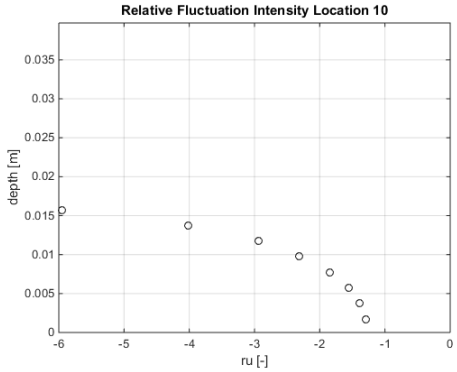

Figure 666; Relative fluctuation intensity location 10

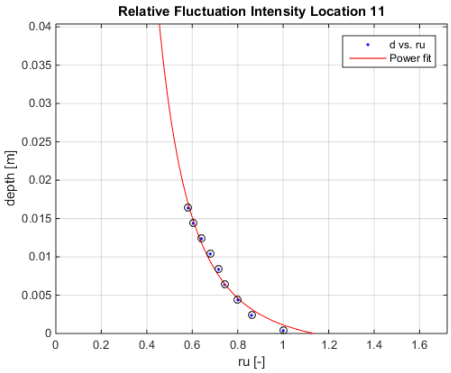

Figure 667; Relative fluctuation intensity location 11

Bed Shear stress

The bed shear stress was determined with Reynolds formula stated in (Schiereck & Verhagen, 2012). Bed shear stresses are determined by averaging the estimation for bed shear stress, over the centimeter measured above the bottom for a time frame of 3 minutes measuring at 50 [hz] per second, excluding all measured values that do not confirm with a signal to noise ratio above 15 and a correlation of 90%.

Bed shear stresses exceed values associated with high level of transport at locations 4,6,8,9,10 & 11. At all locations bed shear stresses were negative.

Table 161; Bed shear stresses [n/m^2]

Location	1	2	3	4	5	6	7	8	9	10	11
	-0,046	-0,062	-0,078	-0,620	-0,074	-0,215	-0,062	-0,285	-0,437	-0,217	-0,234

Estimation of transport

Following the formulations of the bed load transport by van Rijn (van Rijn, 2018). The results are represented as such, that locations at the same longitudinal location are coupled and transport is averaged over these locations (Table 162) For the calculations the absolute value was taken of the measured bed shear stresses. The results are also depicted per sector (Table 163) by calculating the area underneath each cross-sectional measurement. In this way it is expected that scour should primarily occur around the logs, with small scour rates downstream of the logs.

Table 162; Bed load transport [kg/m/s]

Location	1	2 & 7	3 & 8	4 & 9	5 & 10	6 & 11
	NaN	NaN	$3{,}36*10^{-5}$	0,015	NaN	0,0004

Table 163; Bed load transport per sector [kg/day]

Sector	Upstream	Contraction	Constriction	Expansion	Downstream
	NaN	0,4	202,4	4,0	1,8

Water level

The water levels were measured at locations 1,3,5,6 they are depicted in Table 164. The levels were computed by measuring at 1000 [hz] for 15 seconds, and averaging those results. It is observed that the water level shows a drop of 0,8 [cm]. The water level seems to drop during constriction with 1 [cm], and then decreases again with 0,2 [cm].

Table 164; Water level [cm]

Location	1	3	5	6
	39,8029	39,2586	38,8417	39,0501

Measurements after 24h

Bed level

A projection of the bed after running for 24 [h] can be observed Figure 668, the logs have started to move towards a scour hole located on the upstream face of the log layer. The logs show to have assumed semi unstable positions, while the third and fourth counted from upstream have clearly detached from each other. Directly downstream of the logs accretion has occurred while further downstream, near the downstream-section a small narrow scour hole has started to develop.

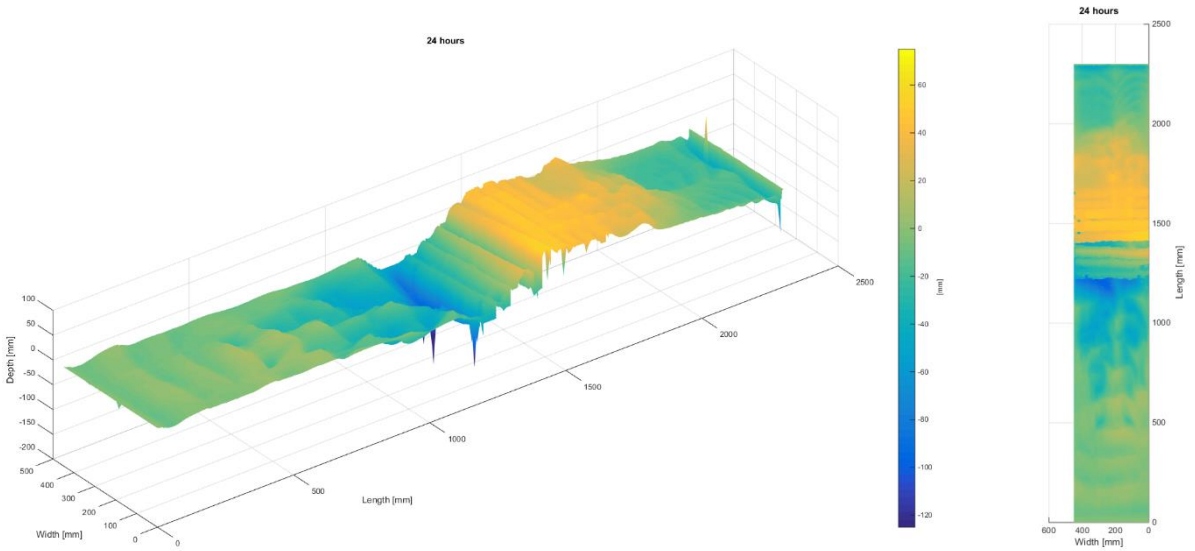

Figure 668; 24[h] bed projection

This can be confirmed with the average transect, observable in Figure 669. Two scour holes can be identified, namely one upstream of the logs with a magnitude of 80 [mm] and one downstream of the logs with a smaller magnitude of 40 [mm].

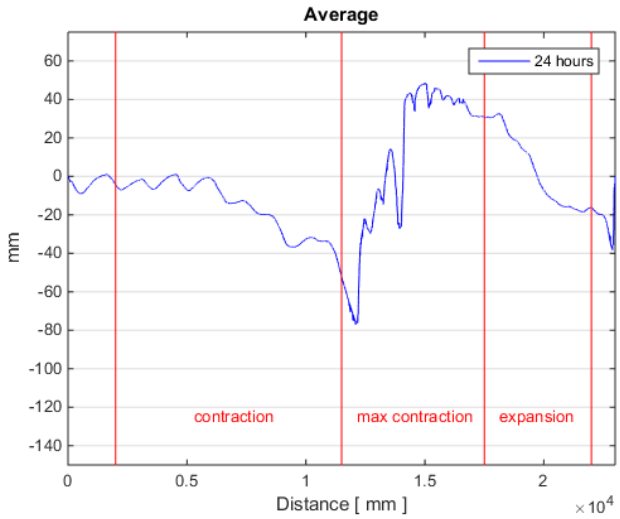

Figure 669; 24[h] average transect

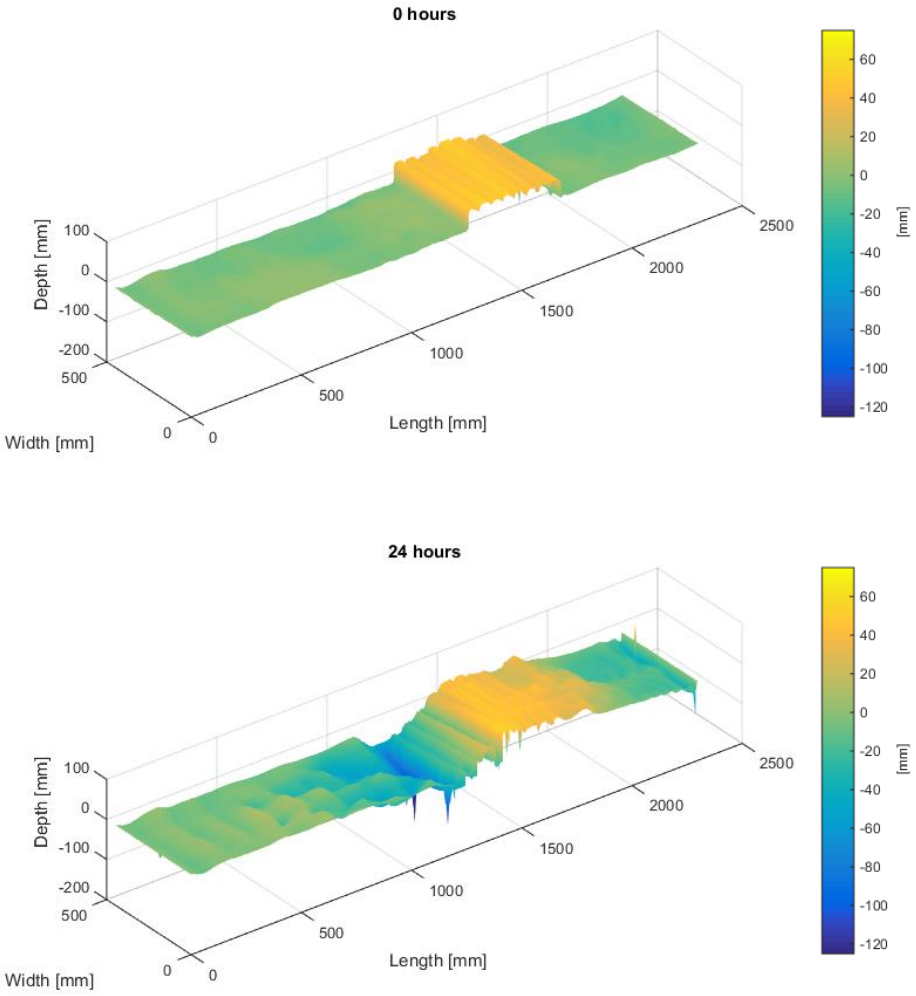

Figure 670; 0[h]-24[h] bed change projection

Table 165; Volume change per sector in [cm^3]

	Upstream	Contraction	Constriction	Expansion	Downstream
Volume	+9	-5379	-5355	+2412	-685

Velocity Profiles

The flow profiles at this time show interesting patterns., the flow profile at location 1 remains relatively unaffected, the flow profile just upstream of the logs shows near zero and occasionally negative velocities near the bed, while further up the water column, flow velocities are much higher. Flow just downstream of the logs show a strong acceleration of flow approximately 10 [cm] from the bed, at location 6 the influence of the narrow scour hole is now clearly observable as velocities near bed are close to zero, while further up the water column flow velocities are much higher. Location 9 shows near bed velocities are to some degree severely disturbed, while flow velocities are relatively uniform higher up the water column.

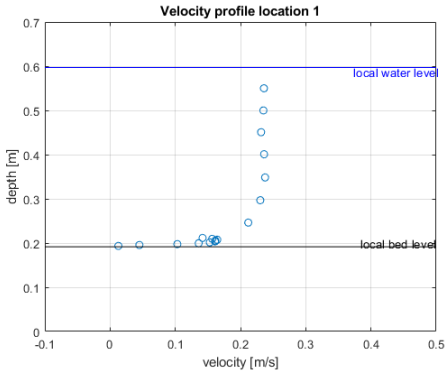

Figure 671; Velocity Profile location 1

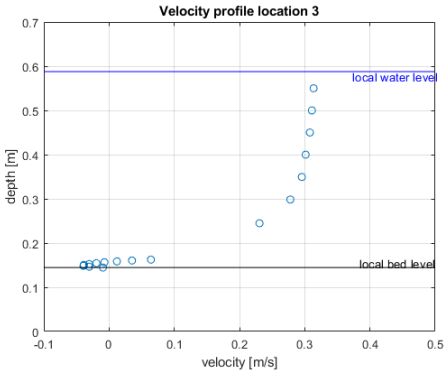

Figure 672; Velocity Profile location 3

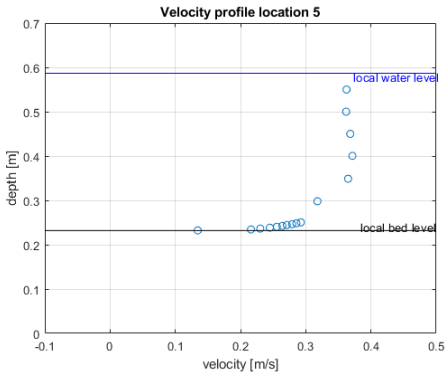

Figure 673; Velocity Profile location 5

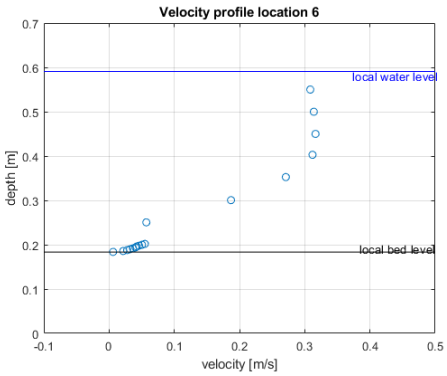

Figure 674; Velocity Profile location 6

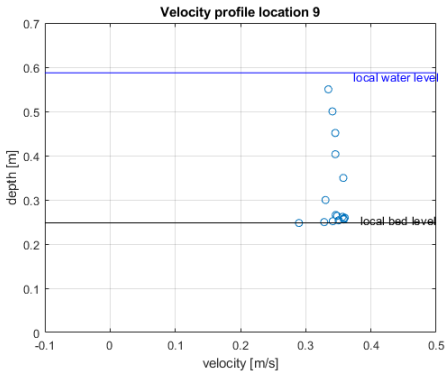

Figure 675; Velocity Profile location 9

Relative fluctuation intensity

RFU now increases from locations upstream towards locations in the constriction-sector (1-2-3 & 7-8), at location 3 strong negative and positive RFU is measured. The magnitude can be explained through near zero velocities, which also explain both negative as positive values. Locations above the log layer (4-9) show a similar, relatively small, and uniform RFU distribution. Location 5 directly downstream of the logs shows values and a distribution usually observed upstream. Location 10 on the other hand shows very strong RFU, most likely due to the void behind the logs in combination with near bed near zero velocities. Locations located at the interface of the expansion-sector and downstream-sector (6-11) show mainly positive and high RFU.

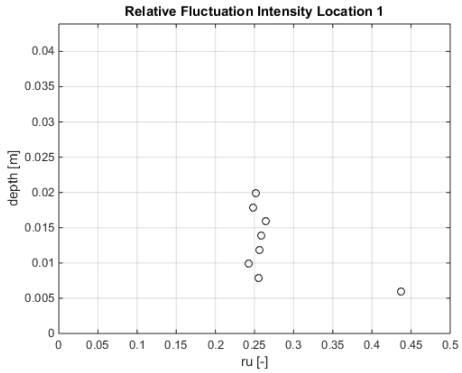

Figure 676; Relative fluctuation intensity location 1

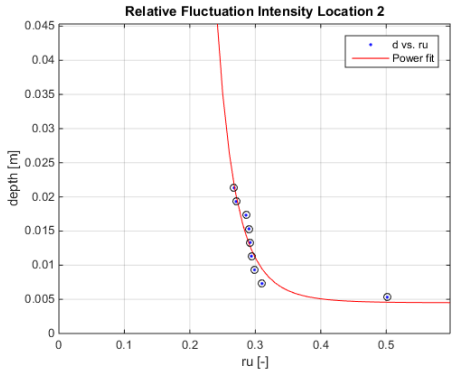

Figure 677; Relative fluctuation intensity location 2

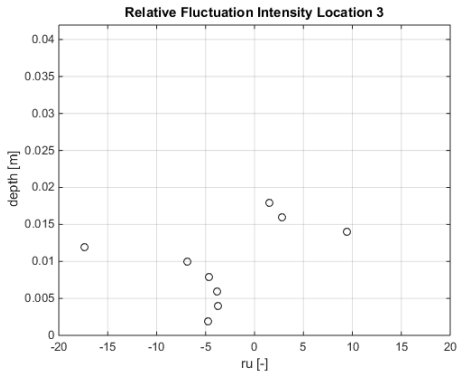

Figure 678; Relative fluctuation intensity location 3

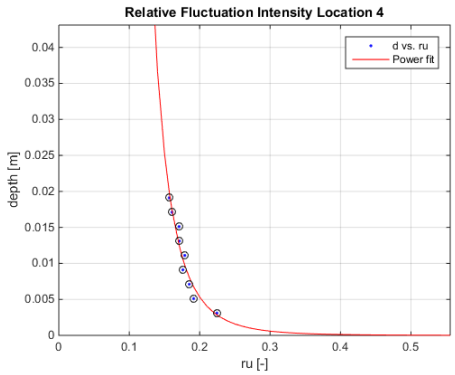

Figure 679; Relative fluctuation intensity location 4

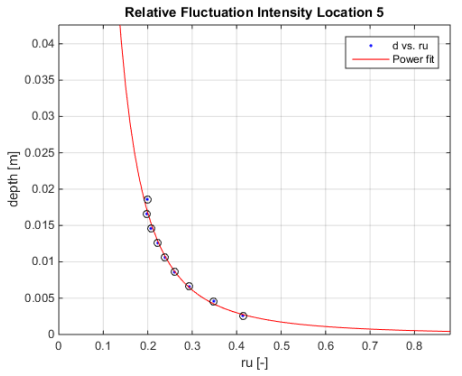

Figure 680; Relative fluctuation intensity location 5

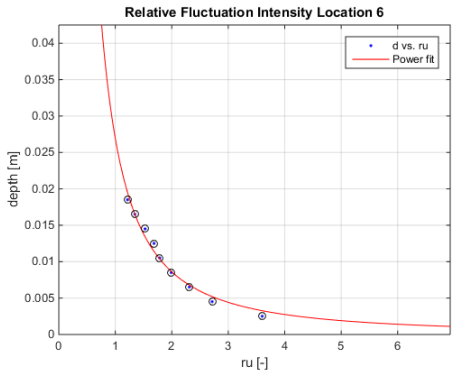

Figure 681; Relative fluctuation intensity location 6

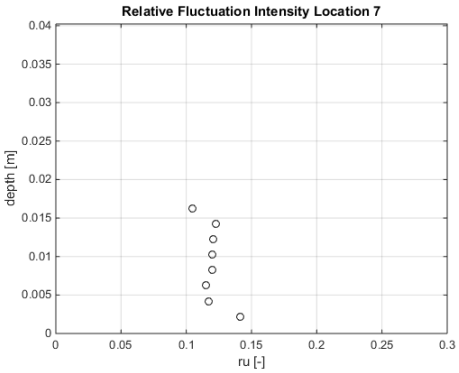

Figure 682; Relative fluctuation intensity location 7

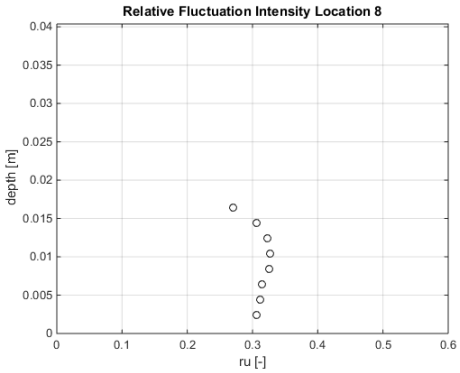

Figure 683; Relative fluctuation intensity location 8

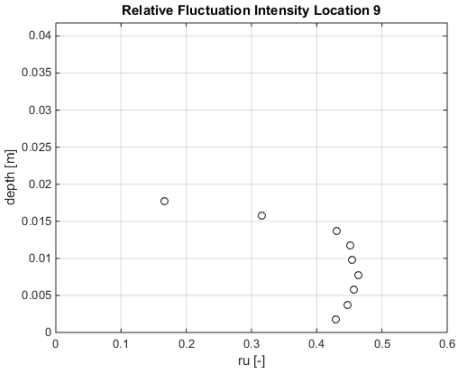

Figure 684; Relative fluctuation intensity location 9

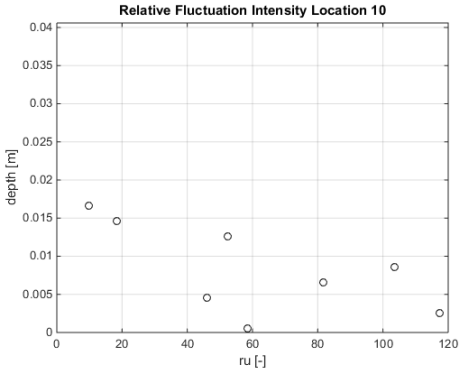

Figure 685; Relative fluctuation intensity location 10

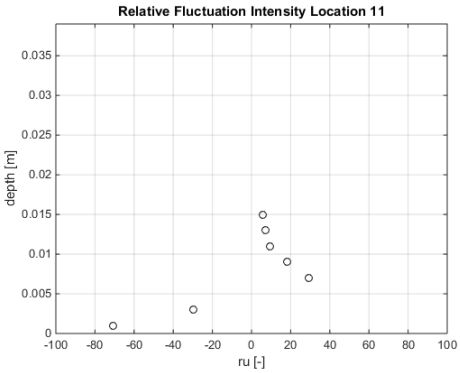

Figure 686; Relative fluctuation intensity location 11

Bed Shear stress

The bed shear stress was determined with Reynolds formula stated in (Schiereck & Verhagen, 2012). Bed shear stresses are determined by averaging the estimation for bed shear stress, over the centimeter measured above the bottom for a time frame of 3 minutes measuring at 50 [hz] per second, excluding all measured values that do not confirm with a signal to noise ratio above 15 and a correlation of 90%.

Bed shear stresses exceed values associated with high level of transport at all locations except at location 7. At all location but location 8 these bed shear stresses were observed to be negative.

Table 166; Bed shear stresses [n/m^2]

Location	1	2	3	4	5	6	7	8	9	10	11
	-0,169	-0,518	-0,334	-0,129	-0,274	-0,129	-0,054	0,266	-0,114	-0,349	-0,218

Estimation of transport

Following the formulations of the bed load transport by van Rijn (van Rijn, 2018). The results are represented as such, that locations at the same longitudinal location are coupled and transport is averaged over these locations (Table 167) For the calculations the absolute value was taken of the measured bed shear stresses. The results are also depicted per sector (Table 168) by calculating the area underneath each cross-sectional measurement. In this way scour is to be expected in the contraction, constriction and expansion sectors.

Table 167; Bed load transport [kg/m/s]

Location	1	2 & 7	3 & 8	4 & 9	5 & 10	6 & 11
	$4{,}34*10^{-6}$	$1{,}74*10^{-3}$	$2{,}17*10^{-3}$	NaN	$2{,}55*10^{-3}$	$1{,}13*10^{-5}$

Table 168; Bed load transport per sector [kg/day]

Sector	Upstream	Contraction	Constriction	Expansion	Downstream
	0,0	63,5	14,7	51,8	0,1

Water level

The water levels were measured at locations 1,3,5,6 they are depicted in Table 169. The levels were computed by measuring at 1000 [hz] for 15 seconds, and averaging those results. It is observed that the water level shows a drop of 0,8 [cm]. The water level seems to drop during constriction with 1,5 [cm], and then increases again with 0,7 [cm].

Table 169; Water level [cm]

Location	1	3	5	6
	39,6885	38,7754	38,6655	39,0764

Measurements after 48h

Bed level

A projection of the bed after running for 48 [h] can be observed in Figure 687. The logs have started to redistribute leaving several gaps in between. Accretion is still observed directly downstream of the logs favoring the right hand side. The contraction-sector shows mild bedforms originating from the interface between the upstream-sector and the contraction-sector.

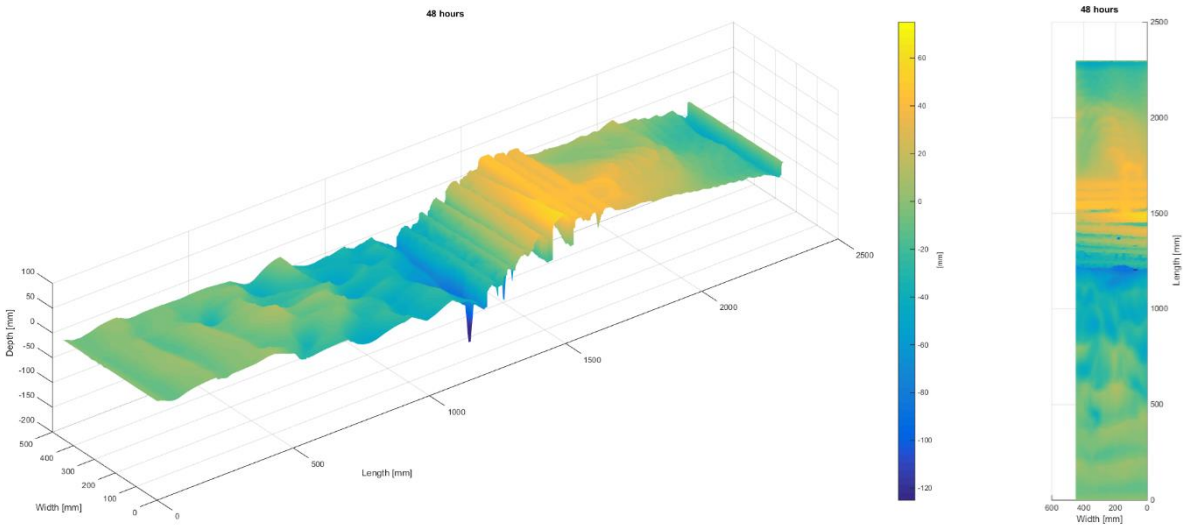

Figure 687; 48[h] bed projection

The average transect (Figure 688), shows the maximum scour upstream of the logs is about 80 [mm] wand the scour hole downstream of the logs reaches a maximum of 40 [mm]. These values have remained similar with respect to the measurements taken after 24 [h].

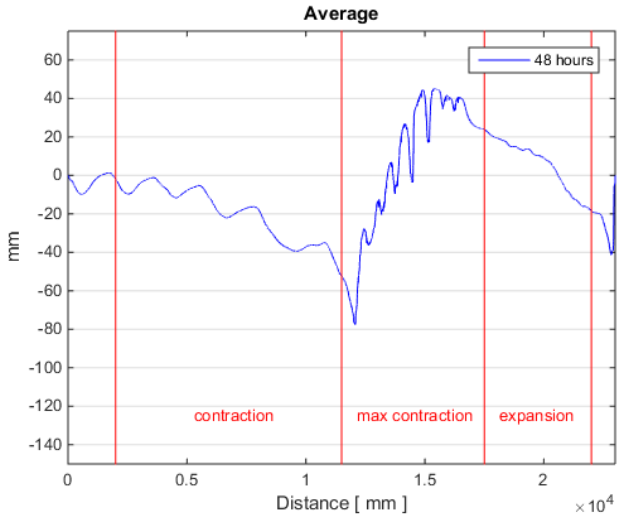

Figure 688; 48[h] average transect

Figure 689 shows that some of the accretion present after 24 [h] just downstream of the logs has scoured away. Bedforms upstream of the logs have intensified but the relative position of the logs seemingly has not changed that much.

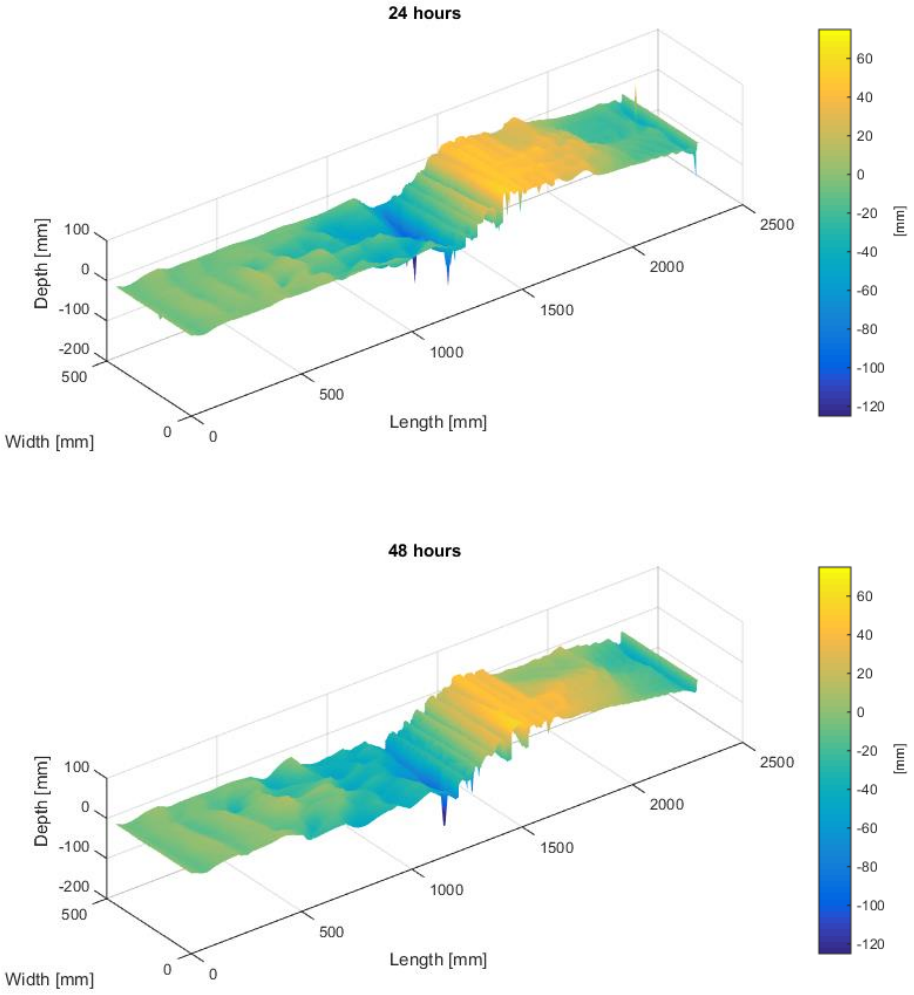

Figure 689; 24[h]-48[h] bed change projection

Table 170; Volume change per sector in [cm^3]

	Upstream	Contraction	Constriction	Expansion	Downstream
Volume	-16	-1878	-1002	+502	-123

Velocity Profiles

The flow profiles at this time show interesting patterns., the flow profile at location 1 remains relatively unaffected, the flow profile just upstream of the logs shows (location 3) shows a normal distribution higher up the water column, while near bed velocities appear to be increasing, this might be caused by the logs. Flow just downstream of the logs show a strong acceleration of flow approximately 10 [cm] from the bed, at location 6 the influence of the narrow scour hole is now clearly observable as velocities near bed are close to zero, while further up the water column flow velocities are much higher. Location 9 shows strongly disturbed measurments.

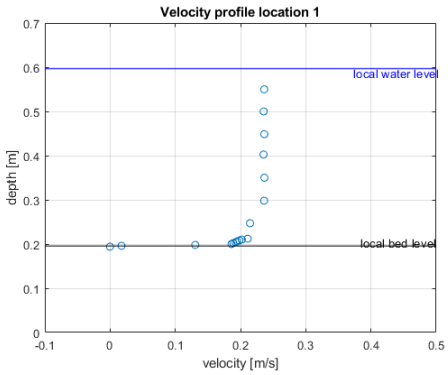

Figure 690; Velocity Profile location 1

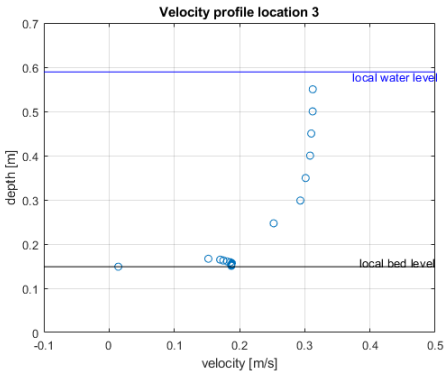

Figure 691; Velocity Profile location 3

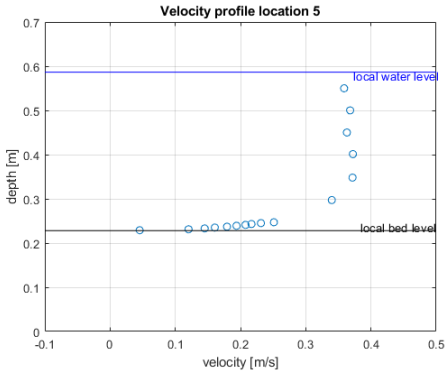

Figure 692; Velocity Profile location 5

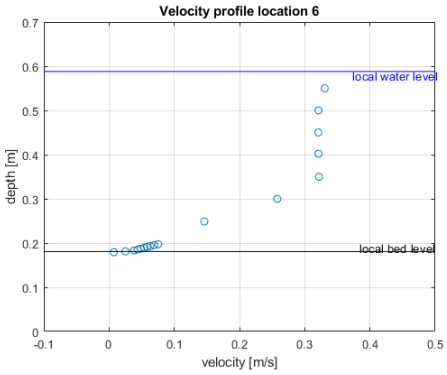

Figure 693; Velocity Profile location 6

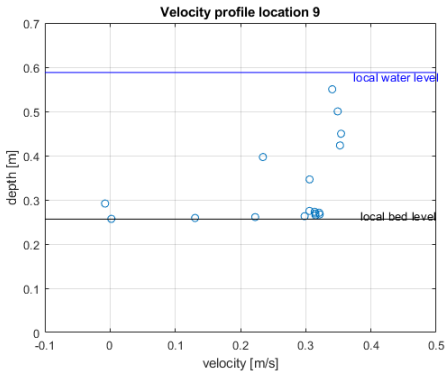

Figure 694; Velocity Profile location 9

Relative fluctuation intensity

RFU now increases from locations upstream towards locations in the constriction-sector (1-2 & 7-8) but decreases from location 2-3. Locations above the logs show relatively small but Uniform RFU. Locations 5 & 10 show moderate fluctuations to average flow velocities and locations located downstream 6 & 11 show strong fluctuations with respect to average flow velocities.

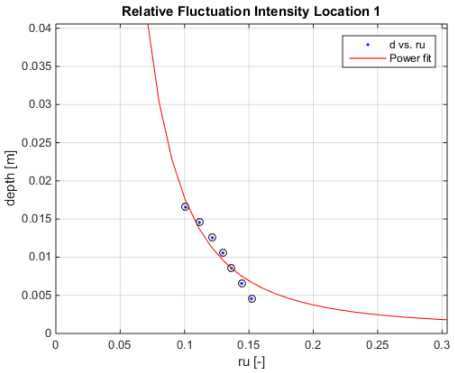

Figure 695; Relative fluctuation intensity location 1

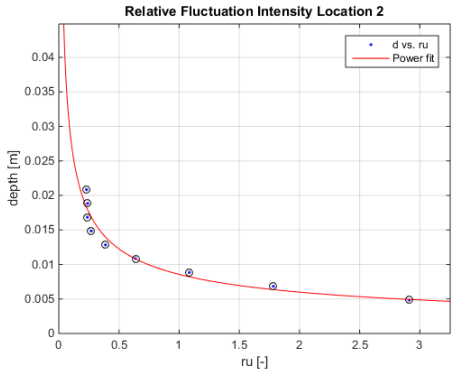

Figure 696; Relative fluctuation intensity location 2

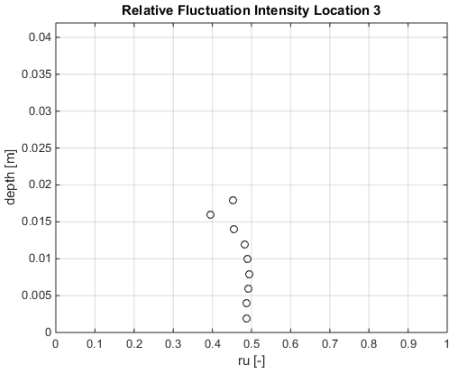

Figure 697; Relative fluctuation intensity location 3

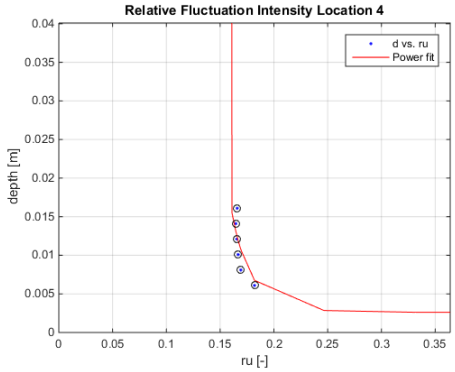

Figure 698; Relative fluctuation intensity location 4

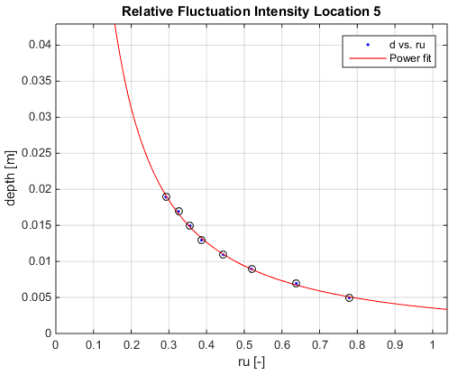

Figure 699; Relative fluctuation intensity location 5

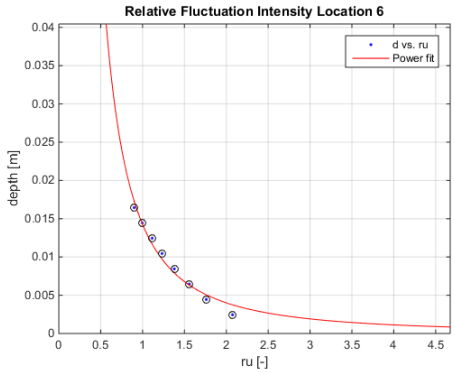

Figure 700; Relative fluctuation intensity location 6

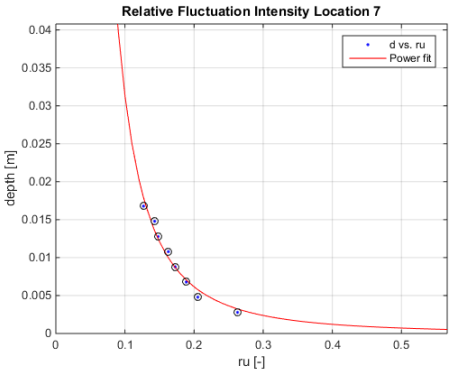

Figure 701; Relative fluctuation intensity location 7

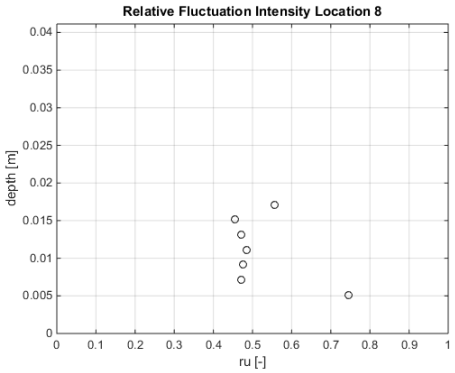

Figure 702; Relative fluctuation intensity location 8

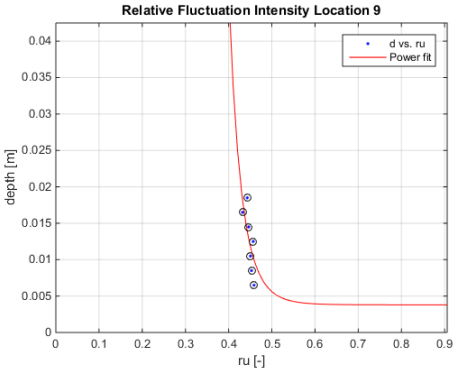

Figure 703; Relative fluctuation intensity location 9

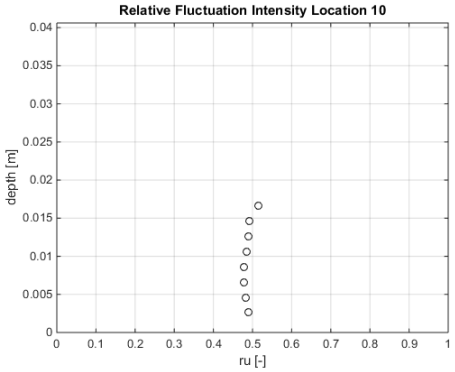

Figure 704; Relative fluctuation intensity location 10

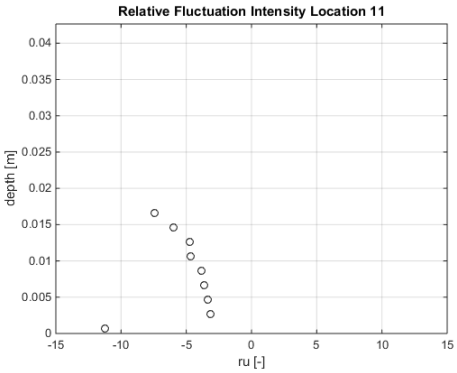

Figure 705; Relative fluctuation intensity location 11

Bed Shear stress

The bed shear stress was determined with Reynolds formula stated in (Schiereck & Verhagen, 2012). Bed shear stresses are determined by averaging the estimation for bed shear stress, over the centimeter measured above the bottom for a time frame of 3 minutes measuring at 50 [hz] per second, excluding all measured values that do not confirm with a signal to noise ratio above 15 and a correlation of 90%.

Bed shear stresses exceed values associated with high level of transport at all locations except at location 1,7 & 11. At all location but locations 4 & 8 these bed shear stresses were observed to be negative.

Table 171; Bed shear stresses [n/m^2]

Location	1	2	3	4	5	6	7	8	9	10	11
	-0,066	-0,397	-0,119	0,847	-0,493	-0,334	-0,083	-0,261	3,783	-0,348	-0,010

Estimation of transport

Following the formulations of the bed load transport by van Rijn (van Rijn, 2018). The results are represented as such, that locations at the same longitudinal location are coupled and transport is averaged over these locations (Table 172) For the calculations the absolute value was taken of the measured bed shear stresses. The results are also depicted per sector (Table 173) by calculating the area underneath each cross-sectional measurement. In this way it is expected that scour should occur in the contraction, constriction and expansion sectors. The values for scour are extremely high especially in the constriction-sector, the presence of logs might make transport less high in this region.

Table 172; Bed load transport [kg/m/s]

Location	1	2 & 7	3 & 8	4 & 9	5 & 10	6 & 11
	NaN	$6{,}58*10^{-4}$	$7{,}26*10^{-5}$	$2{,}81*10^{-1}$	$7{,}55*10^{-3}$	$8{,}57*10^{-6}$

Table 173; Bed load transport per sector [kg/day]

Sector	Upstream	Contraction	Constriction	Expansion	Downstream
	NaN	15,6	3838,8	76,4	0,0

Water level

The water levels were measured at locations 1,3,5,6 they are depicted in Table 174. The levels were computed by measuring at 1000 [hz] for 15 seconds, and averaging those results. It is observed that the water level shows a drop of 0,9 [cm]. The water level seems to drop during constriction with 1,0 [cm], and then increases again with 0,1 [cm].

Table 174; Water level [cm]

Location	1	3	5	6
	39,6552	38,9211	38,6578	38,7879

Measurements after 72h

Bed level

A projection of the bed after running for 72[h] can be observed in Figure 706.The logs are forming a staircase of logs. Bedforms dominate upstream from the logs while downstream from the logs the bed is relatively flat, with a scour hole at the downstream end.

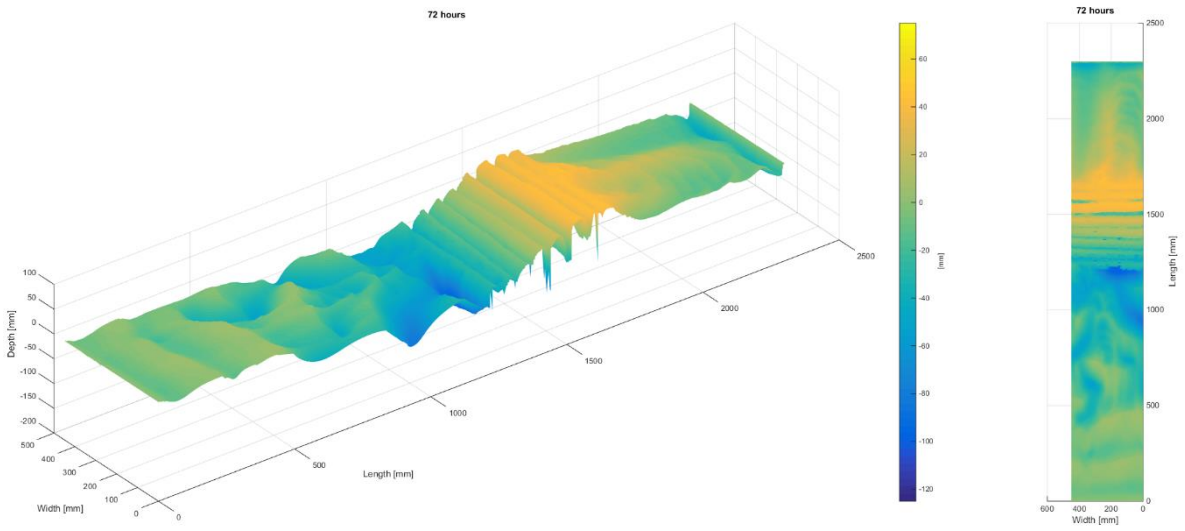

Figure 706; 72[h] bed projection

From the average transect (Figure 707) it can be observed that scour has reached approximately 70 [mm] in front of the log layer. The scour downstream has reached up to on average 40 [mm]. The bed upstream still seems is clearly in motion and the bed downstream of the logs shows slight accretion.

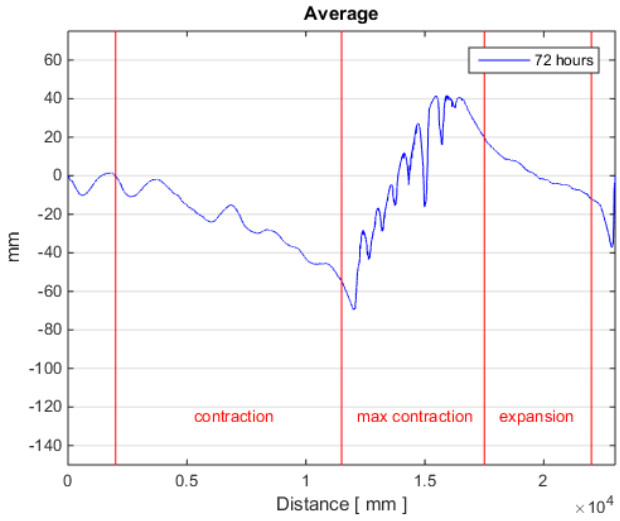

Figure 707; 72[h] average transect

Furthermore Figure 708 shows that compared with the measurement taken at 48 hours scour does not seem to have increased significantly although the bedforms have increased in size and the bed downstream of the logs has seemingly smoothed out.

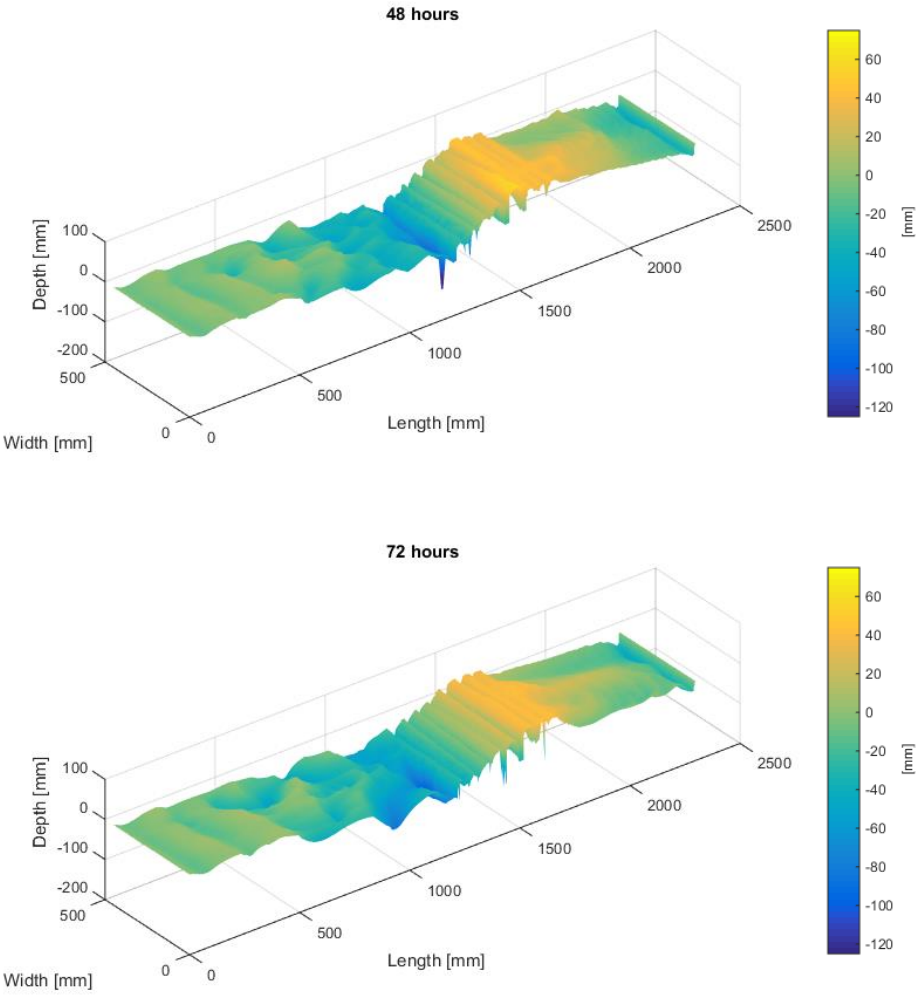

Figure 708; 48[h]-72[h] bed change projection

Table 175; Volume change per sector in [cm^3]

	Upstream	Contraction	Constriction	Expansion	Downstream
Volume	-12	-1558	-1403	-935	+205

Velocity Profiles

Observably, the flow profiles do not seem to change much at all locations although at location 6 it can now be seen that flow is nearly stagnant near the bottom, due the fact that this location is located within the scour hole at the downstream end of the flume, located near a hard barrier.

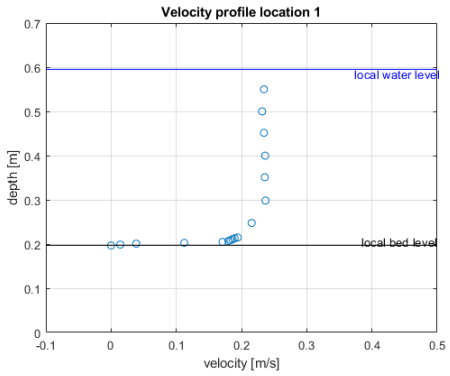

Figure 709; Velocity Profile location 1

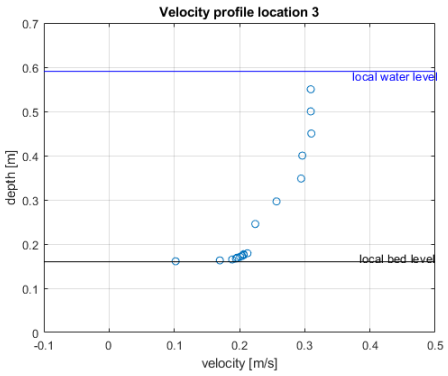

Figure 710; Velocity Profile location 3

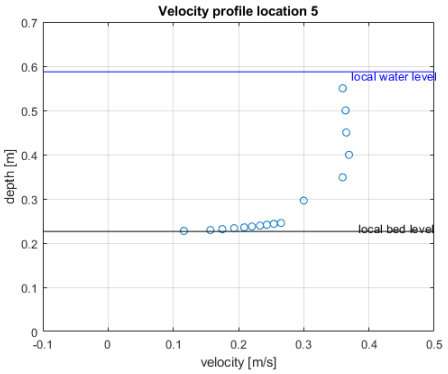

Figure 711; Velocity Profile location 5

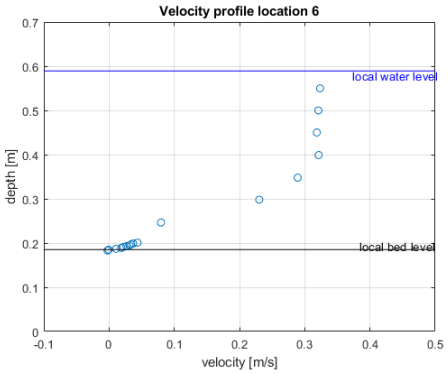

Figure 712; Velocity Profile location 6

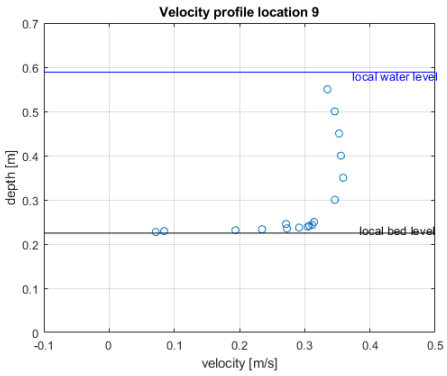

Figure 713; Velocity Profile location

Relative fluctuation intensity

RFU now increases from locations upstream towards locations in the constriction-sector (1-2-3 & 7-8). Locations above the logs show relatively large but Uniform RFU. Locations 5 & 10 show moderate fluctuations to average flow velocities and locations located downstream 6 & 11 show strong fluctuations with respect to average flow velocities.

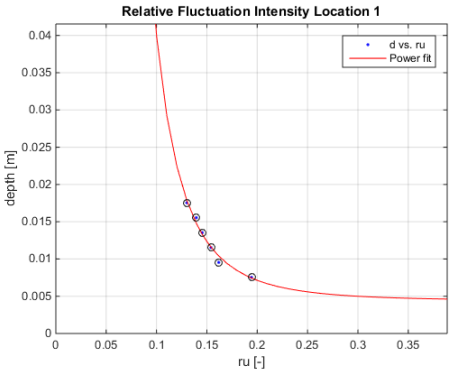

Figure 714; Relative fluctuation intensity location 1

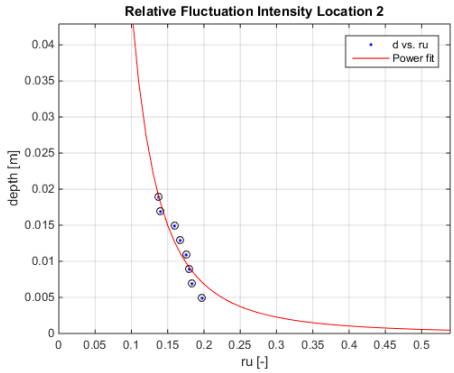

Figure 715; Relative fluctuation intensity location 2

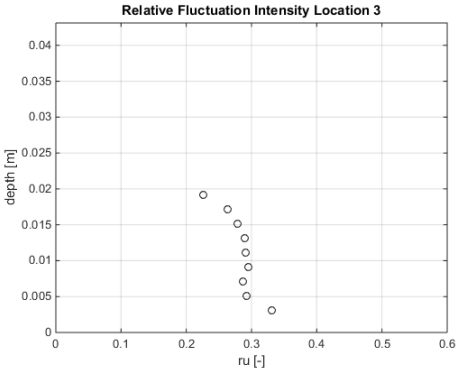

Figure 716; Relative fluctuation intensity location 3

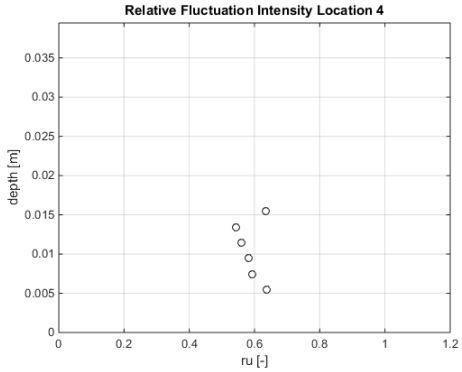

Figure 717; Relative fluctuation intensity location 4

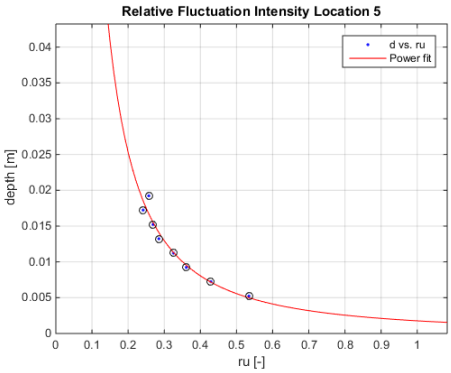

Figure 718; Relative fluctuation intensity location 5

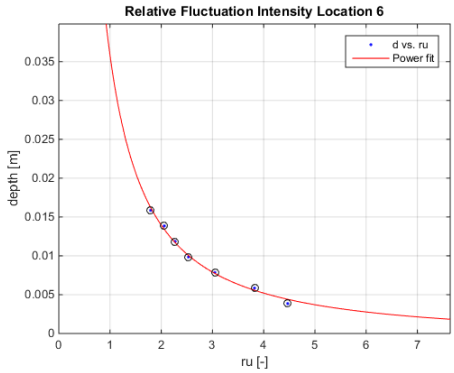

Figure 719; Relative fluctuation intensity location 6

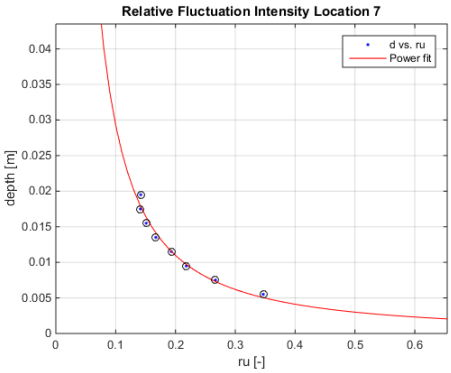

Figure 720; Relative fluctuation intensity location 7

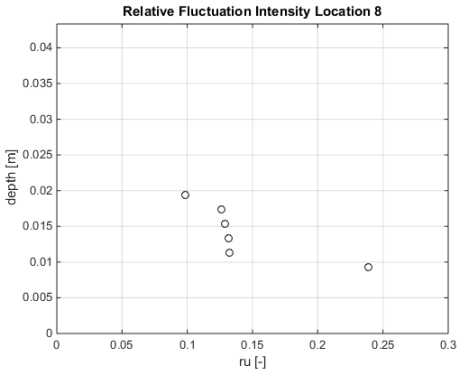

Figure 721; Relative fluctuation intensity location 8

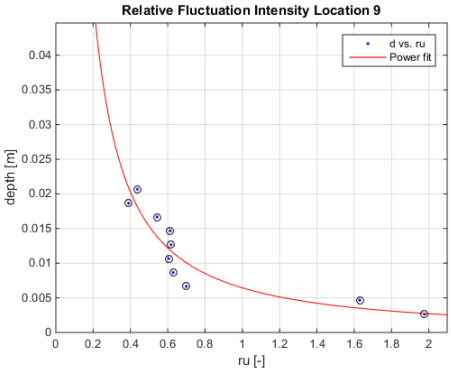

Figure 722; Relative fluctuation intensity location 9

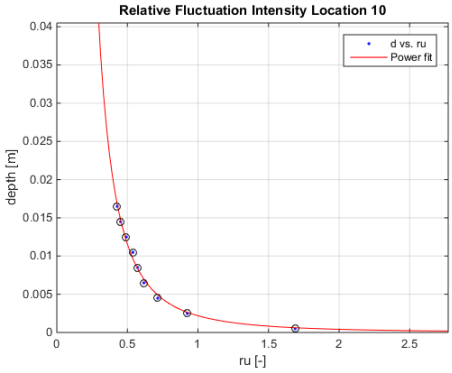

Figure 723; Relative fluctuation intensity location 10

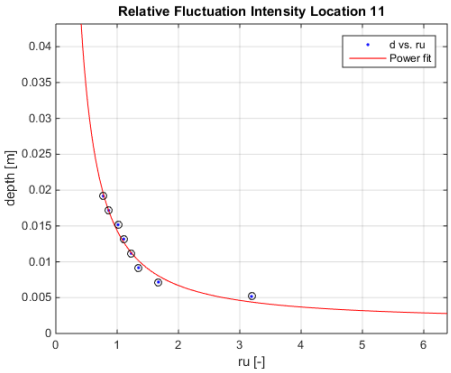

Figure 724; Relative fluctuation intensity location 11

Bed Shear stress

The bed shear stress was determined with Reynolds formula stated in (Schiereck & Verhagen, 2012). Bed shear stresses are determined by averaging the estimation for bed shear stress, over the centimeter measured above the bottom for a time frame of 3 minutes measuring at 50 [hz] per second, excluding all measured values that do not confirm with a signal to noise ratio above 15 and a correlation of 90%.

Bed shear stresses exceed values associated with high level of transport at all locations except at location 1 & 9. At all location but locations 4 & 8 these bed shear stresses were observed to be negative. At location 4 this value was also exceptionally large, most likely caused by the complex flow pattern above the logs.

Table 176; Bed shear stresses [n/m^2]

Location	1	2	3	4	5	6	7	8	9	10	11
	-0,071	-0,124	-0,460	2,694	-0,431	-0,418	-0,232	0,169	-0,097	-0,680	-0,123

Estimation of transport

Following the formulations of the bed load transport by van Rijn (van Rijn, 2018). The results are represented as such, that locations at the same longitudinal location are coupled and transport is averaged over these locations (Table 177) For the calculations the absolute value was taken of the measured bed shear stresses. The results are also depicted per sector (Table 178) by calculating the area underneath each cross-sectional measurement. Scour is to be expected in the contraction, constriction, expansion and downstream sectors. Although the scour rate in the constriction and expansion sector is much higher than the amount of bed material available.

Table 177; Bed load transport [kg/m/s]

Location	1	2 & 7	3 & 8	4 & 9	5 & 10	6 & 11
	NaN	$2{,}22*10^{-5}$	$2{,}66*10^{-3}$	$1{,}18*10^{-1}$	$1{,}66*10^{-2}$	$1{,}32*10^{-3}$

Table 178; Bed load transport per sector [kg/day]

Sector	Upstream	Contraction	Constriction	Expansion	Downstream
	NaN	30,3	1720,2	362,3	5,9

Water level

The water levels were measured at locations 1,3,5,6 they are depicted in Table 179. The levels were computed by measuring at 1000 [hz] for 15 seconds, and averaging those results. It is observed that the water level shows a drop of 0,6 [cm]. The water level seems to drop during constriction with 0,8 [cm], and then increases again with 0,2 [cm].

Table 179; Water level [cm]

Location	1	3	5	6
	39,5022	39,0594	38,7179	38,9293

Measurements after 96h

Bed level

A projection of the bed after running for 96[h] can be observed in Figure 725. The logs have formed a stable a staircase. Bedforms still dominate upstream from the logs while downstream from the logs the bed is relatively flat, with a scour hole at the downstream end.

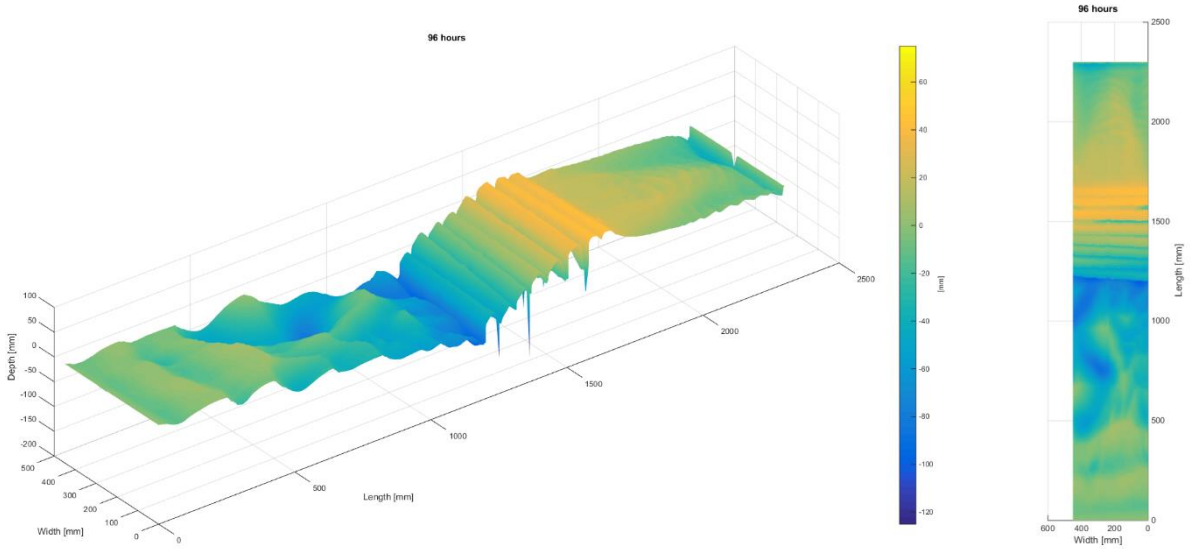

Figure 725; Bed map after 96 [h]

Comparing the average transect with the average transect taken at 0 [h], it can clearly be seen that the bed in the contraction-sector and the constriction-sector is strongly affected. The logs have caused accretion downstream of their location and have formed a clear staircase. Maximal average scour is measured in the constriction-sector with a depth of about 85 [mm]. The scour hole downstream of the logs located in the downstream-sector is about 35 [mm] deep.

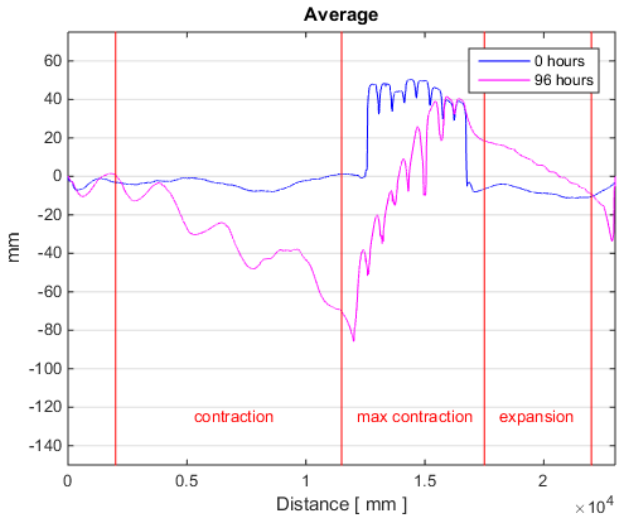

Figure 726; Average transects through time

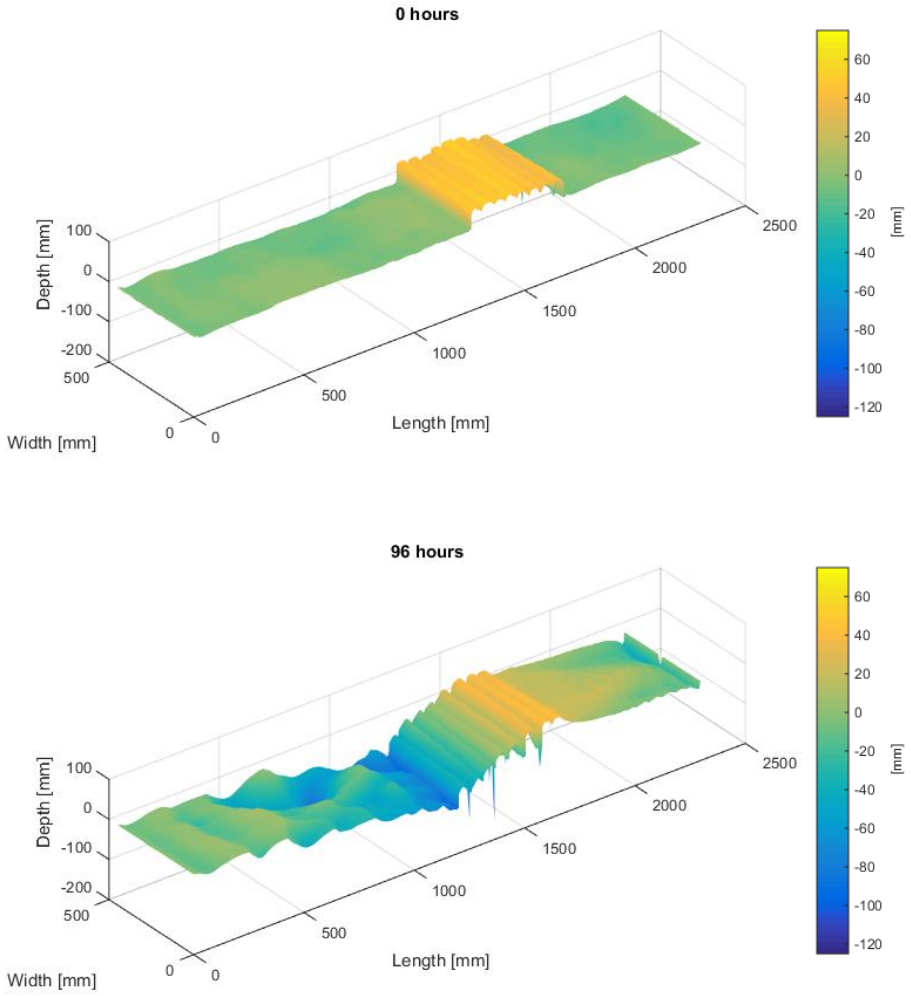

Figure 727; Bed change with respect to 0[h]

Table 180; Volume change per sector in [cm^3]

	Upstream	Contraction	Constriction	Expansion	Downstream
Volume	-20	-3606	-944	+975	+131

Concluding Remarks

This third protected scour B experiment has again shown some promising results. At the point of highest flow velocities, located above the logs, the scour has reduced and even some accretion was observed. The logs have formed a so called staircase of logs, protecting the slope located underneath the logs. Again, a small scour hole downstream of the logs was observed to have formed.

List of Symbols

Symbol	Definition	Unit
$\boldsymbol{B}$	Width	m
$\boldsymbol{B_s}$	Shape correction factor	-
$\boldsymbol{C}$	Chezy coefficient	$m^{0,5}/s$
$\boldsymbol{d_b}$	Soil depth	m
$\boldsymbol{d_s}$	Scour depth	m
$\boldsymbol{D_{15}}$	15% exceedence particle diameter	m
$\boldsymbol{D_{50}}$	50% exceedence particle diameter	m
$\boldsymbol{D_{90}}$	90% exceedence particle diameter	m
$\boldsymbol{D}$	Diameter of logs	m
$\boldsymbol{g}$	Acceleration of gravity	m^2/s
$\boldsymbol{h}$	Water depth	m
$\boldsymbol{k_r}$	(equivalent) roughness of bottom	m
$\boldsymbol{K_\alpha}$	Angle correction factor	-
$\boldsymbol{K_u}$	Velocity correction factor	-
$\boldsymbol{L_l}$	Length of logs	m
$\boldsymbol{n}$	Porosity	-
$\boldsymbol{Q}$	Discharge	m^3/s
$\boldsymbol{r_u}$	Relative fluctuation intensity x-direction	-
$\boldsymbol{r_v}$	Relative fluctuation intensity y-direction	-
$\boldsymbol{r_w}$	Relative fluctuation intensity w-direction	-
$\boldsymbol{s}$	Specific gravity of sand γ_s/γ	-
$\boldsymbol{u}$	Flow velocity in flow direction	m/s
$\boldsymbol{\bar{u}}$	Velocity averaged in time or space in x-direction	m/s
$\boldsymbol{u`}$	Flow velocity fluctuation in x-direction	m/s
$\boldsymbol{u_c}$	Critical velocity	m/s
$\boldsymbol{v}$	Kinematic viscosity	m^2/s
$\boldsymbol{\bar{v}}$	Velocity averaged in time or space in y-direction	m/s
$\boldsymbol{v`}$	Flow velocity fluctuation in y-direction	m/s
$\boldsymbol{\bar{w}}$	Velocity averaged in time or space in z-direction	m/s
$\boldsymbol{w`}$	Flow velocity fluctuation in z-direction	m/s
$\boldsymbol{\rho_h}$	Density wood	kg/m^3
$\boldsymbol{\rho_s}$	Density bed material	kg/m^3
$\boldsymbol{\rho_w}$	Density water	kg/m^3
$\boldsymbol{\sigma}$	Surface tension	$n/\,m$
Δ	Relative density (=$(\rho_s-\rho_w)/\rho_w$)	-
Ψ_c	Shields stability parameter	-

Bibliography

Ettema, R., Melville, B. W., & Barkdoll, B. (1998). Scale Effect in Pier-Scour Experiments. *Journal of hydraulic engineering*, 4.

Haage, S., & Çete , C. (2016). *Bodembescherming met behulp van boomstammen.* Delft: TUDelft.

Mutlu Sumer, B., & Fredsøe, J. (2005). *The mechanics of scour in the marine environment.* Singapore: World Scientific Publishing.

Rijkswaterstaat. (2016). *Korte verkenning plaatsing hout Haringvliet/Hollands Diep tbv inventarisatie KRW maatregelen 2de tranche.* Utrecht: Rijkwaterstaat.

Schiereck, G. J., & Verhagen, H. J. (2012). *Introduction to Bed, bank and shore protection.* Delft: VSSD.

Sibelco. (2017, 5 1). *Sibelco/Producten/Kwartszand*. Retrieved 5 1, 2017, from Sibelco: www.sibelco.be

Sutherland, J., & Soulsby, R. (2010). *Guidelines for physical modelling of mobile sediments.* Barcelona: HR Wallingford.

van Olst, L., van Leeuwen, P., & van der Scheer, B. (2016). *Bodembescherming met behulp van boomstammen.* Delft: TUDelft.

van Rijn, L. (2018, Febuary 20). *simple general formulae for sand transport in rivers, estuaries and coastal waters .* Retrieved from Leo van Rijn: www.leovanrijn-sedimetn.com